

Evaluation of LIDAR and Photogrammetric Elevation Data
for Feature-based Forest Analyses

Thesis

in partial fulfillment of the requirements for

the degree Doctor rer. nat.

at the Department of Earth Sciences

Freie Universität Berlin

Germany

submitted by

S. Mohsen Miri

Berlin

August 2015

Supervisor and 1st Reviewer: Prof. Dr. rer. nat. Bernd Meissner

Advisor: Prof. Dr.-Ing. Martin Kähler

2nd Reviewer: Prof. Dr. rer. nat. Hartmut Kenneweg

3rd Reviewer: Prof. Dr. rer. nat. Stephan van Gasselt

Disputation on: 19.01.2016

Declaration

I declare that I have authored this thesis independently, that I have not used other than the declared sources / resources, and that I have explicitly marked all material which has been quoted either literally or by content from the used sources.

Erklärung

Hiermit versichere ich, die vorliegende Arbeit selbständig verfasst und nur angegebene Hilfsmittel verwendet zu haben. Die aus anderen Quellen übernommenen Daten und Konzepte sind unter Angabe der Quelle gekennzeichnet.

S. Mohsen Miri

Berlin, August 2015

Abstract

For qualitative and quantitative detection of forest resources, there is a demand to extract the stand parameters in forestry not only at stand level but also for single trees; high resolution digital surface models may be suitable for this aim. The dependence of most of stand features on tree height, demonstrates the importance of this element in the characterisation of forest stands from an environmental perspective and for the purpose of the timber industry. Airborne laser point clouds and photogrammetric stereo images are the two main data acquisition sources to generate the digital surface models for detailed and large areas of forests.

The main aim of this research is to study these two surface models for feature extraction approaches based on height data. In the represented research neither the spectral information of the images nor the intensity values of the LIDAR data are used. For this purpose a novel concept, called *eye-finger*, is developed to simulate and analyze the surface models by touching the top levels of the tree crown with closed eyes. To translate the feeling of the *human sense of touch* into the language of machine vision, the geometric and morphological features are defined and evaluated on both laser-based and image-based canopy height models. Because of the high degree of noise in the laser data, a filter should be implemented before the comparison and the segmentation steps. The developed *non-smoothing* filter in this work removes the problematic pixels, while the roughness and the form of the trees remain unchanged.

The work focuses on European mixed-forests, consisting of coniferous and deciduous trees. The roughness parameters used in the production industry are implemented to extract the surface characteristics of mixed-forests. The average-based parameters like R_a show the dependency of these surface evaluators on the age and tree type of the stand. The roughness parameters related to the standard deviation of the surface, measure the finer variations on the surface. An advanced roughness evaluator called R_{fsd} is developed in this research which captures minor height variations on the canopy and is independent from the mean height of the stand.

At the single tree level an object-oriented strategy is mapped out. To extract the position of the single trees, a novel method, called *marble-rolling* is developed. The *seed-objects*, as the result of this process are employed for the supervised *region-growing* algorithm. Simultaneously, the shape characteristics of the growing segments are evaluated and optimized with morphological functions. For the characterisation of the single trees, both geometric features and morphological feature are implemented. The geometric feature provided better results to distinguish the coniferous tree-segments from the deciduous ones. The results of the segmentation are compared with a reference dataset. The test area, with mainly coniferous trees, is defined with a combination of terrestrial laser scanning and close-range photogrammetry. The evaluation of the topological relationships of the reference and target dataset provides high completeness and correctness results for the single tree extraction based on the airborne laser data.

Zusammenfassung

Zur qualitativen und quantitativen Erfassung der Waldressourcen gibt es den Bedarf, Parameter für Waldgebiete nicht nur auf der Ebene von Beständen, sondern auch für Einzelbäume zu erheben; hochauflösende Oberflächenmodelle können dafür zweckmäßig sein. Die Abhängigkeit der meisten Kenngrößen für Waldbestände von Baumhöhen zeigt, dass dieses Element der Charakterisierung von Waldbeständen sowohl für Umweltbelange als auch für die Holzindustrie sehr wichtig ist. Airborne Laser-Scanning und photogrammetrische Stereobilder sind die wichtigsten Datenerfassungsquellen, um detaillierte digitale Oberflächenmodelle für große Waldflächen zu generieren.

Das Hauptziel dieser Forschungsarbeit ist die Untersuchung der beiden Oberflächenmodelle zur Merkmalsextraktion aus den Höhendaten. In der dargestellten Arbeit werden weder die Spektralkanäle der Luftbilder noch die Intensitätswerte der LIDAR-Daten verwendet. Zu diesem Zweck wird das neuartige Konzept „*Eye-Finger*“ entwickelt, um die Oberflächenmodelle durch Berühren der oberen Baumkronenebenen mit geschlossenen Augen zu simulieren und zu analysieren. Um das „*Gefühl des menschlichen Tastsinns*“ in die Sprache der Bildverarbeitung zu übersetzen, werden die geometrischen und morphologischen Merkmale definiert und dadurch sowohl das laserbasierte wie auch das bildbasierte Höhenmodell bewertet. Um den Einfluss des Rauschens bei der Auswertung von der Laserdaten zu minimieren, muss ein Filter vor dem Vergleich und Segmentierung implementiert werden. Der entwickelte „*Non-Smoothing*“ Filter entfernt die problematischen Pixel, während die Rauheit und die Form des Baumes unverändert bleibt.

Diese Arbeit konzentriert sich auf europäische Mischwälder, die aus Laub- und Nadelbäumen bestehen. Um die Oberflächeneigenschaften der Mischwälder zu extrahieren werden in der industriellen Fertigungstechnik entwickelte Rauheitsparameter implementiert. Die Parameter, basierend auf der durchschnittlichen Höhe des Bestandes wie R_a , zeigen die Abhängigkeit dieser Oberflächen-Evaluatoren vom Alter und Baumtyp des Bestandes. Die Rauheitsparameter, bezogen auf die Standardabweichung der Oberflächen, messen die feineren Variationen auf der Oberfläche. Ein weiterer Rauheitsparameter, genannt R_{std} , wurde in dieser Forschungsarbeit entwickelt, um die kleinen Höhenunterschiede auf den Oberflächen unabhängig von der mittleren Höhe des Bestandes zu ermitteln.

Für die Einzelbaumebene konnte eine objektorientierte Strategie entworfen werden. Um die Position der einzelnen Bäume zu extrahieren, wurde das neue Verfahren „*Marble-Rolling*“ entwickelt. Die „*Seed-Objects*“, als das Ergebnis dieses Prozesses, werden für das gesteuerte „*Region-Growing*“ der Baumsegmente verwendet. Gleichzeitig wurden die Formeigenschaften der wachsenden Segmente ausgewertet und mit morphologischen Funktionen optimiert. Zur Charakterisierung der Form und Oberfläche einzelner Bäume werden sowohl geometrische wie auch morphologische Merkmale verwendet. Die geometrischen Merkmale erwiesen sich als besser geeignet, um Nadelbaumsegmente von Laubbaumsegmenten zu unterscheiden. Die Ergebnisse der Segmentierung wurden mit einem Referenzdatensatz verglichen, der aus einer Kombination von terrestrischem Laserscanning und Nahbereichs-Photogrammetrie aufgenommen wurde. In hauptsächlich mit Nadelbäumen bestandenem Testbereich konnte bei der Evaluierung der topologischen Beziehungen zwischen Referenz- und Zieldatensatz eine hohe Vollständigkeit und Korrektheit der Einzelbaumextraktion mit den von Flugzeug gewonnen Laserdaten festgestellt werden.

Acknowledgements

This work would never have been completed without the help of several individuals and institutes. I would like to thank them all, although I feel that words fall short in this regard.

First and foremost, I would like to express my deepest and warmest appreciation to my supervisor and advisor Prof. Dr. rer. nat. Bernd Meissner, who has been a tremendous mentor for me. His many years of experience, together with his insightful supervision, have enabled me to overcome the challenges in the way of my research and develop my problem solving skills. I feel so fortunate to have had him as my advisor and always enjoyed working with his kind team at the geo3 Institute for Geo-research at the Beuth University of Applied Sciences Berlin.

My sincerest gratitude goes to Prof. Dr.-Ing. Martin Kähler, from the Beuth University of Applied Sciences Berlin. Through his professional knowledge and wide experience, he advised and supervised me in many aspects of my PhD. I would like to thank him for providing this PhD position for me. Under his supervision in the laboratory of photogrammetry, I had the opportunity to work in a professionally scientific atmosphere at a very well-equipped workplace. His support, both from a research as well as career point of view has been priceless.

I would like to thank my second reviewer and examiner Prof. Dr. rer. nat. Hartmut Kenneweg from the Technical University of Berlin for undertaking the revision and evaluation of my work. His constructive suggestions played an important role in strengthening the arguments of my research.

I thank my third reviewer and examiner Prof. Dr. rer. nat. Stephan van Gasselt from the Institute of Geological Sciences at Freie Universität (FU) Berlin for his remarkable comments on this work. I appreciate the committee members of the Department of Geosciences at the FU Berlin, for the time taken in organising the examination commission.

At the German Aerospace Center (DLR) in Berlin, Institute of Optical Sensor Systems, sincere thanks to the head of the institute, Prof. Dr. Heinz-Wilhelm Hübers and also to the head of the Department of Sensor Concepts and Applications, Frank Lehmann, for providing the airborne datasets of my research. Especially, I would like to thank Anna Poznanska, who helped me from the beginning of this research with her deep background in the area of remote sensing. Thanks to Steven Bayer and Tilman Bucher for their great organizational help in preparation of the aerial imagery dataset and the terrestrial surveying campaign, and additionally, for their great support by reviewing the first results of my research, published in the 33rd DGPF annual conference in Freiburg, Germany, February 2013.

Special thanks to Dr.-Ing. Arno Bücken from the Institute for Man-Machine Interaction (MMI) at the RWTH Aachen University for organising and providing the airborne datasets and post processing of the LIDAR data.

This research is the result of a great cooperation with the team of GILAN Surveying Engineering Company in Berlin. In this regard, I would like to specifically mention Zeya Deylamipour. This work would not have been feasible without his tireless contribution. I thank him for supporting me with his team and with equipment for the measurement of the field data.

Great appreciation goes also to my friends Marleen and Andreas Tscherch. With their invaluable know-how and experience, they have consistently helped me over the last years. I appreciate their excellent support during the terrestrial data acquisition of the test area and in reviewing my work. I also thank their lovely families for their kind supports and the beautiful moments with them.

I am really thankful to Juliane Saebel from the Institute for Research and Transfer (RIF e.V.) in Dortmund, and also Stefan Teusan from Karlsruhe for the very informative excursions and introductions to forest mensuration.

Thanks to the Center for Geo-Data in North Rhine-Westphalia (Geobasis-NRW), government district of Cologne, for the Digital Elevation Models, the Cadastral Land Registry Office of the district Steinfurt for the surveying data of the reference points in the test area, and also the NRW State Enterprise for Forestry and Timber for the forest data.

Words are not adequate to thank Professor Michael Breuer. For the fortune of having such a friend as well as a professional scientist in my life, I warmly thank him. He supported me on every occasion with all he could do. He always encouraged me by sharing his professional and personal experience, which enabled me to overcome many difficulties.

I would especially like to thank my two invaluable colleagues, Monika Lehmann and Marko Koch in the Laboratory of Photogrammetry at the Beuth University of Applied Sciences Berlin for the very enjoyable time working with them. Reflecting their considerable educational and career backgrounds and very insightful characteristics, they created the best working atmosphere for me.

My sincere thanks also to the other colleagues in the Beuth University of Applied Sciences Berlin, especially to the Dean of the Department III, Prof. Dr. rer. nat. Immelyn Domnick. I would especially like to mention Norbert Knorr who, supported me in the software and hardware solutions. I cordially thank Antje Meissner for her patience and help in the official support of my PhD. Thank you all. I will always treasure the joy of having been a colleague to you.

Thanks also to Joe Kirwan for his precise assistance at the proof reading stage of this work.

Special thanks go to my great friends Susan, Morteza, Sigrid and their families for being beside me. They changed the hard times of my work into enjoyable and memorable moments.

Last but not least, the most special thanks go to my lovely family for their supports in every way. I cannot express how grateful I am to my mother for her good wishes, day and night, for success in my life and to my father for always encouraging and helping me to see the world with new and open eyes. Thanks for all that you have done on my behalf. I feel very lucky to have two brilliant siblings in my life; my sweet-hearted sister Mona and my lovely brother Milad, who stood alongside me over the last years, even though they were very far from me. I am so thankful and proud of you.

Table of Contents

1. <i>Introduction</i>	2
1.1. Geomatics in forestry	2
1.2. Motivation	4
1.3. Statement of the question	4
1.4. Structure of the research.....	6
2. <i>Terms and basics</i>	8
2.1. Single tree in forest mensuration.....	8
2.1.1. Tree height measurement.....	8
2.1.2. Single tree parameters in forestry.....	10
2.2. Remote sensing in forestry	12
2.3. Optical imagery	12
2.3.1. Illumination condition in spectral images	13
2.3.2. Tree measurement in aerial images	18
2.4. Airborne laser scanning.....	19
2.4.1. Ranging systems.....	20
2.4.2. Noise.....	24
2.5. LIDAR-based and image-based elevation data.....	24
3. <i>Image Processing</i>	32
3.1. Pixel-based vs. object-oriented image analysis.....	32
3.2. Scale-space	33
3.3. Segmentation	36
3.3.1. Edge-based and region-based segmentation.....	36
3.3.2. Watershed transformation.....	36

3.3.3. Object-oriented segmentation of single trees.....	39
4. <i>Feature Extraction</i>	50
4.1. Features in single tree extraction	50
4.2. Template-matching.....	50
4.3. Local maxima	52
4.4. Top hat slices	53
4.5. Surface analysis	56
5. <i>Methodology</i>	64
5.1. Eye-finger concept.....	64
5.2. Data preparation.....	66
5.2.1. Noise and filters in processing the LIDAR data	66
5.2.2. Selective or Non-smoothing filter.....	69
5.3. Boundary delineation	71
5.4. Morphological Analysis.....	73
5.5. Marble-Rolling segmentation	76
5.6. Region growing.....	85
5.6.1. Region growing of non-tree areas	86
5.6.2. Segmentation refinement of the stand boundary.....	90
5.6.3. Region growing of single trees	92
5.7. Feature-based classification.....	100
5.8. Segment geometry	101
5.9. Segment roughness	104
5.10. Qualitative and quantitative evaluation.....	106
6. <i>Experimental Results</i>	114
6.1. Study area	114
Accuracy assessment of the DSM datasets	116
6.2. Stand-wise roughness analysis.....	118
Single tree roughness analysis	122
6.3. Reference data for single tree detection.....	126

6.3.1. Traditional methods in forestry	126
6.3.2. Terrestrial laser scanning and photogrammetry of single trees	127
6.4. Stand-wise qualitative evaluation of the CHM	133
6.4.1. Analysis of height variations	133
6.4.2. Form analysis.....	138
6.5. Quantitative evaluation of single tree delineation.....	142
7. <i>Conclusion and outlooks</i>	152
7.1. Height-based forest mensuration.....	152
7.2. From stand-wise analysis to single tree extraction.....	152
7.3. Outlook.....	154
8. <i>References</i>	158
9. <i>Appendices</i>	176
10. <i>Abbreviations</i>	186
11. <i>CV</i>	187



1

Introduction

This chapter has an introductory view on the methods and significance of airborne height data in forestry applications, following with the motivation and the statements of the question.

1.1. Geomatics in forestry

Forest mensuration deals with methods of qualitative and quantitative assessment of forestry areas in different scales. Over the last decade, these aspects have been expanded from determination of logs, trees and stands at a definite point and time [Laar and Akça 2007] to the assessment of wildlife, recreation and watershed management [Hyypä et al. 2004]. In general, forest monitoring can be categorized as a long-term issue in climate protection and carbon preservation analyses, both at regional and national levels [Kenneweg and Weyer 2014]. Higher precision in forest mensuration can be used in biomass analysis and CO₂ preservation approaches. In forest management applications, detection of forest damages with remote sensing data can help to control tree diseases and plan for reforestation [Meissner et al. 2004]. In the wood industry, according to the demand for raw materials, efficient management in transporting timber from the forest directly to the related manufacturing factories needs higher precision for measurements of the fell plans [Shan and Toth 2009]. For all of these reasons, more accurate qualitative and quantitative information on individual trees is requested in the base studies. Concluded in [Laar and Akça 2007], “*the forest mensuration deals with the technical aspects of tree and forest stand measurements, such as:*

- *Measurement of tree and stand variables, e.g. diameter, height, basal area, bark parameters, and volume of standing and felled trees*
- *Determination of form and age of trees and forest stands*
- *Determination of volume of standing and felled trees*
- *Measurement of live crown and quantity of foliage*
- *Estimation of biomass and biomass components of individual trees and stands*
- *Estimation of the total and merchantable stand volume and its size class distribution*
- *Estimation of the diameter, basal area, height, and volume growth of single trees and forest stands*
- *Estimation of the damages and the quality of individual trees and forest stands*

Over the last decade, developments in remote sensing of the forest have changed profoundly, both from the technical and processing points of view, which shows the potential of

implementing these methods in regional and national levels for forest monitoring [Ackermann et al. 2014]. Especially for mixed forests, the necessity and the great interest in more detailed forest information systems for single tree delineation and classification based on height and spectral data has been noted since the last decade [Pyysalo and Hyyppa 2002; Bayer et al. 2013]. Such information systems require detailed three dimensional positioning and accurate attributing of single trees. Employing high quality digital elevation models acquired from forest areas, in addition to the high resolution multi-spectral information at single tree level, can provide the essential data for such geographical information systems.

In geospatial applications, trees are one of the most complicated objects to survey. The difficulties in single tree delineation are basically due to the variety of tree types and their complexity of form and color. Textural changes in the tree crown occur relatively faster than its geometric characteristics. However, such geometric information is difficult to measure on the ground [Sheng et al. 2001]. In forest information systems, geometric feature extraction of single trees, by means of airborne data-acquisition sensors, focuses mostly on finding the trees positions by delineating the crown boundaries. This indicates that employing reasonable surveying sensors on the one hand, and appropriate tree extraction methods on the other, are the most challenging issues at this level of detail. Thanks to rapid developments in Airborne Laser Scanning (ALS) technology and High Resolution Stereo Cameras (HRSC), both from the technical [Baltsavias 1999c] and processing points of view [Pfeifer et al. 2007], the provision of valuable geospatial information in forestry applications has been increasing [Leckie et al. 2003]. Using the potential of the recent photogrammetric sensors and the capabilities of the combined datasets are the current research topics in this area [Straub et al. 2013].

Regarding the cost-efficiency parameters, higher updating rate of the data acquisition [Straub and Seitz 2011] and due to the different characteristics of laser-based and optical techniques, one might ask whether or to what extent the digital surface models, provided with solely photogrammetric progresses, can meet the demands of forestry applications. Due to the different characteristics of high-resolution stereo images and ALS data, the demand for comparison and integration of these two data-acquisition methods arises to ensure automatically accurate and detailed single tree extraction. To achieve this goal, assessment of the strengths and weaknesses of each method should be taken into account [Mielonen et al. 2005; Sato 2010; Leckie et al.

2003; Heinzl et al. 2008; Wang et al. 2008]. This evaluation can be extended from spectral analysis of the data-acquisition sensors to the image-processing methods in machine vision algorithms. Additionally, the variety of the forest types from tropical jungles to the Scandinavian forest stands shows the range and diversity of research approaches in this area.

With a particular focus on forest inventory at individual tree level in middle European mixed forests, this research aims at evaluating Digital Elevation Models (DEM), including Digital Surface Models (DSM) and Digital Terrain Models (DTM), generated from airborne laser scanners and high resolution aerial photogrammetric cameras. With the goal of developing an automatic algorithm for single tree extraction based on only DEM data and without the spectral channels, the challenging aspects for definition of optimized parameters are evaluated.

1.2. Motivation

The goals stated in the introduction are considered broadly, including the topics from forestry demands to the capabilities of the laser scanning and photogrammetry in this field and are detailed further in the next chapter. Airborne laser scanners and aerial imagery sensors are the most important sources for high resolution data acquisition in forestry. In the interest of improving the accuracy of the statistical analyses and also to save time and expenditure compared to traditional terrestrial forestry methods, there is a resulting increased demand for automatic extraction of single trees from these airborne platforms. Evaluation of acquired data focuses mainly on the end products, with the aim of developing computer-vision algorithms. In summary, the demand for optimization of accurate and detailed geospatial data in forest GIS is the overriding concern of this thesis.

1.3. Statement of the question

Single tree delineation requires 3D positional information on trees. That means the height of individual trees is a crucial element for biomass analysis and stem volume estimation which can be provided by remote sensing methods. Observing the forestry areas using high resolution airborne sensors has been implemented to define the position and extract the relevant attributes of a single tree. In this way, a dense point cloud of LIDAR data describes the complex geometry of the upper canopy of forest, suitable for extraction of tree height information [Pyysalo and Hyypä

2002]. Along with airborne laser scanning, high resolution aerial images, as one of the basic and rich sources of detailed geospatial information for forest inventory, has been used for the relevant applications to a large extent. In contrast to airborne laser scanning, aerial images are updated more regularly for national or regional mapping aspects in several countries [Straub et al. 2013].

The problematic scope for readily generating Digital Elevation Models (DEM) from spectral imagery data as passive sensors on the one hand, and the shortcoming of LIDAR data in textural information on the other [Miri et al. 2013; Arbeitsgruppe Forstlicher Luftbildinterpreteten 2012], illustrate the demand for evaluating the accuracy and correctness of these two data acquisition methods for single tree extraction. Leckie et al. (2003) achieved automated tree isolation from imagery data in the range of 80%-90% based on ground data. However problems occur in the shadowed areas, on surfaces with low contrast [Arbeitsgruppe Forstlicher Luftbildinterpreteten 2012] or homogeneous texture and in the open plots where sunlit ground vegetation exists [Leckie et al. 2003]. These weaknesses of optical imagery can be covered by employing the LIDAR data.

From another point of view, tree isolation using only the LIDAR data has the disadvantage of poor delineation of the crown outline. Seamless integration with optical data is also important to possible savings in data acquisition and increased automation in the processing [Shan and Toth 2009]. Several methods have been proposed and implemented to overcome these challenges. To succeed in an efficient single tree extraction model, synergy of imagery and LIDAR data is suggested [Leckie et al. 2003; Heinzl et al. 2008; Wang et al. 2008], which confers the advantage of the supplementary characteristics of each method onto the other. The objective of this research is to develop an automatic approach for evaluation of canopy height models from LIDAR-based and image-based sensors in order to investigate the following arguments:

- To what extent can the digital elevation models, generated from imagery data, provide the required geometric data for single tree detection methods, in comparison to LIDAR data?
- What are the characteristics of tree height models in LIDAR and photogrammetry elevation data and how can these specifications be measured?
- Which parameters are to be considered for designing and developing automatic single tree detection methods using high density LIDAR data and high resolution aerial images?

To answer these questions, the potential and quality of airborne laser scanning and digital imagery to generate digital elevation models (DSM and DTM) needs to be evaluated. Keeping the characteristics of the datasets, challenging areas should be discussed and relevant parameters will be defined for automatic extraction of single trees. This investigation can be implemented in different levels, covering the sensor assessment up to the evaluation of the final products. In this research the focus is on the DEM products and post processing algorithms.

1.4. Structure of the research

After this introduction, the forestry terms related to airborne surveying as well as the technical characteristics and challenging aspects of imagery and LIDAR data in forest mensuration will be discussed in the next chapter. In chapter 3 the significant parameters in image-processing, affecting the relevant segmentation and classification algorithms will be indicated. Chapter 4 deals with the definition and extraction of forest features from the LIDAR-based and photogrammetric surface models. In chapter 5 the proposed methodology for characterization of the forest stand and single tree extraction is explained in detail. The experimental results of the test area are discussed in chapter 6. Finally, in chapter 7 the conclusion of the research and the outlook for future work are discussed. The references and appendices are presented in chapters 7 and 8.



2

Terms and Basics

This chapter reviews the forestry terms used in airborne surveying of single trees, followed by the basics of aerial imagery and LIDAR in this area. The state of the art, limitations and advantages of both methods are compared focusing on forestry applications.

2.1. Single tree in forest mensuration

The structure of a single tree begins at underground level, with the organs of the roots. On the ground, the tree bole connects the roots to the limbs of the tree trunk. In the upper parts the limbs are expanded into branches and twigs, forming the tree crown. This part of a tree is the most discussed area in biomass studies and can be observed by remote sensing methods. The tree crown might be covered by leaves depending on the tree type and season. The valuable limb of the tree in wood industry is, however, the tree trunk or bole, which is covered in bark. This part of the tree forms its structure to provide a support to the leaves, flowers or fruits while connecting them to the roots. In most cases it may not have leaves sticking out of it. In other plants, this connecting part is also called the stem of the plant. The term tree stem, in this research, has the same meaning as the tree trunk. The main goal of single tree delineation, using remote sensing techniques, is to extract the position of the tree stem through processing the tree crown analyses.

2.1.1. Tree height measurement

The tree height is defined as a parameter to determine the site class or site index of a stand for volume calculations [Laar and Akça 2007], which can be seen in Figure 1:

“Total tree height is defined as the distance between the top and base of the tree, measured along a perpendicular, dropped from the top.”

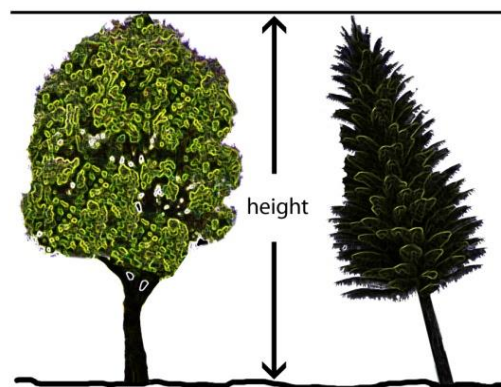


Figure 1: Tree height based on definition of [Laar and Akça 2007]

A detailed definition and comparison of the existing devices for measurement of tree height with traditional methods in forestry can be found in [Laar and Akça 2007]. In most of these methods, the measured tree height might differ, depending on the experimental skills of the forester and considering the different conditions of the forest area. Figure 2 shows one of the terrestrial methods, using a vertical scale and based on the inclination angles:

$$h = \frac{L \cdot (\tan \alpha_3 - \tan \alpha_1)}{\tan \alpha_2 - \tan \alpha_1}$$

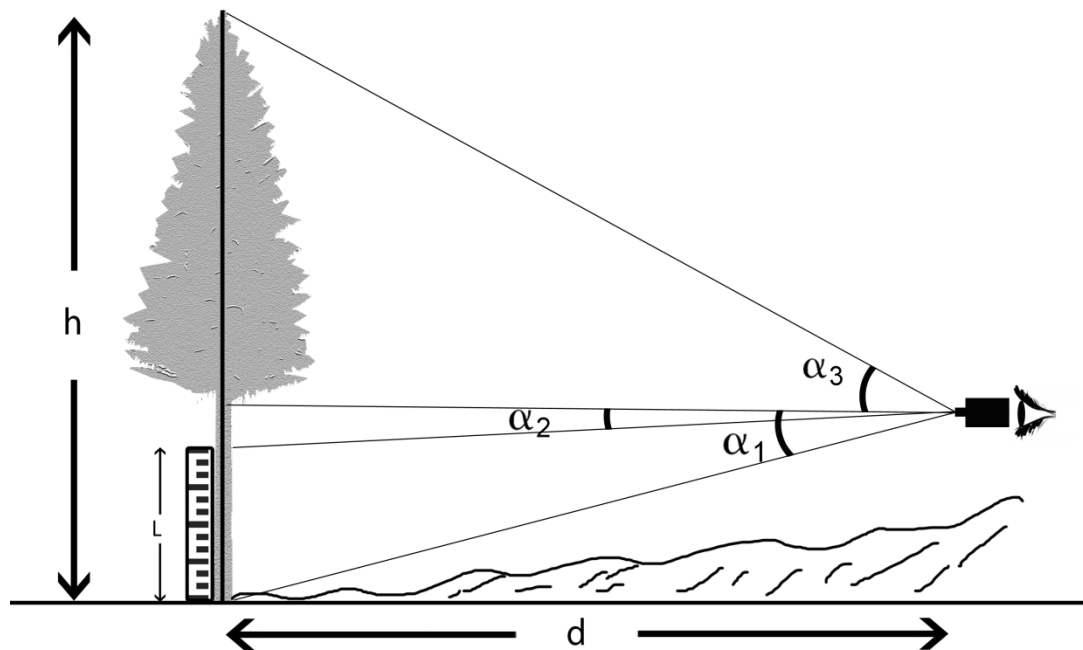


Figure 2: Measurement of height with a vertical scale

Using other terrestrial methods like Hypsometers¹, the tree height can be obtained by measuring the horizontal distance (d) and the vertical angles:

$$h = d \cdot (\tan \alpha_3 - \tan \alpha_1)$$

In the equations above, the vertical angles have positive and negative values if they are higher or lower than the horizontal level.

¹ www.forestrytools.com.au

2.1.2. Single tree parameters in forestry

Geometric demonstration of the form of a tree is based on parameters defined in forest indices. Based on these parameters, including *Diameter at Breast Height*² (*DBH*), *Crown Length* (*CL*), *Crown Width* (*CW*), and considering the height of the tree, new relational parameters can be extracted (Figure 3).

According to [von Gadow 2005] the *DBH* can be used to calculate the *Basal Area* (*BA*) of the stand as one of the most used parameters in forest mensuration.

$$BA = \frac{\pi}{4} \sum_{i=1}^n (DBH)_i^2$$

Standwise parameters, like Stand Density Index (*SDI*), are related to the amount and density of the single trees, which can be calculated by:

$$SDI = N \cdot \left(\frac{n}{d_g} \right)^{-\beta_i}$$

where N is the stem quantity per hectare, n is the amount of the stems, β is a known parameter for the related stand and d_g is the average basal area which can be calculated by:

$$d_g = \sqrt{\frac{4}{\pi} \cdot \frac{BA}{N}}$$

As can be seen in Figure 3, according to [Laar and Akça 2007], most of these parameters are related to the tree position and height. Parameters like *Crown Ratio* (*CR*), which is related to the age of the tree, can be obtained from its 3D extension.

The crown ratio is defined with a logistic function [Hasenauer and Monserud 1996] using the linear combination of input variables and estimated coefficients (x):

$$CR = \frac{1}{1 + e^{-x}}$$

² In general the breast height of the tree is 1.3m above the tree base. The parameter *DBH*, which is mostly used in stem analysis, is measured at this height of the tree.

$$\text{Crown Ratio} = \frac{\text{Crown length}}{\text{Tree Height}}$$

$$\text{Crown Form Index} = \frac{\text{Crown length}}{\text{Crown Width}}$$

$$\text{Crown Thickness Index} = \frac{\text{Crown Width}}{\text{Crown Length}}$$

$$\text{Linear Crown Index} = \frac{\text{Crown Width}}{\text{DBH}}$$

$$\text{Crown Spread Ratio} = \frac{\text{Crown Width}}{\text{Tree Height}}$$

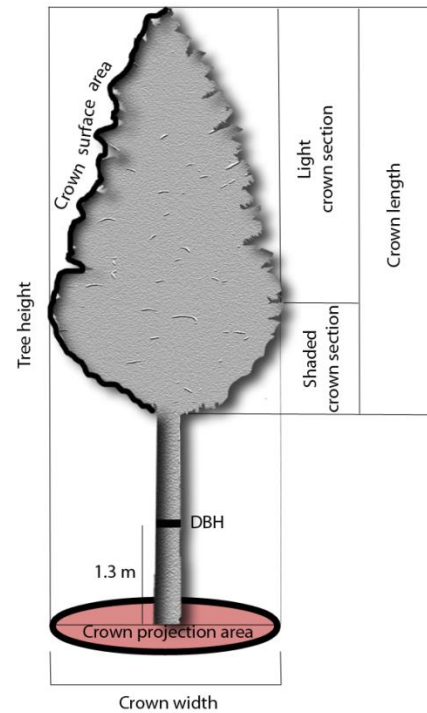


Figure 3: Forest parameters based on characteristics of the tree crown

However, in the developed models of the crown ratio, the competitive status of the subject tree should also be taken into account:

$$x = a + b \cdot \text{SIZE} + c \cdot \text{COMP} + d \cdot \text{SITE}$$

The variable $b \cdot \text{SIZE}$ can be defined as a factor of tree height and DBH, whereas the factor $d \cdot \text{SITE}$ depends on the environmental parameters like elevation above sea level, slope and azimuth of the aspect. The factor $c \cdot \text{COMP}$ represents the competition measures, calculated by the basal area per hectare of the trees which are larger in diameter than the subject trees. The crown competition factor is calculated from the crown width for open-grown trees [Hasenauer and Monserud 1996].

In the case of competition, [Holdaway 1986] defines a model with the coefficients of (b_i) extracted from:

$$CR = b_1 \cdot \left(\frac{1}{1 + b_2 G} \right) + b_3 \cdot (1 - e^{-b_4 \cdot d})$$

Assuming G is the basal area per hectare and d as the diameter of the subject tree, the coefficient b_1 estimates the CR in the case of complete absence of competition and b_2 is the rate of decrease of crown ratio in an increasing competition.

In biomass estimation, the Crown Surface Area (CSA) of the tree can be defined as the covering surface of the live crown. Representing the crown of a coniferous in a parabolic form, the crown surface can be calculated as follows [Laar and Akça 2007]:

$$CSA = \frac{\pi CW}{12 CL^2} \cdot (4CL^2 + \frac{1}{4}CW^2)^{3/2}$$

As can be seen, along with the spectral properties of the tree crown, extracting the geometric characteristics of the crown closure (CW, CR, CSA) plays an important role to define the vital parameters in forestry.

2.2. Remote sensing in forestry

Remotely sensed methods provide techniques to observe the forest area from above and extract the needed parameters in relevant applications in forestry. Preparing forest maps from aerial photographs goes back to 1887 [Hildebrandt 1969], when an airborne balloon was used as the platform for photography of forest around Berlin [Laar and Akça 2007]. Since then, forest observation from aircraft systems has been developing in platforms, sensors, optics and processing algorithms. The remote sensing of forest areas ranges from satellite imagery to airborne data acquisition systems. The potential demand for implementation of the recent technologies and processing methods for countrywide forest applications has been outlined in [Ackermann et al. 2014]. The focus of this research is on the very high resolution aerial images and laser data.

2.3. Optical imagery

The spectral reflectance of the objects in aerial images depends on the material of the object and the incident rays. Depending on the tree type, the crown surface might change its texture and color in different seasons. Geometrically, trees do not have a regular flat shape, but rather a round surface. Furthermore the crown surface is covered by leaves, needles or twigs, with different density and scattering directions. That leads to a heterogenic surface on the tree crown. Due to

these two facts, the optical reflectance of the tree crowns might change in different times, different lighting angles and different observing views.

2.3.1. Illumination condition in spectral images

For a better understanding of the influence of illumination conditions on the texture of the crown, a 3D model of a single tree was generated from a photogrammetric digital surface model. Figure 4 shows different reflectance of deciduous tree crown surface from top view. The lighting source is set artificially at the height of 45 degrees in four azimuths (0, 90, 180 and 270 degree). In this figure, the hill-shaded model shows that even with a unique texturing color (in this case gray) the texture of the surface model changes in different lighting of crown surface.

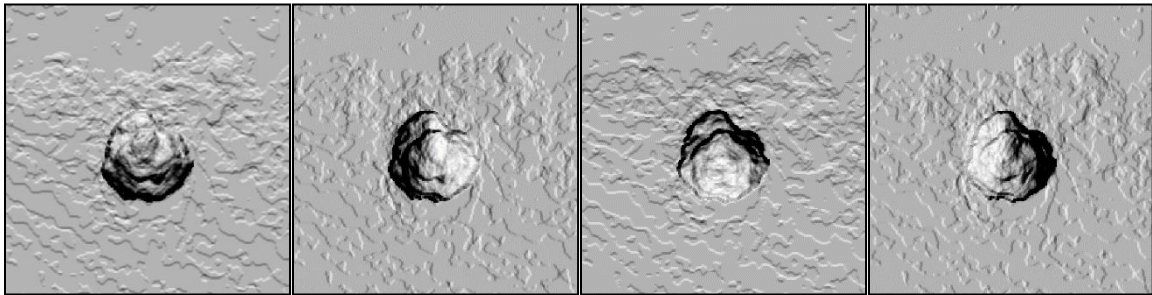


Figure 4: Artificial reflectance of the crown surface, setting the light source at a height of 45 degree and azimuth of (from left to right) 0, 90, 180 and 270 degree

A detailed optical modeling of the parameters, indicating different surface types and distribution of scattering and penetration can be found in [Larsen 1997].

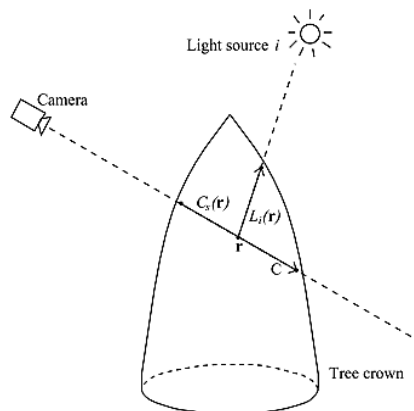


Figure 5: Illumination elements in spectral imagery of tree crown [Larsen 1997]

In the scattering model of Larsen, the passed ray of light in the direction of L through the foliage (Figure 5), which is also called the transmitted portion of light by the tree crown, can be gained by:

$$p_{tr}(L) = \exp\left(-\int_L \sum_{t \in T} f^{(t)}(\mathbf{r}) dw\right),$$

where the surface of the tree crown is modeled with $\mathbf{r} = (x, y, z)$ and the density function of $f^{(t)}(\mathbf{r}) \geq 0$, $t \in T$ refers to type and density of the tree surface. This can be calculated by:

$$p_{refl}(\mathbf{r}) = \frac{\sum_{t \in T} p_{refl}^{(t)} f^{(t)}(\mathbf{r})}{\sum_{t \in T} f^{(t)}(\mathbf{r})},$$

$$P(C) = K_{refl} \sum_{i \in lights} P_i R(i, C),$$

$$R(i, C) = \int_C \sum_{t \in T} p_{tr}(C_s(\mathbf{r})) \cdot p_{tr}(L_i(\mathbf{r})) \cdot p_{refl}(\mathbf{r}) \left(\sum_{t \in T} f^{(t)}(\mathbf{r}) \right) \left| \frac{d\mathbf{r}}{dw} \right| dw.$$

To practically demonstrate these parameters on a single tree surface, Figure 6 shows the effect of shadows on the surface model compared to the colored data. As can be seen, in multispectral images, the tree crown of a single tree, without surrounding objects is affected by the illumination condition, which changes the intensity values of the surface.

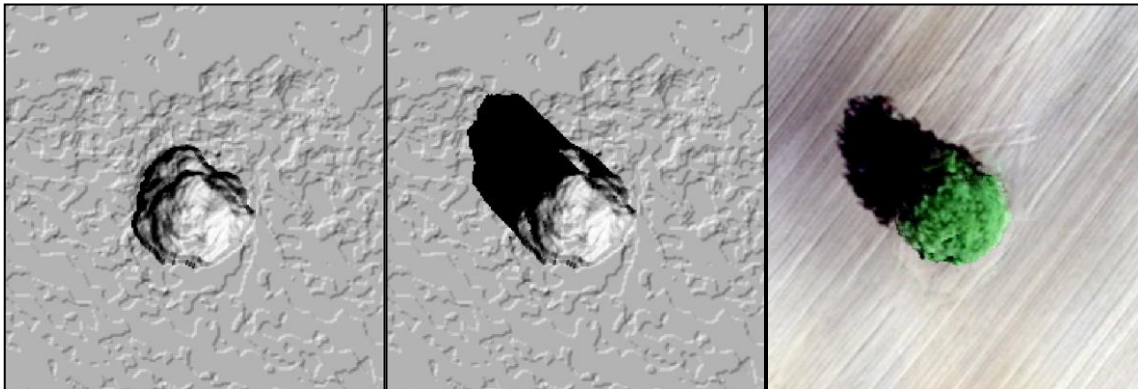


Figure 6: Different texture caused from the shadows on tree surface (left) and from the tree height on the ground (middle) and effect of the shadows on colored data (right)

The shadows in multispectral channels can be categorized in two groups. The first group is caused from the roughness of the tree surface. Such shadows affect the intensity value of the tree surface and results in heterogeneity on the texture of the tree crown. This puts the segmentation of the images in challenge. The second group of shadows resulted from the height of the tree, lead in covering the surrounding objects. This causes problems for distinguishing the crown boundary from the neighboring trees. In Figure 7, the segmentation of the single tree, affected by these two types of shadows, is represented and compared to the colored data. A multiresolution segmentation in eCognition (with scale parameter 100, shape 0.1 and compactness 0.5) is applied on shaded surfaces. Due to the additional textural information in color data, the scale parameter should be set to 1000 to gain a reasonable result. As a proper solution for removing shadows in spectral data, the vegetation indices, i.e. NDVI are applied in multispectral segmentation procedures.

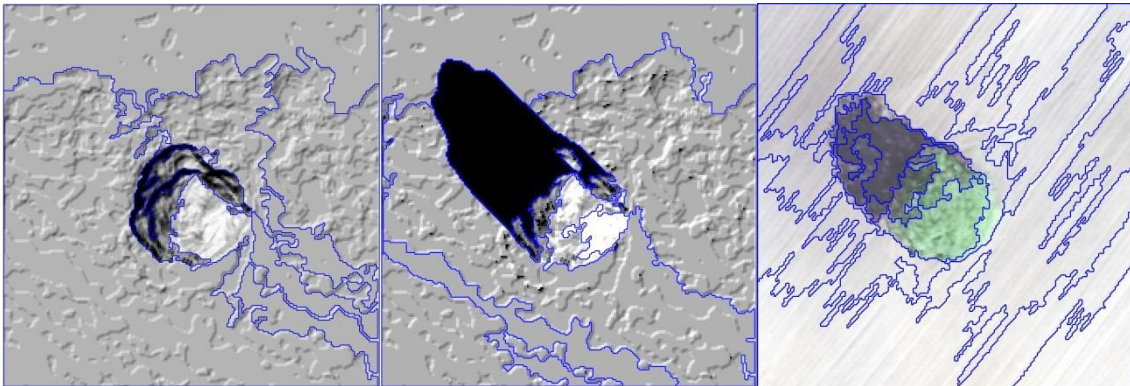


Figure 7: Multiresolution segmentation of shaded surface of a single tree with roughness shadows (left) and height shadows (middle) compared with spectral data (right).

In Figure 8 the length of the shadow caused by the height of the tree is demonstrated and can be gained by:

$$S = h / \tan(\alpha)$$

where, α is the angular altitude of the sun.

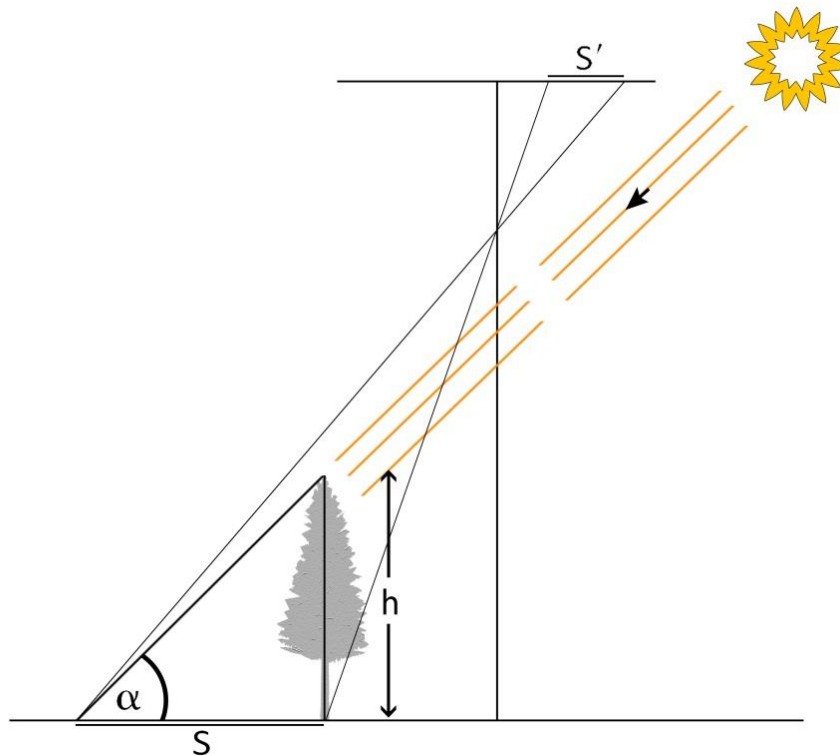


Figure 8: The length of shadows (S) in aerial images

Additional to shadows, the occluded areas are also important to be discussed. This problem, which is caused by the geometry of the data acquisition and also the shape of the object, in this case the trees, results in no data areas in digital orthophotos.

The occlusion problem is not only dependent on the tree height but also on the topography of the terrain. That means the lighting and reflectance of the trees in aerial images are also influenced by the terrain height variations. A detailed discussion about the influence of sunlight direction, topography of the ground and the geometry of the imagery on the illumination condition of the single trees can be found in [Adler 2001].

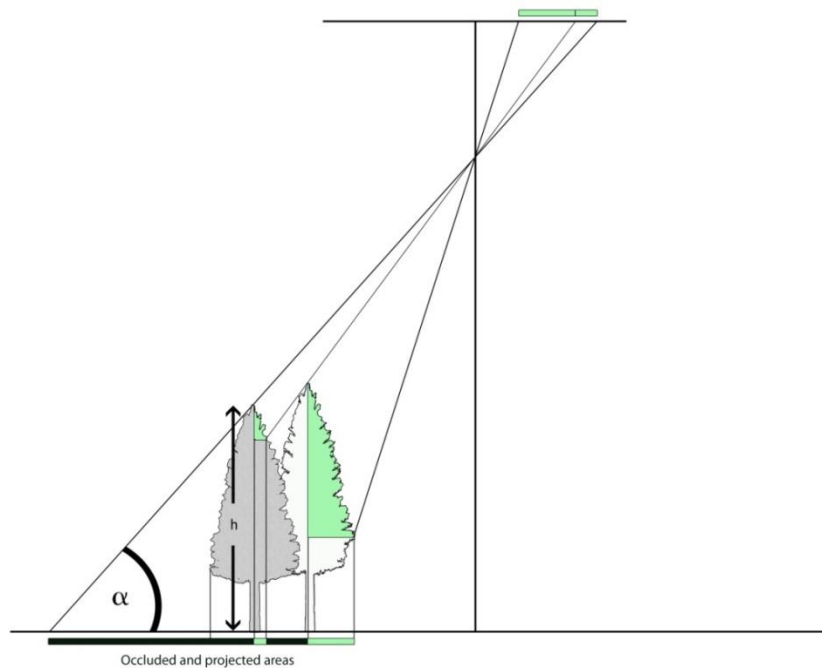


Figure 9: Occluded areas (black) and projected surface of the tree crowns (green) in aerial images

In [Larsen 1997] a geometric optical model is developed to extract the position of the single trees from aerial images with circular correlation templates. For the near-nadir parts of a stand in the image, more templates in different directions should be used. The radius of the templates varies, depending on the viewing angle, crown geometry and tree density within the stand. The image contrast is one of the decisive factors for effective recognition of the trees in this method.

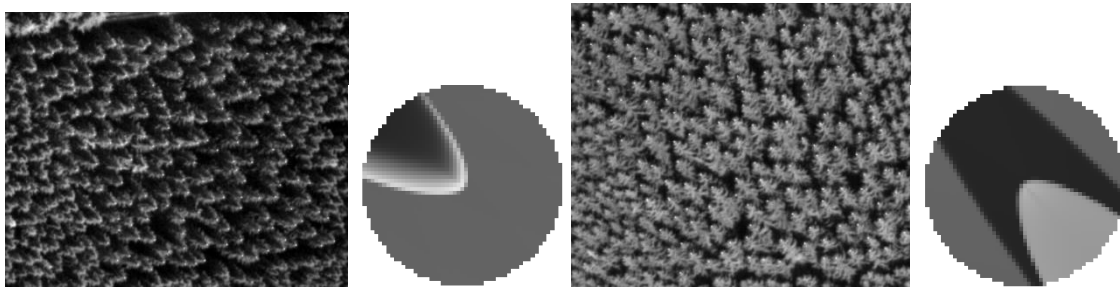


Figure 10: Different viewing angles and templates for STE from high resolution images [Larsen 1997]

In the model of Larsen, 86%-92% of the trees were found from an even-aged stand of Norway spruce with 1m distance. For the delineation of the tree regions, the little shadows on the crown boundaries are advantageous; however these ideal shadows are not always available, especially in coniferous stands.

2.3.2. Tree measurement in aerial images

The tree height can be measured, using the traditional methods in photogrammetry, by the difference of parallax in stereo images [Laar and Akça 2007] using:

$$\Delta h = \frac{h_g \cdot \Delta p}{b + \Delta p}$$

where Δh is tree height, h_g is the flight altitude above the tree base, Δp is the parallax difference of top and base of the tree and b is the base of stereo images (Figure 11). In a developed version of this formula for topographic areas, the tree heights can be calculated by [Laar and Akça 2007]:

$$\Delta h = \frac{h_0 \cdot (\Delta p_1 - \Delta p_2)}{b + \Delta p_1 + \Delta p_2 + \frac{\Delta p_1 \cdot \Delta p_2}{b}}$$

where h_0 is the flight height above the principal point of the left image, $\Delta p_1, \Delta p_2$ is the parallax difference between the base of the tree and the principal point of the left and right image respectively (Figure 11). As the element of $\frac{\Delta p_1 \cdot \Delta p_2}{b}$ is near to zero, the approximated value can be gained by:

$$\Delta h = \frac{h_0 \cdot (\Delta p_1 - \Delta p_2)}{b + \Delta p_1 + \Delta p_2}$$

For detection of the tree height from aerial images, the image resolution plays an important role. Particularly in coniferous trees, the higher the resolution, the more precise is the calculation of the height from stereo images. In the final steps, to reduce the loss of precision, a proper bit depth should be selected for the storage of height values in 2.5D raster images.

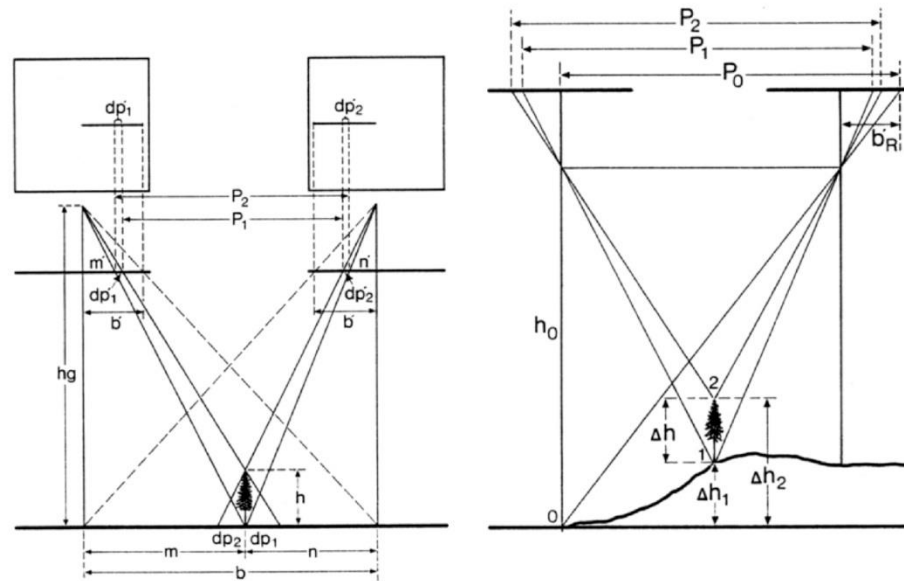


Figure 11: Stereoscopic measurement of tree height in flat (left) and topographic (right) areas (Laar and Akça, 2007)

2.4. Airborne laser scanning

The technology of laser scanning has been employed to provide a digital surface model of objects, both in terrestrial and airborne systems. The platform of an airborne laser scanner is a fixed wing aircraft or a helicopter. The principle of distance measurement with laser scanners is the measurement of the sent and received pulses of the laser beam considering the travel time of the light. The commercial Airborne Laser Scanning (ALS) systems operate at a wavelength between 800 and 1550 nanometer.

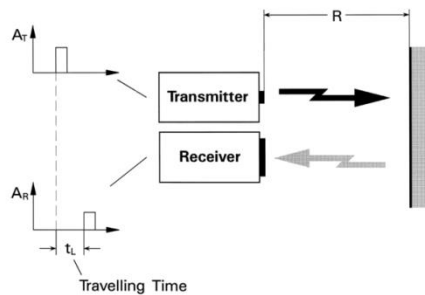


Figure 12: Transmitted (A_T) and received amplitude (A_R) in time-of-flight ranging [Wehr and Lohr 1999]

The main components of LIDAR (Light Detection And Ranging) devices consists of two components. First, the laser scanner to measure the distance to spotted points on the ground and

second the GPS/IMU units for the exact positioning and orientation of the system [Beraldin et al. 2010]. The final result of this measurement is a huge amount of points, with 3D coordinates for each, called point cloud. The density of the point cloud depends on the aircraft velocity, flight height and the scanning rate, which varies between 0.2 and 50 points/m². After timely synchronization between the measured points and the GPS/IMU data in a control unit, the point clouds will be saved in the storage unit. An operator laptop is used to set up the mission parameters and also for communicating with the control and recording unit. The preplanned flight lines are displayed for the pilot in a flight management system [Beraldin et al. 2010].

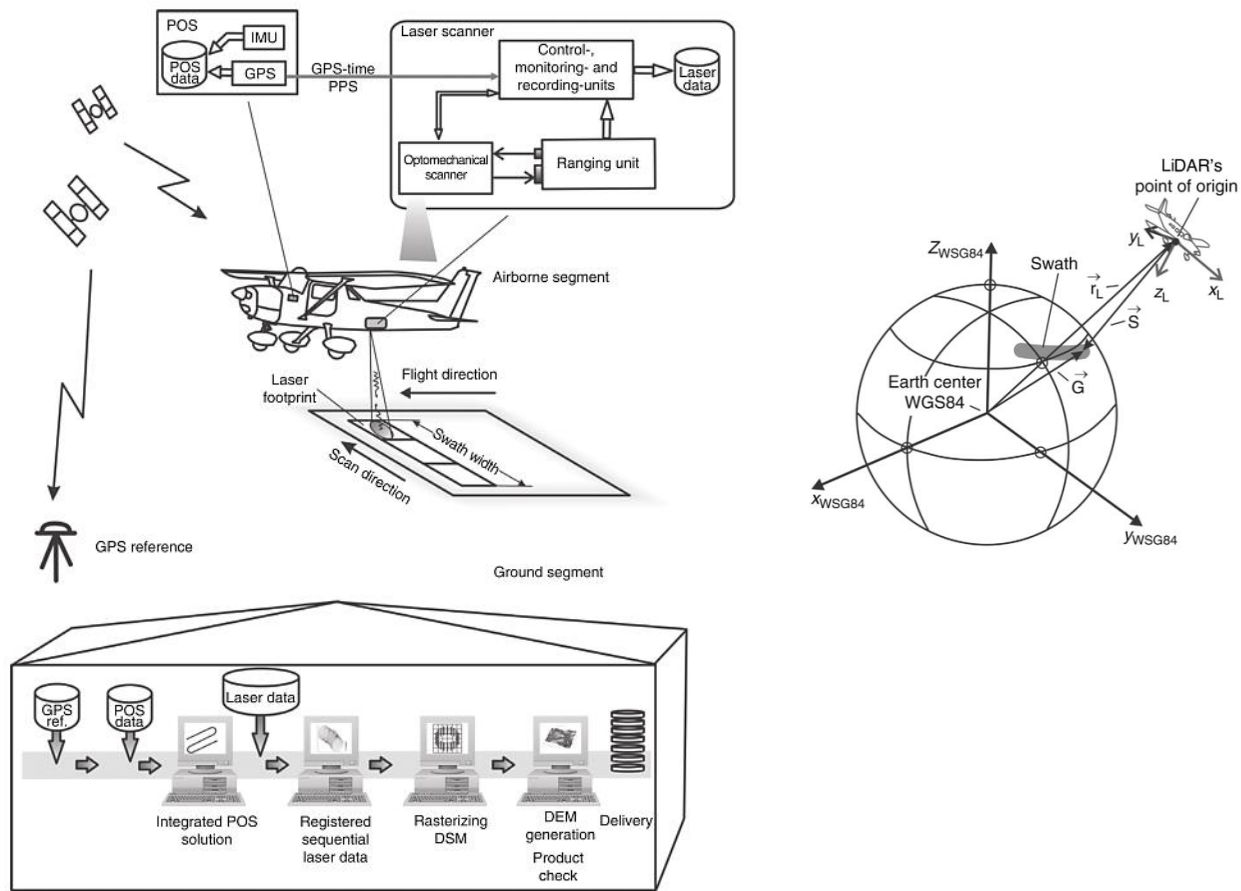


Figure 13: Left, ALS units from data acquisition to processing phases, right: Vector setup for geocoded LIDAR data [Shan and Toth 2009]

2.4.1. Ranging systems

With regard to the geometry of distance measurement, ALS systems can be classified in two types; *light transit time* and *triangulation*. In the former, the distance is calculated with

measurement of the send-receive time delay, whereas the latter calculates the distance with the triangular geometry created by the sent and the received pulses. Considering the ranging principle, the light transit time laser scanners, also known as time of flight, can be categorized in two systems of *pulse* and *phase* measurement systems, for discrete and continuous wave (CW) respectively [Shan and Toth 2009], [Beraldin et al. 2010].

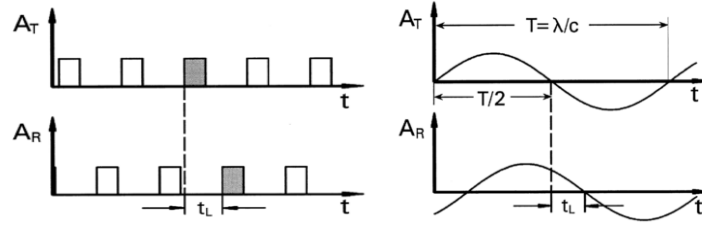


Figure 14: Measuring principle of pulse (left) and continuous waves (right) [Shan and Toth 2009]

In both systems, the ranging accuracy is affected by the signal to noise ratio (S/N) of the sensor. However the ranging resolution depends on the measuring precision of the travel time of the laser beam. Due to the principle of discrete measurement in pulse systems, the ranging resolution depends on the counting precision of the reflected and received pulses (Δt_L). However in CW systems, the measuring precision of the phase difference ($\Delta\Phi$) determines the ranging resolution. Table 1 summarizes the relative equations from [Baltsavias 1999a] and [Shan and Toth 2009] for calculation of distance, resolution and measurement precision of these two ranging techniques.

	Pulse	Continuous Wave
<i>Range:</i>	$R = \frac{1}{2}c \cdot t_L$	$R = \frac{1}{4\pi} \frac{c}{f} \cdot \Phi = \frac{1}{2}c \cdot \left(\frac{\Phi}{2\pi} T\right) = \frac{\lambda}{4\pi} \Phi$
<i>Range resolution:</i>	$\Delta R = \frac{1}{2}c \cdot \Delta t_L$	$\Delta R = \frac{\lambda}{4\pi} \Delta\Phi$
<i>Range precision:</i>	$\sigma_{R_{pulse}} \sim \frac{c}{2} \cdot t_{rise} \frac{\sqrt{B_{pulse}}}{P_{R_{peak}}}$	$\sigma_{R_{cw}} \sim \frac{\lambda_{short}}{4\pi} \cdot \frac{\sqrt{B_{cw}}}{P_{R_{av}}}$

Table 1: Comparison of ranging methods in ALS systems

In [Wehr and Lohr 1999] typical reflectivity of various diffuse reflecting materials for 900 nm wavelength are provided. Recently, the Full-Wave-Form (FWF) analyses of LIDAR data opens new aspects in recognition of the object types, based on the form of the backed pulses.

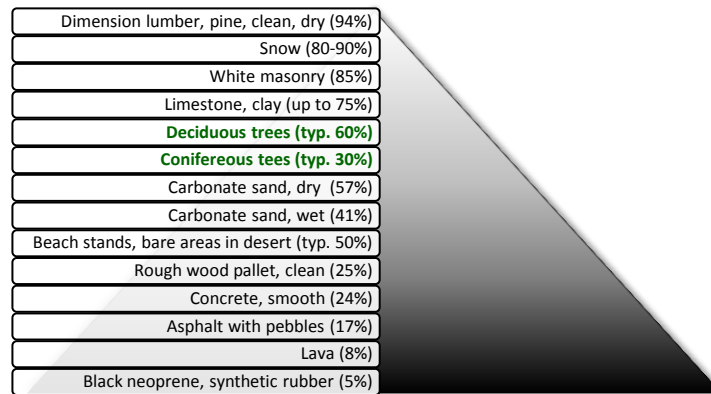


Figure 15: Typical reflectivity of deciduous and coniferous trees (in percent) in comparison with various diffuse materials for 900nm wavelength (values from Wehr and Lohr, 1999).

To reach the optimized detection of the objects on the earth, the laser wavelength will be suited to the reflectivity of the object surface. As limitations, two factors of flight height and eye-safety of the laser beam should be specifically taken into account. An approximate equation for calculating the relation between transmitted (P_T) and received power (P_r) can be found in [Baltsavias 1999a]:

$$P_r = \rho \frac{M^2 \cdot A_r}{\pi R^2} \cdot P_T$$

where R is the range, ρ/π is an assumed Lambertian Bidirectional Reflectance Distribution Function (BRDF), A_r is the receiver area and M is the atmospheric transmission.

This equation shows that, to obtain a predefined power in the receiver for a specific canopy type and atmospheric condition, the transmitted power should be increased in higher scanning flights. However, due to the eye-safety limitations during laser scanning projects, the amplitude of laser power should be controlled. This limitation is mostly of concern in urban areas, though is not a problematic issue in forests. The advantage of laser scanners as active sensors, and the better reflectance results during night, opens the possibility of data acquisition with higher laser power in forests to achieve better quality of intensity values. According to [Baltsavias 1999a] the minimum detectable object within the laser footprint, depends largely on its reflectivity and not on the object size.

In addition to the atmospheric conditions and the parameters related to data acquisition procedure (as well as range, laser power, wavelength, laser aperture, detector sensitivity and noise level), the parameters caused from the object side like background irradiation, type of target reflectivity (defuse, specular or both), inclination and the 3D structure of the object surface, can influence the detection procedure of the object.

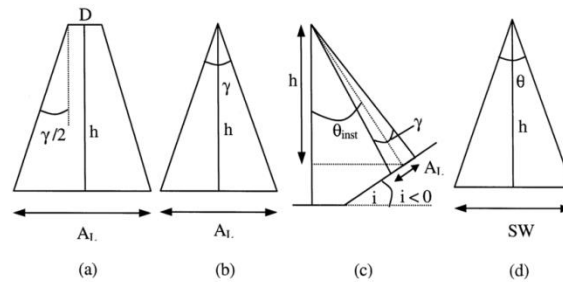


Figure 16: Footprint (a, b, c) and swath width (d) in scanning geometry [Baltsavias 1999a]

From the point of view of scanning geometry, the mentioned parameters might be affected regarding the position and the orientation of the single trees in scanning corridors. Furthermore the stand density and the surface type of the tree foliage influence the quality and quantity of the acquired point clouds. As the laser scanners are active sensors, the direction of the light source (sender) and the viewing direction of the imaging sensor (receiver) are almost the same. In this case the term shadow (the not illuminated areas) has the similar meaning to the occlusion (areas with obstacle in the viewing direction) in photogrammetric imagery.

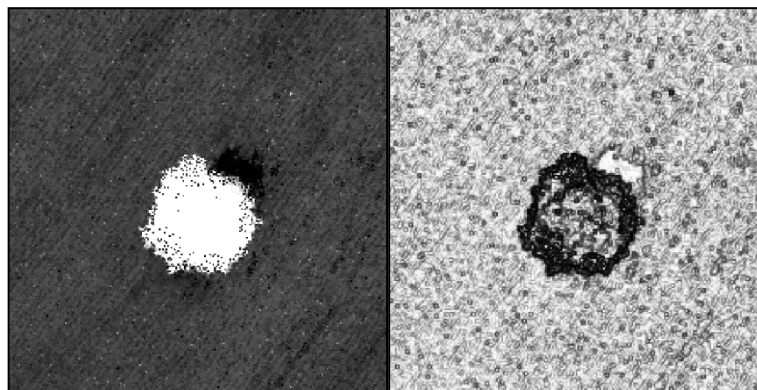


Figure 17: nDSM of a single tree from LIDAR data (left) and the shaded model of the point cloud (right). The lack of data at the occluded area shows where the laser beam could not reach the ground.

2.4.2. Noise

As mentioned in section 3.2, segmentation of laser data in forest areas suffers from noise. The sources of the fluctuations on the Canopy Height Models (CHM) can be seen from two aspects; *sensor-dependent* or *object-dependent*. The former group of noises is caused from the wrong signals achieved or recorded by the sensor. This stems from the problems in sensor or backed pulses from the flying objects in the scanning direction [Shan and Toth 2009]. The second source of fluctuated points is the complex form of the tree crown. As laser beams can penetrate through the crown closure, the crown shape will contain some points under the tree crown surface and even on the ground. Such points remain even in the calculation of the nDSM. To overcome this problem, an advanced filter is needed, in which the problematic points will be first detected and then replaced with new values, calculated from the neighboring pixels. This should allow filtering of the crown closure without changing the crown shape. A comparison of neighborhood filters and a novel filtering method will be discussed in section 5.2.1.

2.5. LIDAR-based and image-based elevation data

As two basic and rich sources of detailed geospatial information in forest inventory, characteristics of photogrammetry and LIDAR have been issued and compared to a large extent in the literature [Baltasvias 1999b]. Airborne laser scanning showed its efficiency in forest mensuration in various algorithms and methods [Hyypä et al. 2004]. Along with the LIDAR sensors, in recent decades, generation of digital elevation models from high resolution aerial images has been improving with respect to rapid developments in sensors and automatic matching algorithms [Haala and Wolff 2009], [Lemaire 2008], [DeVenecia et al. 2007]. However in optical imagery, the 3D measurement of the canopy surface models fronts with the challenges in stereo analysis and matching algorithms. A comparison of laser-based and image-based methods for acquiring the geospatial data in this area is discussed in [Miri et al. 2013]. Contrary to the laser data³, the advantage of aerial images rests on their spectral and textural contents. Such

³ The current commercial laser scanners use mostly only one laser beam in a definite range of infrared wavelengths. Multi spectral lidar systems are developed to send multiple infrared laser beams to the canopies to extract more textural information from the forest surface. An exploration about a multi spectral canopy lidar system tested on different ages of single trees is provided by the school of Geo-Sciences at university of Edinburgh (www.geos.ed.ac.uk).

information is mostly used for delineation of tree species. Table 2 shows an overview of the strength and weaknesses of both data acquisition methods in extracting geospatial attributes in forestry.

Capabilities and Potentials	ALS	Imagery
Direct measurement of the surface	✓	✗
Textural contents	!	✓
DSM generation	✓	✓
DTM generation in dense forests (or in leafy season)	✓	!
DTM generation in sparse forests (or leafless season)	✓	✓
Independence from illumination conditions	✓	✗
Costs for repeatable measurement	✗	✓
Independence from texture of the object	✓	✗
Spectral information	!	✓

Table 2: Comparison of laser-based and image-based data potential for forestry applications (potential level: ✓ high; ! medium; ✗ low) [Miri et al. 2013].

Comparing these two sensors, the ALS data seem preferable to generate the digital elevation models of canopies. However, high costs of lidar projects, on the one hand, and the richness of information in image-based methods are the main reasons for the great interest in employing image-based technologies in forest mensuration.

Due to the variations in terrain elevation, the DSM of the forest does not show the height variations of the trees. To eliminate the influence of the elevation changes on the ground, the normalized Digital Surface Model (nDSM), which is also called Canopy Height Model (CHM), can be calculated by subtracting the DTM from DSM. This shows the significance of both DTM and DSM data for more detailed information on individual trees. As a remarkable advantage, the capability of ALS data in capturing both surface models has been proven. Laser-based Digital Terrain Models (DTM) in the leafless seasons, can be used as a reference ground surface for generation of nDSM, because over time the terrain surface remains more unchanged than the crown surface [Miri et al. 2013].

On the other side, image-based techniques, based on stereo matching algorithms like Semi Global Matching [Hirschmuller 2005], provide confidential results in DSM generation of forests. Due to the fact that the repetition rate of statewide coverage with airborne imagery is performed every 2-3 years, these data represent a cost-efficient potential for forest monitoring. The complication in aerial imagery to reach the ground surface under the canopy, particularly in deciduous stands during leaved seasons is counted as a limitation of this method.

To investigate whether or to what extent the image-based digital surface models fulfill the forestry requests, both laser-based and image-based DSM data are evaluated in [Miri et al. 2013]. This evaluation was performed over closed mixed forests in NRW province, Germany. For the image-based DSM, two sets of aerial images captured by UltraCam XP (Microsoft) with 8cm and 20cm GSD of the forest area in Hoppengarten are compared.



Figure 18: True-orthophoto of the test area Hoppengarten [Miri et al. 2013]

For a better comparison of the tree forms in image-based and laser-based datasets, digital surface models are demonstrated in Figure 19. Although the laser data is filtered and free of noise and flying points, because of the measuring characteristics of laser scanners and the roughness of the tree surfaces, the DSM is represented as relatively heterogeneous. As can be seen, the SGM method, also results in an appropriate representation of the canopy surface, though with smoother surfaces, especially in 20cm resolution.

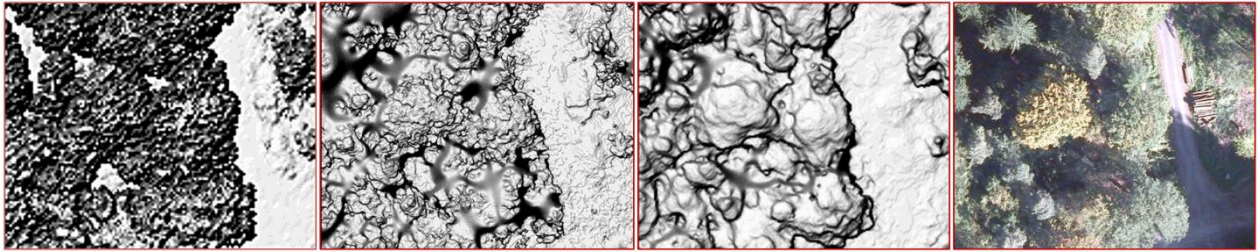


Figure 19: Test area Hoppengarten; DSM Laser 40cm, photogrammetric DSM 8cm and 20cm, RGB 8cm [Miri et al. 2013]

A comparison between the image-based and laser-based DSM is carried out on the 8cm and 20cm images in this area. To provide an independent reference dataset, the LIDAR data of this area is used. Both image-based DSM are subtracted separately from the DSM of LIDAR data. The differentiated images (Figure 20) demonstrate well-fitted results (green colors) on the ground and also at the highest levels of canopy elevation in both resolutions. The interpolated areas, mostly shows in blue colors, confirm the well-known problems of stereo matching algorithms in shadowed and occluded areas. This comparison shows that, although in many cases an increase in spatial resolution of aerial images leads to more detailed DSM, the outcome is not necessarily a better surface model. The red areas, which can be found for the most part along the outer boundary of stands, are assumed as matching faults. In this case the height value of laser data is more than the image-based DSM. The blue areas are mostly the no data areas where, after interpolation, the image-based DSM has more value. Occlusion, complexity of the texture on the trees, different representation of trees in overlapping areas of stereo images and inappropriate illumination conditions can be regarded as problematic aspects stemming from the object space (tree crowns) and the geometry of the imagery (see section 2.3), which influence the performance of matching algorithms.

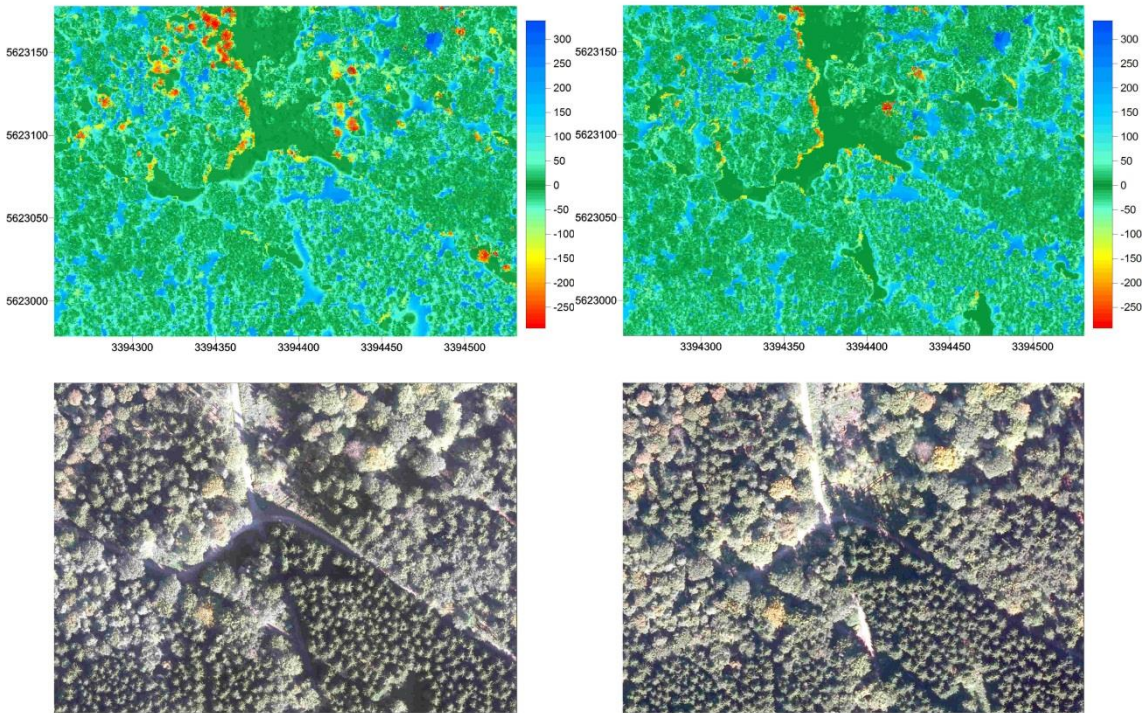


Figure 20: Top: difference images with colorized height differences in decimeter; $DSM_image_8cm - DSM_LIDAR_40cm$ (left), $DSM_image_20cm - DSM_LIDAR_40cm$ (right). Bottom: True orthophotos 8cm (left) and 20cm (right)[Miri et al. 2013].

For further evaluations on the second test area, the photogrammetric images with 20cm resolution have been used. This dataset is representative as a standard data type, which can be provided using SGM or other similar matching algorithms.

In the second test area (description in chapter 6) some single trees were not detected in the image-based DSM (Figure 21). The absence of these trees, which is checked with LIDAR data (the blue points in the differentiated image) and also compared to existing shadows of them in the orthophoto of the same processed images, occurs mostly in open areas.

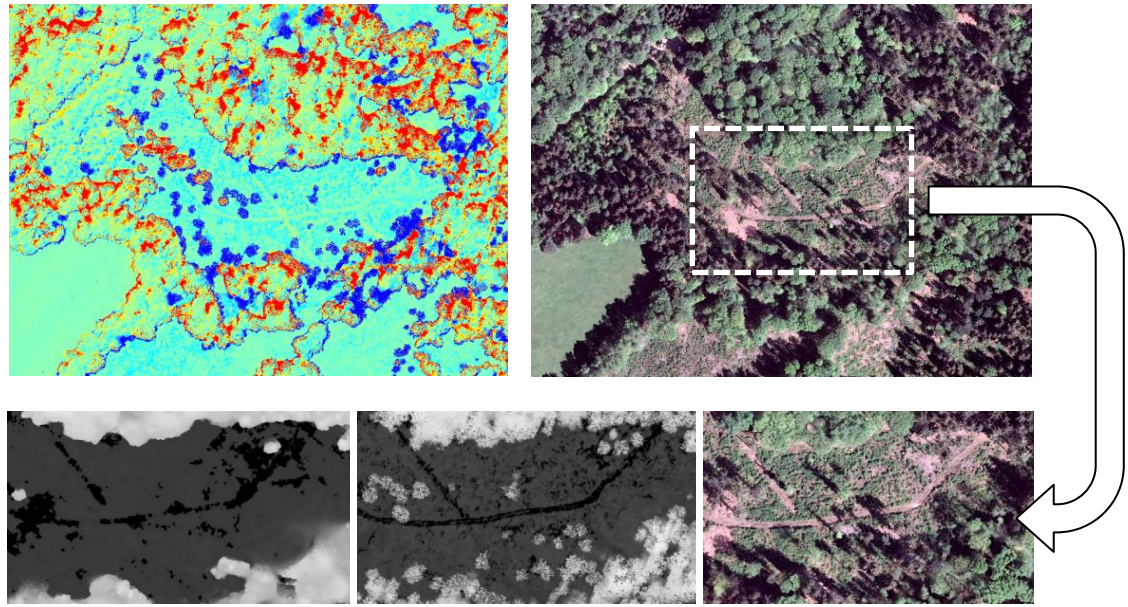


Figure 21: Existence of single trees in clearing areas: left and right; the existence of the trees through their shadows in the true-orthophoto and laser-based DSM, middle; the lack of the trees in image-based DSM.



3

Image Processing

In this chapter, the basis for image-processing and remote sensing in single tree extraction will be reviewed.

3.1. Pixel-based vs. object-oriented image analysis

In the classical definition of image classification, pixel based image analysis is based on both supervised and unsupervised methods, where the textural content of the images is used as the main criteria to delineate the objects of interest. Before classifying the image objects, the texture-based criteria are used for segmentation algorithms (see section 3.3). In other words, in pixel-based approaches, it is the texture of the image that defines the homogeneity criteria based on gray level values. The approach of *Object Based Image Analysis* (OBIA) facilitates spatially relevant management issues in a more intelligent way by exploiting the geospatial information from the Very High Spatial Resolution (VHSR) data [Lang 2008]. In contrast to pixel-based image analysis, in OBIA, it is possible to insert some additional properties or features to influence the segmentation process.

To achieve more intelligence in image interpretation of the geospatial based monitoring of the objects, the machine vision techniques should approach the ultimate goal of human comprehension. Since the last decade, the OBIA could bridge the gap between the image analysis software (as the producer of the geospatial information) and the geospatial information systems (as the analyzer of such information) via integrating different processing techniques. To solve the problem of complexity of the data, Lang (2008) explains the efficiency of the image analysis methods, considering the *intelligence* facets, as the way of:

“... supervised delineation and categorization of spatial units, how implicit knowledge or experience is integrated and the degree, in which the output are contributing to an increase of knowledge and understanding of complex scene contents...”

In [Baatz et al. 2008] an advanced approach of OBIA is discussed, which is called *Object-Oriented Image Analysis*. The main idea in this context is the fact that the objects are not only used as information carriers but are modeled as moving from object primitives to the final stage of analysis with continuous extraction and accumulation of expert knowledge. This can be structured in modular and fractal procedures.

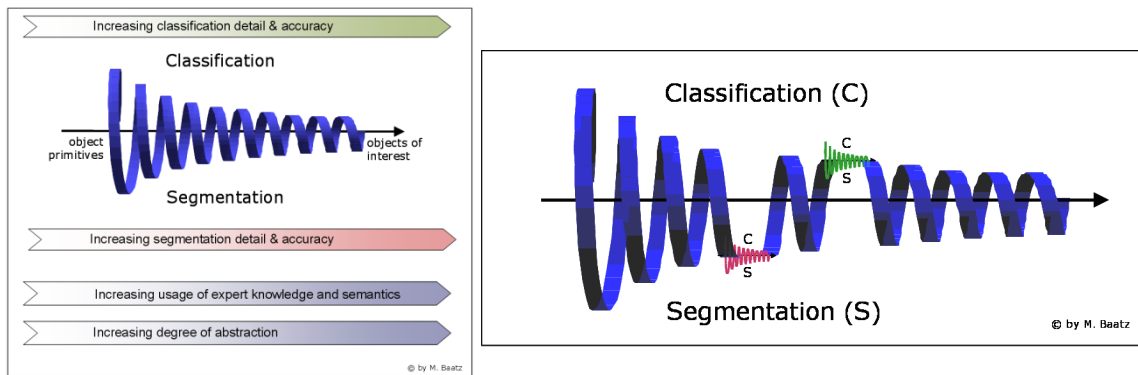


Figure 22: The generic procedure of object-oriented image analysis (left) and the fractal approach of segmentation and classification in a workflow [Baatz et al. 2008]

To design such procedures, a workflow designed from some rules containing definite parameters can be set. In object-oriented approaches these workflows are also known as *rule-sets*. A simple example of a fractal workflow for the case of single tree delineation is demonstrated in Baatz et al., 2008, implementing basic segmentation⁴ and classification methods. In general, isolating the objects of interest (single trees) can be performed in two classification ways. In the first method, the focus is on extracting the objects which contain the candidates (called *tree areas*). Whereas in the second way, declassification of the other objects, where the existence probability of the target objects are at the lowest degree (called not tree areas) is the main task. In this research, integration of these two approaches will be implemented and evaluated.

3.2. Scale-space

Extracting the objects from the image data needs to work in an appropriate scale space. To extract the single trees from airborne datasets, an appropriate scale relating to the required level of detail (LOD) should be defined. In [Straub 2003], the problem of scale is indicated as a “*chicken and egg*” issue which means a trade-off problem. In general the problem of scale space can be discussed from two different points of view. In the first aspect, called *data-based*, the scale can be defined based on the level of detail of the dataset, which is interpreted as the geometric and spectral resolution of the image. In the 2.5D height data, the pixel size defines the LOD of the dataset in XY plane, whereas the radiometric resolution of gray levels demonstrates the

⁴ The term segmentation is defined in Baatz et al., 2008 as all the procedures, those build, modify, grow, merge, cut or shrink objects. See section 3.3 for more explanation about segmentation algorithms.

geometric precision in the 3rd dimension. In the case of LIDAR, the relevant parameters affecting the resolution include the flight altitude, velocity and scan rate. For photogrammetric imagery the flight height, the base/height ratio, sensor size and bit depth of the spectral channels play significant roles in precision of final DSM data.

The other aspect for the definition of the scale space can be followed in post processing steps. How the dataset is stored, filtered or smoothed, which template size should be set in template-matching algorithms and what type of segmentation is used, are the main issues in the so called *process-based* approaches.

One solution for the problem of the scale space is to work in multiple scale-spaces. Two of the earliest methods of multi-scale representation of an image are the *3.3quad-tree partitioning* (see section 3.4) and the *pyramid space definition* [Lindeberg 1993]. Using pyramid layers, the image is calculated and saved in different levels of detail from coarse resolution to fine. The advantage of scale-space representation in the pyramid spaces is the rapid calculation and demonstration of the image elements, which plays an important role in saving the computational memory. In segmentation methods, it is possible to provide such pyramids using similar methods like chess-board segmentation, where each segment is a square with the calculated size from the required resolution.

Defining $f : \mathbb{R}^N \rightarrow \mathbb{R}$ as a function for representing any signal and $t \in \mathbb{R}^+$, the linear form of scale-space representation of $L(x, t) : \mathbb{R}^N \times \mathbb{R}^+ \rightarrow \mathbb{R}$ in [Lindeberg 1994] is constructed as follows:

$$L(x, t) = g(x, t) \cdot f$$

where $g(x, t)$ is the Gaussian kernel:

$$g(x, t) = \frac{1}{(2\pi t)^{N/2}} e^{-\sum_{i=1}^N x_i^2 / (2t)} \quad , \quad x_i \in \mathbb{R}$$

The standard deviation of the kernel $g(x, t)$ can be calculated by the root of the scale parameter:

$$\sigma = \sqrt{t}$$

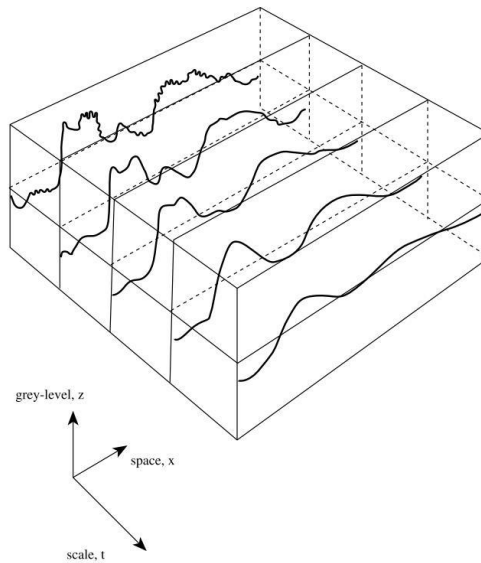


Figure 23: Schematic 3D demonstration of the scale-space representation of a 1D signal [Lindeberg 1993]

In 2.5D height images, Persson et al., (2002) attempts to define an appropriate scale space by smoothing the tree canopy with a 2D Gaussian filter in the way that each single tree has a single height maximum.

$$G(x, y) = \frac{1}{\sqrt{2\pi}\sigma} e^{-\frac{x^2+y^2}{2\sigma^2}}$$

For this, the smoothing operation σ was set in three steps from fine to coarse level with values of $4/\pi$, $6/\pi$ and $8/\pi$. Thereafter, the tree positions are searched by finding the local maxima followed by a region growing algorithm to define the crown boundaries.

Generally, the scale-space representation models can be equivalently defined in the form of diffusion equation:

$$\partial_t L = \frac{1}{2} \sum_{i=1}^N \partial_{x_i^2} L$$

This form is the well-known physical equation of heat distribution over time t in a homogeneous medium with uniform conductivity [Lindeberg 1994].

3.3. Segmentation

Different definitions of the term segmentation can be found in the literature. In general, segmentation is the process of isolating objects of interest from the background (not relevant areas) based on partitioning the image into disjoint regions, called segments. After segmentation, each region is a homogeneous area with respect to some criteria such as gray value or texture [Roerdink and Meijster 2001],[Wah 2008]. In other words, a segmented image contains regions, which totally cover the entire image and are separated via specific criteria.

Since in OBIA approaches, the image segmentation is the customary technique to extract the primitive units, image segments are mostly equated to image objects [Castilla and Hay 2008]. To obtain proper image objects, subdivision of an image varying from pixel level to larger segments (the whole image as the maximum segment size) is required. Due to different textural characteristics of objects in different images, it is not possible to define a unique segmentation algorithm for all image types. However, knowledge about the specificities of the objects of interest leads us to design the appropriate rule-set for this.

3.3.1. Edge-based and region-based segmentation

Based on the concepts of following the discontinuity or homogeneity properties of the image, the basic segmentation algorithms can be categorized in two types of *edge-based* or *region-based* methods [Hanbury 2008]. Considering the homogeneity criteria, the region-based methods partition the image by *region growing* (adding homogeneous pixels to a region) or *region splitting* (splitting the heterogeneous pixels that cannot satisfy the criteria). In advanced cases a combined method called *region splitting and merging* will be implemented. In region-based segmentation, the homogeneity value of each region will be evaluated, which is highly dependent on the imaging conditions and the characteristics of the objects of interest. In contrast, the edge-based methods focus on separating the image by finding the borders of the image objects.

3.3.2. Watershed transformation

In image-processing, watershed transformation is a method of image segmentation, which is based on the combination of region-based and edge-based aspects [Wah 2008]. Recently, this method has been used in single tree delineation of both coniferous and deciduous stands with

combination of height data and spectral channels [Bayer et al. 2013]. The first attempts on implementation of the watershed contours in morphological analysis of images dates from the late 1970s by [Beucher and Lantuéjoul 1979] which is improved in the last decades for image partitioning algorithms [Vincent 1992; Vincent and Soille 1991; Roerdink and Meijster 2001; Wah 2008]. In practice, watersheds are one of the classical objects in topography [Vincent and Soille 1991]. A drop of water falling on the sides of watershed lines (like mountain ridges) flows down until it reaches a flat area, a river or other body of water. The water drops gather to shape the catchment *basins* like lakes. In image segmentation approaches, a gray scale image is assumed as topographical reliefs, where the gray value of each pixel stands for its height value. Contrary to topography, in the case of single tree delineation, this algorithm should be implemented on the inverted image of canopy height model, where the catchment-basins are the tree tops and the separating lines (watersheds) represent the crown segments.

As can be seen in Figure 24, the concept of this method is to grow the regions around the local minima of an image until they reach the ridges in the grayscale values. The boundary of the image partitions are based on these extracted ridge lines. As well as the region-based techniques, this method can also be implemented in hierarchical levels of homogeneity. The difference between split and merge hierarchy and watershed hierarchy is the starting point. In region growing methods the starting points, called seed points, should be previously specified, whereas in watershed transformation the starting points are the local minima of the gray scale.

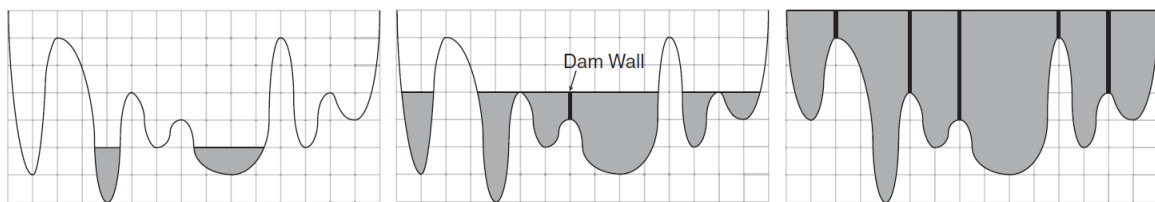


Figure 24: Different phases of watershed segmentation by flooding on the landscape. The segment boundaries are demonstrated with thick lines [Wah 2008]

A detailed explanation of watershed transformation can be found in [Vincent 1992; Vincent and Soille 1991; Roerdink and Meijster 2001; Wah 2008]. In 2D space with domain of $D \in \mathbb{Z}^2$, assume the gray scale image f as an element in the differentiable continuous space; $f \in C(D)$.

The *Topographical Distance* between points p and q inside D is defined by the infimum⁵ of the path γ on the surface S as followed:

$$T_f(p, q) = \inf \int_{\gamma} \|\nabla f(\gamma(s))\| ds$$

For this image, which has the minima $\{m_k\}, k \in I$ for some index set I , the Catchment Basins $CB(m_i)$ can be defined by:

$$CB(m_i) = \{x \in D \mid \forall j \in I \setminus \{i\} : f(m_i) + T_f(x, m_i) < f(m_j) + T_f(x, m_j)\}$$

The catchment basins are the sets of points $x \in D$ which are topographically closer to m_i than to any other regional minimum m_j . Based on these two preliminaries, the watershed transform of f , represented in [Roerdink and Meijster 2001] can be defined by a set of points which belong to the complement of the catchment basins:

$$W(f) = D \cap \left(\bigcup_{i \in I} CB(m_i) \right)^c$$

In other words, the segment lines are the connected points, which do not belong to any catchment basins.

The challenging aspect in watershed transformation is controlling the partitioning stages of the image. A solution in this case is the hierarchical partitioning of the image by synchronous flooding using depth parameters. In this case, the first basins, which could be connected by depth 1, obtain the weighting value of 1. At the next flooding depth (e.g. gray scale or height depth value) there is no new connection in basins, whereas in depth 3, new basins could join each other. The new connection gets the depth value of 3. This process goes on until all image pixels are filled. The joining vertices (in 2D) or the ridge lines (in 3D) show the dams or segment boundaries.

⁵In mathematics, *infimum* is the greatest lower bound of a set S , defined as a quantity m such that no member of the set is less than m , but if ε is any positive quantity, however small, there is always one member that is less than $m + \varepsilon$. (<http://mathworld.wolfram.com/Infimum.html>)

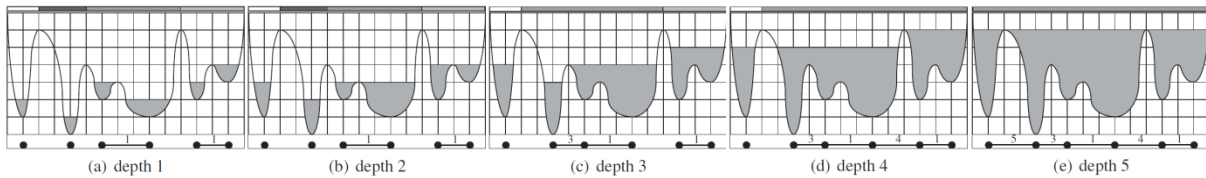


Figure 25: Construction of a partition hierarchy by synchronous flooding using depth function. On top of each diagram, the separated segment values caused from connection weights of depth are demonstrated in different gray values [Wah 2008]

This progress shows the high dependence of watershed transformation on the image resolution and the bit depth of the image. Furthermore the contrast and the complexity of the object contours in the image play a decisive role in this segmentation method. For manmade objects where the image contours on the object have a significant contrast to each other, this method is recommended. However for natural objects, specifically for trees, where the separating contours are not even visually easy to detect, this method leads to oversegmentation in image partitioning. The specific characteristic of watershed transformation is that this method works only in the image space and not in feature space and is independent of the scale space [Straub and Heipke 2007].

In the discrete case, the watershed transformation confronts the problem of plateaus, i.e. regions with constant or non-minimum gray value [Roerdink and Meijster 2001]. In this situation the falling drop might not find the appropriate steepest path to the basins. This can be solved by calculation of the vectors called *Skeleton by Influence of Zones (SKIZ)*. For this, the cheapest distance function will be calculated [Meyer 2001; Vincent 1992]. Schardt et al. (2002) and based on [Roerdink and Meijster 2001] a lower completion algorithm should be applied to convert such plateaus into hills, leading the drops to the next lower neighbor pixel. A detailed review of different watershed transformation algorithms can be found in [Najman and Couprie 2003].

3.3.3. Object-oriented segmentation of single trees

Choosing appropriate segmentation algorithm is one of the challenging aspects in object based image-processing, because it significantly influences the scale-space representation of the scene. In this way, the characteristics of some common algorithms in object-oriented image-processing will be reviewed in the following. To gain a better understanding, each algorithm will be implemented on image-based and laser-based canopy height models of a single tree using the

eCognition software. Note that, the RGB channels from true-orthophotos are also demonstrated in the background; however, they are not implemented in the segmentation procedures.

Chessboard segmentation

One method of changing the scale-space is to change the unit of the detail (pixel size) in the image space. Subdividing an image (or image object) into equally square parts (grids) can be performed with chess-board segmentation [eCognition 2013]. In this method of segmentation the pixel values or the image texture are not taken into account. The grid size defines the extend to which the information should be detailed in the image object space, while the pixel-based properties are still saved in the new cells. Figure 26 shows the segmentation of an image-based nDSM with 20cm pixel size, segmented in grids of 10 pixels each (2m grid size). This segmentation method is usually used as the first step, before any other segmentation step, to define the level of resolution pyramid at which we are working. This varies from pixel size (smallest object size in an image) to larger grid sizes (the largest size is the whole image).

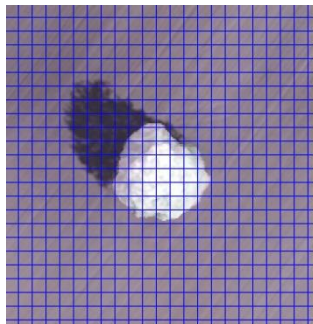


Figure 26: Chess-board segmentation of an image-based nDSM with grid size of 10 pixel (2m)

Quad-tree segmentation

In this method, the scene will be divided into square objects with sides of power two, varying from the pixel size to the maximum square object of $2^k \times 2^k$ for some $k \in \mathbb{Z}$. Quad-tree segmentation is one of the earliest types of multi-scale representation of image data (Klinger, 1974 in Lindeberg, 1994). In the first step, the scene will be divided into four objects and if the segment value does not exceed the threshold, the subdivision process will be continued. The threshold can be based on the defined measure e.g. mean value or standard deviation.

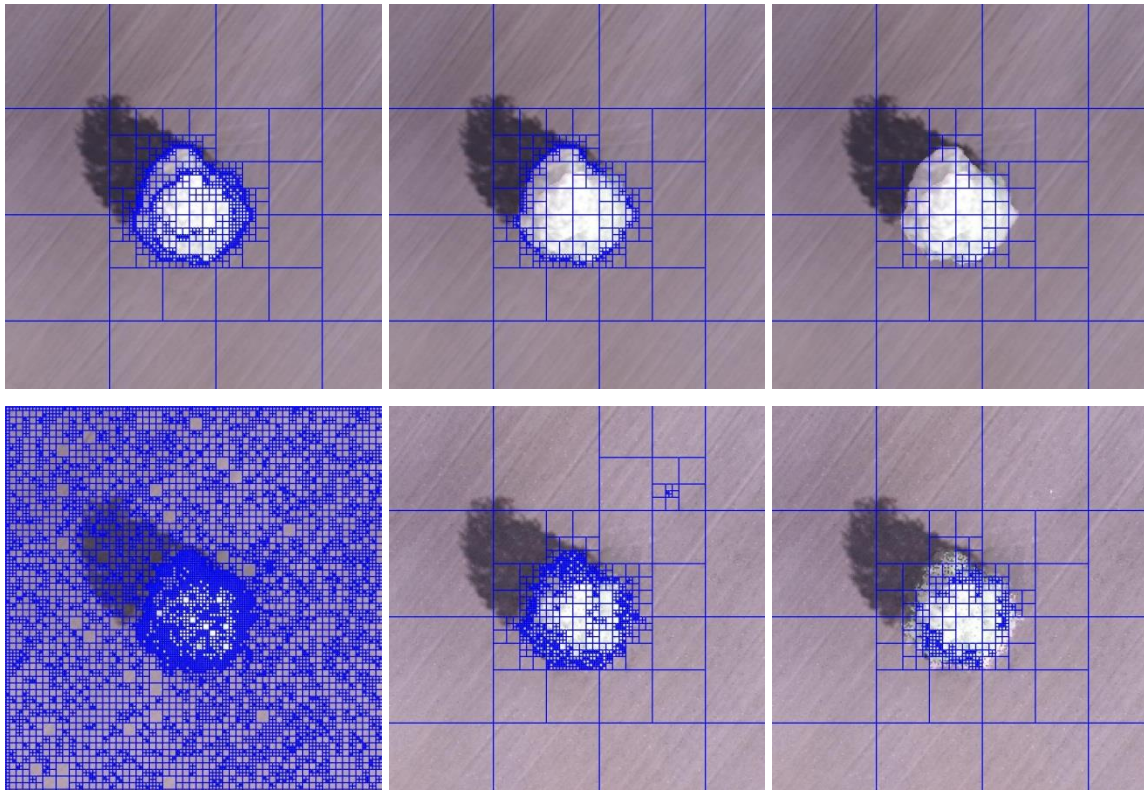


Figure 27: Quad-tree segmentation of image-based (top) and laser-based (bottom) nDSM of a single tree with scale parameter of 10, 50, 100 and 200 (left to right)

Figure 27 shows the quad-tree segmentation of the single tree. As can be seen, the structure of the object is not easily detected.

Threshold or contrast splitting segmentation

With definition of a threshold, an image can be split into dark and bright areas (Figure 28). Based on the object level, the contrast splitting segmentation starts with a chessboard segmentation, followed by stepwise splitting of the objects or pixels [eCognition 2013].

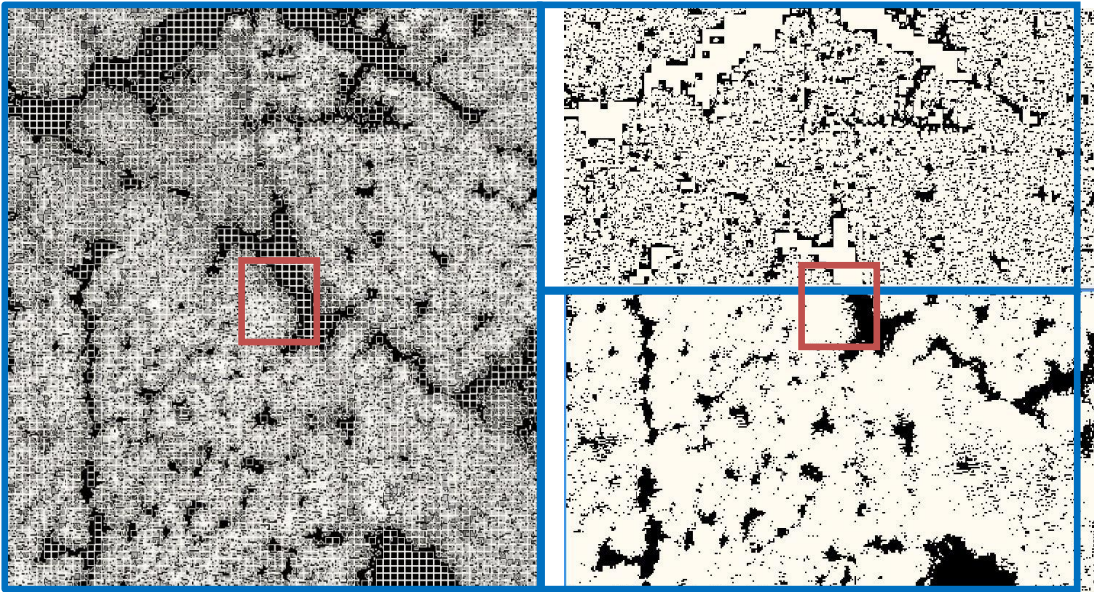


Figure 28: Contrast split segmentation with step 10, chessboard object size 10 pixels or 2m (left and top-right) and 100 pixels (right-down)

The number of split segments depends on the radiometric resolution of the image. In the case of DSM images this equates to height difference steps. As demonstrated in Figure 29, due to the radiometric resolution of 10 centimeter in the dataset, there is no significant difference between the contrast steps of 10 and 20.

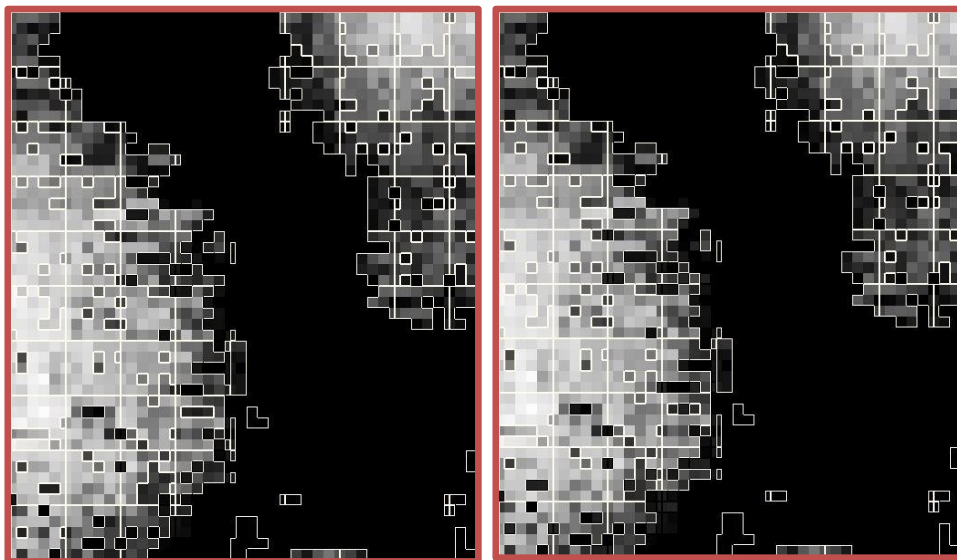


Figure 29: The small difference in Contrast Split with step 10 (left) and step 20 (right) with chessboard object size of 100 (the red subset from previous figure)

The strength of this segmentation method lies in the delineation of the tree crown boundaries. However the influence of noise, especially in nDSM of LIDAR data, is a disadvantage to this method. Due to these two facts, a proper filter which can remove the high frequency noises within the tree crown and simultaneously preserve the edges on the tree boundaries needs to be implemented on LIDAR data, before using this segmentation method.

Spectral difference segmentation

This method merges the segments, according to their gray value. Spectral difference segmentation is basically for refining the previously segmented images with other algorithms [eCognition 2013]. That means using this method on small object sizes, i.e. pixel size level, might result in oversegmentation, which is a disadvantage to rough LIDAR data (Figure 30). To deal with this problem, one might determine high threshold values, however this results in losing more details of the image texture. Therefore, using this method needs a previously strong filtered dataset for laser-based CHM.

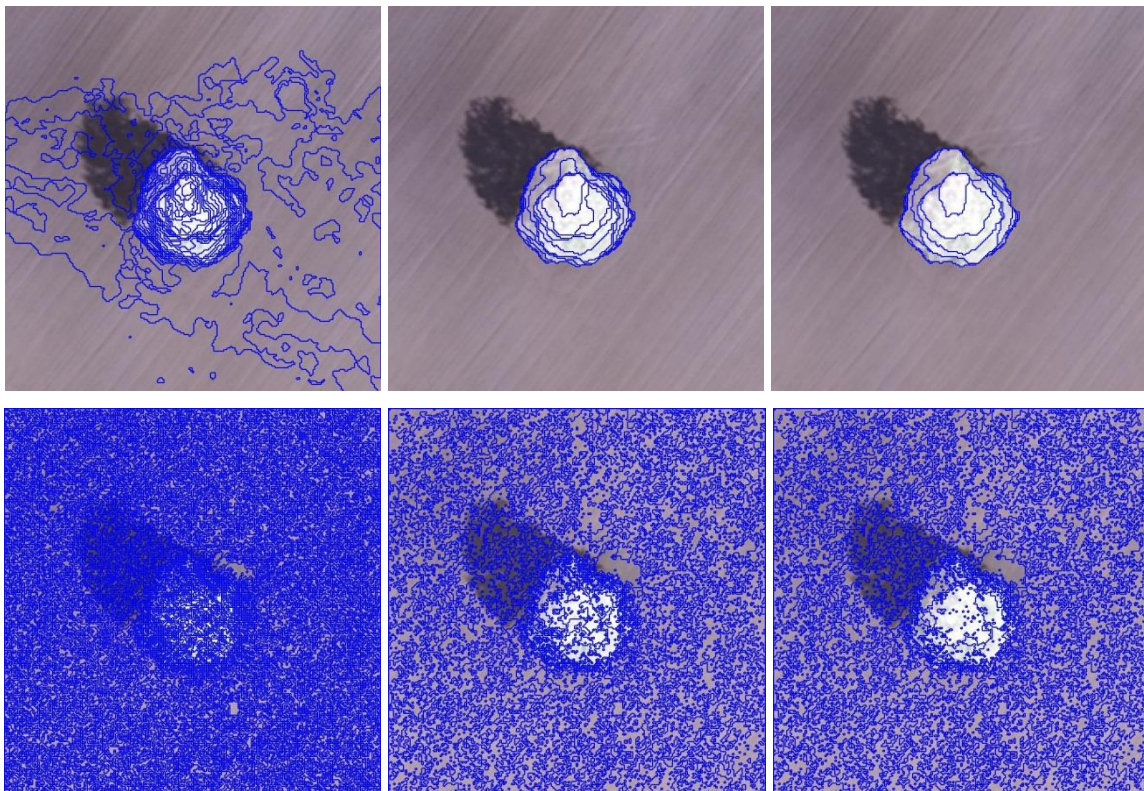


Figure 30: Spectral difference segmentation of image-based (top) and laser-based (bottom) nDOM with maximum difference of 1, 5 and 10 (left to right) after a chessboard segmentation at pixel size

Multiresolution segmentation

In multiresolution segmentation, the image layers can be weighted considering their significance and influence on the segmentation process [eCognition 2013]. Additionally, the level of details (LOD) on the image object can be defined with scale parameters. To define an appropriate scale parameter, one should consider which layers have more influence on the segmentation. As demonstrated in Figure 31, some objects might not change in different scales (like the large open air region). However, the smaller objects (e.g. the free space area) might not be recognized as a separated segment in lower LOD.

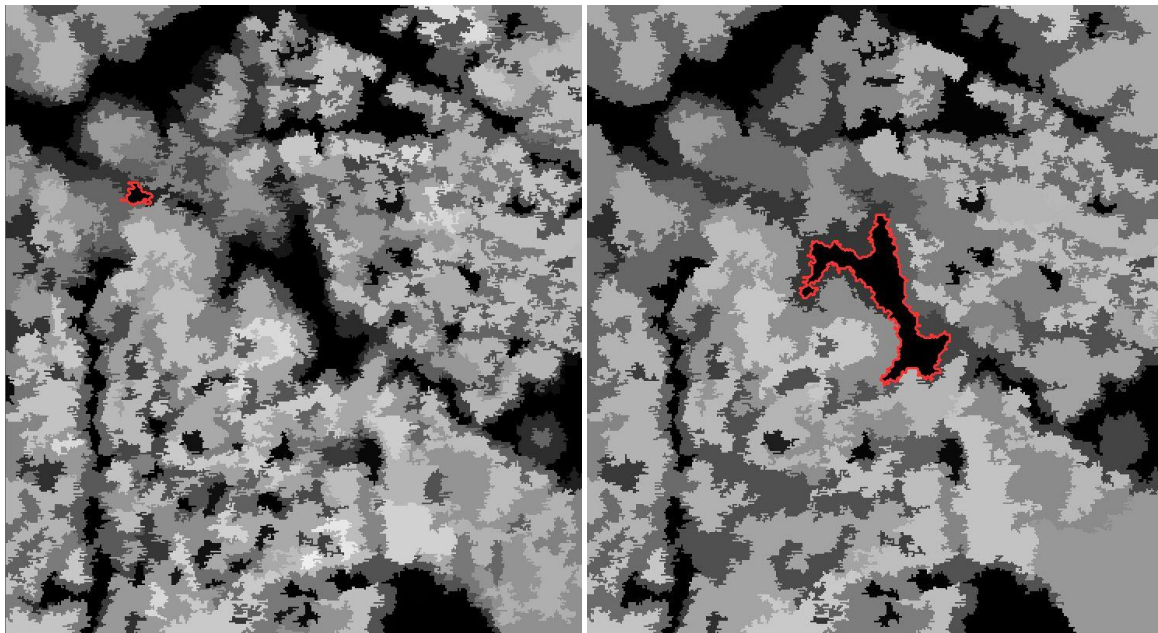


Figure 31: CHM image segmented with multiresolution algorithm in eCognition with scale parameters 100 (left) and 200 (right) with shape parameters 0.1 and compactness of 0.5

It should be noted that reducing the scale parameter will increase the influence of noises in the dataset, which is a considerable issue in LIDAR datasets. Figure 32 shows the differences in segmentation of image-based and laser-based nDSM with different scale parameters.

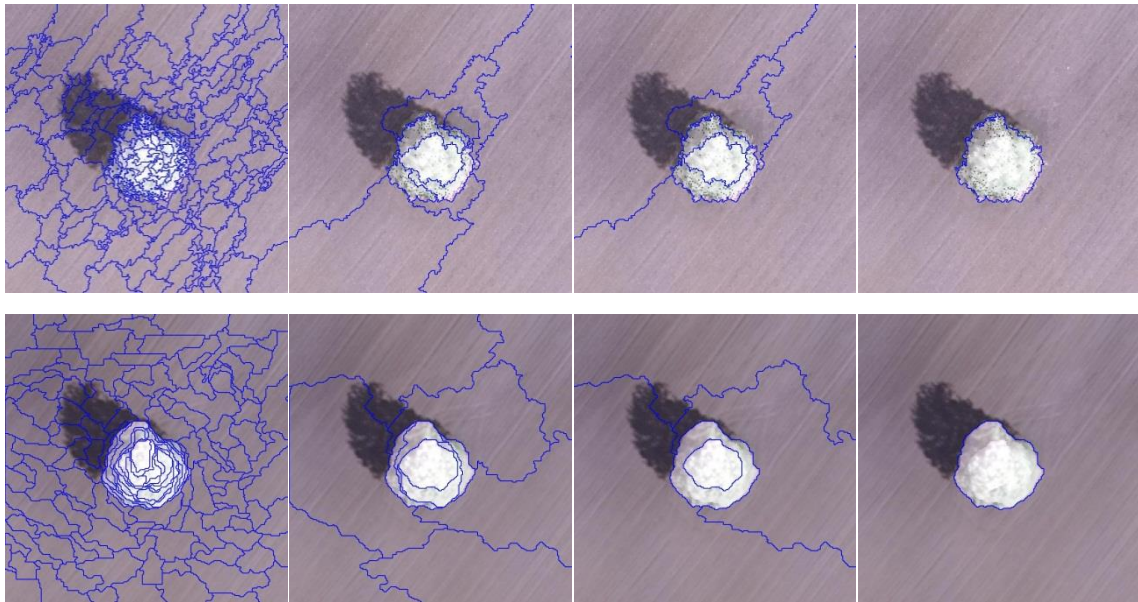


Figure 32: Multiresolution segmentation of laser-based (up) and image-based (bottom) nDSM of a single tree with scale parameter of 10, 50, 100 and 200 (left to right)

As can be seen, in areas where the trees are separately isolated, for example in urban areas or farm trees, the height differences provide a contrast between the gray scale values and the background (buildings or ground). This means that in bigger values of scale parameter the tree crown can easily be segmented in both datasets. Comparison of the multiresolution segmentation of both datasets at the scale parameter 10 shows that the structure of the object influences the final form of the segments. At this level, one can observe that in laser-based nDSM the segments are more or less in line with the direction of the background object (southwest to northeast on the plowed ground in Figure 32). However in the image-based nDSM, this structure would not affect the segments.

Combination of segmentation methods

In the software eCognition, the segmentation methods can be combined, taking account of the characteristics of the requested objects and the results of each algorithm. Therefore, choosing the order and the image object level of each algorithm plays a significant role to enhance or lose the initial elements of the object. In Figure 33 two segmentation results are demonstrated where the chessboard segmentation with a big grid size (2m) under a multiresolution segmentation (scale 200) results in losing the edges on the boundary of the tree crowns.

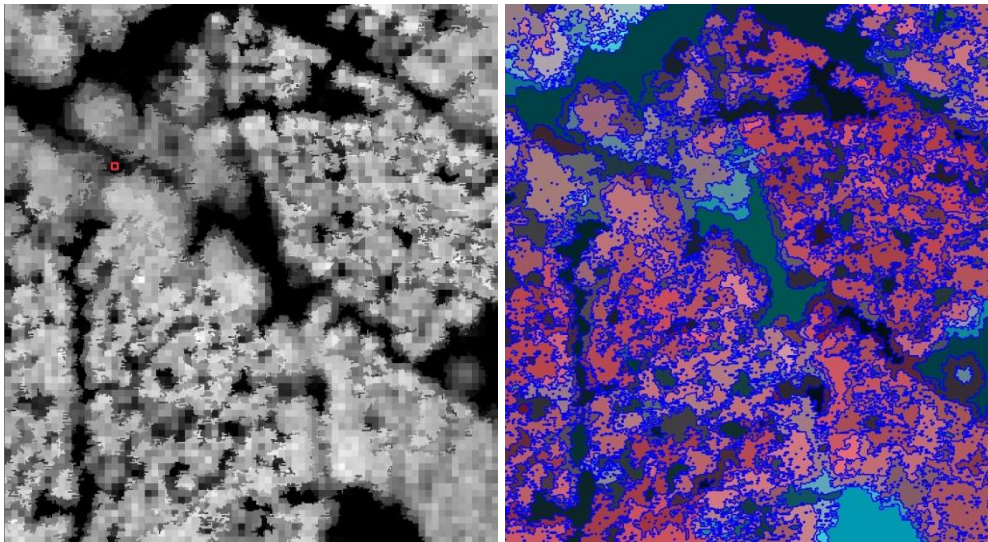


Figure 33: Chessboard 10 pixel or 2m (the cell represented in red) under a multiresolution with scale 200 (left) and spectral difference segmentation (sp.diff. =100) on LIDAR nDOM after a multiresolution segmentation with scale 100 (right).

On the other side, with the order of multiresolution after spectral difference segmentation, the tree edges seem to be refined, but the gaps between trees are wrongly filled. Figure 34 shows the appropriate separation of the tree stands area and ground, using spectral difference segmentation on the nDSM data after a multiresolution segmentation.

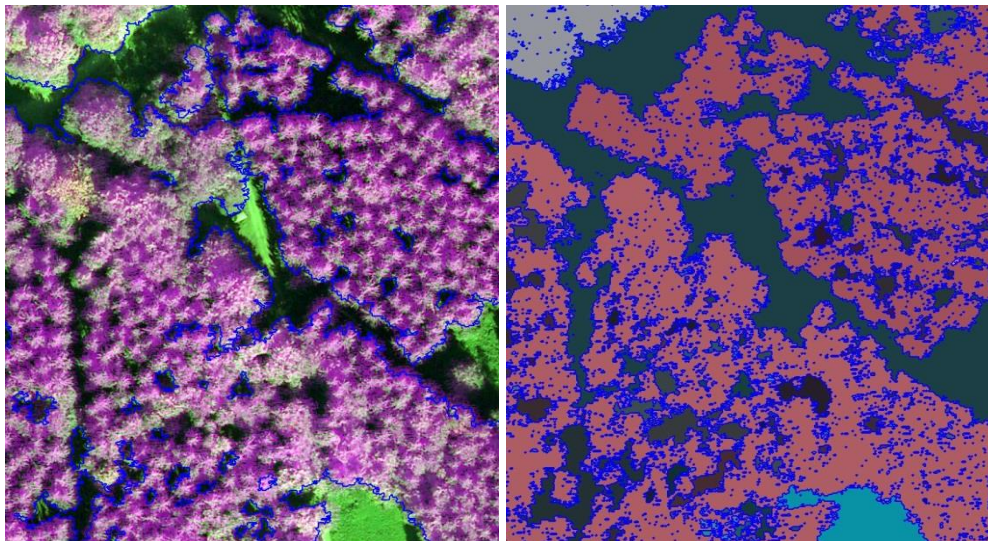


Figure 34: Spectral difference segmentation on nDOM with 10 maximum difference after a chessboard segmentation at pixel size

Compared to the color data, the stand boundaries and the gaps between the trees are enhanced properly, whereas the noisy characteristic of the LIDAR data caused some small dots in the segments. These can be easily removed with a size filter in the stand classes. It should be emphasized that in this thesis, all of the spectral analyses are implemented on the height data. The spectral channels (R,G,B and NIR) are shown for visual comparison and imagination of the reader and never used in the algorithms.

To isolate the single trees in segmentation procedures, one should provide a proper object space. In a rule-set, the object space varies from one rule to the other. The output of one step can be the input of the other step. This means the features, defined in the rules, should carry the requisite characteristics of the target object in each level. The term segmentation level can be discussed from different aspects considering these parameters:

- At which height level should the features be created?
- Which features can represent the characteristics of the object?
- In which scale-space (see section 3.2) can these features be more efficiently provided?

As mentioned in [Miri et al. 2013], in the image-based DSM, because of the problems in the interpolated areas, which are caused by shadows, the most reliable segmentation level is within the highest parts of the nDSM. In this research, this elevation level of the canopies will be investigated for both image-based and laser-based datasets. In the next chapter, appropriate features are developed to perform this evaluation.



4

Feature Extraction

This chapter will discuss the features; these represent the geometric and morphologic characteristics of tree crown.

4.1. Features in single tree extraction

In general, extractions of single trees are categorized in *bottom-up* or *top-down* methods [Maar 1982 from Bechtel 2007], which can also be referred as *data-driven* and *model-driven* approaches [Straub 2003].

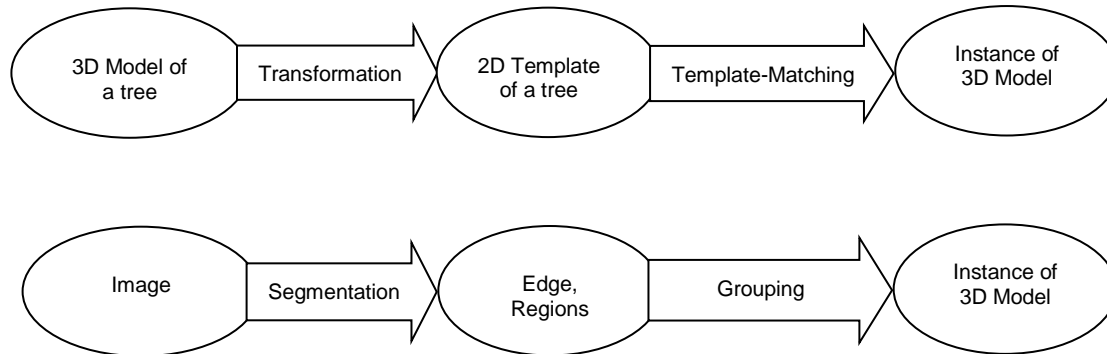


Figure 35: Top-down or model-driven (up) and bottom-up or data-driven approach in tree extraction [Straub 2003]

The main issue in the top-down strategies is how to find the single trees if a previously mathematic model of the trees is provided. This case is similar to template-matching algorithms. On the other side, the bottom-up approaches focus on the delineation of single trees with extraction of image objects using segmentation and classification algorithms.

4.2. Template-matching

Feature extraction by template matching methods is sensitive to the texture and shape of the object of interest. For man-made objects, these algorithms are mainly based on the spectral data. The key point in such algorithms is providing an appropriate level of detail considering that:

- *More spectral channels will increase the levels of textural information.*
- *Higher resolution might increase the level of detail, but depending on the sensor type, shape and complexity of the object, and the parameters of the processing method, it might lead to inconsistent or inappropriate results.*

Template matching techniques for single tree detection are for the most part used in coniferous stands. This is because of the quasi star shape of the single trees in airborne images. It should be

noted that some coniferous trees like pine do not satisfy such form and have primarily the form of deciduous trees. However, it is the imaging conditions, resolution and the DSM generation method which influence the quality of the true-orthophotos. As can be seen in Figure 36, the true orthophoto with higher resolution (8cm) shows more detailed parts of the tree crown, though the star form of the trees has lost its symmetric geometry.

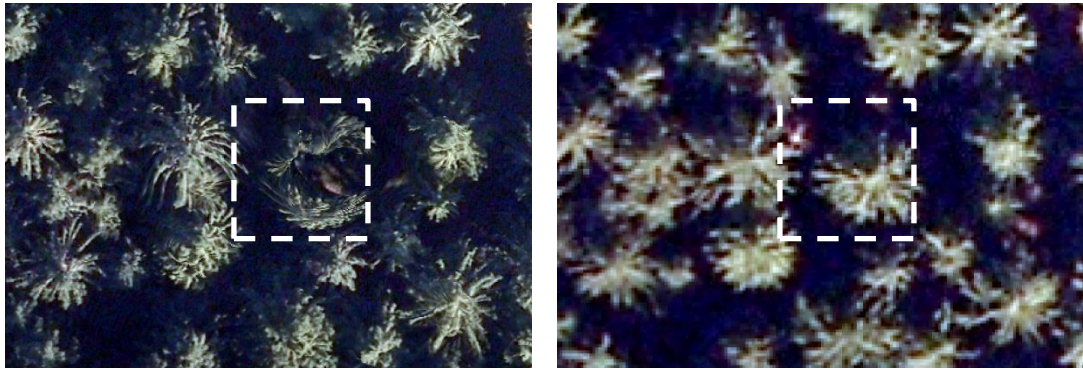


Figure 36: Different projection of trees in true orthophotos with resolutions of 8cm (left) and 20cm (right)

When using the height data, the tree template can be defined with a mathematical form. As the single trees of even a particular stand type are different in size, a dynamic template is needed, which changes its size related to the forest parameters of the stand.

In model-based approaches the trees can be defined as geometric objects. Considering the parameter Z as the crown height data in the ellipsoidal model of [Larsen 1997], a tree can be modeled with:

$$\frac{(z^2)^{n/2}}{a^n} + \frac{(x^2 + y^2)^{n/2}}{b^n} = 1$$

In a simple form, this model can be replaced with the generalized ellipsoid of revolution from [Pollock 1996]:

$$\frac{(z - z_0)}{a^n} + \frac{((x - x_0)^2 + (y - y_0)^2)^n}{b^n} = 1$$

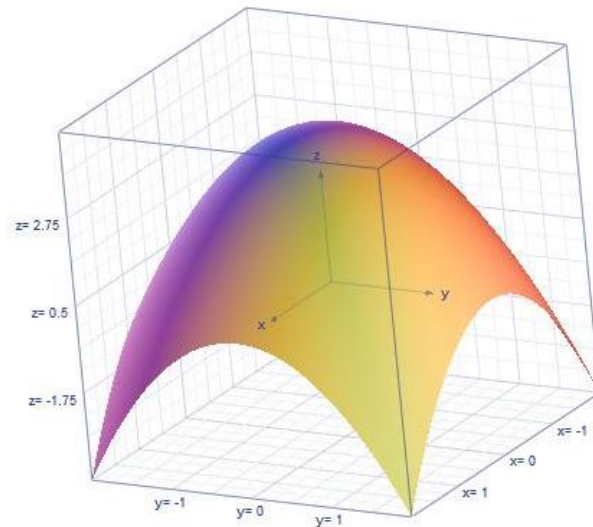


Figure 37: Generalized ellipsoid of revolution with $a = b = n = 2$

The advantage of using the height information is that, based on the geometric parameters, the templates can be fitted on the crown surface. However, as the trees have different form and height within a stand, a single mathematical model which fits all the trees cannot be defined.

4.3. Local maxima

In object oriented approaches, the local maximum, as one of the commonly used features to reach the highest point of trees has been discussed in the literature [Solberg et al. 2006]. The local maximum is defined as a pixel where all the 4 connective neighborhoods have lower height values [Koch et al. 2006]. In the case of equal height pixels, they will be connected and form a plateau. Generally, local maxima are used as seed points in region growing algorithms. However, to avoid false seed points (local maxima on the lower vegetation), a height threshold is implemented at the beginning of such algorithms. Baatz et al., 2008, defined a workflow in object oriented image analysis to find the local maxima in ALS data (0.5 m) which is based on the object primitives. However, the background of the forest should be defined as non-tree area at the first step using a height threshold. In [Koch et al. 2006], the stand is classified into two classes of low trees and high trees. In this way, the basic object domain is prepared for the next processing steps. For extraction of the tree crowns in this method, the positions of the trees are needed as seed points. They are extracted in the next steps, where the segments are broken down into primitives of the size of one pixel (using chessboard segmentation). This step is followed with a

searching window to find the local maxima as probable tree positions. By comparison of the grey value of the current pixel with its neighboring pixels, the local maxima in tree-areas are classified as tree positions. Finally, the tree positions are used as seed points for a region growing segmentation. For analysis of the tree crown diameter, the quality of the tree shape is very important [Batz et al. 2008]. That means an appropriate refinement algorithm is required for best fitted tree crown boundaries.

To find the local maxima in spectral data, the most illuminated part of the tree should be searched for. It is to be noted that, depending on the elevation of the sun and the position of the tree in the image, the peak point of the tree is not necessarily the most illuminated point of the tree. This means, to use the RGB datasets, the topography, illumination condition, shape and inclination angle of the tree at the time of imagery should be taken into account (see section 2.3). These conditions should be predefined in color-based template matching algorithms to model the tree on the top levels. More detail about the template matching of tree models in spectral data can be found in [Erikson and Olofsson 2005].

4.4. Top hat slices

As well as local maxima, the top slices can also be defined as seed objects. The main problem in finding the local maxima is the definition of the scale space. In detailed scales (i.e. higher resolution) the local maxima are confronted with oversegmentation. That means the number of local maxima are more than the number of the existing trees. In coarse scales, this results in undersegmentation. In the single tree detection flowchart of [Miri et al. 2013], the top hat slices are found as a segmentation step before finding the local maxima. In this way, the candidate points, as the maxima of the crown surface, will be searched in the top hat slices. The advantage of this workflow is that classifying the low and high trees can be undertaken in the preliminary steps and before classifying the low and high vegetation. As defined, extracting these segments is also dependent on the segmentation algorithms and their relative parameters. In other words, segmentation of the height data at top hat level is an advanced solution for the problem of scale space to find the local maxima. However, definition of appropriate top hat segments is also related to the characteristics of the data acquisition method and to the geometry of the tree types.

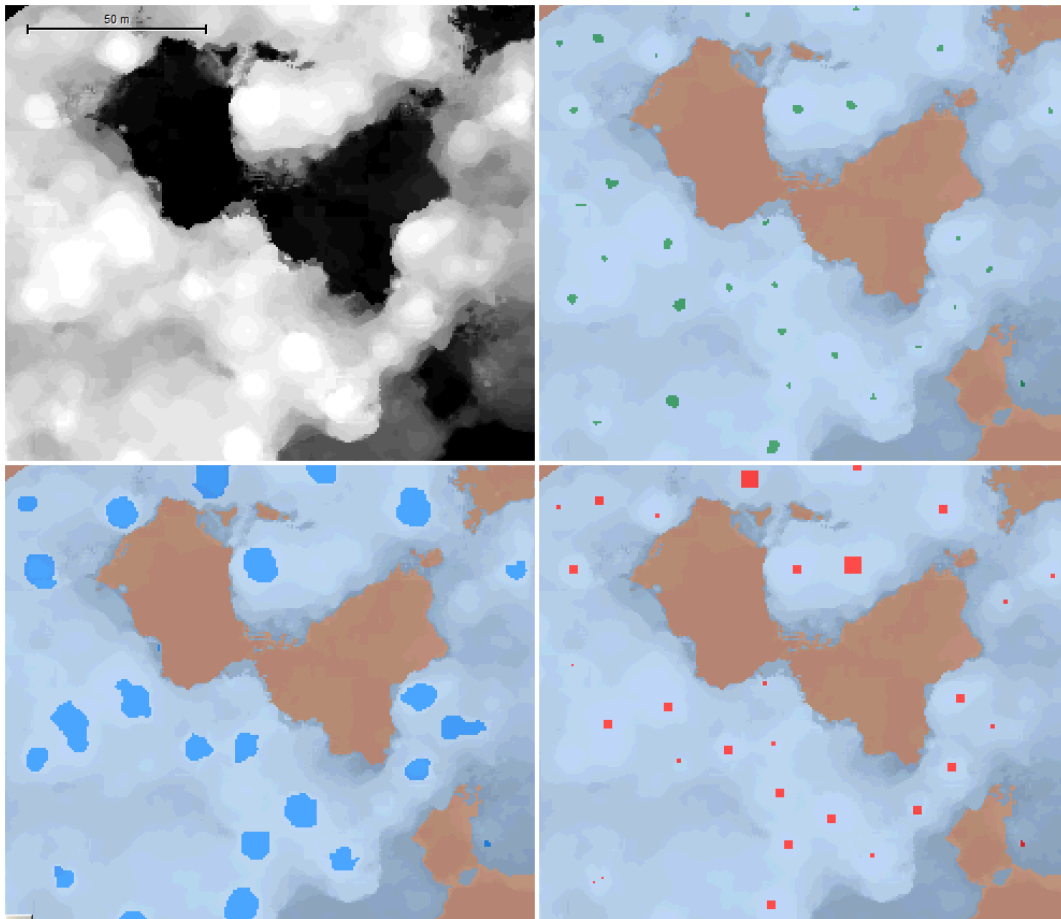


Figure 38: Top hat segments on an image-based nDSM with 20cm resolution (top left) using spectral difference segmentation (top right), multiresolution segmentation (down left) and Quadtree segmentation (down right)

Figure 39 shows the difference in the multiresolution segmentation of image-based and laser-based nDSM, with scale, shape and compactness parameters of 50, 0.1 and 0.5. As can be seen, such trade-off parameters result in slight undersegmentation in coniferous trees and a high oversegmentation in the deciduous tree (lower left corner of the area).

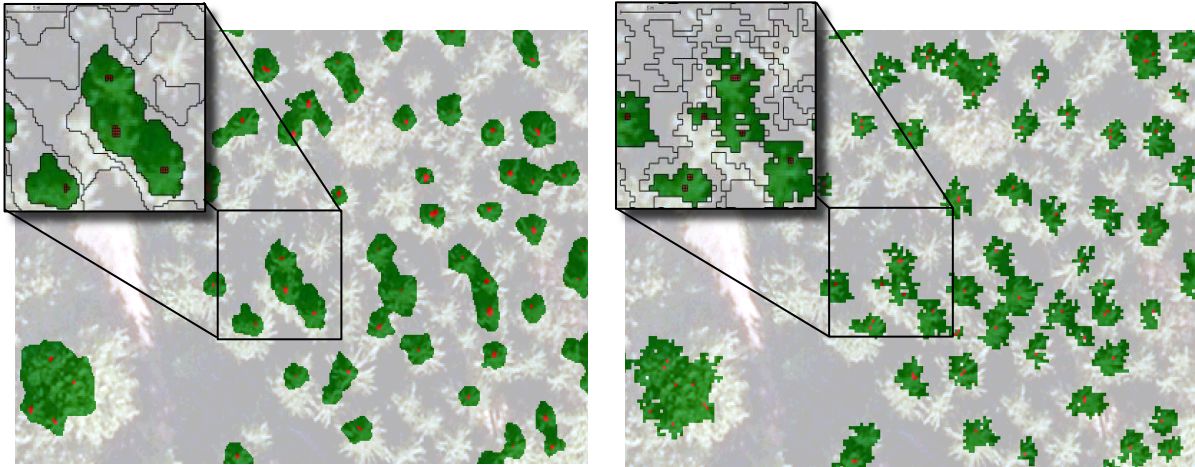


Figure 39: Different top hat levels (green segments) and local maxima (red pixels) in different nDSM; image-based (left) and laser-based (right)

In [Miri et al. 2013], before evaluating the geometry and morphological characteristics of the crown model, the top level slices are extracted using the colored contour maps, defining the trees in different segmentation heights. Figure 40 represents the workflow of this procedure.

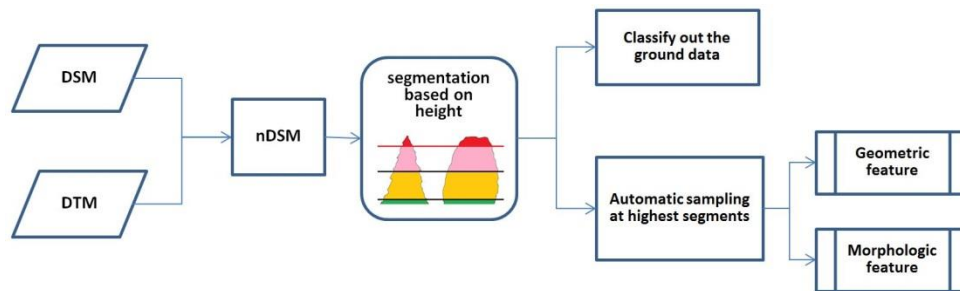


Figure 40: Processing workflow of the feature-based evaluation of the DSM data at the level of THS (red) [Miri et al. 2013]

In the first step, the nDSM is extracted from the DSM with 20cm pixel size and the laser DTM of one meter. Thereafter, an automatic segmentation, based on the elevation data of the nDSM is implemented. This step is followed by the selection of the local maxima segments on the top hat slices. This has the advantage that the classification of ground and not ground areas is performed after top hat segmentation. In later techniques, like in [Andersen et al. 2001], highest levels of CHM data are used to detect the tree positions using a structural element in the form of a flat disk [Adams 1993], [Jones and Soille 1996]. The critical point in [Andersen et al. 2001] is the 2D form of the structural element. To solve the problem of scale space, they used different filters (0.9m, 1.2m and 1.5m cell size), which meant losing the crown form of the trees.

This model can be improved by definition of a 3D form parameter while adding the height dimension to the morphological analysis and the problem of scale space can be solved by using different structural elements. The main idea in this part is to create a multi-layer scale-space by putting several hats in different size and form groups on the tree crowns. Theoretically, these hats are created by running 2.5D morphological features in spherical, ellipsoidal or conical forms.

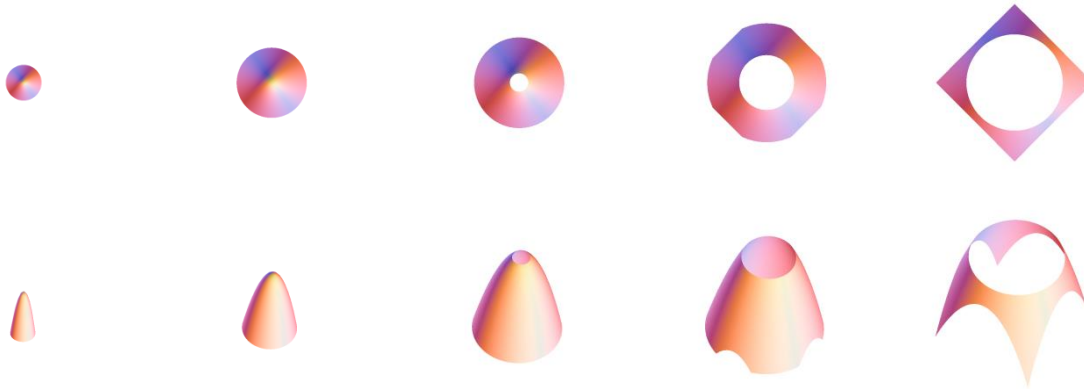


Figure 41: 2D and 3D fitness of structural elements in five scale spaces and different height sections for the hat with the formula of $\frac{z}{a^2} + \frac{x^2+y^2}{b^2} = 1$, with $a = 2$, $b = 2$

Presetting the size and shape of the hats can determine the non-linear multi-scale space of the model. Obviously, the type and quantity of these layers vary depending on the tree type (coniferous or deciduous) and the forest density. To improve the efficiency of this method, the most appropriate section of the structural elements on the surface model should be calculated for different height sections.

4.5. Surface analysis

Interpretation of the height data for single tree extraction requires consideration of the characteristics of the containing stand. The arguments which will be put forward in this section are relevant to the understanding of 3D surface characterization. Such analyses are rather important in forest stands, where estimated values for the stand height are required for the pre-definition parameters of single tree extraction. The *mean height of the stand*, *height of the trees with the basal area* and *mean height of the dominant trees* are discussed in [Laar and Akça 2007] through a height profile as significant values for stand-wise analysis of forests. Such surface

analysis can be compared to similar cases in industrial spaces. Quality assessment of industrial pieces with irregular variations or analyses of ceramic, cement or other surfaces in microscopic dimensions give rise to similar discussions as in this area. These methods are categorized into mechanical (direct contacting the surface) or optical (without touching the surface) systems. Figure 42 shows the 1D (profile), 2D and 3D results of a light-based measurement of a concrete surface using coherence scanning interferometry.

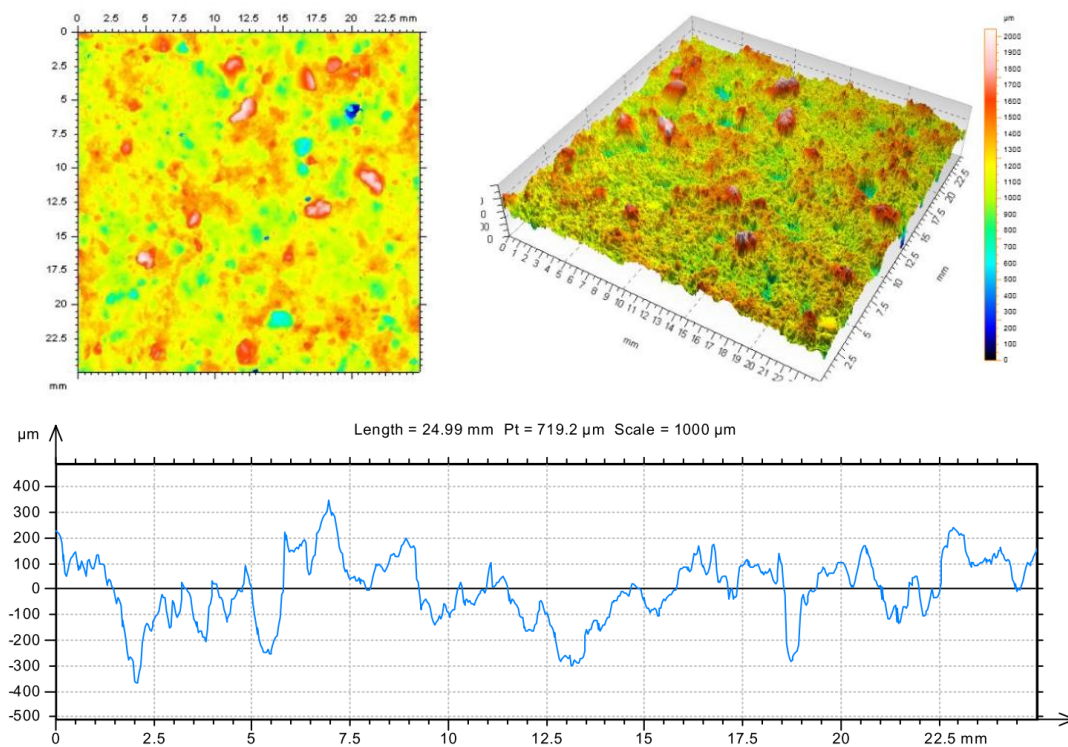


Figure 42: Results of micrometric measurement of a concrete surface using coherence scanning interferometry demonstrated in 2D, 3D and profile on the blue line (www.nanovea.com)

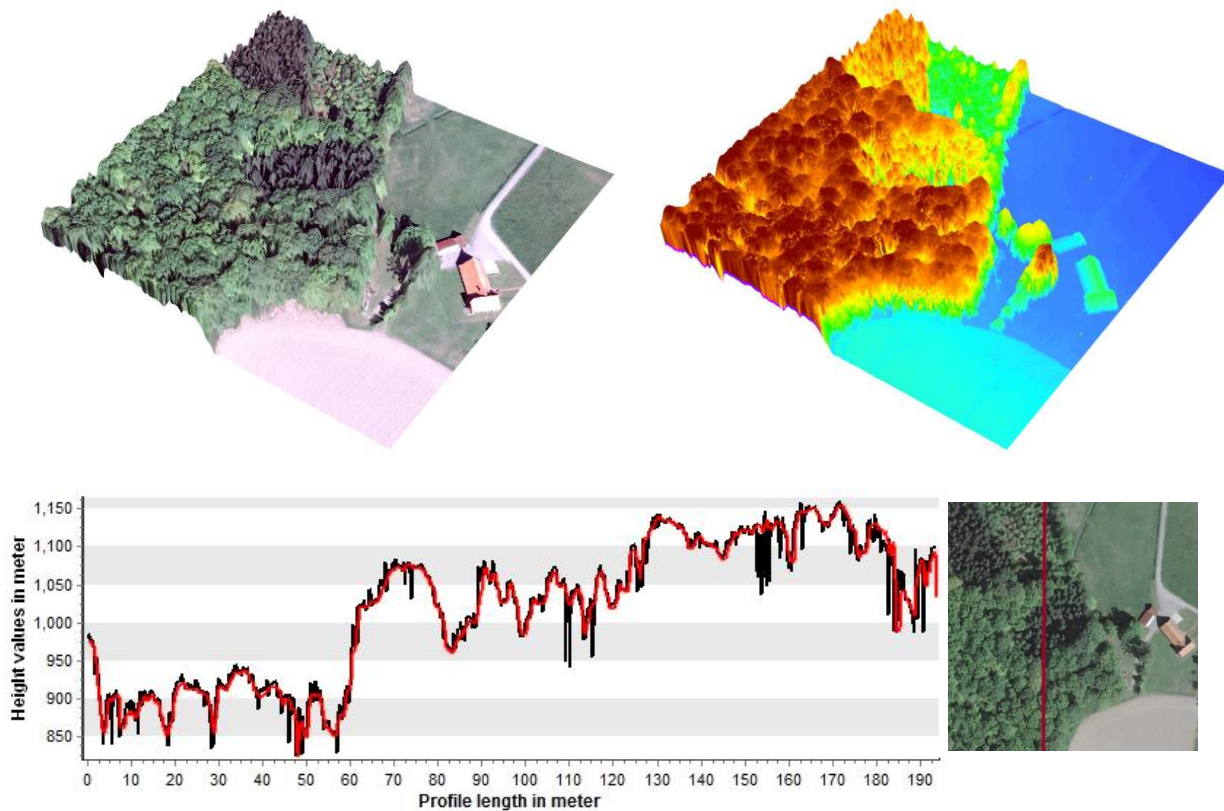


Figure 43: Top: True-color and false-color surface model of a mixed forest near to other flat surfaces. Down: 2D profile of the laser-based nDSM the rough surface (black) and the filtered surface (red)

A detailed review of experiments in this area can be found in [Blunt and Jiang 2003]. For engineering production purposes, an already measured digital surface can be analyzed using several mathematical parameters to explain the difference from design to the final product.

To demonstrate the texture of a surface, the so-called *Birmingham 14 parameters* were developed in the early 1990s and improved under the *SURFSTAND* project into the *15 S-parameter set* in numeric forms, which are now taken up by the European and International Standard Organizations (CEN/TC 290 and ISO/TC 213) for 3D texture analysis of surfaces [Blunt and Jiang 2003]. These parameters are categorized in five types, *amplitude*, *spacing*, *hybrid*, *fractal* and *other* parameters (Table 3).

Amplitude parameters	Spacing parameters	Hybrid parameters	Fractal parameters	other parameters
<ul style="list-style-type: none"> •Root mean square deviation - Sq •Skewness -Ssk •Kurtosis - Sku •Maximum peak/valley height - Sp, Sv •Maximum height - Sz •Arithmetical mean height of the surface - Sa 	<ul style="list-style-type: none"> •Density of summits - Sds •Fastest decay auto-correlation length-Sal •Texture aspect ratio - Str 	<ul style="list-style-type: none"> •Arithmetic mean peak curvature - Spc •Root mean square slope - Sdq •Developed interfacial area ratio - Sdr 	<ul style="list-style-type: none"> •Fractal dimension - Sfd 	<ul style="list-style-type: none"> •Texture direction - Std •Ten point height of surface - S10z

Table 3: The S-Parameter Set

Depending on the surface type and the required features, the relevant parameters can be applied. In general, the texture of a surface can be defined as a rough, wavy or primary surface. According to [Blunt and Jiang 2003] the amplitude parameters focus on the height deviation, whereas the other ones focus on the texture and forms on the surface. For this reason, the amplitude parameters will be investigated for analysis of forest surface models in this research.

Feature	Value	Description
μ	Mean height of the profile	Arithmetical average of the surface
R_a	Averaged roughness over the entire measured length of profile	Standard deviation of the pixel values from μ
R_q	Root mean square roughness.	Height between the highest peak and the mean plane
R_{sk}	Skewness of the surface.	Depth between the mean plane and the deepest valley
R_{ku}	Kurtosis on the surface	Difference between the peak and the valley point.

Table 4: The R-Parameter Set

Roughness can be defined as fine variations on the surface model, which are caused by the irregular structure of the crown surface. The strength of the roughness depends also on the data capturing method, including the sensor type and the (re)sampling method of the surface. In

general, roughness evaluators are sensitive to the signal to noise ratio of the sensor. Table 4 shows a list of some of these parameters⁶ for a 2D profile on the surface.

Based on the definitions in [ISO_4287 1997; ASME_B46. 1 1985] and [Blunt and Jiang 2003] the advanced mathematical formula of these parameters is explained below for a continuous surface model.

The *average roughness* (S_a) of surface can be calculated from:

$$S_a = \frac{1}{A} \iint_A |Z(x, y) - \mu| dx dy$$

where A is the area and μ indicates the arithmetical *mean height* of the surface:

$$\mu = \frac{1}{A} \iint_A Z(x, y) dx dy$$

The standard deviation of the surface roughness can be calculated from the distribution of the height data using the *root mean square* (S_q) on the surface model:

$$S_q = \sqrt{\frac{1}{A} \iint_A (Z(x, y) - \mu)^2 dx dy}$$

Skewness (S_{sk}) qualifies the symmetry of the height distribution by measuring the average of the first derivative on the surface. A negative value of skewness indicates that the surface is made up of valleys and the distribution slopes to bottom, whereas positive values relate mainly to the occurrence of peaks and asperities. That means the distribution slopes to the top. Due to the large exponent used, this parameter is very sensitive to the sampling and noise of the measurement:

$$S_{sk} = \frac{1}{S_q^3} \left[\frac{1}{A} \iint_A (Z(x, y) - \mu)^3 dx dy \right]$$

Kurtosis (S_{ku}) qualifies the sharpness of the peaks on the height distribution and as well as skewness, noisy data can affect this parameter too:

⁶ The roughness parameters are defined in the ISO 4287/1: 1997, DIN 4768 and DIN 4776. They are generally used in metrology of industrial and optic surfaces: www.imagemet.com, www.smt.zeiss.com.

$$S_{ku} = \frac{1}{S_q^4} \left[\frac{1}{A} \iint_A (Z(x, y) - \mu)^4 dx dy \right]$$

In this research the surface analyses of the forests will be performed using these amplitude parameters. However, for the height data in raster format, the continuous form of roughness parameters should be transformed into discrete form.



5

Methodology

In this chapter the existing methods of analyzing digital elevation models in forestry areas will be discussed and the algorithm used in this work will be introduced.

5.1. Eye-finger concept

As single tree extraction is directly related to the characteristics of the stand type, surface evaluation of canopy height models is required for presetting a couple of parameters in forest partitioning. By means of these parameters, the real form of a tree will be shaped and evaluated for automatic algorithms. A workflow to define and set the parameters for the relevant features in height data is needed to describe the methodology of this research. In terms of rule-sets, the fractal form of object-oriented workflows was explained in section 3.1. To structure an intelligent system, an efficient workflow should be able to transform, process and reproduce the required information for recognizing the object of interest. In other words, an intelligent machine should be able to train itself to some extent. In the approach to single tree extraction through the height data, the single tree detector machine can be assumed as a blind person. The sense of feeling or touching the forest canopy, without seeing it, will be simulated via a novel concept, called *Eye-fingers*. In this concept, to extract, define and visualize the parameters, the human sense of touching will be simulated by machine vision techniques. Like a trained blind person, this algorithm attempts to recognize the forest type and find single trees. In this vision, the trees are imagined in very small dimensions, where, one can feel the forest with closed eyes, without any additional spectral information. To translate this feeling from the language of human perception into machine language, an object-oriented approach in image analysis of digital surface models is implemented. For feeling small objects, thanks to the human sense of touch, one can evaluate the geometry (e.g. size and shape) and morphology (e.g. roughness and texture) of surfaces to interpret the surface and recognize the objects of interest. In the case of designing an intelligent system, these parameters should be mathematically translated into machine language.

This chapter represents a novel workflow of single tree extraction (Figure 44), categorized in five units. The first unit deals with *Data preparation*. Separating the tree and non-tree areas is undertaken in the next unit, entitled *Tree boundaries*. Thereafter, the provided layers and the tree boundaries are imported into the segmentation units, called *Marble rolling segmentation* and *Tree crown segmentation*. Finally, the delineated tree crowns are compared with the reference measurements in the *Evaluation* unit.

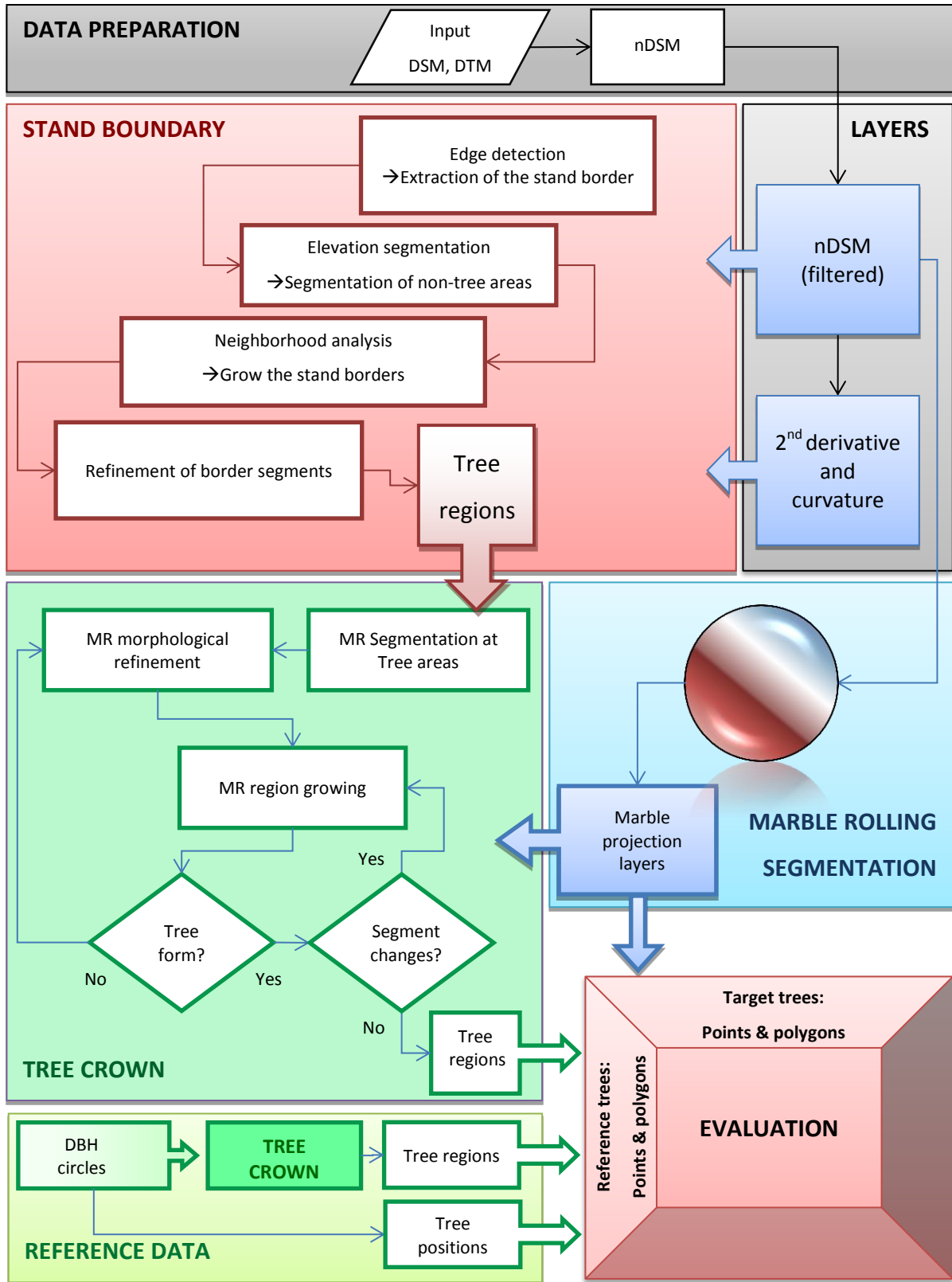


Figure 44: Object oriented workflow for single tree extraction

5.2. Data preparation

To provide the appropriate layers, two-sided image-processing of height data is considered. In this concept, both model-based and data-based methods (top-down and bottom-up) for single tree extraction are implemented. As a basic layer, the nDSM of both the laser-based and image-based are prepared. As explained in previous chapters, the laser dataset needs to be filtered for a supervised reduction of the problematic points on the surface model. During the interpolation steps in generation of the image-based DSM, the digital surface models are rather smoothed and need no more filters. In the next section, a novel approach of filtering the laser dataset is introduced. From the filtered nDSM, the curvature images are extracted and will be used for the delineation of the stand boundaries.

5.2.1. Noise and filters in processing the LIDAR data

Due to the flying points from the false measurements and the rough surface of LIDAR data that arise because of the complexity of crown surfaces, an appropriate filter is needed for removing the outliers in the nDSM data, while keeping the form of the tree structure. To develop such filters, two aspects should be considered; first the positioning method of the tree and second the boundary of the crown region. In general, the problematic points during the segmentation of CHM datasets can be categorized in four groups, described below:

1- Flying points over the tree surface, which cause false local maxima on the tree surface and challenge the positioning of the trees (e.g.), should be replaced with points laid on the *crown surface*.

2- Flying points over the ground surface, which result in false peaks on the ground, should be replaced with the points on the *ground*.

3- Ground points under the tree surface, which stem from penetration of the laser beam through the tree crown, lead to oversegmentation of the crown segment; they should be replaced with the points on the *crown surface*.

4- Holes on the tree surface, which are caused from the complex structure of the crown surface or due to the penetration of the laser beam, should be replaced with the points on the *crown surface*.

Figure 45 demonstrates a side view of these outliers on tree height models in LIDAR data, coded with above numbers.

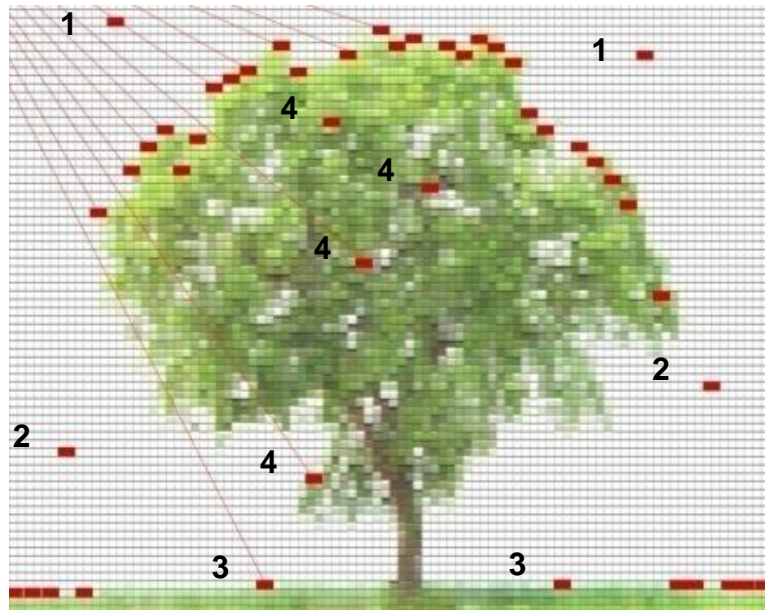


Figure 45: The problematic points in the laser-based height data⁷

Table 5 demonstrates an overview of the existing focal filters in the software ArcGIS 10.1, with size of 3 pixels. Due to the high frequency of the height variations in forest surfaces, filters dealing with the number of pixels (*variety*, *majority*) are not recommended. Such filters search for unique values while the other pixels remain unchanged. This is not the appropriate solution on smoothing the crown surface.

The filter *minority* detects values that occur least often in the neighboring cells, but will not remove them. The *minimum* filter results in shrinking the crown boundary. Whereas using the *maximum* filter the tree region grows to some pixels. Before rasterizing the point cloud datasets, these two filters are appropriate for generating the ground surface models (DTM) and crown surface models (DSM) from the last pulses and the first pulses of the laser data.

Among the other statistical filters, *Mean* and *SUM* reduce the high frequency noises. Losing the sharpness of crown boundaries and smoothing the top points of the segment, are the two main disadvantages of such filters. The *Range* and *STD* filters enhance the high frequency changes in

⁷ The original form of the tree symbol is from www.pngimg.com.

the neighborhood pixels, which can be used for a rough segmentation of the crown boundaries. To remove the high frequency noises, while keeping the sharpness of the crown boundary, *Median* filter shows the most satisfying results. As a weakness, this filter cannot preserve the upper structure of the crown surface and removes the peak points, though not as strong as *Mean* filter.

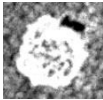





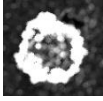


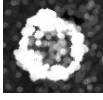


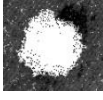


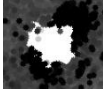


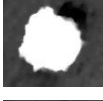








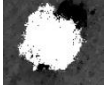


Filter Type	Description	Filtered crown model	Tree structure	Tree boundary
Variety	the number of unique values of the cells in the neighborhood			
SUM	total of all values of the cells in the neighborhood			
STD	standard deviation of the cells in the neighborhood			
Range	difference between largest and smallest value of the cells in the neighborhood			
Minority	value that occurs least often in the neighbor cells			
Minimum	smallest value of the cells in the neighborhood			
Median	median of the cells in the neighborhood			
Mean	average value of the cells in the neighborhood			
Maximum	largest value of the cells in the neighborhood			
Majority	value that occurs most often in the neighbor cells			

Table 5: Some geospatial filters in software ArcGIS 10.1

5.2.2. Selective or Non-smoothing filter

To overcome this problem, a new approach in filtering the LIDAR data will be introduced in this section. A *non-smoothing* filter based on a threshold value is developed. Using this filter the problematic points, i.e. the flying points (above the crown surface or ground) and the holes (within the tree crown) are detected and replaced with relevant height values. Figure 46 shows the workflow of this filter in three steps.

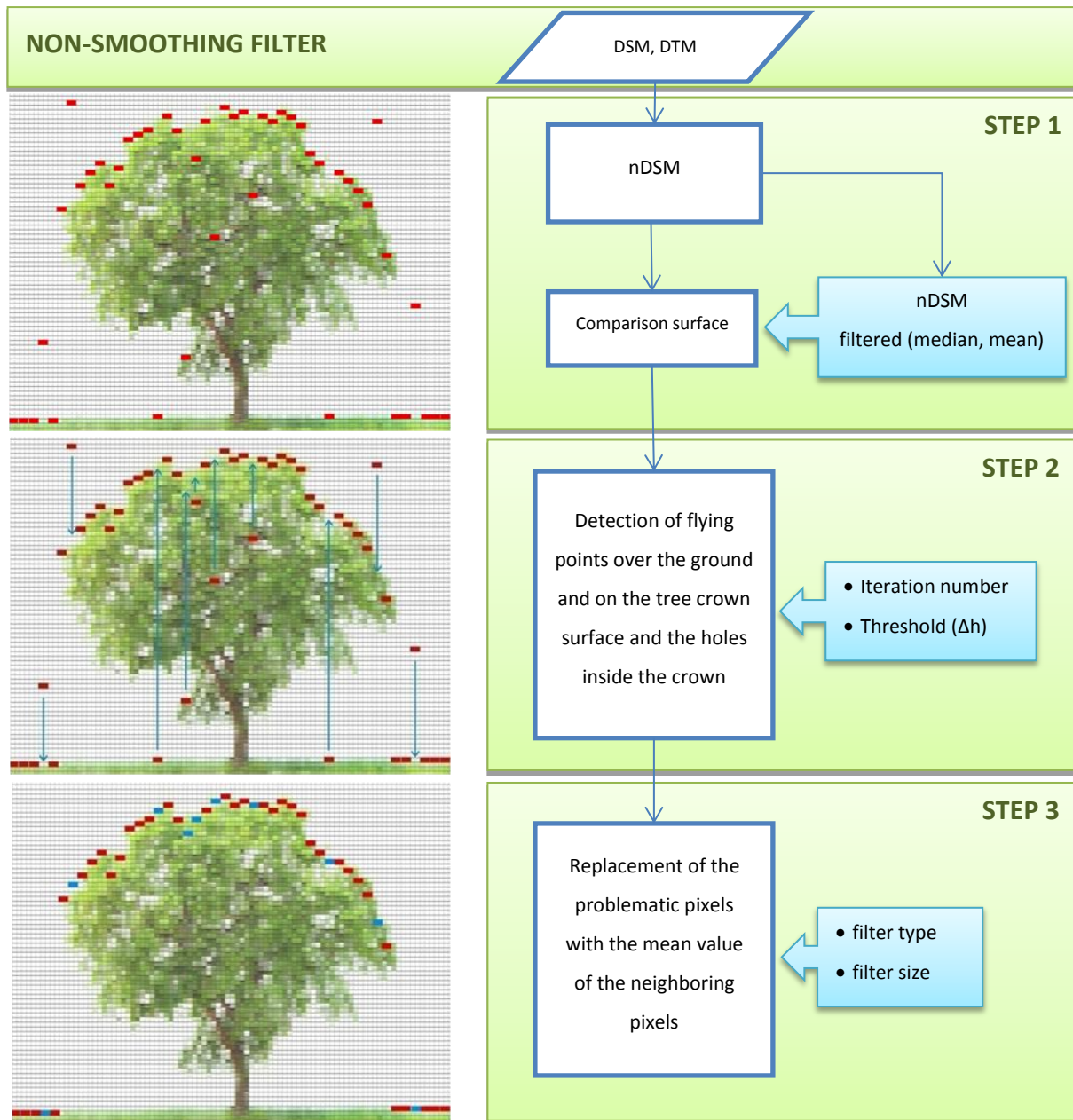


Figure 46: Non-smoothing filtering of the laser-based nDSM data

In the first step, after providing the nDSM dataset, a comparison surface layer is calculated using a smoothing statistical filter (e.g. median). The filter size depends on the resolution and the noise frequency of the surface model. Thereafter, the four problematic pixels (explained before) are detected using a differentiated image of both original and comparison surface. The quantity of these pixels (red in Figure 47) depends on the tree type of the stand.

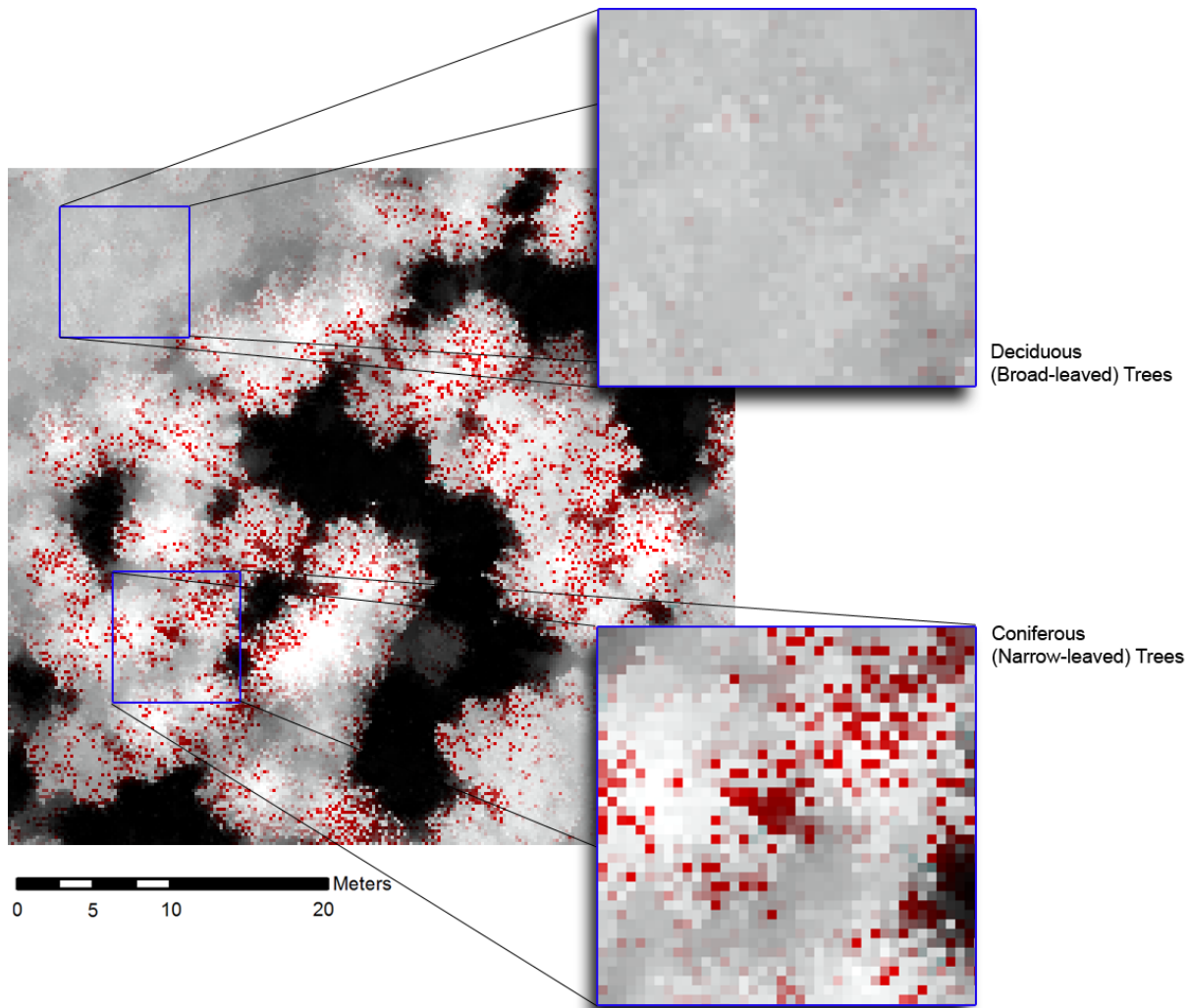


Figure 47: The problematic pixels in laser surface models of deciduous and coniferous trees

Higher amounts of repaired pixels in coniferous stands show more roughness of the surface models for narrow-leaved trees than the deciduous ones. The strength of the filter for detecting such areas can be set by a threshold value. In the last step, the problematic pixels are replaced

with the mean or median value, calculated from the neighboring pixels. Figure 48 shows the nDSM of a LIDAR dataset, before and after filtering.

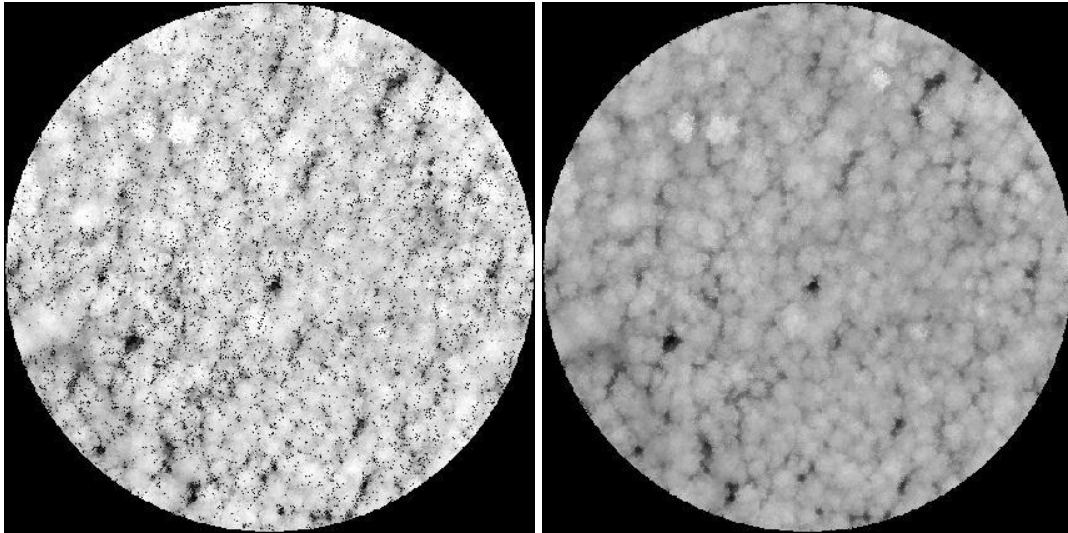


Figure 48: Laser-based nDSM data before (left) and after (right) filter

5.3. Boundary delineation

A tree stand consists of outer and inner boundaries. The outer boundaries are usually defined by setting a threshold for sudden differences on the nDSM. Figure 49 shows such boundary lines in red, which separate the outer border of a stand from the neighboring ground area (or neighboring stand). However, the most challenging regions are the boundaries inside the stand (demonstrated with blue lines).

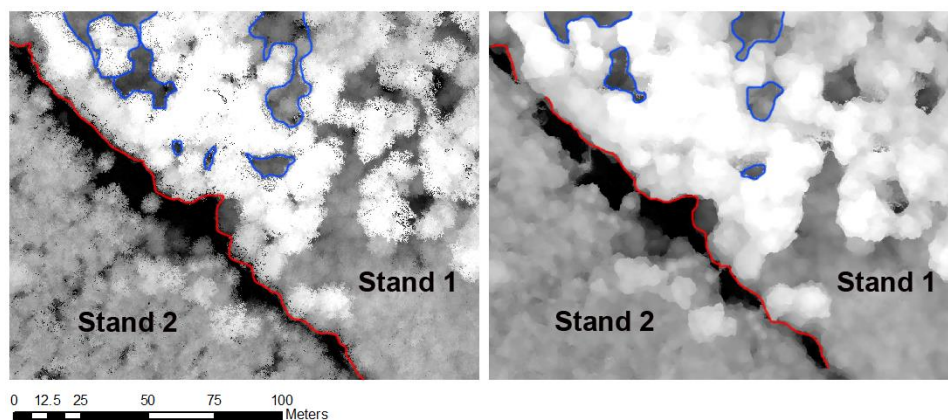


Figure 49: The outer boundary (red) and some inner boundaries (blue) of the mixed *Stand 1* on laser-based (left) and image based (right) canopy height model

To extract the valley regions (e.g. the gaps inside the stand), setting a unique height threshold might not result in proper bordering of the valleys. In the next unit of the workflow, to enhance the slight variation on the height data, the 2nd derivative and curvature of the stand surface are provided as additional image layers. For each point on a continuous surface, infinite curvature values can be calculated, regarding the direction of the cutting vertical plane. The curvature of a point on a surface can be calculated from its two principal directions, where the curvature values have maximum ($k_1 = \frac{1}{R_1}$) and minimum ($k_2 = \frac{1}{R_2}$). These values are called principal curvatures. R_1 and R_2 indicate the radii of the fitted circles on the curve along the principal directions. The angle between these two directions can be defined with (φ) [Fuchs 2003].

$$k(\varphi) = k_1 \cdot \cos^2 \varphi + k_2 \cdot \sin^2 \varphi$$

Using these parameters, the mean curvature value ($k_m = \frac{k_1+k_2}{2}$) and the Gaussian curvature ($k_g = k_1 \cdot k_2$) can be obtained. The Gaussian curvature determines whether the surface has a flat ($k_g = 0$) convex ($k_g > 0$ & $k_1, k_1 > 0$), concave ($k_g < 0$ & $k_1, k_1 < 0$) or saddle ($k_g < 0$) form. To extract the crown boundaries, the curvature along the slope direction (k_s) can represent the form and sudden changes on the CHM data. Figure 50 shows an image-based canopy height model generated from SGM algorithm and the derived curvature values along the slope (ArcGIS 10.1). As can be seen, in addition to separating the tree areas from the ground surface, the abrupt changes in different tree heights can also be used recognise the tree groups in different ages.

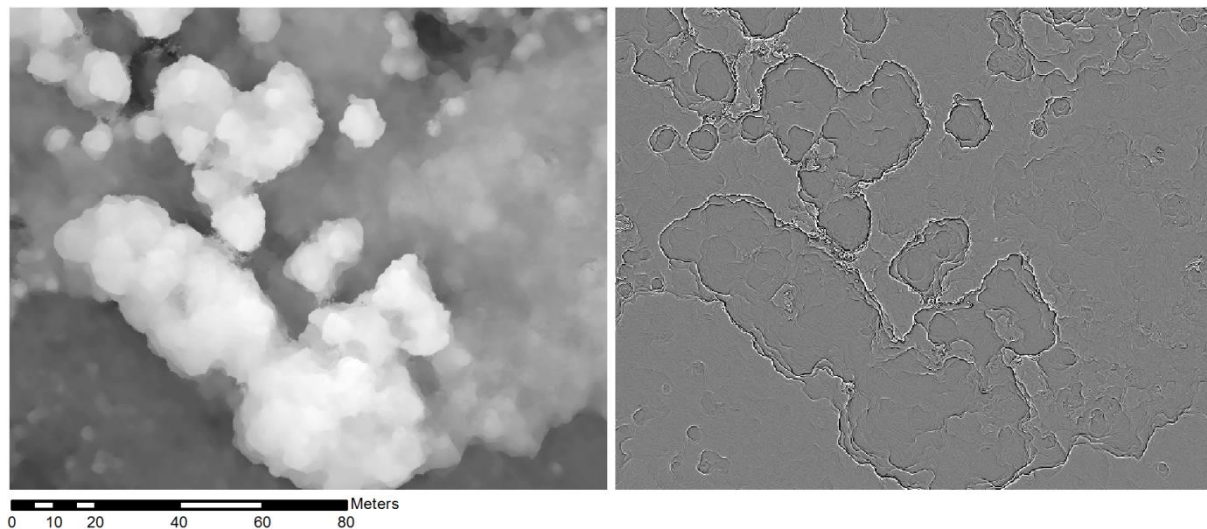


Figure 50: Image-based nDSM (left) and its curvature along the slope (right) of a mixed forest area

In laser-based canopy height models (Figure 51), the locally dominant trees can be recognized in k_s images although, the heterogeneity of these lines, specifically near to the boundary of tree groups in the same age, confirms the demand on filtering the LIDAR data, without changing the crown shape.

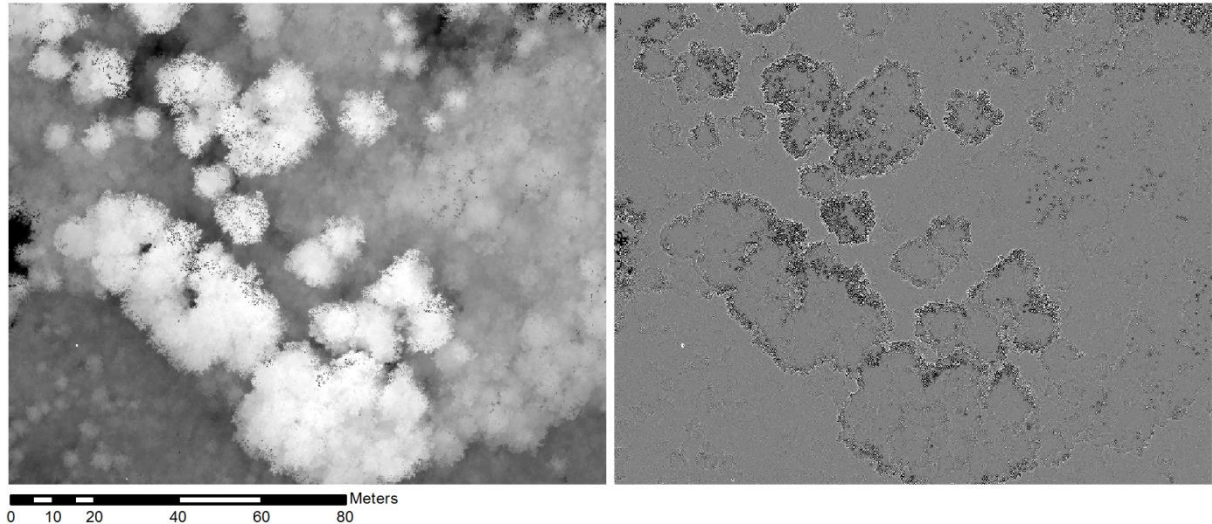


Figure 51: Laser-based nDSM (left) and its curvature profile (right) of a mixed forest area

As well as other edge-detection methods, the edge pixels do not produce continuous lines to partition the image [Hanbury 2008]. Due to the complexity of the geometry of the boundaries, in this thesis, this layer will be combined with region-based techniques.

5.4. Morphological Analysis

To determine the geometric structure of the canopy surface in a quantitative way, morphological functions can be employed. The concept of such functions is originally for 2D binary images to extract predefined geometric objects. According to [Andersen et al. 2001] the goal of any morphological operation is:

“... to gain information relating to the geometric structure of an image by probing the image with another set of specified size and shape, known as a structuring element.... In formal terms, a morphological operation is an image transformation with the structuring element serving as the parameter for the transformation.”

Such structures can be used for 3D grayscale images, in which the gray values represent the form of the object in the third dimension. The four important morphological operations are *dilation*, *erosion*, *opening* and *closing*. According to the theory of sets, detailed mathematic terms of these operations are described in [Soille 2003] and [Andersen et al. 2001]. Assuming set A as the entire image and set B as a smaller set of structuring elements both from an Euclidian d -dimensional of the real space (R), the relative morphological operations are shown below:

$$\text{Dilation: } A \oplus B = \{c \in R^d \mid c = a + b \text{ for some } a \in A \ \& \ b \in B\}$$

$$\text{Erosion: } A \ominus B = \{x \in R^d \mid x + b \in A \text{ for every } b \in B\}$$

In image-processing, the opening and closing operations are combinations of dilation and erosion. With definitions of *addition* and *subtraction* operations of Minowski from [Young et al. 2007] for $\tilde{B} = \{-b \mid b \in B\}$, the 2D operation of the dilation and erosion can be defined.

$$\text{Addition: } A \oplus B = \cup_{b \in B}(A + b)$$

$$\text{Subtraction: } A \ominus B = \cap_{b \in B}(A + b)$$

$$\text{Dilation: } D(A, B) = A \oplus B = \cup_{b \in B}(A + b)$$

$$\text{Erosion: } E(A, B) = A \ominus \tilde{B} = \cap_{b \in B}(A - b)$$

Commutative, non-commutative, associative, translation invariance and duality are the main properties of these operations which are detailed in [Young et al. 2007]. In practice, dilation and erosion are used together forming the opening and closing operations:

$$\text{Opening: } O(A, B) = A \circ B = D(E(A, B), B)$$

$$\text{Closing: } C(A, B) = A \bullet B = E(D(A, \tilde{B}), \tilde{B})$$

For example, an erosion followed by a dilation makes up the morphological operation opening. Figure 52 shows an object, reshaped by morphological operations.

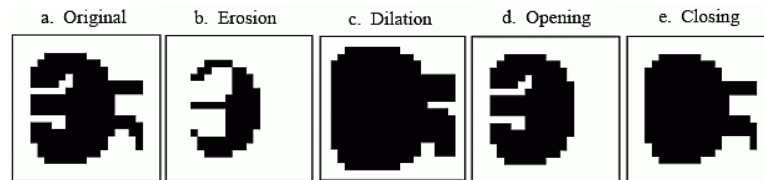


Figure 52: Morphological operations on an object in a binary image space [Smith and Scientist 1999]

In image-processing, the dilation is used for region growing, filling, and expansion of an image object, whereas the erosion is implemented for shrinking, reducing or thinning purposes to extract the skeleton of the object. For an efficient reshaping of image objects, the opening and closing operations can be used for the refinement of final objects with removing the irrelevant parts (sharp concave or convex edges, noise and holes). The standard forms of the structural elements are defined with 4 and 8 neighborhood objects. Additional to the two dimensional binary images, in the third dimension, the geometric analysis of image objects can be performed by the gray level values of each pixel. This means, the subset B can be defined in the 3rd dimension using the gray values as height data.

In single tree delineation, analysis of the crown boundaries can be evaluated like the binary images in two dimensions, however the form of the tree crown can be analyzed with 3D structural elements. Looking at a profile of a tree, Figure 53 shows the effect of two 3D morphological operations on the 3rd dimension. The dilation and erosion operations are implemented running a spherical structural element on the 3D model of the crown.

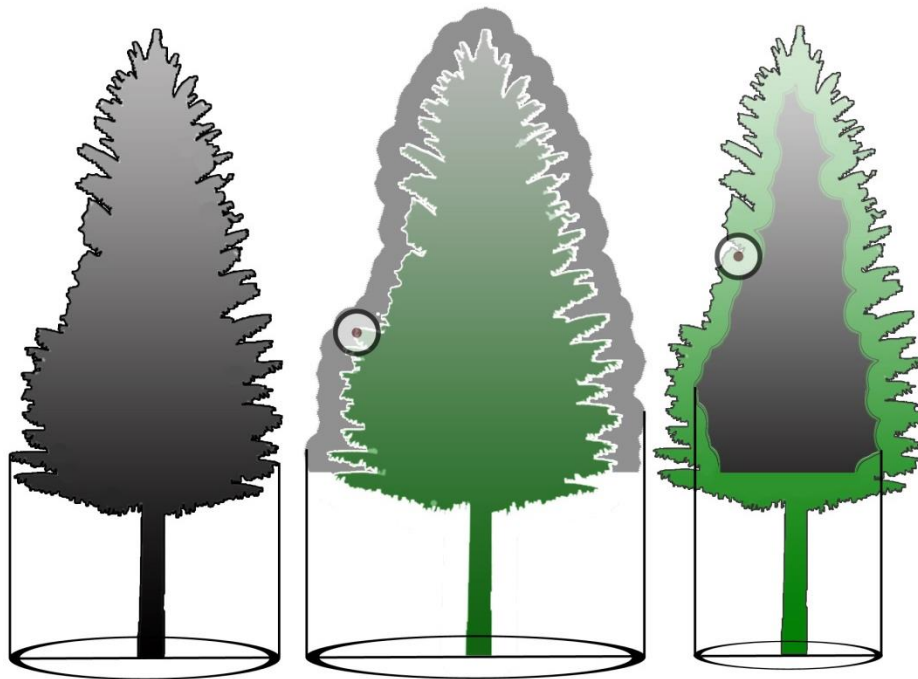


Figure 53: Profile of a tree height model (left) after dilation (middle) and erosion (right) with a spherical structural element

As can be seen, these operations affect the two significant elements of the tree structure in CHM models; crown projection (crown width) and tree height (crown length). As a consequence, one can say that the morphological operations influence the scale space of the image in a non-linear form. In other words, an advanced erosion operator can be used for extracting the tree positions as seed points. As the dilation operator changes the crown boundary, a supervised workflow is needed, in which the opening and closing operations can control the reshaping of the crown structure.

5.5. Marble-Rolling segmentation

The main geometric assumption in 2D structuring elements is the circular form of the crown projection (see section 4.4). To model the growth form of the tree in the third dimension the crown model is assumed as having an elliptical shape [Pollock 1996], [Straub 2003]. In reality, due to the irregular form of tree crowns, defining a single model for even a particular forest type needs additional assumptions like vitality (e.g. vegetation indices) to be obtained from the spectral channels [Straub 2003]. In this way, an adequate contrast between the trees and the environmental objects (ground, asphalt, buildings, etc.) improves the efficiency of these methods.

The question is how to reach the tree positions without such information, while only using the height data.

In this chapter, a novel approach, called *Marble-Rolling (MR)*, will be introduced. This method is independent from the spectral information and is based only on the geometric form of the tree crown in digital surface models. For this, the flat circular structural element (disk) in [Andersen et al. 2001] will be developed in the third dimension, transforming into marble (spherical) forms as the morphological objects⁸. The probable positions of the trees are extracted based on the projection of these marbles. To aid understanding, the concept of this method will now be explained. Imagine an inverted grayscale image with basins as demonstrated in Figure 54. Then, try to roll several marbles with a unique size into the basins until they find their fixed positions.

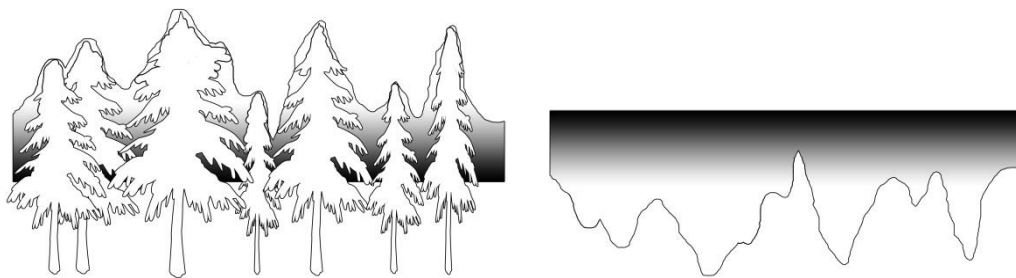


Figure 54: Profile of a tree height model with a ground threshold (left) and the inverted one (right)

Each marble will project a circle on the XY plane from its most fitted parts to demonstrate the probable position of the tree peak point in this scale space. The projection image will be saved in a binary image layer as the first probability image of the tree positions. This step will be repeated with bigger marble sizes (Figure 55) to create a multi-layer scale space. The main idea in this method is that, the side branches of a tree can be automatically removed. If an already detected tree position in fine scales is not repeatedly detected by other marbles, this will not be considered as the tree top, but as a false neighboring branch. Therefore such positions can be automatically removed in the coarser scale spaces (larger marbles). The advantage of this method is that it does

⁸ In this thesis, the extraction of marble projections layers is a function of a surface analysis tool (FEATsurf), developed by the author in the Graphical User Interface (GUI) of the software MATLAB (see Appendix 2 und Appendix 3). For this function the sphere structuring element in MATLAB is used.

not need a height threshold. Therefore, even very small neighboring trees in lower elevations will be detected.

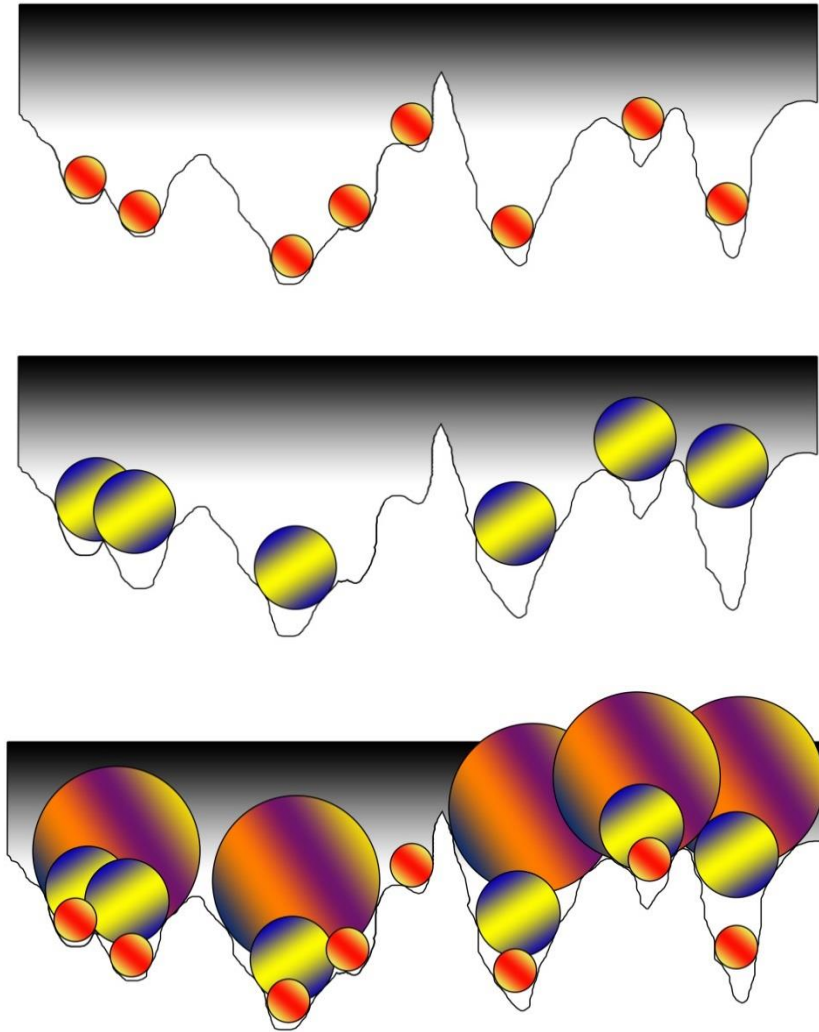


Figure 55: Marble rolling with different marble sizes (top and middle) and combined format

To set the size of the marbles the linear relationship between the crown width and the DBH is calculated by:

$$CW = a_0 + a_1(\bar{d})$$

where \bar{d} denotes an average value for DBH in the stand. According to the forest parameters, defined in the forest management book at the University of Goettingen in Germany [von Gadow

2005], the equation can be defined individually for deciduous and coniferous trees in different forms. For example for spruce and beech stands the following formulas can be used.

$$CW_{Spruce} = 1.64 + 0.14(\bar{d})$$

$$CW_{Beech} = 1.39 + 0.18(\bar{d})$$

To design these marbles into a raster format, the round form of a sphere should be transformed into voxels. Depending on the resolution of the dataset and the size of the image objects the precision of the voxel spheres can be defined (Figure 56).

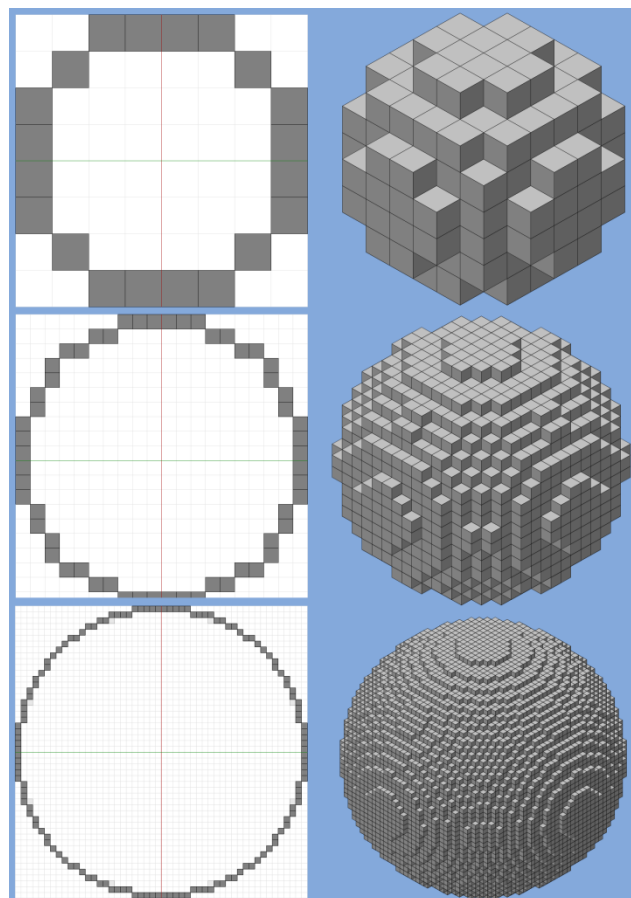


Figure 56: The voxel spheres⁹ in 2D (left) and 3D (right) with diameters of 8 pixels (top) 20 pixels (middle) and 50 pixels (bottom)

After rolling the marbles (moving the voxelized spheres) on the height data, the projection layers will be extracted in binary images (Figure 57).

⁹ The voxels are generated using the online tool *plotz* (www.plotz.co.uk).

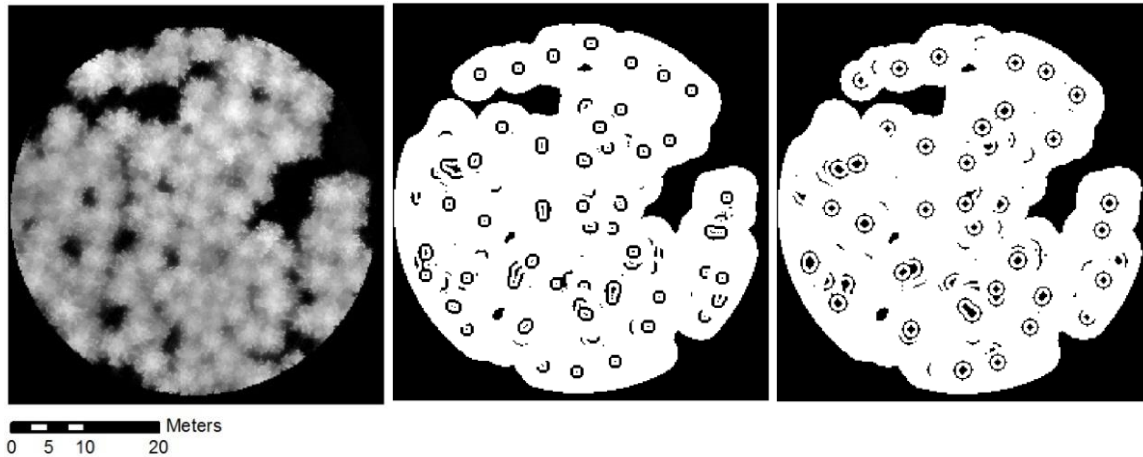


Figure 57: Binary images of the 3D marbles with 2m and 3m radius in a coniferous stand

It should be emphasized, that this method provides the seed layers (in this case they are not called seed points anymore) required for the region growing steps. This decision is taken because each peak point on the tree top might not necessarily be the highest point of the tree. To get the top level segment of a tree, a relative portion of the highest level from the tree crown is required [Miri et al. 2013]. That means the size of the marbles is dependent on the tree geometry. The difference in geometric characteristics of coniferous and deciduous stands leads to different grouping of the marbles. For coniferous stands, the workflow can start with smaller marbles than for deciduous ones. Furthermore, the conic form of these tree types shows more changes in marble images from small to bigger sizes, whereas, the deciduous stands show less necessity to work with different marble sizes. As a solution, based on the tree type, the projection layers are also weighted during the segmentation steps.

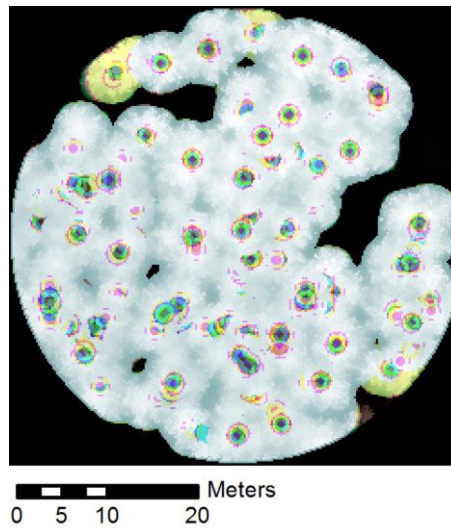


Figure 58: Multi-layer demonstration of the structural elements for three marble sizes

To extract the top portion of the crown surface, the marble projection layers can be extracted and weighted (between 0.0-1.0) through object-oriented with multi-layer segmentation methods. In coniferous stands the weighting value of small marbles, as the top point of the tree, is to be set near to one, whereas the bigger layers get less weighting values.

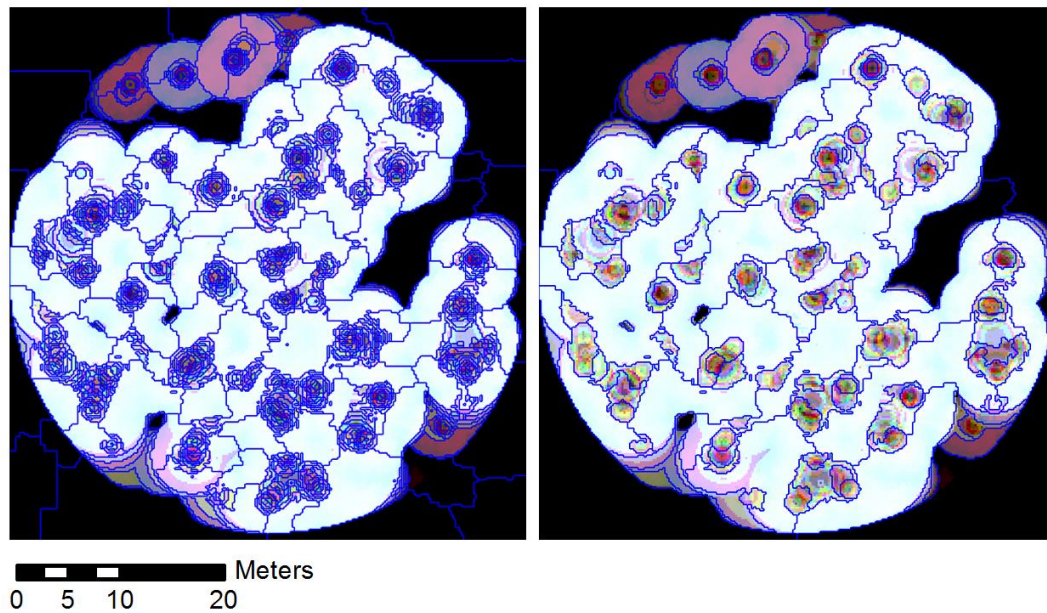


Figure 59: Multiresolution segmentation of marble layers of a coniferous stand in eCognition with parameters: shape 0.1, compactness 0.5 and scales 10 (left) and 50 (right). Marble layers are weighted from 0.0 to 1.0 with 0.1 intervals

In the case of deciduous stands, the weighting value on the smaller marbles should be less than the bigger ones. This is because the deciduous trees might have more than one local maximum on their crown surface.

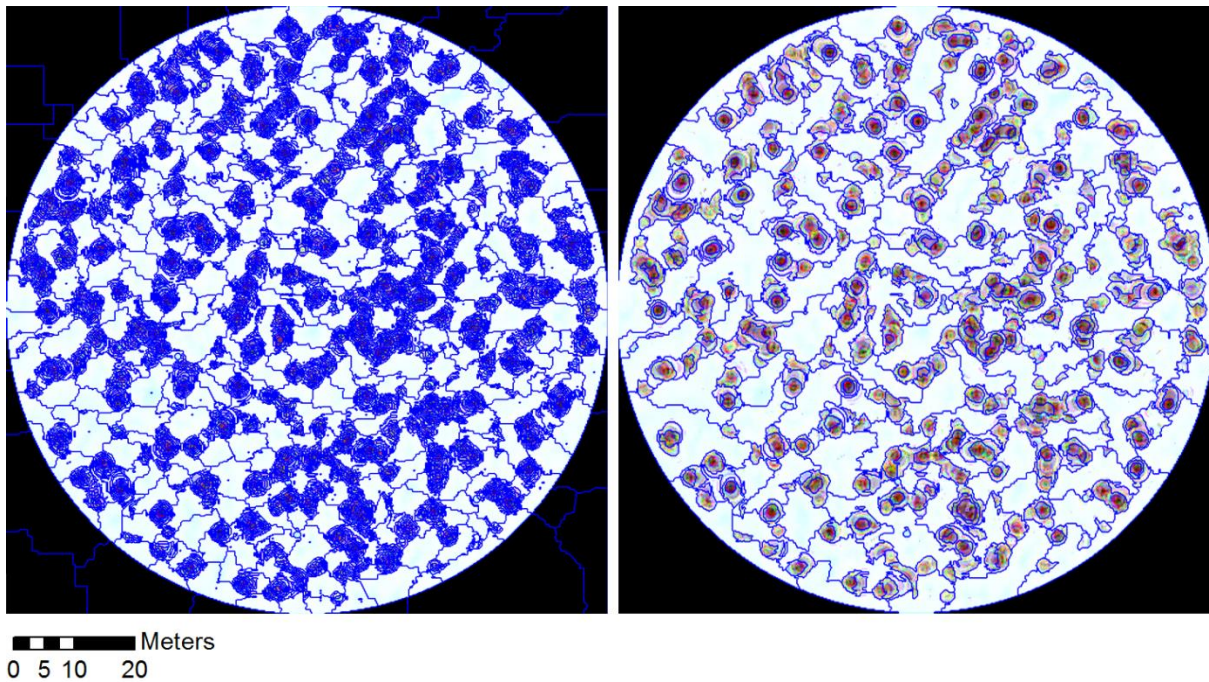


Figure 60: Multiresolution segmentation of marble layers of a deciduous stand in eCognition with parameters: shape 0.1, compactness 0.5 and scales 10 (left) and 50 (right). Marble layers have the same weighing value of one

Figure 61 and Figure 62 show the results of multiscale segmentation of marble layers with sizes from 1 to 9 pixels (radiuses between 0.2 – 1.8 m) for laser-based and image-based plot data. The segmentation is performed in two scales (10 and 50). Compared to the segmentation results in Figure 59 the tree tops are more accurately recognized than in the case using marble layers with 10 - 20 pixel radii.

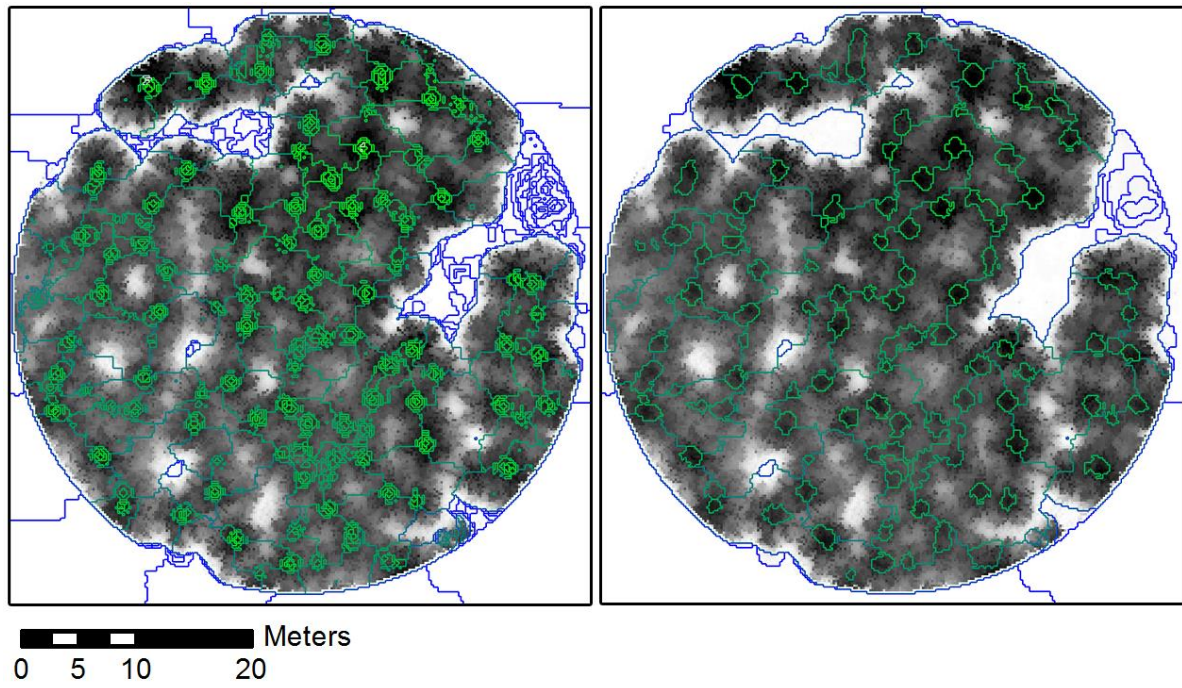


Figure 61: Multiresolution segmentation of marble layers of a laser-based nDSM of a coniferous stand before (left) and after (right) merging the marble segments

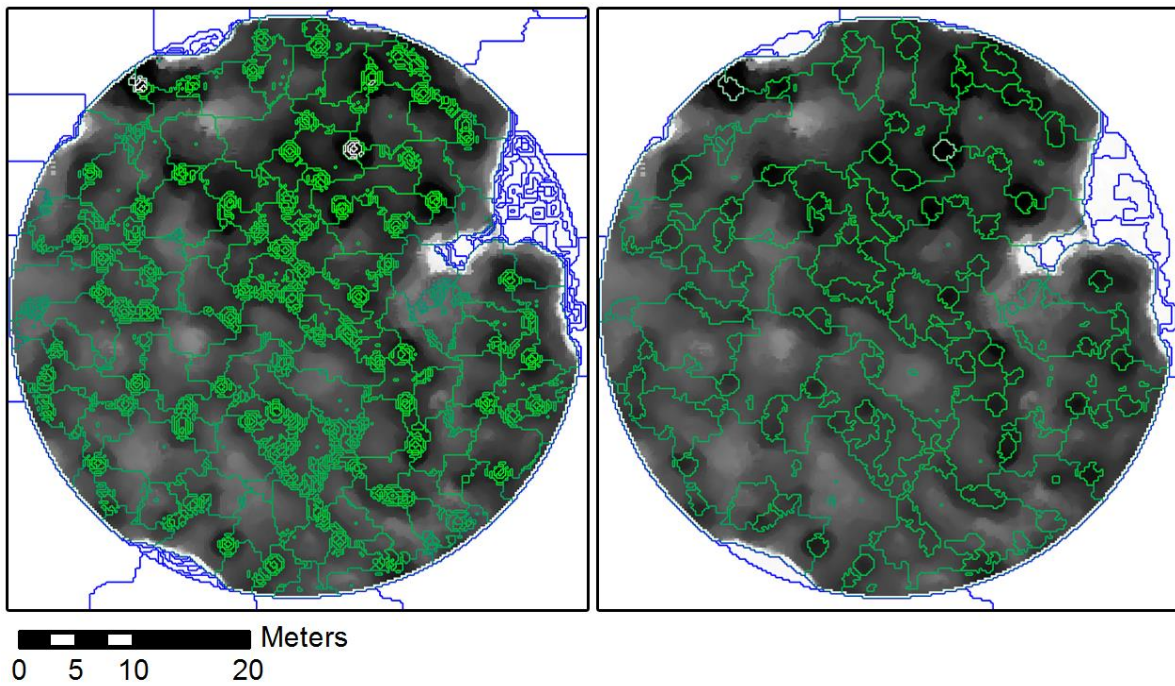


Figure 62: Multiresolution segmentation of marble layers of an image-based nDSM of a coniferous stand before (left) and after (right) merging the marble segments

A comparison between these two datasets demonstrates that the laser data distinguish the top level of the crown more accurately than the image-based data. As well as the black colors of the projection areas in the marble layers, the inverted nDSM has also lower (darker) grey values in higher elevations. One might decide to apply the inverted image as a weighting parameter for segmentation of these layers. However, this decision is dependent on the segmentation algorithm. Employing the nDSM values lead to small segments in the regions between the tree tops. This might make the refinement procedure a challenging situation (for example for merging based on *Area*).

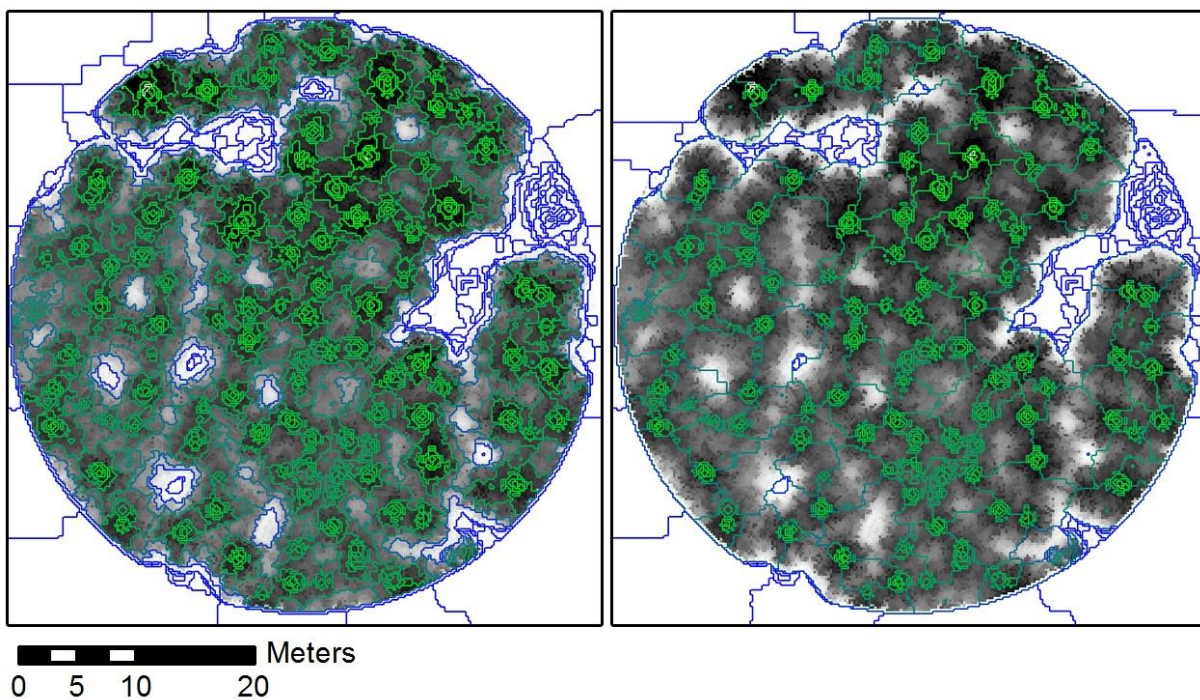


Figure 63: Multiresolution segmentation of marble layers on a laser-based nDSM of coniferous stand in eCognition. Inversed nDSM is involved (left) and is not involved (right) as weighting values

Another application of the marble rolling method, specifically for coniferous stands, is to define the orientation of single trees such as inclination (β) and the azimuth of inclination (α), which can be calculated from the position of the largest and smallest marbles (Figure 64). These features can be used in investigation of the influence of wind, sun and topography on the growth direction of the trees. However, this study is beyond the scope of this research.

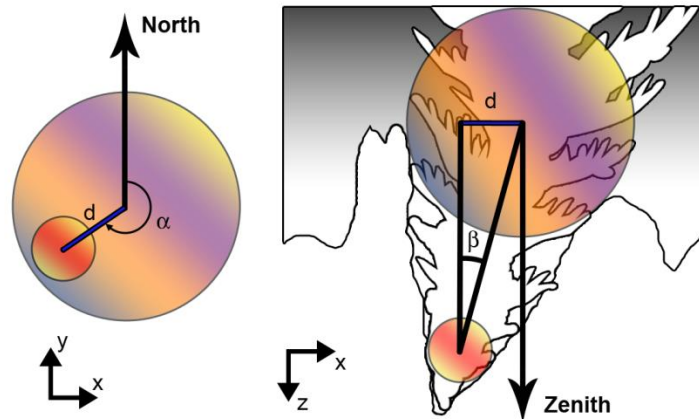


Figure 64: Definition of amount and direction of tree inclination using marble rolling layers

5.6. Region growing

The importance of region growing algorithms for the estimation of different types of tree heights, e.g. mean height and top height, is emphasized in [Laar and Akça 2007]. By definition, region growing is a segmentation method to partition the image by clustering the pixels, starting from a limited number of pixels [Batz and Schäpe 2000], called seed points or seed objects.

For region growing algorithms in forestry, seed objects are the first and most challenging issue. In the case of the delineation of tree areas, they can be obtained from local maxima or the points with highest illumination (usually based on spectral data). On the other hand, the non-tree areas are mostly defined as the ground or low vegetation, mostly defined by a height threshold or local minima in valley following techniques [Gougeon 1998]. Extracting these areas in dense forests is a challenging approach, which can be solved by region growing techniques. In this thesis, for both cases, appropriate seed objects are provided to be used for growing from tree and non-tree regions to each other. The purpose of region growing in this methodology is to distinguish the *tree regions* and separate them from the *non-tree* areas. To achieve this aim, two strategies are implemented:

- Growing the seed objects of the non-tree areas (boundaries), to define the stand borders
- Growing the seed objects of the tree regions (marble projections) to the non-tree areas

5.6.1. Region growing of non-tree areas

Delineation of the non-forested areas is a defining issue to border the tree stand. One of these methods is valley following, developed and introduced by [Gougeon 1998]. In this method, the gaps between trees are found by finding a local minimum and growing to reach the stand boundaries. The main problematic question in the method of Gougeon is the limiting value of region growing. In most cases a height threshold value is defined (Figure 65). All the objects over the threshold value are categorized as tree areas. The further steps, e.g. region growing of single trees, will be implemented on these remaining island segments. The critical point is that, due to the complex geometry of tree crowns in forests, defining only one threshold value leads to classifying some small trees as low vegetation or non-tree classes. The decisive solution lies in recognition of the tree boundaries at the early steps. Defining such separating areas can control the resizing algorithm.

In contrast to [Gougeon 1998], a new aspect in this thesis is developed which is growing the non-tree areas from the tree boundaries. This method has an advantage to the valley following technique, in so far as the limiting value (stand boundary) is already equal to the seed objects.

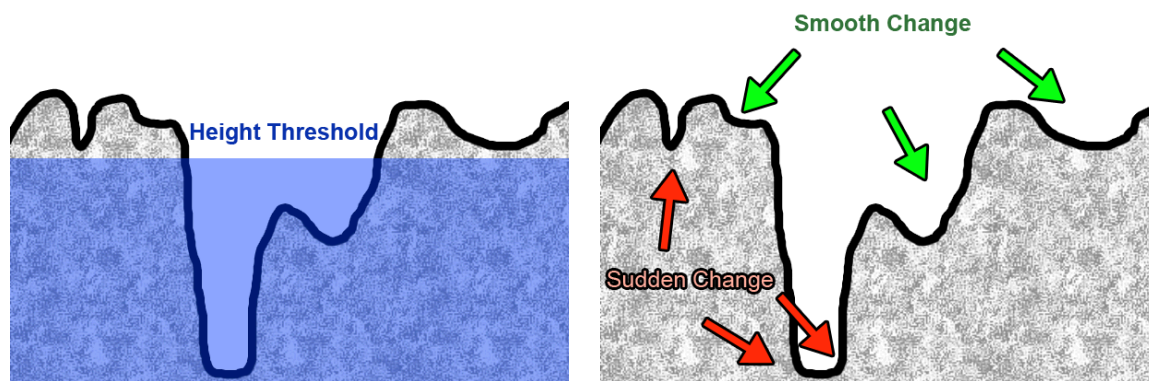


Figure 65: Definition of growing limits with setting height threshold (left) and recognition of changes in curvature values (right)

For this, the curvature image of the height data is implemented (see section 5.3). The curvature profile layer, which is provided in software ArcGIS v.10.1, shows the sudden changes on the surface model. Figure 66 demonstrates these layers for laser and image based nDSM.

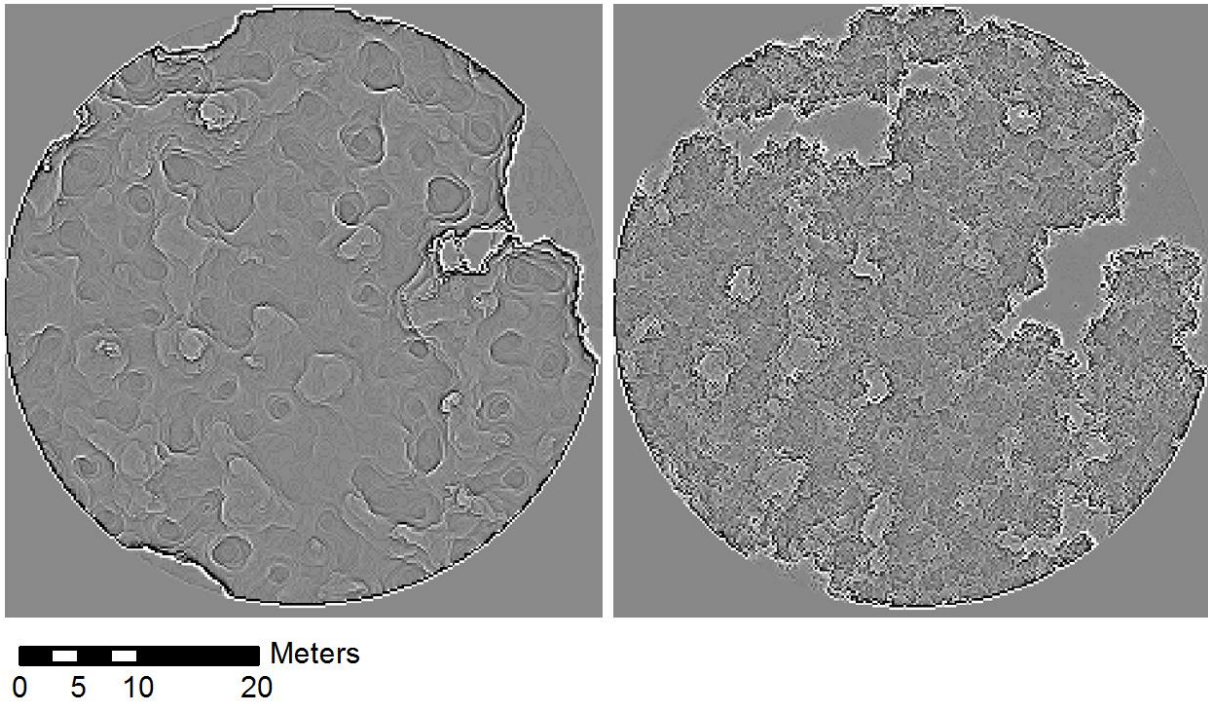


Figure 66: Curvature profiles of image-based and laser-based nDSM in a coniferous stand

Due to the different characteristics of the laser and image dataset, the curvature lines differ from the point of view of softness and shape. With image-based surface models the curvature profiles are rather smoothed. Whereas in laser datasets the heterogeneity of point cloud on tree crowns makes it difficult to find a closed polygon. However the boundaries, separating the tree areas from the non-tree ones are more ambiguous in image nDSM. In laser surface models, it is easier to separate these two regions. The common issue in both datasets is within the sudden areas, where the higher contrast (the neighboring bright pixels near the dark ones) can help to define a rule-set for recognizing these boundaries. This feature can be defined by calculating the mean pixel value of the outer and the inner boundary of an image object. In software eCognition, the set of all pixels belonging to the inner and outer border pixels of an image object v is defined as followed:

$$P_v^{Inner} = \{(x, y) \in P_v : \exists(x', y') \in N_4(x, y) : (x', y') \notin P_v\}$$

$$P_v^{Outer} = \{(x, y) \notin P_v : \exists(x', y') \in N_4(x, y) : (x', y') \in P_v\}$$

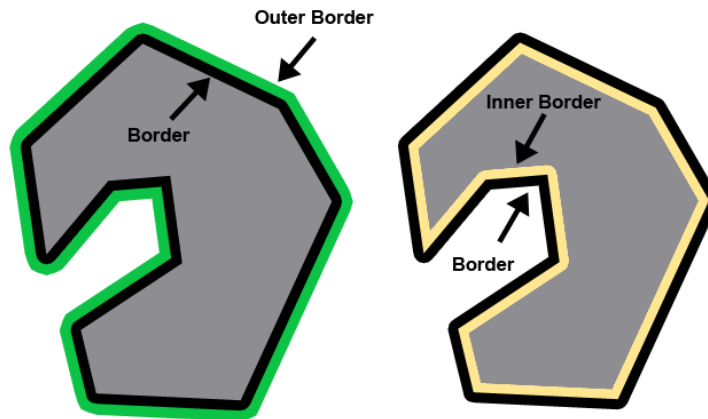


Figure 67: Definition of the inner border and the outer border of a segment

To define the border pixels, the characteristics of the inner and outer borders of image objects can be used. For the pixels along the border areas, the difference between the gray values of outer and inner border in curvature images is more than the threshold value t .

$$P_v^{Border} = \{(x, y) \in P_v : \exists(x', y') \in N_4(x, y) : |P_v^{Outer} - P_v^{Inner}| \geq t_1\}$$

Finding these areas at pixel level might be a challenging task in laser nDSM. This is because even after filtering steps and due to the complex structure of the tree surface, the small points with high variations might be detected as border pixels (Figure 68).

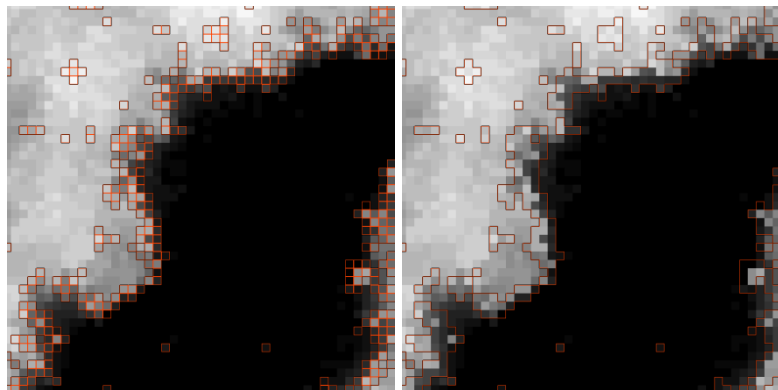


Figure 68: Candidate border pixels (with orange boundaries) based on curvature values before (left) and after (right) merging

The border objects (classified as border in the last step) are kept as seed objects, to start the region growing from the neighboring pixels (inner border) into the non-tree objects (nt).

In this condition, a feature should be defined to possess both neighborhood and height comparison criteria:

$$P_v^{nt} = \{(x, y) \notin P_v : \exists(x', y') \in N_4(x, y) : |z' - \overline{P_v^{Border}}| \leq t_2\}$$

where z' is the height value at (x', y') from the nDSM, and $\overline{P_v^{Border}}$ is the mean height value of the border segment.

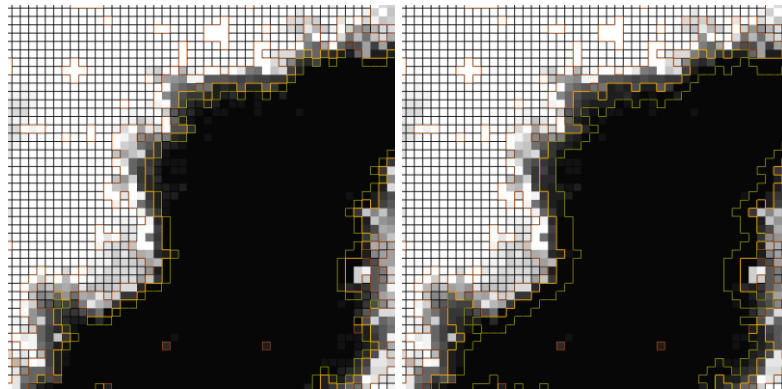


Figure 69: Start of the region growing of the non-tree area (with yellow boundaries) at the first (left) and second (right) growth iteration

From this level of classification, the P_v^{nt} objects grow into the unclassified pixels towards the slope direction of non-tree area (Figure 70) until filling or reaching a border or tree object, represented as island.

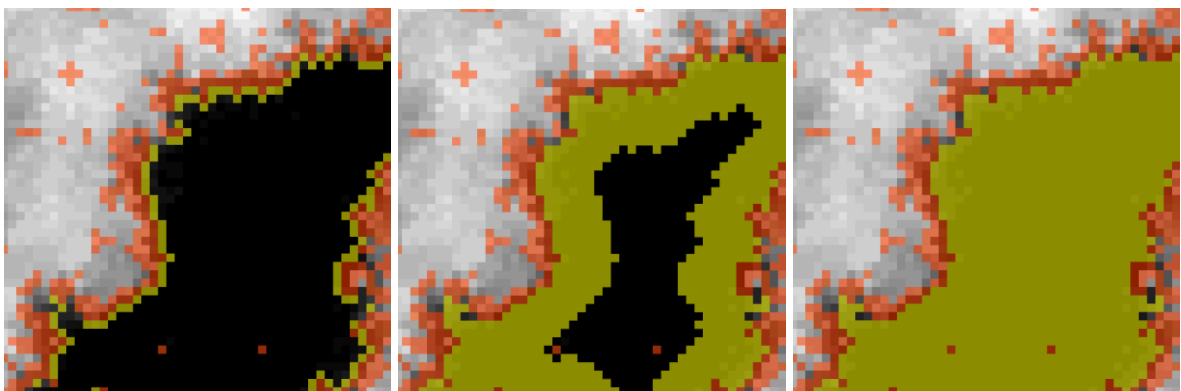


Figure 70: Region growing of the non-tree area (yellow-green) from the first to the last growth iteration

After classifying the non-tree areas (yellow), the border classes (orange) are classified back into the tree areas.

5.6.2. Segmentation refinement of the stand boundary

In segmentation procedures, some irrelevant segments might remain in the destination object space because they could not satisfy the distinguishing conditions. For evaluation of the segmentation results two problems should be taken into account, *oversegmentation* and *undersegmentation*, which can be solved by proper merging or splitting algorithms respectively. In general the oversegmentation is less problematic than the undersegmentation. In other words, a successful segmentation leads to little oversegmentation and no undersegmentation [Castilla and Hay 2008]. The term segmentation *refinement* can be defined as removing or reclassifying these segments to improve the priori results of a segmentation procedure. The refinement should be implemented along the segment borders to reach an exact match of the object boundaries [Iwanowski and Soille 2005] or inside the destination object space to remove the small islands.

In this thesis the destination objects are the single trees, which can be found within the tree areas. However, the refinement of the not-tree areas, e.g. the gaps, is needed before. This is because the boundary of not-tree areas defines the outer limits of region growing of the single trees in the stand. Removing the concave gaps at the higher elevations, detection of the small segments enclosed by the tree and not-tree classes, as well as false edges at borders are the main tasks in this phase (Figure 71).

After defining the not-tree regions, the remaining regions are to be used for marble rolling algorithm. It should be mentioned that the order of region growing and marble rolling is dependent on the user. For detection of very small trees or lower vegetation, region growing can be implemented after marble rolling.

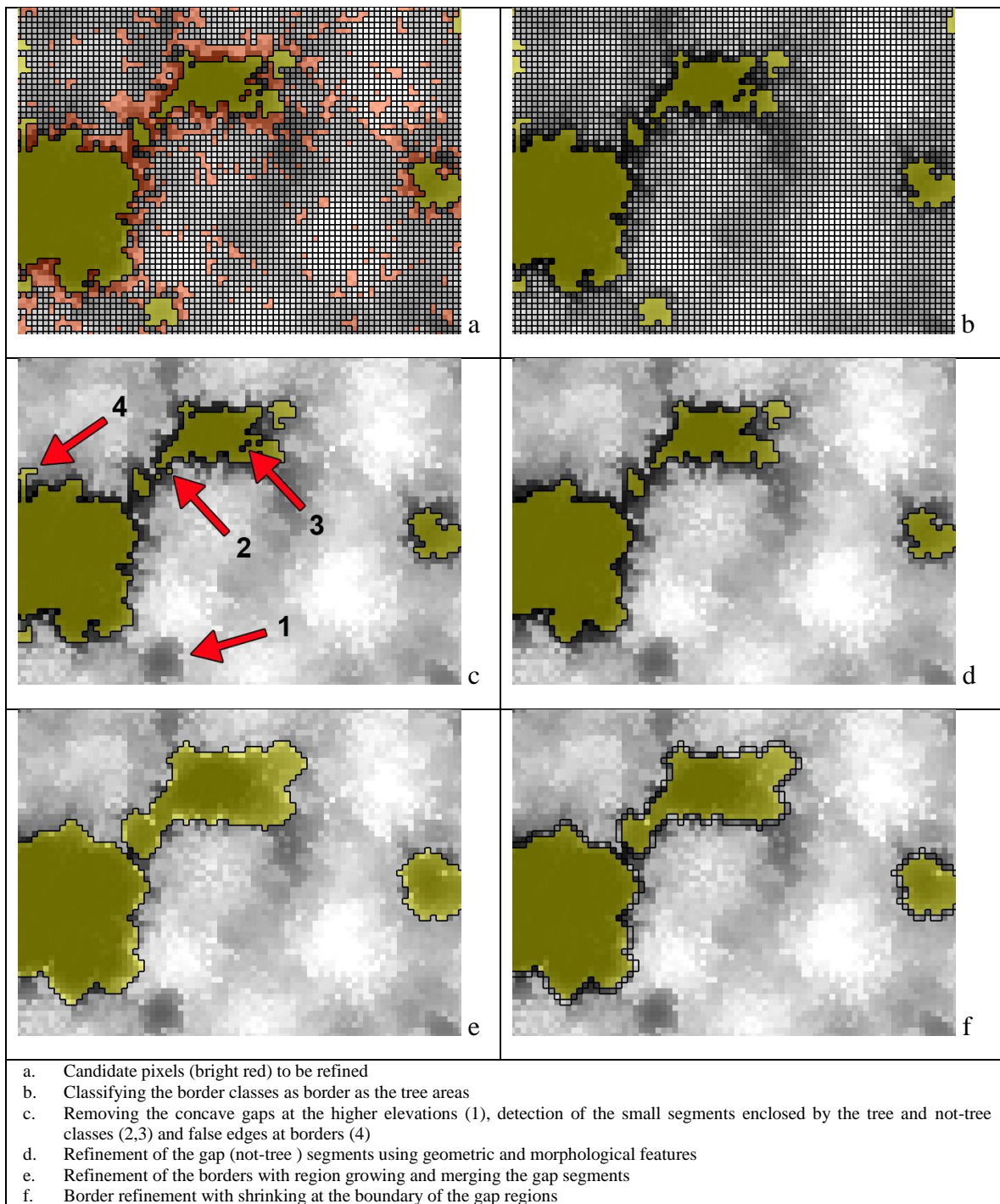


Figure 71: Segmentation refinement of the not-tree area in a laser-based nDSM

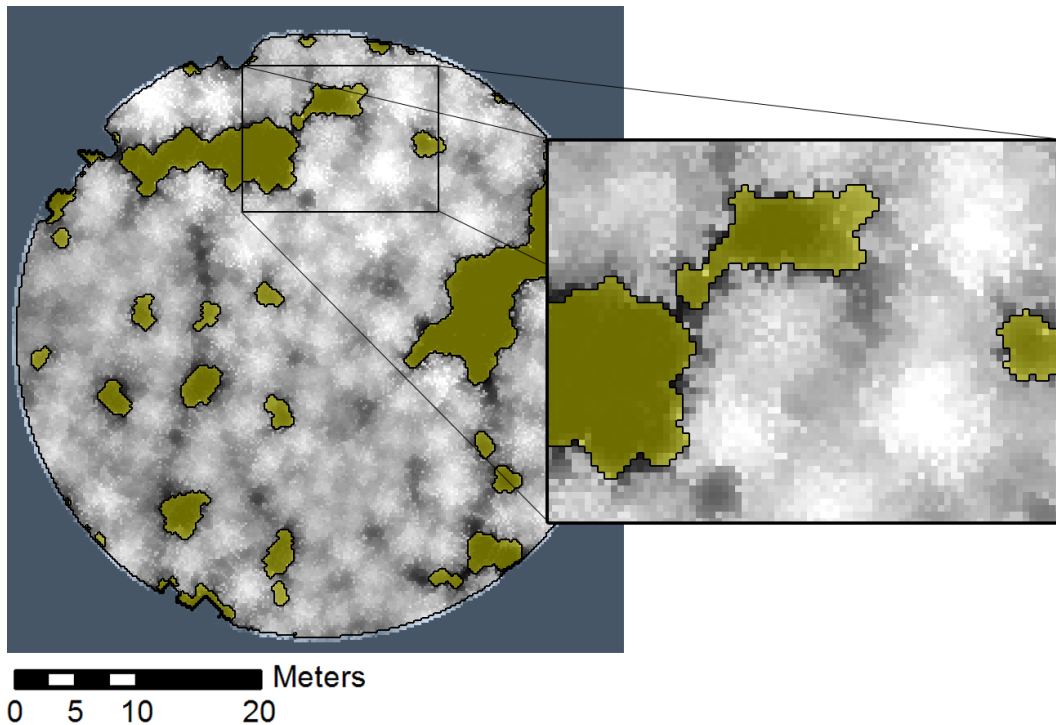


Figure 72: Final result of the segmentation refinement of the not-tree areas (yellow) in a laser-based nDSM of a coniferous stand

5.6.3. Region growing of single trees

Due to the smooth variation of the tree heights at the upper part of the canopy, the border of the tree regions in digital elevation models can be defined by reference to the changes in curvature or the second derivative values. For single trees in urban areas, this can arise if sudden changes in elevation between the tree crown surface and the manmade objects (e.g. street, yard) occur. Separating the trees from the objects with near height values (e.g. neighboring buildings) can be implemented on the basis of the sudden changes in textural characteristics of the homogeneity of the surface, like the standard deviation of the height values on the surfaces. In dense forests, setting these features is a challenging approach.

In recent research, separating the single trees in the 3D space is based on the point cloud clustering, taking account of the characteristics of the implemented sensor. In hyper-spectral remote sensors, the reflectance characteristics are used to classify the tree regions. For LIDAR data, the Full-Wave-Form (FWF) analysis is one of the main approaches for classification of the point clouds. Based on the wave form of the return pulses, the characteristics of the target surface

can be analyzed to detect if it is ground, trunk, branch or leaf surface of a tree. However such analysis is beyond the scope of this research.

According to [Miri et al. 2013] the most reliable part of the surface models, specifically in image based datasets, are the tree regions at the highest levels of elevation which should be chosen for region growing of the CHM data. At this level, without considering the wave form or spectral analysis of the tree species, the canopy surfaces are separated in regions according to the geometric and morphological features over the LIDAR and image-based nDSM.

Region growing of single trees begins with seed objects, which in general are provided by features like local maxima [Solberg et al. 2006]. The critical issues in defining a single point (one pixel in raster form) as a seed point for region growing are:

- The upper parts of the tree crown are considered as similar objects (points) with the same growth conditions.
- Trees with more than one peak (local maxima), i.e. the deciduous trees, will be segmented in more than one tree-region, which requires additional constraints in merging steps.
- Setting the growth conditions at the beginning of the growing algorithm, e.g. height variations, shape and compactness of the tree regions does not satisfy the growth procedure, due to the different environmental conditions for each single tree.

In this thesis, the seed objects on the tree areas are acquired from the segments extracted from the marble-rolling method. Implementation of marble projection segments has the advantage of keeping a bigger slice of the tree top for growing. Compared to the local maxima, this increases the reliability of seed objects. Furthermore the growth procedure can be weighted from the beginning of the region growing. Seed objects, as the initial portions of the tree segment, show the top slices of the trees.

In general, growing algorithms on the 2.5D space focus on the height (gray) values in the rasterized height images. Due to the complicated form of the tree surfaces, the regions extracted from only the height variations might not demonstrate the typical forms of the trees. Figure 73 shows the region growing of the seed objects based on the absolute height changes. In eCognition, the comparison of the currently growing pixel value can be performed using a reference parameter as an absolute value or a variable feature. Predefinition of the reference

segment as an absolute value and its comparison with a threshold for maximum height difference, restricts controlling the shape of the segments during growing the regions.

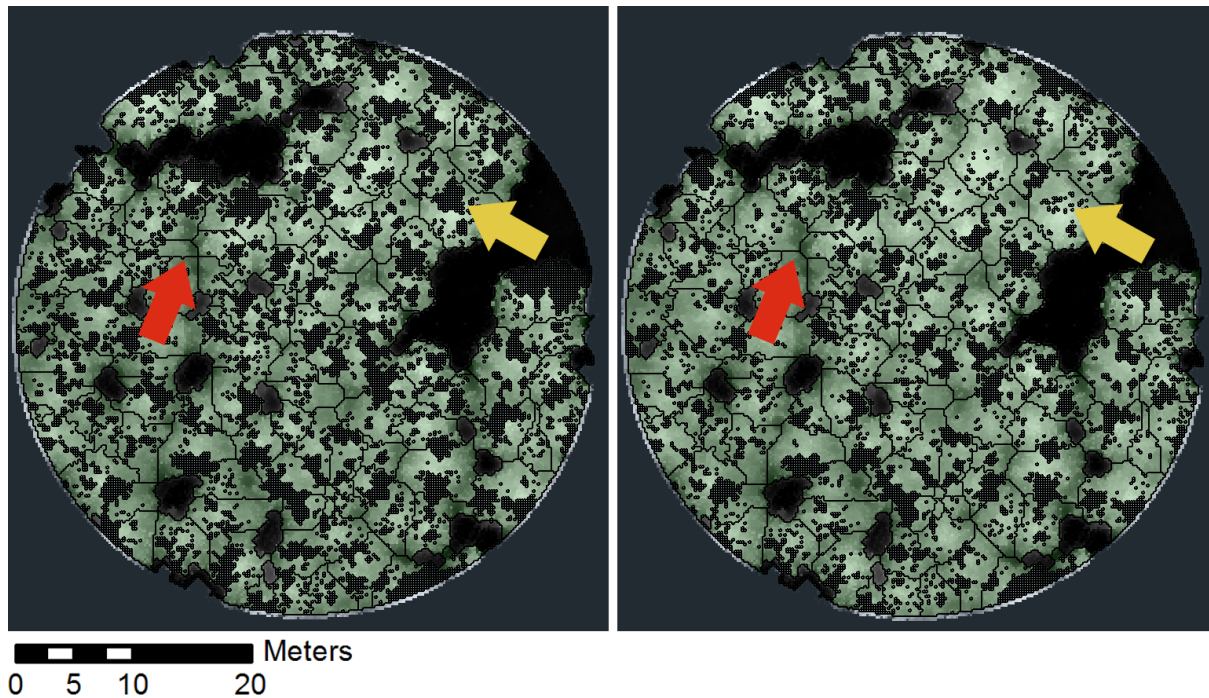


Figure 73: The problem of region growing based on height value of the current growing pixel as absolute reference comparing with the mean height of the inner border pixels (left) or the mean height of the segment (right)

On the other side, region growing, combined with multiresolution segmentation cannot satisfy the geometric form of the trees (Figure 74). This is because the shape and compactness parameters of the segments are based on polygons with a definite geometry. These parameters can be considered if the texture of the objects leads the segment to grow or to stop growing. For example, on the top of buildings, the homogeneity of the slope value (texture-based feature) allows the segment to grow, whereas the sharp and straight lines along the roof edges can stop the growing procedure. In the form of a rule-set, these parameters can be defined by setting the compactness and shape settings of the segmentation at the early steps, followed by textural features [Haralick et al. 1973]. This solution is not applicable for the surface model of trees, because considering the low contrast in textural values on the CHM, there are no sharp edges to define the geometry of the edges. Additionally, trees do not have a predictable and fixed geometry.

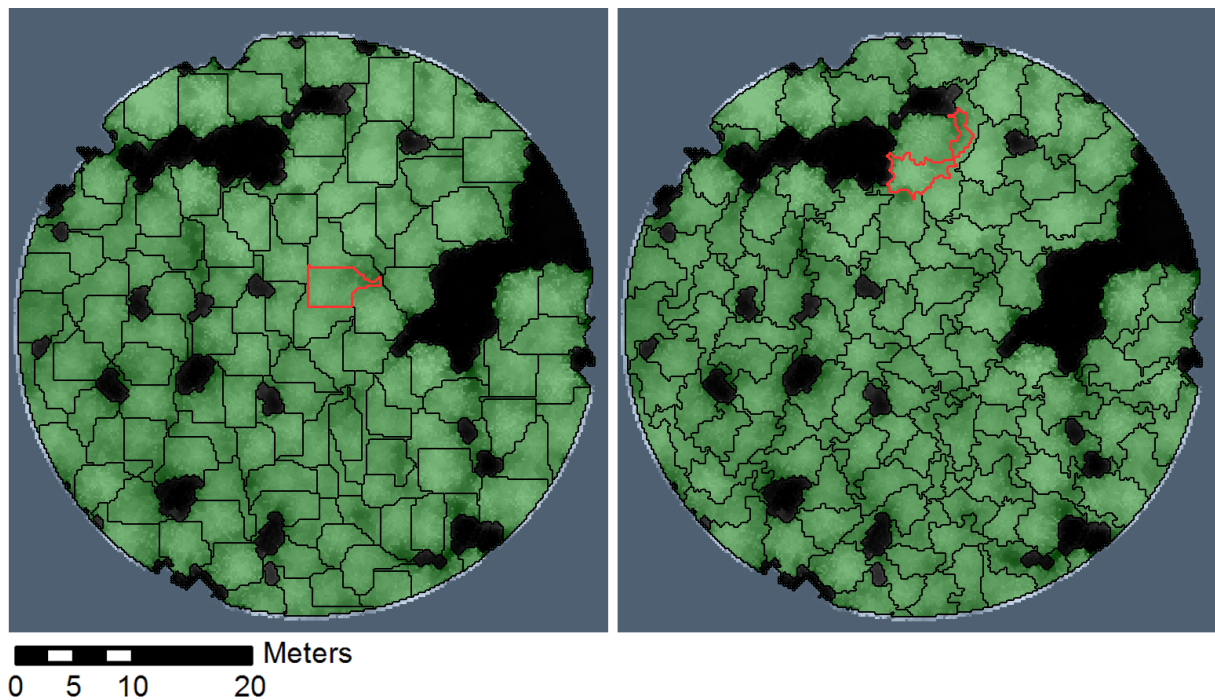


Figure 74: Uncontrolled segmentation of the single trees based on extreme values of compactness (left) and shape (right) parameters leads to wrong region growing of the seed objects

However, in these irregularities, there exist some rules to be set in machine-vision to define a segment as a tree. As a rule-set, a tree might not finally reach a definite geometry during its life in the forest, but it tries to stay in a *balanced* and *stable* form in the competition for growth.

To translate this sentence into the language of machine-vision, a successful region growing algorithm should be able to simulate the growth procedure in an iterative process. Different illumination, terrain height differences, soil quality, etc. might change the growth form of the trees in their competitions in forest areas. Because of that, some geometric and morphologic parameters should be predefined to control the growing form of each segment. In [Bechtel 2007] some hypotheses are defined for the definition of the tree form in region growing algorithms. *Circularity*, *3D convexity*, *symmetry*, *compactness*, *size* and *distance* are the basic prerequisites in region growing algorithms. In nature, a very single tree tries to grow in a round (circular form in 2D horizontal profile) shape. In forest, due to the different environmental conditions, each single tree grows differently. This means defining a circular crown closure (an ideal form of a tree) with the radius obtained from the forest tables (in relation to the height, age and forestall quality grades of the stand) is not the best solution for extracting the tree regions. However these

parameters can be used to control the growth. Size, compactness (the length/width relation), shape index and the ecliptic fit of the segments are the main constraints, which will be investigated for the growth algorithms, in this research.

At the beginning of region growing, evaluating the form parameters is not recommended. Because the small seed objects, which might already have just a cross form containing five pixels, might be removed with circular morphological elements. This means that at least two growth iterations with no refinements are required at the first steps. Setting the size of the Morphological Element (ME) is one of the challenging areas in this work. A big morphological element removes the smaller segments and the small MEs cannot function properly to round the border of the tree segment.

To keep the stability of tree regions, morphological elements in the form of opening are used. The question is the optimal form and size of the morphological element. To round the unstable parts of a segment the circular form of crown projection is chosen. However, a fixed form and size cannot be predefined for all of the trees in the stand. As a solution, a morphology association machine in the form of a rule-set provides a set of morphological elements for different sizes and different growing iterations (Figure 75).

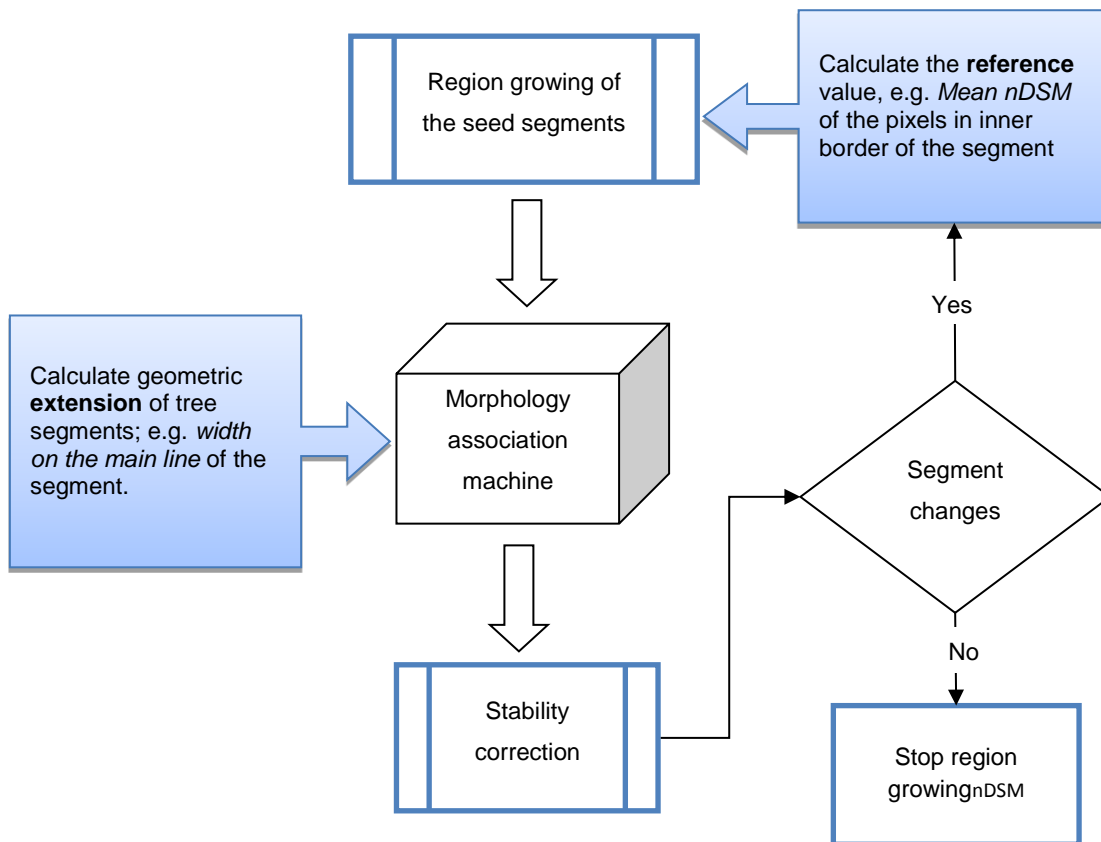


Figure 75: Schema of a supervised region growing model

For comparison, geometric parameters like *Area (size)* are not proper features. Because an unstable segment (a very long segment) might have the same area as the morphological element, which can be removed through the implementation of the ME. In addition, the iterative growing of the seed objects in eight directions leads to reshaping the current tree segments (seed objects for the next iteration) into rhombus forms. Another advantage of using circular MEs is to convert them into a stable shape with round edges.

The optimized size of the ME should be around the maximum width of the segment. There are several types of segment width, depending on the calculation method of the segment shape parameters. In the software eCognition, this value can be calculated in two ways (Figure 76), called *width* (using the bounding box) and *width on the main line*. In the former method a bounding box is defined to calculate the smallest eigenvalues of the segment (the semi-minor of

the approximated ellipse). A more accurate method of defining the shape of the segment is using the approximate polygon, based on the skeleton lines of the image object. In this way the width of the segment will be calculated using the average width along the main line (longer axis) created from a Delaunay triangulation of the polygon [eCognition 2013].

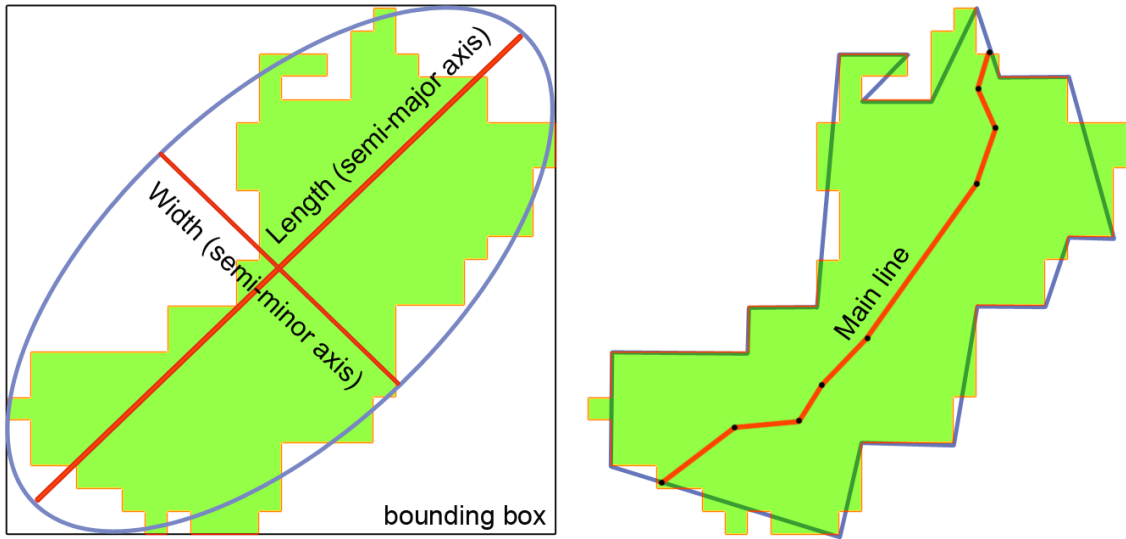


Figure 76: Definitions of the length and width of a segment based on the ellipse parameters in the bounding box (left) or the main line of the skeleton polygon (right)

This value is set as the input of this association machine and classifies the seed objects based on their geometric extension in every growing session. Definition of width values with minimum interval (1 pixel) results in higher flexibility of the allocation process, though this increases the computation time of the morphology allocation. The maximum size of the ME can be calculated based on the forest parameters of the specific tree type. Figure 77 shows different morphological elements (in this case opening masks) defined for different segment widths with one pixel interval. Choosing several ME sizes results in keeping those parts of the segment which have the round form of a tree. If needed, the segment will be separated into more parts to be analyzed with fitting ME in the next iterations.

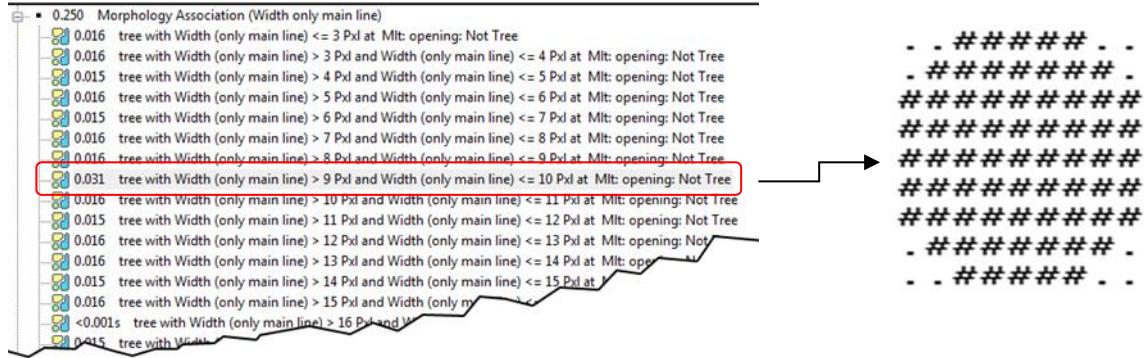


Figure 77: Circular opening elements among the MEs within an allocation rule-set

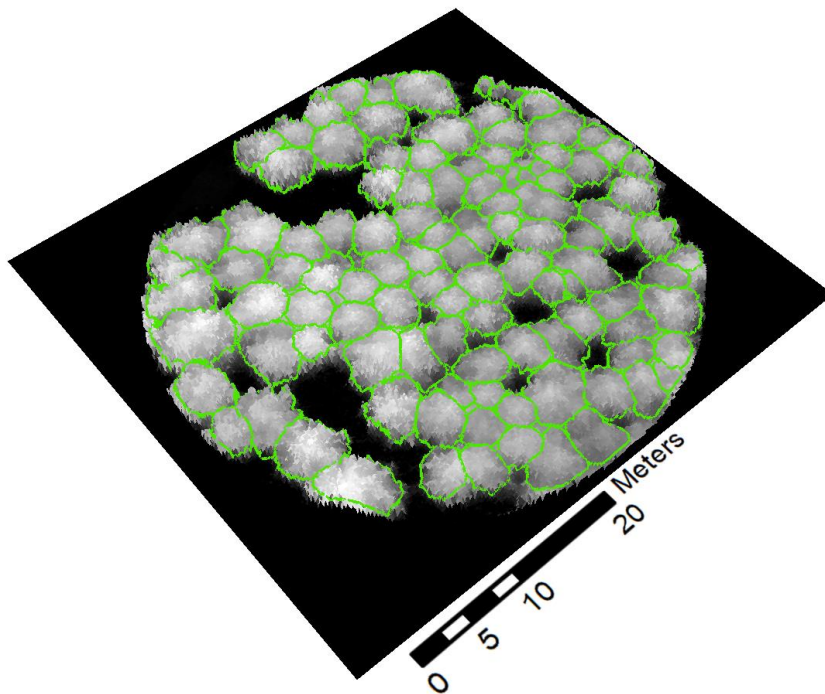


Figure 78: Result of a supervised region growing model on LIDAR-Data (for better demonstration of the regions, the scale at height values is set to 0.1)

As explained in section 5.6.2, the outer limits of the stand are previously delineated from the not-tree areas. Within the stand, the regions will grow under these conditions until their borders reach each other. For the final segmentation results, one might be satisfied to keep working with these segments, leaving the small gaps between trees. Another decision can be taken if the gaps

between the trees should be avoided. For this, the last growing session will be performed without implementation of the morphological elements (Figure 79).

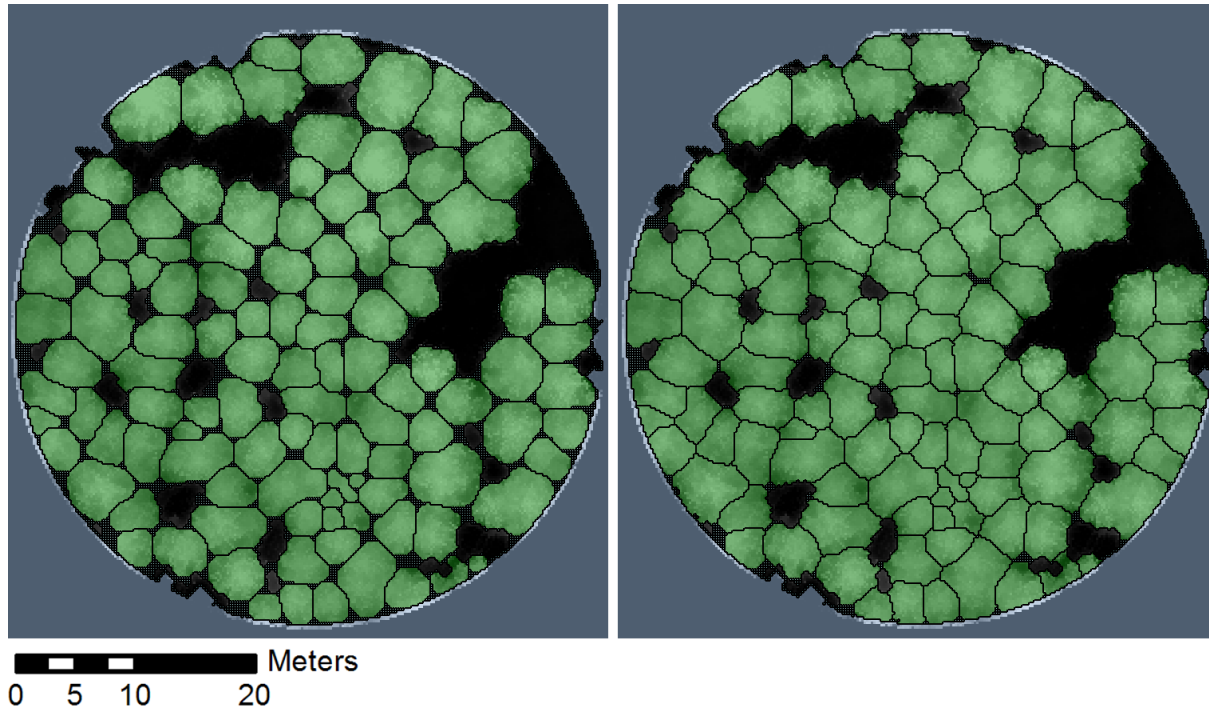


Figure 79: Final segmentation results with the gaps between trees (left) and the extended tree regions without the final implementation of MEs (right)

5.7. Feature-based classification

Due to the different characteristics of the coniferous and deciduous trees the segmentation results vary, depending on the parameters used in the marble rolling procedure. For an efficient segmentation, it is advantageous to define the type of the stand at the initial steps of the segmentation. This increases the consistency of the results. In mixed forests, distinguishing the boundary of the coniferous and deciduous stands from the height data, at the beginning steps is however an impossible task.

In this research, the separation of the tree types occurs after the region growing step. Based on the geometric characteristics of the tree segments, the coniferous and deciduous trees will be separated to improve the classification results.

5.8. Segment geometry

Geometric features provide information about the form and shape of digital surface models at segment level. In this work, such features are mostly concentrated at single tree level. In [Miri et al. 2013] a geometric feature, called Inversed Quasi Flatness (IQF), is introduced which describes the flatness of the trees at the highest elevation of the nDSM. At this level deciduous trees are expected to be flatter than coniferous ones, which yield higher values in IQF. Figure 80 shows the color-coded results of this feature. Comparing the spectral data, the estimations on the laser nDSM show satisfying results for coniferous trees but relatively poor recognition of the deciduous ones. This is mainly due to the small segment size at the top elevation level, which overestimates the IQF. In contrast, the results in the photogrammetric nDSM show relatively good recognition of true segments in deciduous trees.

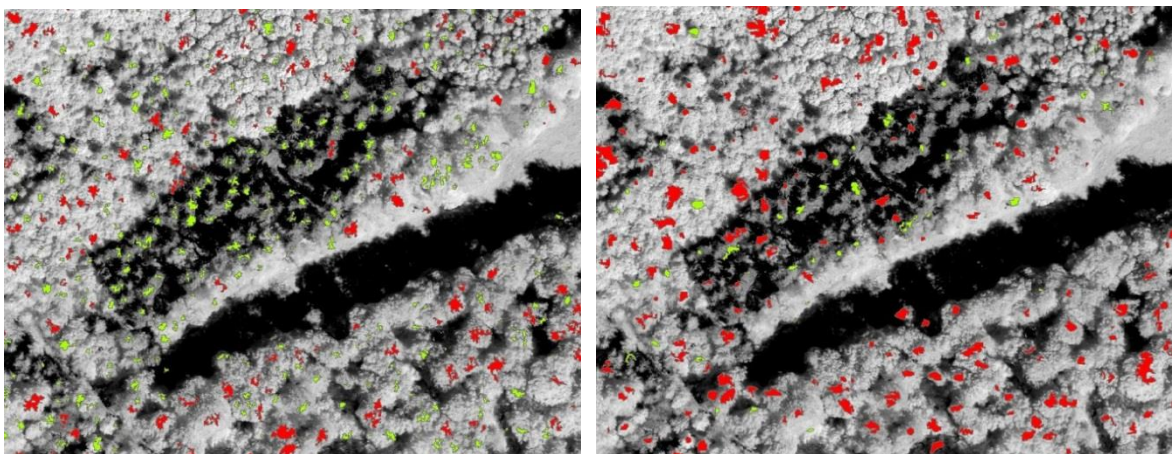


Figure 80: Comparison of IQF on laser-based nDSM (left) and image-based nDSM (right) at low segmentation level for ■ coniferous and ■ deciduous tree types from [Miri et al. 2013]

By nature, the deciduous trees might have more peak points, producing small segments after region growing. Figure 81, demonstrates that for the same plot size, an oversegmented deciduous single tree represents more tree numbers than three correctly segmented coniferous ones.

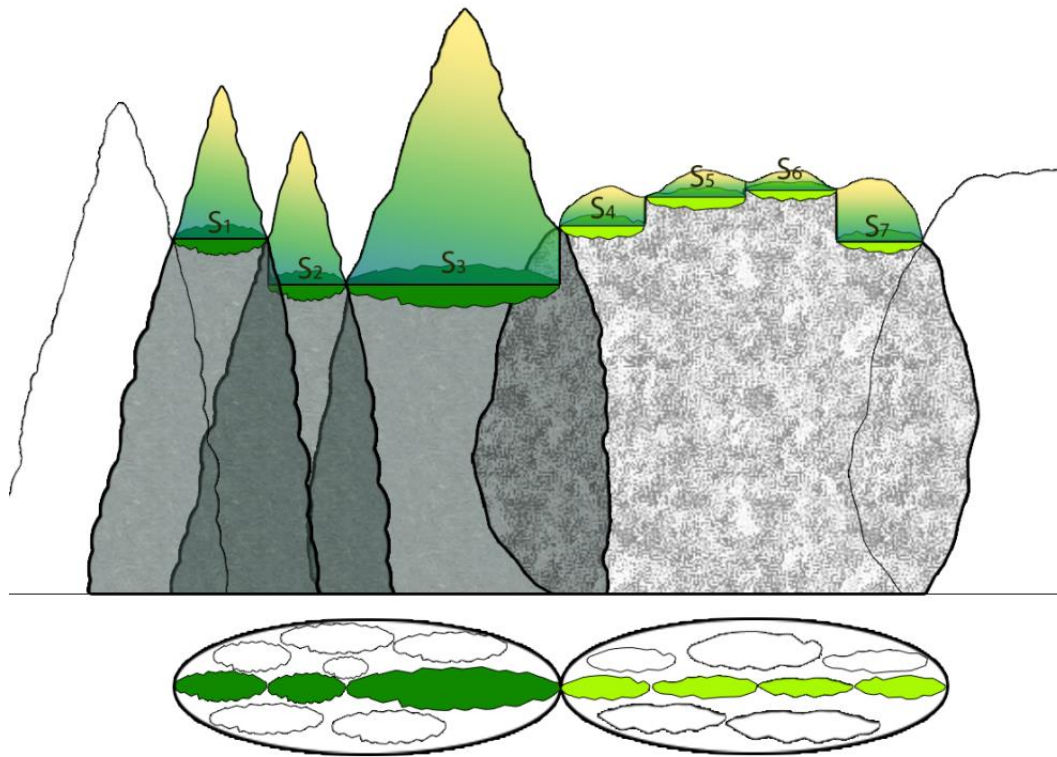


Figure 81: 2D and 3D demonstration of the results of region growing-comparison of the segments in a dense coniferous area (S1 to S3) with a deciduous tree (S4 to S7)

One should consider that the profile of a tree segment in dense forests might not be a horizontally flat plane. Considering the borders of the neighboring trees, there can be an inclination on this surface. This affects the mean value of the height at segment level. To better demonstrate the segment section, Figure 82 shows the relationship of the height values of the pixel within a segment in a 3D form. In the projection of the height data into a 2D segment, the gray values at the inner border of the segment might have a maximum and minimum value (an inclined segment). The mean height of the cutting plane can be calculated from the average of these two values. The segment height is the difference between the maximum height value of the segment and the mean of inner border.

Table 6 indicates some of the basic features including *average height*, *area*, *peak point* and *valley points* of the segment used to generate the advanced ones as well as *Quasi Flatness* and the *Mean Quasi Flatness*.

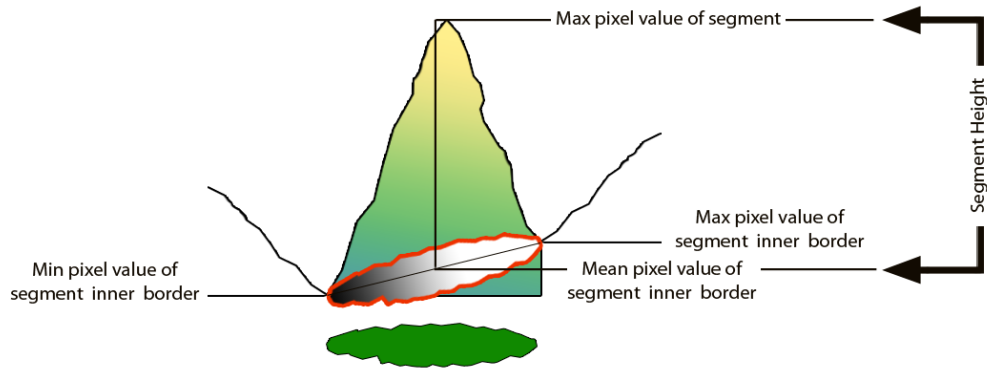


Figure 82: Geometry of the final segments in 2D and 3D space

To obtain the actual mean height of the segment the *Mean of inner border* in segment should be used:

$$MQF = ([\text{Max. pixel value nDSM}] - [\text{Mean of inner border nDSM}]) / [\text{Segment Area}]$$

Feature	Value	Description
H_{av}	Average height of the segment	Arithmetical mean value of height in segment
$H_{av_F_m}$	Average height of the filtered layer in the segment	Arithmetical mean value of height in the filtered layer of m in the segment (F includes mean, median, maximum, minimum)
A	Area of the segment	Sum of the number of pixel
H_p	Maximum peak point in segment	Height between the highest peak and the mean plane
H_v	Minimum valley point in segment	Depth between the mean plane and the deepest valley
D	Segment domain	The height difference between the peak and valley point
H_{in_b}	Mean of inner border	Mean of height values along the inner border of the segment
QF	Quasi flatness of the segment	H_{av}/A
MQF	Mean quasi flatness of the surface	$(H_p - H_{in_b})/A$

Table 6: The geometry-based features of a segment

5.9. Segment roughness

Different tree types have different degrees of roughness (see section 04.5). To define a proper feature, based on the roughness characteristics of the surface, the height variations should be measured. The Standard Deviation (STD) of the surface in each segment can be a candidate for this feature. As a similar feature, in [Miri et al. 2013] the Averaged Height Variation (AHV) is measured in some sample segments at the highest levels of the CHM.

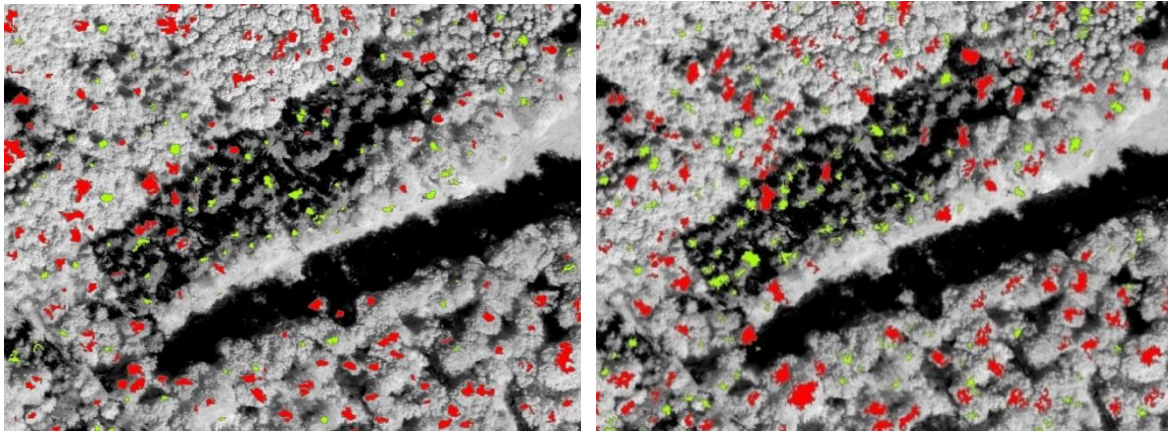


Figure 83: Comparison of AHV on laser-based nDSM (left) and image-based nDSM (right) at low segmentation level for ■ coniferous and ■ deciduous tree types [Miri et al. 2013]

The discussion on this point is the reference value, from which the deviations should be calculated. In the theory, the mean value of the segment (mean height) can be used. Due to the dependence of this feature on the elevation values, the efficiency of this parameter will be investigated in this research. In CHM, high elevations neighboring to lower height levels (ground or low vegetation) increase the STD value of the segment, which results in false representation of the high roughness in the segment. As can be seen in Figure 84, the high variation of the height values from the *Mean of segment*, demonstrates a very rough surface. However in reality, there exist both high and low degrees of surface roughness.

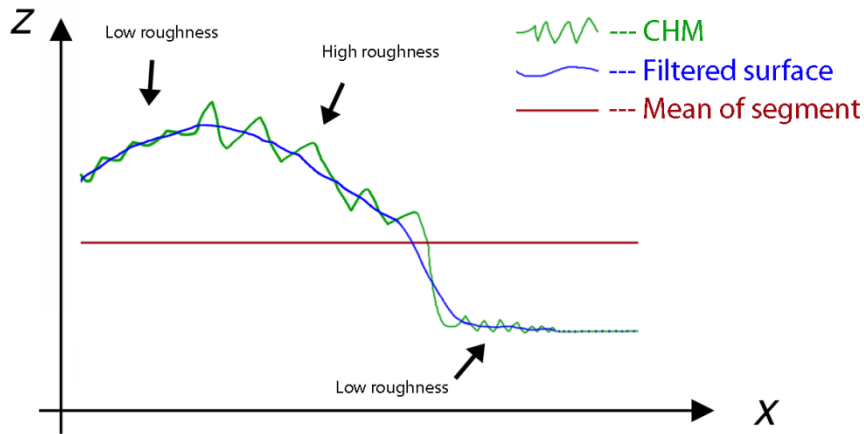


Figure 84: Roughness and height variations considering different reference values for calculating the standard deviation of a segment

Furthermore, if the STD feature is used together with the geometric ones, the combined feature (roughness and geometric) results in correlated classification. This is because the mean height value contains geometric information of the tree segment, which can be calculated from the maximum and minimum values of the segments. To solve the correlation problem, a novel feature is defined, in which the height variations of the CHM are calculated from the difference of the raw nDSM from the filtered surface model. In this way the STD of the segment is normalized on the filtered surface and shows significantly more reliable results. This feature, which in this research is called *Filter-based Standard Deviation (fSTD)*, is evaluated for the classification of the tree types to demonstrate the roughness characteristics of the CHM. This surface evaluator can analyze the surface model with different sensitivity (different scales) and is able to calculate the standard deviation of the surface in a finer moving window with an arbitrary size. The deviation of the height value in each pixel will be compared with the filtered (median or mean) value of neighboring pixels in the moving window (μ_f). In other word, the result is the standard deviation of the surface normalized on the filtered surface of the plot sample. Obviously, the size of the window denotes the sensitivity of the roughness evaluator. To understand the spread of this filter, for the minimum window size (in pixel), the mean value is equal to the pixel values ($Z_{(x,y)}$), whereas the maximum window size yields the mean height of the plot (μ).

$$Z_{(i,j)} \leq \mu_f \leq \mu$$

The *Filter-base Standard Deviation* (S_{fstd}) of surface can be calculated by:

$$S_{fstd} = \sqrt{\frac{1}{A} \iint_A (Z(x, y) - \mu_f)^2 dx dy}$$

where A is the area of the segment and μ_f indicates the height value of the pixel on the filtered surface (median or mean) of the nDSM:

$$\mu_f = \frac{1}{A_f} \iint_{A_f} W(x, y) dx dy$$

where A_f is the area of the moving window.

Another application of this roughness evaluator is to find an optimized iteration number in filtering steps of the height data.

$$0 \leq S_{fstd} \leq S_q$$

If after some iteration number, the roughness of the surface does not change, this shows that the surface has reached the required smoothness. This number can be used for the dataset with the same stand type.

5.10. Qualitative and quantitative evaluation

The evaluation of the digital elevation models in the test area is performed in both *qualitative* and *quantitative* aspects in this thesis. The object-oriented approaches (section 3.1) are implemented for the classification of the tree types. The qualitative evaluation is mainly concentrated on the segmentation results of the elevation data.

In this research, the geometric and the roughness features are investigated on the laser-based and image-based datasets. Additionally, in the quantitative approach, the positioning and boundary delineation of the single trees will be evaluated. Several methods can be implemented for the quantitative assessment of single tree extractors. The *point to point* methods focus on the allocation of the tree position based on the Euclidian distances. In Figure 85 three allocation areas with 1m, 2m and 3m buffer around the reference points are demonstrated.

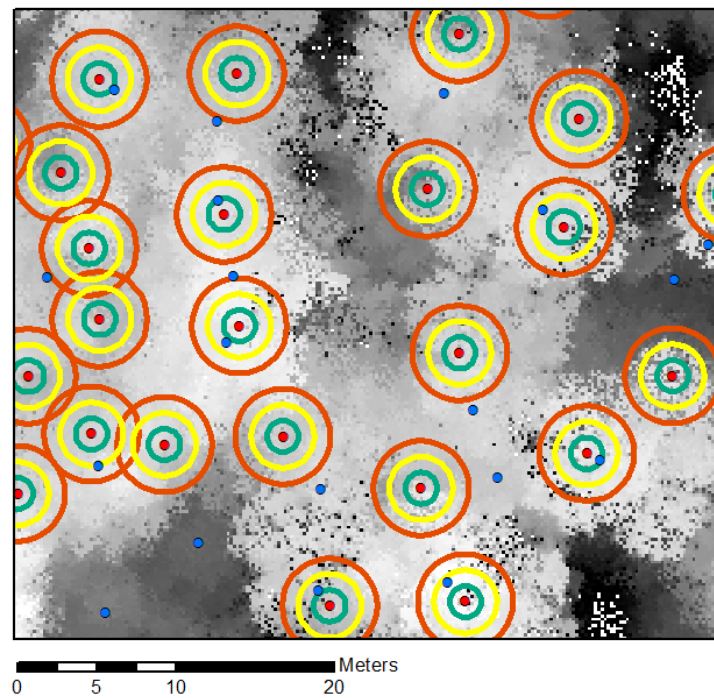


Figure 85: Allocation areas for the automatically found tree positions (blue points) with search buffers of 1m, 2m and 3m (green, yellow and orange lines) around the reference trees (red points)

The main hypothesis in such methods is that the trees are considered as straight columns and the inclination stems are not taken into account. That means a tree position, which might be in the tree crown area but out of the buffer regions, will not be allocated as a truly found tree. It should be that the data acquisition of the reference trees is based on the positioning of the tree stems, whereas the automatically extracted trees are acquired from the crown surface models. This means that for quantitative evaluation the relations between the points and polygons should be defined. Topologic relations describe the relative position of two objects, without considering their metrics [Gerke 2006].

According to [Egenhofer and Franzosa 1991] these relations (R_i) between two spatial regions can be described in terms of the boundary (∂) and interior ($^\circ$) of the sets A and B in sixteen binary topological specifications¹⁰(Table 7).

¹⁰ Defining the *closure* of the set A as the smallest closed set containing A, the *boundary* of A is the intersection of the closure of A and the closure of the complement of A. The *interior* of A is the largest open set contained in A.

	$\partial A \cap \partial B$	$A^\circ \cap B^\circ$	$\partial A \cap B^\circ$	$A^\circ \cap \partial B$	Semantics of the nine region relations
R_0	0	0	0	0	A and B are disjoint
R_1	1	0	0	0	A and B touch
R_2	0	1	0	0	A equals B
R_3	1	1	0	0	
R_4	0	0	1	0	
R_5	1	0	1	0	A is inside of B or B contains A
R_6	0	1	1	0	
R_7	1	1	1	0	A is covered by B or B covers A
R_8	0	0	0	1	A contains B or B is inside of A
R_9	1	0	0	1	
R_{10}	0	1	0	1	A covers B or B is covered by A
R_{11}	1	1	0	1	
R_{12}	0	0	1	1	A and B overlap with disjoint boundaries
R_{13}	1	0	1	1	
R_{14}	0	1	1	1	A and B overlap with intersecting boundaries
R_{15}	1	1	1	1	

Table 7: The sixteen specifications of binary topological relations and the terminology for the nine relations (grey rows) between two spatial regions

Among them, nine relations can be specifically used for *polygon to polygon* topology of neighboring regions. This combination can be defined for two polygonal datasets of reference (C as circles) and target trees (S as squares) with:

\cap	S°	∂S	S'
C°			
∂C			
C'			

where ($^\circ$, ∂ , $'$) are the interior, boundary and exterior of a set, respectively. In [Straub and Heipke 2004] and [Gerke 2006] these relations are reduced to eight situations of *disjoint*, *touch*, *overlapped*, *cover*, *covered by*, *contain*, *contained by* and *equal*, and are represented in Figure 86.

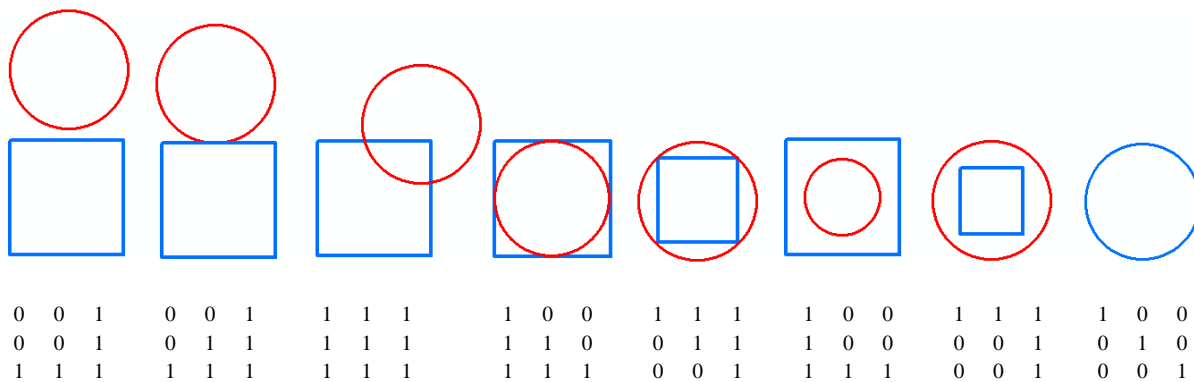


Figure 86: Topological relations between the reference dataset (red circles) and the target tree segments (blue squares) based on [Gerke 2006] and [Straub and Heipke 2004]

The overlapping strength, demonstrates the transition from disjoint to equal [Straub 2003] and can be calculated by Overlapping Factor [Winter 2000]:

$$OF_{A,B} = \frac{C \cap S}{\min(|C|, |S|)}$$

$$0 \leq OF_{A,B} \leq 1$$

Based on the definitions of the commission error (False Positive or FP) and the omission error (False Negative or FN) in [Straub 2003], the completeness (producer accuracy) and correctness (user accuracy) of a classification can be calculated with values between zero and one. The True Positive (TP) value is the overlapping area of the reference and the extracted segments.

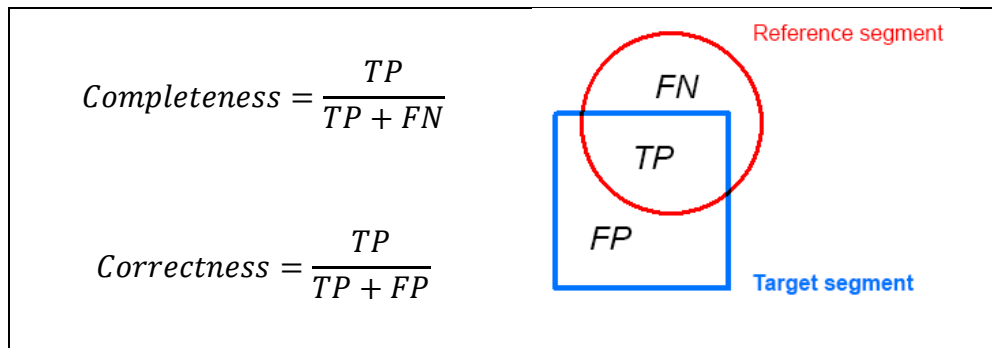


Figure 87: The explanation of completeness and correctness according to [Straub 2003]

As can be seen in Figure 87, the reference dataset contains the false negative and the true positive, whereas the target segments possess the true positive and the false positive. Regarding the overlapping factor (OF), a target polygon is positioned exactly on the reference polygon if one of the last five topological relations in Figure 86 occur ($OF=1$). However, this factor cannot efficiently represent the quality of the crown delineation. Theoretically, a successful tree extraction algorithm has both completeness and correctness near to one. In this thesis An Advanced Overlapping Factor (AOF) is implemented which is calculated by multiplication of completeness and correctness.

$$AOF_{R,T} = Completeness \cdot Correctness = \frac{O^2}{R \cdot T}$$

$$0 \leq AOF_{R,T} \leq 1,$$

where O is the overlapping area and R and T are the areas of the reference and the target segment. The minimum value of this factor (zero) occurs if the segments do not overlap. The maximum value (one) can be seen in the last topological relation in Figure 86, where both segments cover each other completely. However, as both datasets are assumed identical with polygonal characteristics, the positional evaluation of the single trees is not considered explicitly in the overlapping factors. This is because the position of the single trees in reference and target segments might not be the same, even if both segments cover each other completely.

Another controlling factor is the *quality* assessment of the segmentations results from [Rutzinger et al. 2009]:

$$Quality = \frac{TP}{TP + FP + FN} = \frac{Comp \cdot Corr}{Comp + Corr - Comp \cdot Corr}$$

The best quality in segmentation will be obtained if both reference and target segments are equal ($FP = 0, FN = 0$).

For the linking of the point datasets (reference tree positions) to the polygon datasets (extracted tree segments) the characteristics of both identities (point-polygon) should be considered. For this, the topological relationships between automatically extracted trees and the buffer areas are required. To overcome this problem, an advanced point-polygon evaluation factor is defined, in which, both point-point and polygon-polygon relationships are integrated. For this, the distance (D) between the reference points and the target points are calculated from different features and are normalized on the maximum distance in the dataset (D_{max}) to provide a factor called *Weighting Distance (WD)* for the point-point quantitative analysis.

$$WD = \frac{D_{max} - D}{D_{max}}$$

$$0 \leq WD \leq 1$$

Based on the WD factor, the maximum distance ($D = D_{max}$) represents the lowest weighting value ($WD = 0$), whereas an exact tree positioning ($D = 0$) yields the highest precision of single tree positioning ($WD = 1$). The position of the target single trees can be extracted from different features like the centroid of the segment or from the marble growing segments.

Combination of the polygon-polygon and the point-point evaluation factors yield a novel factor called *Weighted Distance and Overlapping (WDO)*, which can be used for single tree delineation.

$$WDO = WD \cdot AOF_{R,T}$$

$$0 \leq WDO \leq 1$$

Using this factor, a successfully delineated single tree can be defined if both reference and target segments have a complete overlap with an exact positioning of the trees.



6

Experimental Results

This chapter deals with the experiments implemented on both LIDAR and photogrammetric datasets. The algorithms introduced in the last chapter will be tested and evaluated based on the reference data.

6.1. Study area

To evaluate the proposed methods and algorithms in this research, a mixed forest in the state of North Rhine-Westphalia (NRW) in Germany is investigated. The LIDAR data are acquired by the airborne laser scanner RIEGL LMS-Q560. The photogrammetric stereo images are captured by the aerial camera Z/I Imaging DMC 1. Table 8 shows the technical data of both sensors and the related raw datasets. A detailed comparison of the aerial cameras in forestry applications can be found in [Arbeitsgruppe Forstlicher Luftbildinterpreten 2012]. The packages of the datasets include the DSM of LIDAR data and aerial images. The photogrammetric DSM is generated with Semi Global Matching (SGM) provided by the Institute of Optical Sensor Systems at the German Aerospace Center (DLR) in Berlin (Adlershof). The pulse analysis of the Laser data has been performed by the Institute for Man-Machine Interaction at RWTH Aachen University. The laser dataset includes the first pulse and last pulse point clouds. As a very advantageous specification of LIDAR technology in forestry, the last pulse data can provide DTM of the forest ground under the canopy with relatively higher resolution. However, to perform a confidential comparison between LIDAR and photogrammetric DSM, the available filtered DTM with one meter resolution is used from the officially available DTM of the geo-database¹¹ center in the state of NRW.

To provide the required layers in the workflow of this research (see section 5.1), the First Pulse (FP) data is converted into a raster image with resolution of 20cm. Due to the different resolution of the DSM and DTM data, to avoid the sudden changes in the nDSM data, the DTM dataset is interpolated and smoothed to 20cm GSD. The height data are stored in 16bit format images with 10cm height depth resolution. The forestry information is provided with the cooperation of the Institute for Research and Transfer (RIF. eV.) in Dortmund and the State Enterprise for Forestry and Timber North Rhine-Westphalia¹².

¹¹ www.geodatenzentrum.nrw.de

¹² Landesbetrieb Wald und Holz NRW (www.wald-und-holz.nrw.de)

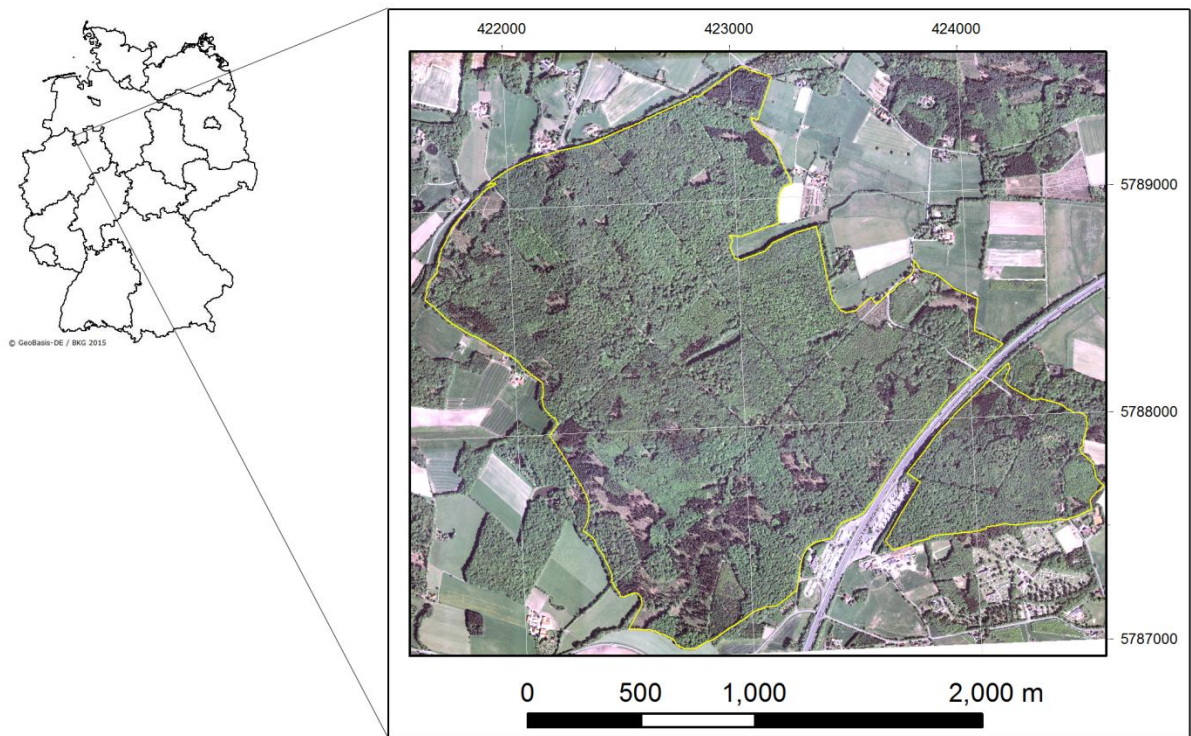


Figure 88: The study area Habichtswald in the state of NRW, Germany

Airborne laser scanning		Aerial photos	
Scanner:	RIEGL LMS-Q560	Camera:	Z/I Imaging DMC 01
Date of scanning:	March, 20 th , 2011	Date of acquisition:	May, 2 nd , 2011
Flight altitude:	600m above ground	Flight altitude:	2000m above ground
Point density and resolution:	1 p/m ² converted to 20cm GSD	Resolution:	8 cm, 20 cm GSD
Data package:	First Pulse (FP), Last Pulse (LP)	Data package:	RGB, NIR, raster DSM
Range resolution on natural targets $\rho \geq 80\%$ reflectivity:	2cm (<1500m dist.) or 1cm (<650m dist.)	Virtual focal length:	Pan: 120 mm Color: 30 mm
Data format:	2.5D raster image	Data format:	2.5D raster image
Bit depth resolution:	16 bit	Bit depth resolution:	16 bit
Height depth resolution:	10 cm	Height depth resolution:	10 cm
Scan geometry:	Parallel lines with ± 22.5 up to ± 30 deg. Field of view and 0.3m spot diameter at 600m dist.	Imaging geometry:	60% length and 40% side overlapping

Table 8: Technical data for airborne sensors used for the test area Habichtswald (HBW)

Accuracy assessment of the DSM datasets

To investigate the accuracy of the digital surface models of the test area, a differentiated image of the DSMs is provided. As Figure 89 shows, the maximum differences occur mostly around the edges where the sudden height differences exist (the red, yellow and blue areas). The light green regions are the most fitted areas. The dark blue color demonstrates where the LIDAR height values are over the image-based DSM ($H_{\text{Laser}} > H_{\text{Image}}$). They are the levels, where the small branches of the trees are measured by laser; those are smoothed during the interpolation steps in the SGM process. Such differences can be found around the separated single trees. Additionally, the flying points in the LIDAR data, which are mostly categorized as noises, can be seen in small blue points.

In the yellow and the dark-red areas, the image-based DSM is superior to the laser one ($H_{\text{Laser}} < H_{\text{Image}}$), which is mostly related to the interpolation of the height values in the gaps between the trees. These problematic regions complicate the delineation of the crown boundaries in forest areas.

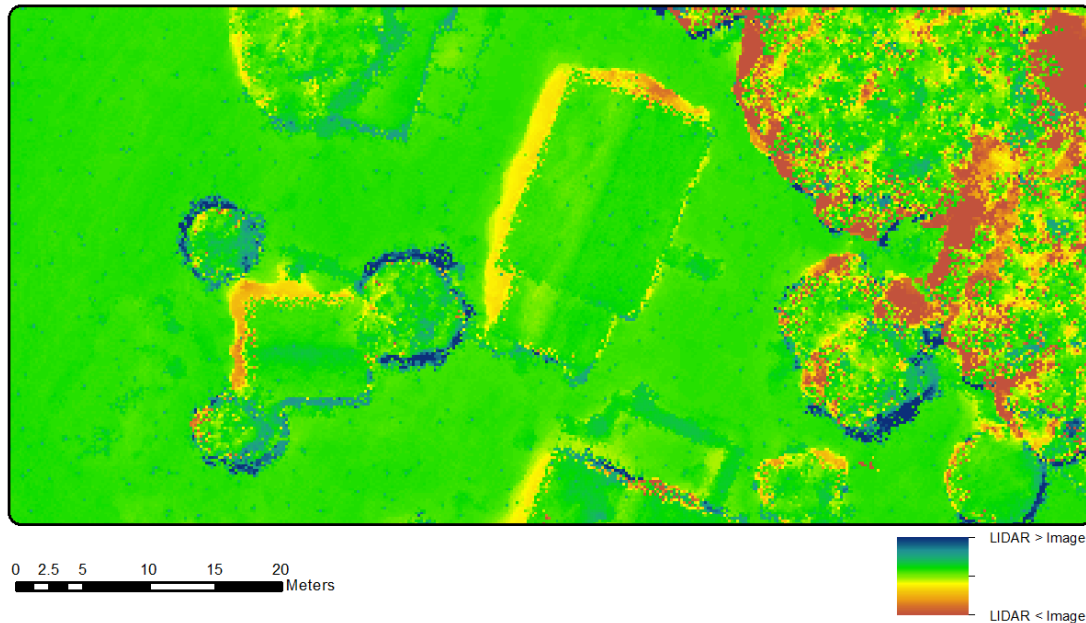


Figure 89: Difference image of DSM data (LIDAR - Image)

For quantitative comparison of the datasets, some surfaces are selected as assessment patches within the study area (Figure 90). Due to the weakness of the laser scanners in measurement of

the edges on the one hand, and the interpolation problems of the SGM method in abrupt edges, on the other, the evaluation areas are selected inside the boundary of the surfaces. Table 9 shows the statistical information of the investigated regions. The averaged mean height difference of about 9cm (less than one depth in gray level) shows the adequate coincidence quality of the selected surfaces and confirms the reliability of the DSM datasets for further analyses.

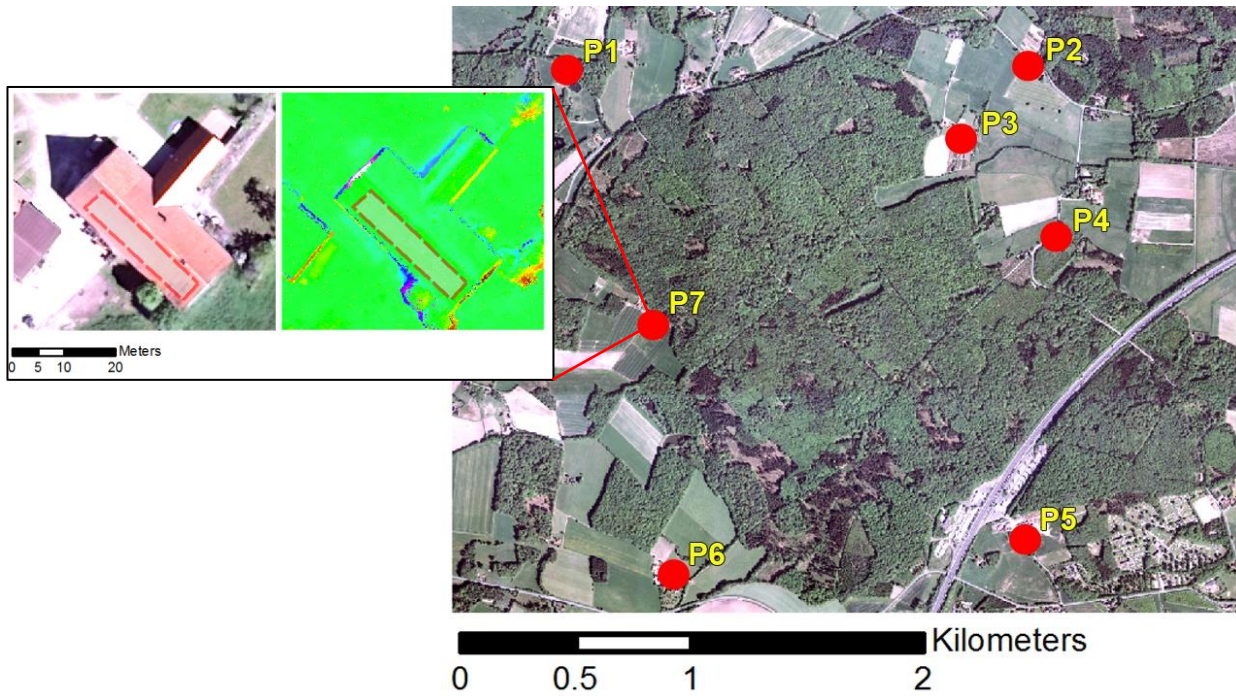


Figure 90: Contribution of the assessment patches around the study area

Patch	Pixels	Area (m ²)	Min. Diff. (m)	Max. Diff. (m)	Range (m)	Mean Diff. (m)	Std (m)	Majority (m)	Minority (m)	Median (m)
P1	1437	57.5	-0.3	2.1	2.4	0.03	0.17	0.0	0.9	-0.1
P2	1047	41.9	-0.6	1.6	2.2	0.06	0.21	0.0	0.8	0.0
P3	3933	157.3	-0.4	2.2	2.6	0.16	0.18	0.2	-0.4	0.2
P4	1388	55.5	-0.1	2.2	2.3	0.13	0.16	0.1	0.7	0.1
P5	5476	219.0	-0.2	2.1	2.3	0.02	0.16	0.0	1.8	0.0
P6	3569	142.8	-0.1	2.3	2.4	0.14	0.14	0.1	2.3	0.1
P7	2965	118.6	-0.5	2.7	3.2	0.10	0.20	0.1	-0.5	0.1

Table 9: Statistical assessment of difference surfaces of laser-based and image-based DSM

6.2. Stand-wise roughness analysis

The roughness parameters described in section 4.5 are used to evaluate the surface characteristics of forests in different stand types. However, to analyze the 2.5D digital surface models the roughness equations should be transformed into a discrete space (Table 10). This is because the height surfaces are in raster format.

Feature	Mathematic form
Mean height	$\mu = \frac{1}{mn} \sum_{k=0}^{m-1} \sum_{l=0}^{n-1} Z(x_k, y_l)$
Average roughness	$R_a = \frac{1}{mn} \sum_{k=0}^{m-1} \sum_{l=0}^{n-1} Z(x_k, y_l) - \mu $
Root mean square roughness	$R_q = \sqrt{\frac{1}{mn} \sum_{k=0}^{m-1} \sum_{l=0}^{n-1} (Z(x_k, y_l) - \mu)^2}$
Skewness	$R_{sk} = \frac{1}{mnR_q^3} \sum_{k=0}^{m-1} \sum_{l=0}^{n-1} (Z(x_k, y_l) - \mu)^3$
Kurtosis	$R_{ku} = \frac{1}{mnR_q^4} \sum_{k=0}^{m-1} \sum_{l=0}^{n-1} (Z(x_k, y_l) - \mu)^4$

Table 10: The sets of roughness parameters in 2D form

For analysis of these surfaces some circular samples with radii of 25m to 50m from the deciduous and coniferous stands in the test area of Habichtswald are chosen based on the age and type of the trees (Table 11).

Deciduous			Coniferous		
Forest	Stand type / Age class		Forest Code	Stand type / Age class	
430b1	Beech (<i>Fagus sylvatica</i>)	>80	432a1	Spruce (<i>Picea abies</i>)	41-60
437a1	Beech (<i>Fagus sylvatica</i>)	>80	433a1	Spruce (<i>Picea abies</i>)	41-60
432a3	Beech (<i>Fagus sylvatica</i>)	>80	434a4	Spruce (<i>Picea abies</i>)	41-60
436a1	Beech (<i>Fagus sylvatica</i>)	>80	433a8	Spruce (<i>Picea abies</i>)	21-40
430c2	Oak (<i>Quercus robur</i>)	21-40	433a6	Douglas fir (<i>Pseudotsuga</i>)	21-40
432b1	Beech (<i>Fagus sylvatica</i>)	21-40			
429a1	Beech (<i>Fagus sylvatica</i>)	61-80			
430a1	Beech (<i>Fagus sylvatica</i>)	61-80			
424h1	Oak (<i>Quercus robur</i>)	21-40			

Table 11: Characteristics of the sample areas in the forest region of Habichtswald

Figure 91 demonstrates the first three parameters which are dependent on the arithmetic average of the pixel values. As these parameters are closely related to the mean height of the stand, it can be seen that the roughness variations in the same stand types are rather similar; however, they vary in different stands. This indicates that the parameters μ , R_a and R_q can be used to border the outer boundaries for stand-wise analyses.

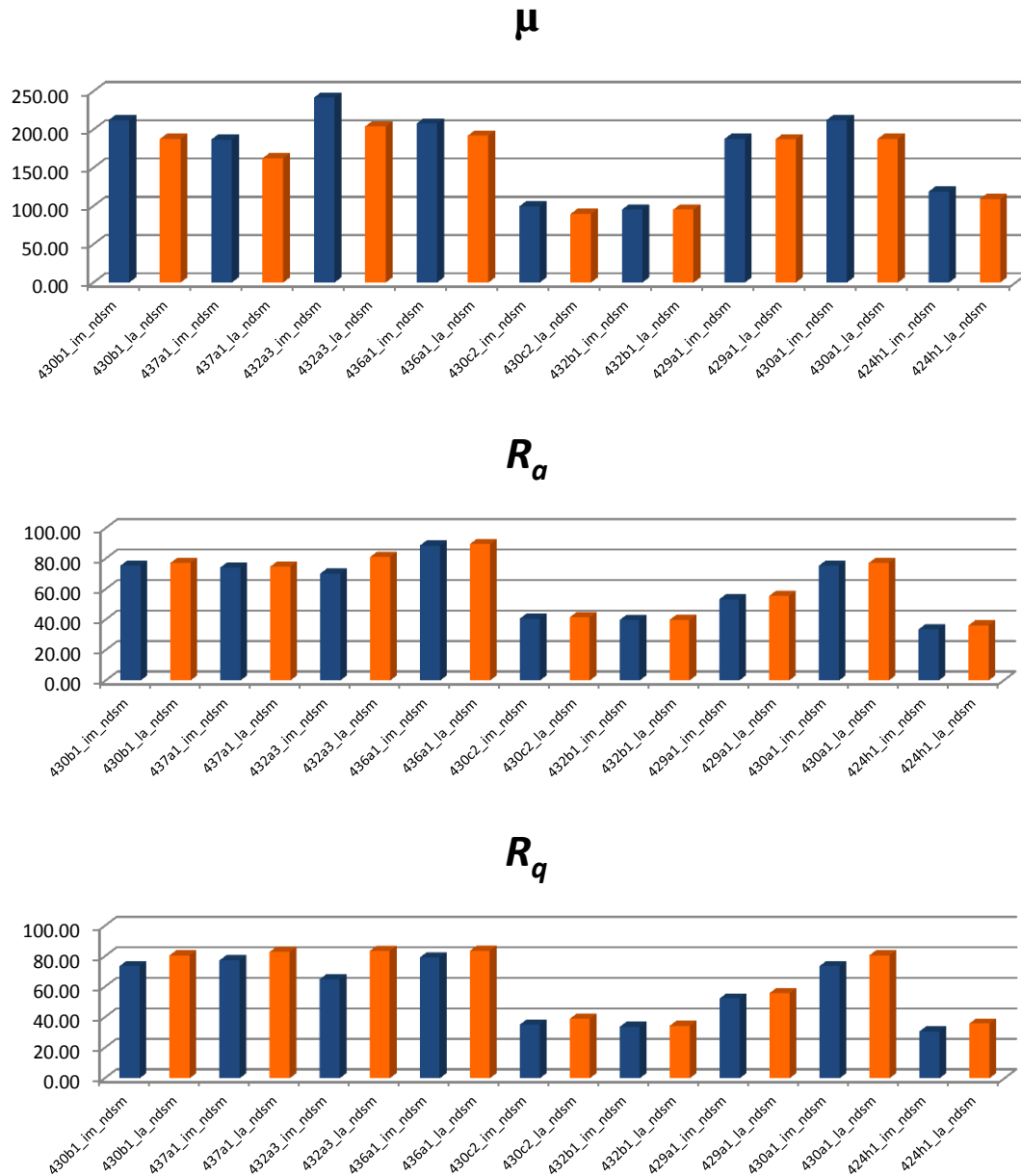


Figure 91: Roughness parameters (in decimeter) on image-based ■ and laser-based ■ surface models based on the arithmetic average of different deciduous stands

Due to the direct relation of the parameter μ to the elevation of the stand, this parameter is almost in the range of the height values, but larger than R_a and R_q . As the parameters μ and R_a are affected from the false height in the interpolated gap areas, the higher values of R_q show more reliability for this parameter. Furthermore, the tree types are also better distinguished. As a result of the roughness parameters, which are related to the standard deviation of the surface, Figure 92 shows little variations on the crown surfaces of the deciduous stands. Therefore they cannot explicitly distinguish the stand types in height models.

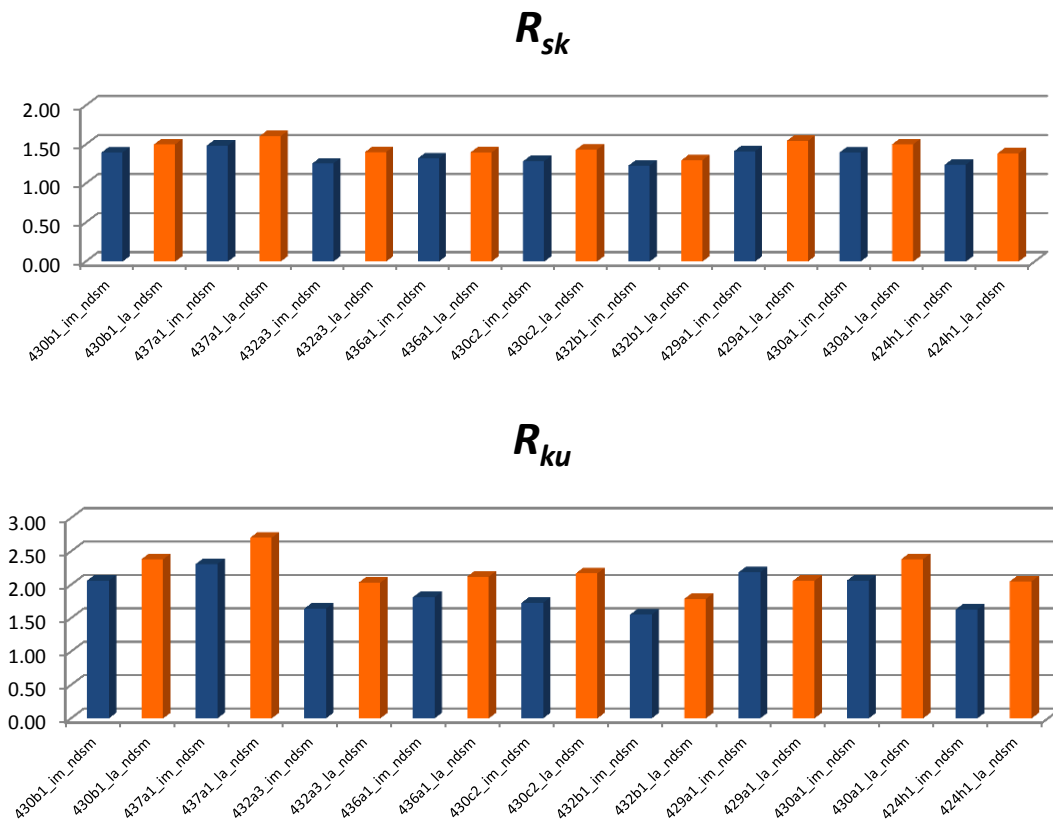


Figure 92: Roughness parameters (in decimeter) on image-based ■ and laser-based ■ surface models based on the standard deviation of different deciduous stands

Comparing the two data acquisition methods, both laser and image data show relatively similar roughness values in average-based parameters (Figure 93). Though, in the cases of R_{sk} and R_{ku} , the roughness of the laser data is more than the image dataset. This is due to the characteristics of LIDAR in direct and detailed acquisition of crown surfaces. In contrast to the deciduous stands, the coniferous ones did not show a regular change in the mean height parameters (μ). For the

image-based nDSM, this value is more than the LIDAR one. This is because of more gap valleys in the coniferous surface models, where the interpolated height between the trees results in false height calculation. This problem does not occur in R_a and R_q . This signifies the greater reliability of these two parameters in the case of image-based DSM.

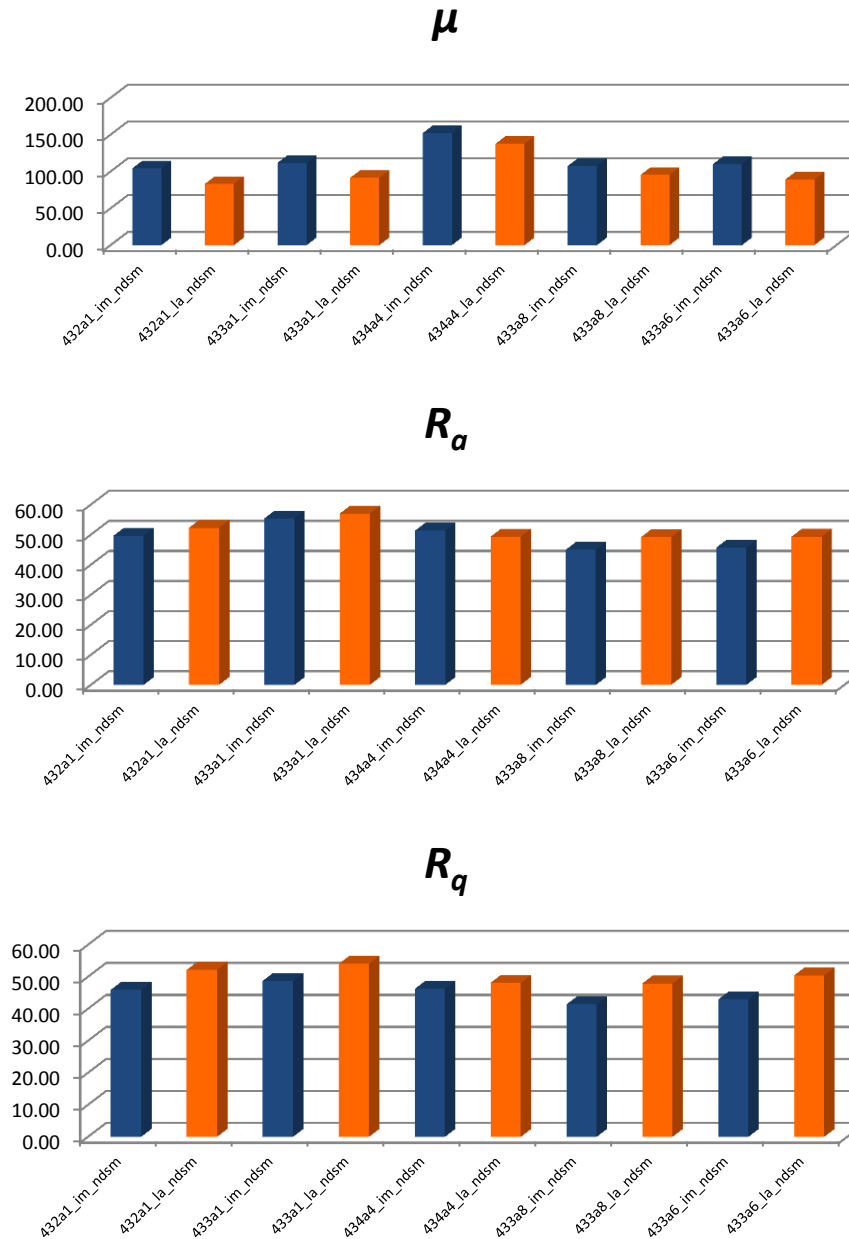


Figure 93: Roughness parameters (in decimeter) on image-based ■ and laser-based ■ surface models based on the arithmetic average of different coniferous stands

In both coniferous and deciduous stands, the LIDAR data show more roughness values, based on the standard deviation parameters (R_{sk} and R_{ku}). Though, the parameter R_{ku} varies dramatically in the coniferous stands with different ages. This can be seen in the two last larger values (young coniferous stands) in Figure 94.

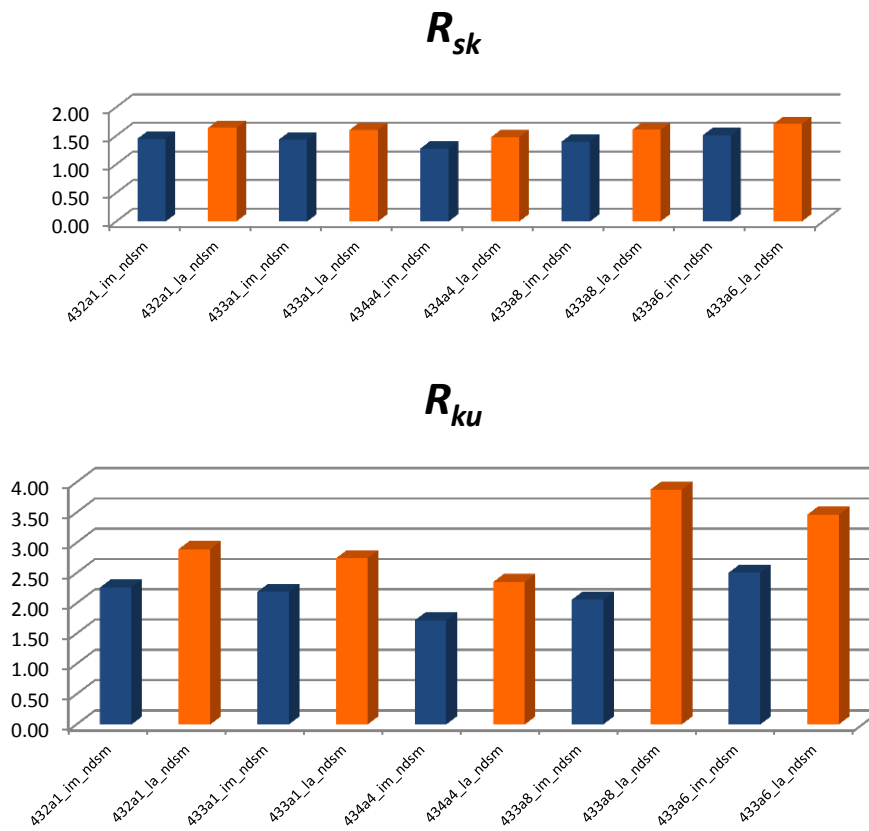


Figure 94: Roughness parameters (in decimeter) on image-based ■ and laser-based ■ surface models based on the standard deviation of different coniferous stands

These roughness measures are still dependent on the mean height of the sampled datasets. For instance, a young deciduous stand (lower height values), represents less roughness although it might have similar surface variations to a dense older stand (with higher trees).

Single tree roughness analysis

The influence of the mean value (μ) on the other roughness parameters shows that, they can be affected by the structure of the stand (deciduous, coniferous or mixed), tree height (stand age) and the forest density. This can be significantly seen in the coniferous stands due to the more peak and valley forms. To redress this weakness of the existing surface analyzers, a roughness

evaluator is needed to measure the surface quality in finer scales. Furthermore, there is a demand for segment analysis at single tree level. As explained in the previous section, the roughness parameters can be used as measuring instruments to describe the characteristics of forest surfaces. To remove the problematic points on the surface models (especially for LIDAR data), they should be filtered without changing the surface characteristics (see section 5.2.1). To set the optimized parameters, the filter strength in the laser-based and image-based nDSM should be measured using a fine roughness evaluator.

A rough surface needs more filter iterations to be free of noises. This indicates that another way of defining the roughness degree of a surface is the iteration number of filtering until the surface does not change. In other words, comparison of the surface roughness with a *filtered surface* (e.g. mean or median) instead of the mean plane of the surface patch, gives more information about the fine variations on the surface. The developed roughness evaluator, introduced in section 5.9, is used to calculate the standard deviation of the surface in a finer scale. The discrete form of the *fine standard deviation* (R_{fstd}) for a rasterized surface with the size of $m \times n$ can be calculated from:

$$R_{fstd} = \sqrt{\frac{1}{m \cdot n} \sum_{k=0}^{m-1} \sum_{l=0}^{n-1} (Z(x_k, y_l) - \mu_f(x_k, y_l))^2}$$

where $\mu_f(x_k, y_l)$ indicates the grey level value of the filtered image at the point (x_k, y_l) . For example, this value for a mean filter with square window size of $i \times j$ can be gained by:

$$\mu_f(x_k, y_l) = \frac{1}{i \cdot j} \sum_{p=k-i/2}^{k+i/2} \sum_{q=l-j/2}^{l+j/2} F(x_p, y_q)$$

To find an optimized iteration number in filtering the height data, the parameter R_{fstd} should stay unchanged after some iteration numbers. As expected, by implementing this surface evaluator, the laser data possesses more roughness on the CHM than the image-based height models. As can be seen in Figure 95, after 5 iterations, the laser surface is smoothed from 20cm to 12cm, whereas the value for the image data is almost unchanged (from 8.82cm to 8.59cm). The slight variations

in the image-based CHM (ca. 2cm) indicate that the SGM datasets do not need to be filtered due to the smoothing during the interpolation steps.

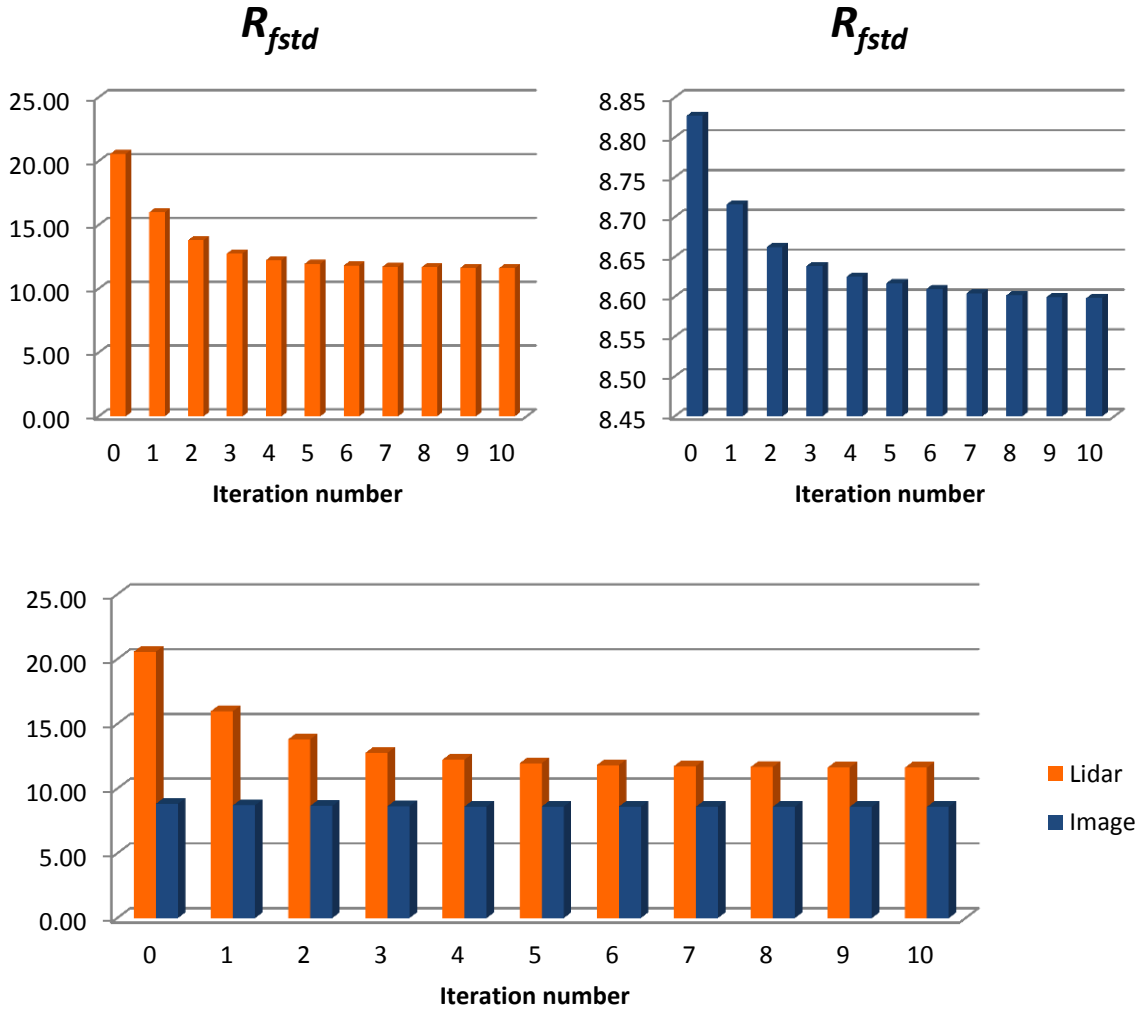


Figure 95: Roughness analysis (in decimeter) over the CHM of an old beech stand using the R_{fstd} evaluator with window size of 3 pixels in different filter iterations

A comparison of the height data for two completely different stands (a young coniferous and an old deciduous) is demonstrated in Figure 96. The fine roughness analysis of the filtered surface models demonstrates the very slight change of the image-based surface models in the iteration steps for both coniferous and deciduous stands, whereas the LIDAR data become smoothed after 4 or 5 iterations. Regarding the results for each data acquisition method, the old deciduous stand shows more R_{fstd} roughness on their canopy than the young coniferous. This means, in addition to

the tree type, the age and density of the trees should also be considered in characterizing the stands with the roughness parameters.

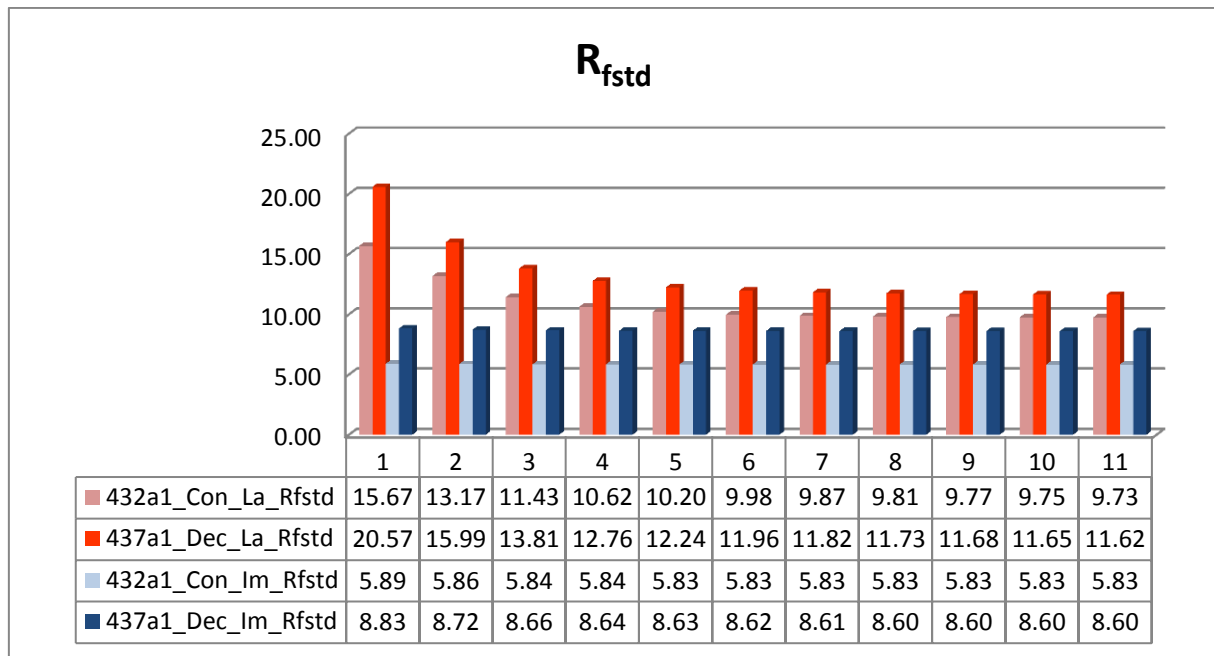


Figure 96: Roughness analysis (in decimeter) over laser (red) or image (blue) CHM of a young spruce (Con) stand (432a1) and an old beech (Dec) stand (437a1) using the R_{fstd} evaluator in eleven filter iterations

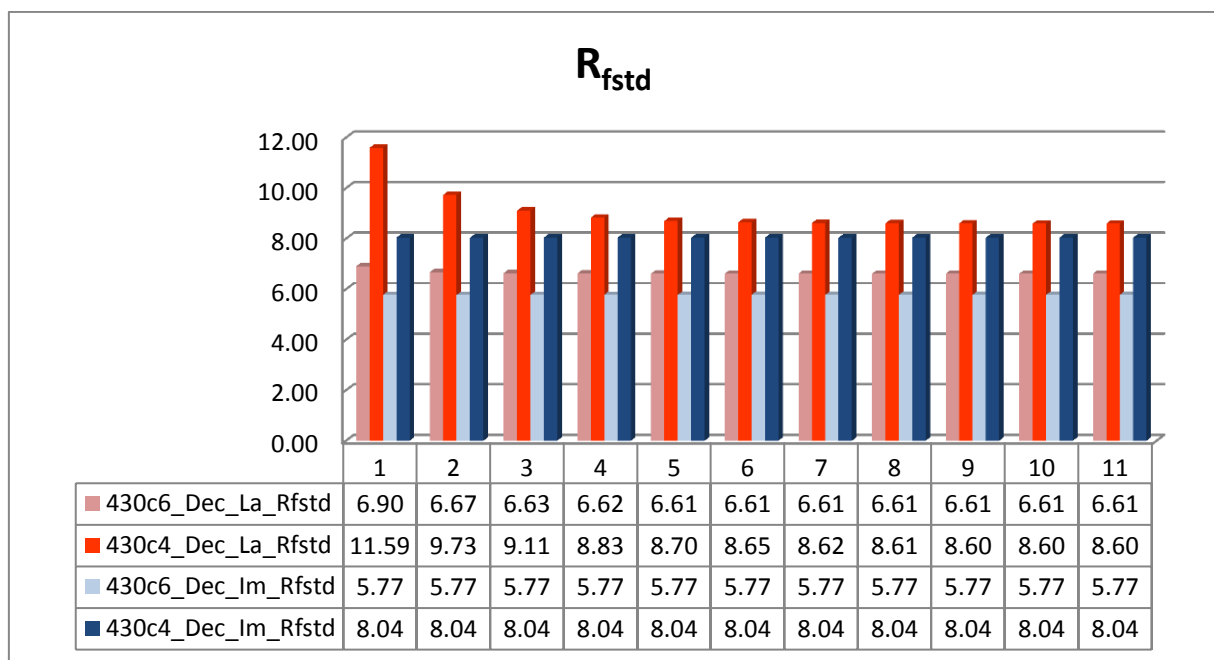


Figure 97: Roughness analysis (in decimeter) over laser (La) or image (Im) CHM of a very young mixed deciduous stand (430c6) and a young beech stand (430c4) using the R_{fstd} evaluator in eleven filter iterations

The influence of the stand age on the characteristics of the surface is shown in Figure 97. Due to less competition success in younger stands, they stay in higher densities with less roughness value on their canopy surface.

6.3. Reference data for single tree detection

Preparing reliable reference data for evaluation of single tree segments is one of the most challenging issues in forest mensuration. The goals of terrestrial data acquisition in this thesis are measuring the position of the single trees and also extracting the DBH. To compare the current methods in traditional forestry and the surveying methods for single tree extraction in mixed European forests, two practical excursions, in the Tegel forest in Berlin and in the Habichtswald forest in North Rhine-Westphalia were organized. The advantages and disadvantages of both methods are described below.

6.3.1. Traditional methods in forestry

In the first excursion, a traditional method of single tree mensuration in forestry (see section 2.1.1), is evaluated for a test area in Tegel forests. For this, an ultrasound Hypsometer (Vertex) is employed. Different interpretation of the tree height and the tree positioning is for the most part dependent on the physical and experimental characteristics of the forester. Furthermore, considering the required accuracy $\delta < 10\text{cm}$ (one bit depth) for evaluation of the aerial datasets, the positioning accuracy could not reach the existing surveying methods. Figure 98 shows two steps of measuring the distance and the diameter of the single trees at the breast height (DBH). However, easiness and completeness of the data in the field are the advantages of such methods. A detailed explanation for forest mensuration methods can be found in [Lar and Akça 2007] and [Nagel 2001].



Figure 98: Experimenting the preparation of the reference data using traditional methods in forestry

The problematic cases in mensuration of single trees result by nature from the wildness of the forest. Figure 99 shows that measuring the tree parameters at the breast height might not always be a simple task. The number of trees and the tree positions are the main challenging issues. This leads to a vast difference between the measurements of the trees under the canopy and the tree position from the top of the crown surface.



Figure 99: Complexity of tree positioning and counting

6.3.2. Terrestrial laser scanning and photogrammetry of single trees

For a confidential reference dataset, the existing surveying methods are compared. To satisfy the completeness and the accuracy of the reference dataset, Terrestrial Laser Scanning (TLS) is used in combination with a Smart Station (Total Station and GPS). Employing this equipment provides

a 3D point cloud of the forest area under the canopy surface in a global coordinate system (Figure 100).

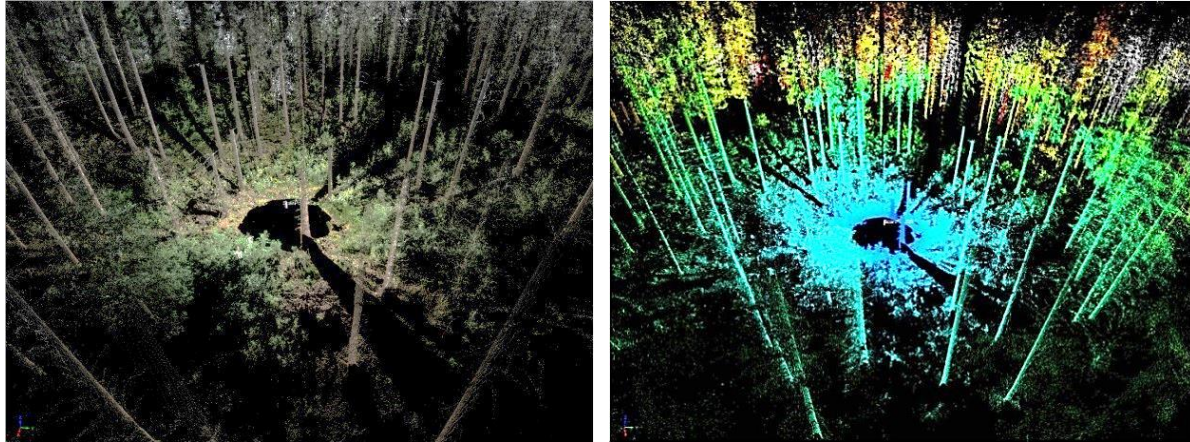


Figure 100: Point cloud of a TLS station in a coniferous stand with true colors (left) and height false colors (right)

For better detection of the tree trunks in the forest, using only the point cloud data might be a challenging task, especially in leaved seasons, as well as in dense forests. The solution is to support the point cloud with color data (Figure 102Figure 100 and Figure 101), which means integrating a photogrammetric camera with the laser scanner¹³.



Figure 101: Panorama view of the point cloud of a scan position with RGB information

¹³ In Leica HDS 7000 systems, colorizing the point cloud can be performed by replacing the scanner with a camera to provide a cubic panorama space. Contrary to the Riegl Systems, it takes more time for registration of these scans and the panoramic cubes in the office.

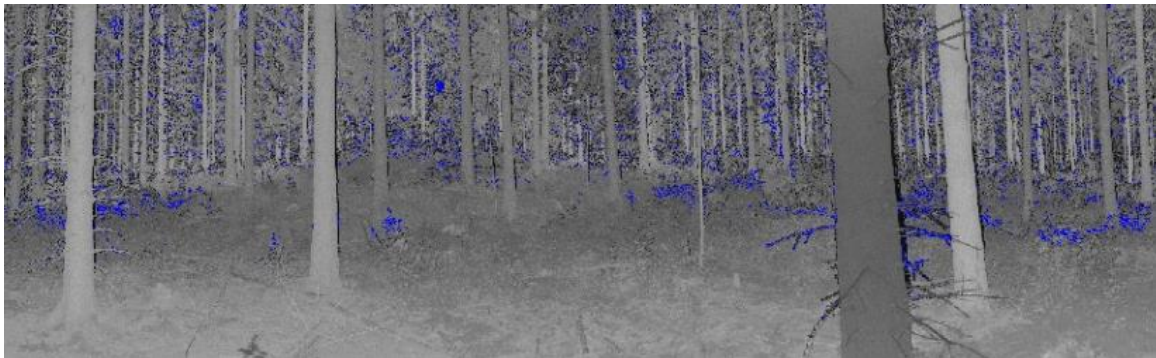


Figure 102: Panorama view of the point cloud of a scan position with intensity values

Two TLS systems, Leica HDS 7000 and Riegl LMS 620, are compared for this purpose (Figure 103). The Riegl LMS 620 with a measurement range of 2m to 2000m for natural targets with reflectance of more than 80% (750m for reflectance of 10%) is chosen. The claimed registration accuracy of 10mm, the beam divergence of 0.15 milli-radian and the field of view of $80 \times 360^\circ$ can be cited as the main characteristics of this system¹⁴.



Figure 103: Leica HDS 7000, Riegl LMS Z620

The advantage of the already calibrated and mounted camera on the Riegl LMS scanner facilitates using combined close range photogrammetric images within the point cloud data in the photogrammetry software PHIDIAS¹⁵. In this way, extracting the geometric parameters of single trees will be based on both the laser data and the integrated images from the metric camera Nikon D300, mounted on the laser scanner. This increases the measurement accuracy of the tree position, DBH and identification of the tree type, even more so than using colored point cloud.

¹⁴ www.riegl.com

¹⁵ PHIDIAS is a development in area of photogrammetric evaluation systems and is implemented as an application on the CAD system MicroStation (www.phocad.de).



Figure 104: Surveying the reference points at field, required for geo-referencing the terrestrial dataset

Along with the laser scanning, measurement of the registration targets is carried out using the total station Leica 1202, integrated with a smart station differential GPS. The surveying data are to be registered to the global coordinate system UTM (WGS84), acquired by GPS from an open air region within the forest and the geodetic fixed points around the test area¹⁶. Figure 104 shows the surveying of one of the fixed points. Two surveying campaigns in two different seasons are organized for the field data acquisition¹⁷. The first took place at the end of August 2012 and the second was undertaken in March 2013. Obviously, the August data acquisition was a rather problematic one. Due to the leafy time at the lower vegetation level, acquiring the DBH of the

¹⁶ The geodetic fixed points are provided by the cadastral land registry office Steinfurt in North Rhine-Westphalia.

¹⁷ The surveying campaign was supported by the equipment and personnel of GILAN Eng. Co. (www.gilan-survey.de) and the German Aerospace Center (DLR) in Berlin, Adlershof.

trees was a challenging task. However, with complementary scan positions and the aid of integrated photogrammetric images, the breast height levels were achieved even in this season.



Figure 105: Terrestrial laser scanning of the targets in the clearing area for the global registration (right) and the single trees within the stand (left)

After terrestrially scanning the under canopy of the test area, extracting the single tree positions is carried out with the software PHIDIAS. For this, the point cloud of the single trees with diameters more than 15cm will be selected exactly at the DBH level (1.3m). Using the integrated images and the selected point cloud, a horizontal circle will be fitted on the profile of the point cloud on the stem. The center of this circle is considered as the position of the tree at the DBH level. The DBH circles will be used later as weighting values for the simulation of the reference segments. As demonstrated in Figure 106, this procedure should be performed in the multi-view environment of the software MicroStation to achieve the completeness of the dataset and confirm the correctness of the tree positions in the TLS data. Based on the panorama images provided from the mounted camera on the laser scanner, the tree types are identified¹⁸.

¹⁸ The identification of the tree types is performed by the forest specialists at the Institute for Research and Transfer (www.rif-ev.de) in Dortmund, Germany.

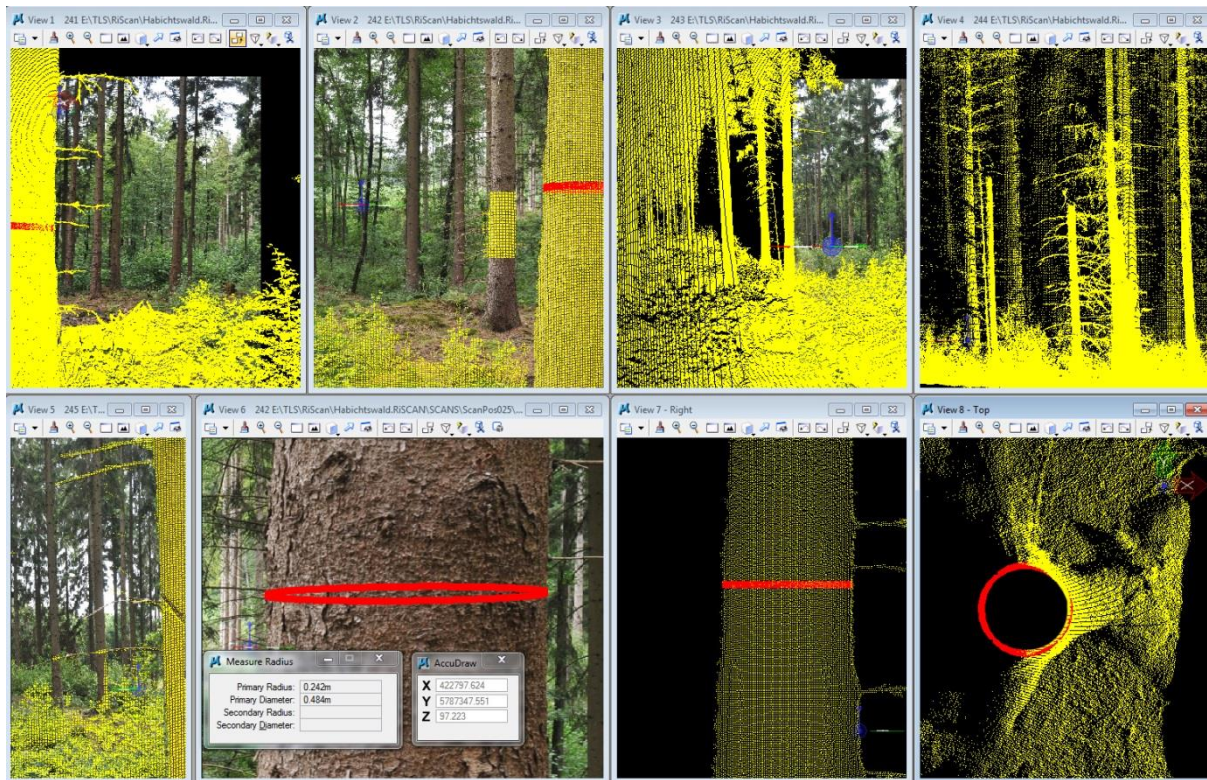


Figure 106: Terrestrial data acquisition of the single trees with TLS and close range photogrammetry in PHIDIAS

For acquisition of the reference data, there are several aspects to be considered:

- The tree position can be obtained from the center of the circle at the DBH level. In relation to the under-canopy vegetation, choosing an appropriate season for data acquisition plays an important role in a time-saving process.
- In the interests of suffice the completeness of the dataset, planning the (complementary) scan positions depends on the forest density.
- For the extraction of the tree heights or the diameter circles at the upper height levels (required for definition of the tree inclination), leafless seasons should be used for data capturing.
- To obtain the best fit of the DBH circle with the combined photogrammetric images, working in a multiple-view environment is recommended (Figure 106).
- Definition of the breast height level differs depending on the terrain surface of the forest area. On a flat DTM, a cutting plane at breast height (1.3m from the ground) provides a profile of the point cloud of the trees. In a non-flat area (bumpy or slope grounds), the

DBH circle should be defined for each tree separately from the ground and along the growth direction of the tree (Figure 107).

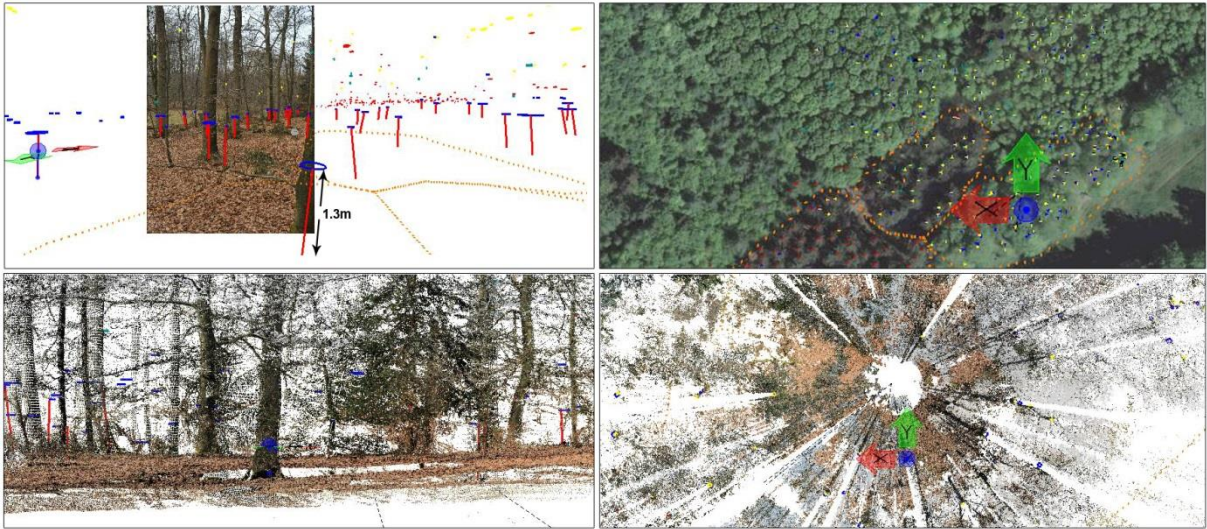


Figure 107: Multiple-views for provision of the reference data. Top-left: the DBH circles (blue) and the 1.3m breast height (red lines); Top-right: the test area (marked with orange dashed lines). Below: colored point clouds.

6.4. Stand-wise qualitative evaluation of the CHM

To analyze the characteristics of the surface models in mixed forests, the laser-based and image-based nDSM data are evaluated by the features developed in this research (see section 5.7). The geometric feature of Mean Quasi Flatness (MQF) and the roughness feature of Normalized Height Variation (NHV) are implemented to classify the test area into deciduous and coniferous areas. For the laser-based surface models, the normalized roughness of the surface is calculated. This process is performed for each segment on the filtered surface. For evaluation of the surface models at different heights, the segmentation results are not filtered by segment size and segment height.

6.4.1. Analysis of height variations

To avoid the influence of noise in laser data, the height variations should be compared to a statistically filtered surface. The statistical filters like mean and median are affected from the problematic points (flying points, gaps of penetration, etc.). Therefore, the deviations are compared to the non-smoothing filter developed in this research (see section 5.2.1).

Regarding the hypothesis, that the coniferous stands have more averaged-based roughness on their canopy surface than the deciduous ones, the classification of tree types is implemented on a mixed stand in the Habichtswald test area possessing spruce (*picea abies*) stands and European beech (*Fagus sylvatica*). The results of the segmentation (Table 12) show the quality of the STD feature in both laser-based and image-based datasets to classify the coniferous and deciduous stands. The roughness feature STD on the image-based nDSM of the coniferous stand has a mean value of 2.13m. The same feature (STD) on the filtered laser dataset shows a mean value of 3.05m. This is due to the higher roughness in the laser dataset. More confidential results are achieved with the feature NHV from laser data with a mean value of 1.80m, which is independent from the mean height values.

Tree Type	Values for	Tree height (image)	Image-based STD	Tree height (laser)	Laser-based NHV	Laser-based STD
Coniferous	Min	6.63	1.00	5.44	0.40	0.53
	1st Quartile	18.52	1.40	17.33	0.72	2.12
	Median	21.07	1.89	19.96	1.44	3.01
	3rd Quartile	23.00	2.59	21.71	2.51	4.03
	Max	26.76	6.76	25.88	6.64	6.65
	Mean	20.28	2.13	19.14	1.80	3.05
Deciduous	Min	1.79	0.00	3.30	0.00	0.23
	1st Quartile	19.06	0.27	18.46	0.06	0.69
	Median	20.50	0.49	20.74	0.12	0.92
	3rd Quartile	23.21	0.70	22.45	0.24	1.33
	Max	26.02	1.00	25.85	0.40	4.11
	Mean	20.49	0.50	21.01	0.15	1.14

Table 12: Analysis of roughness parameters on laser-based and image-based surface models

Using quartile distribution analysis, Figure 108 shows the segment characteristics and the quality of the segmentation for the coniferous class. To compare the roughness values with the tree heights of the stand, the statistical value of the mean height extracted from the nDSM of the tree segments are also demonstrated. This shows that 50% of the segments have height values around 20m in both surface models. This feature can classify the coniferous area in the same height range in image-based and laser-based surface models. The first quartile of the segment height begins with the minimum value of more than 5m in both surface models. This means the low vegetation segments are automatically excluded during the classification.

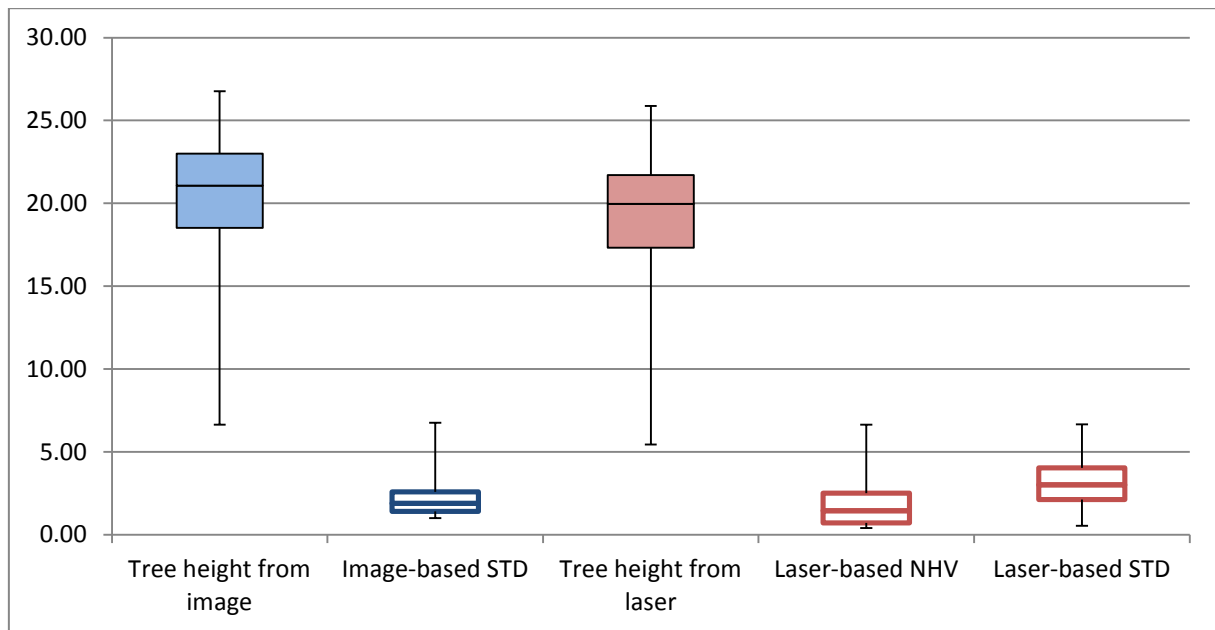


Figure 108: Segment specification of coniferous classification using roughness parameters on image-based and laser-based surface models (values in meter)

However, in the image-based segmentation 75% of the classified segments have a height value of more than 18m. In the case of laser data, this value is around 17m. The problem comes from the shadowed areas, where the gaps are interpolated in higher elevations in the image-based datasets.

In Figure 109 the distribution analysis of the classification is demonstrated for the deciduous segments. As in can be seen, in the case of the coniferous results, 75% of the classified segments are at the top elevations (approx. 19m for image-based and 18m for laser-based). Compared to the coniferous segments, the height variations of the deciduous ones (0.5m in image-based STD and 0.15m for laser-based NHV) are significantly lower, which confirms the hypothesis of less average-based roughness on the deciduous canopies.

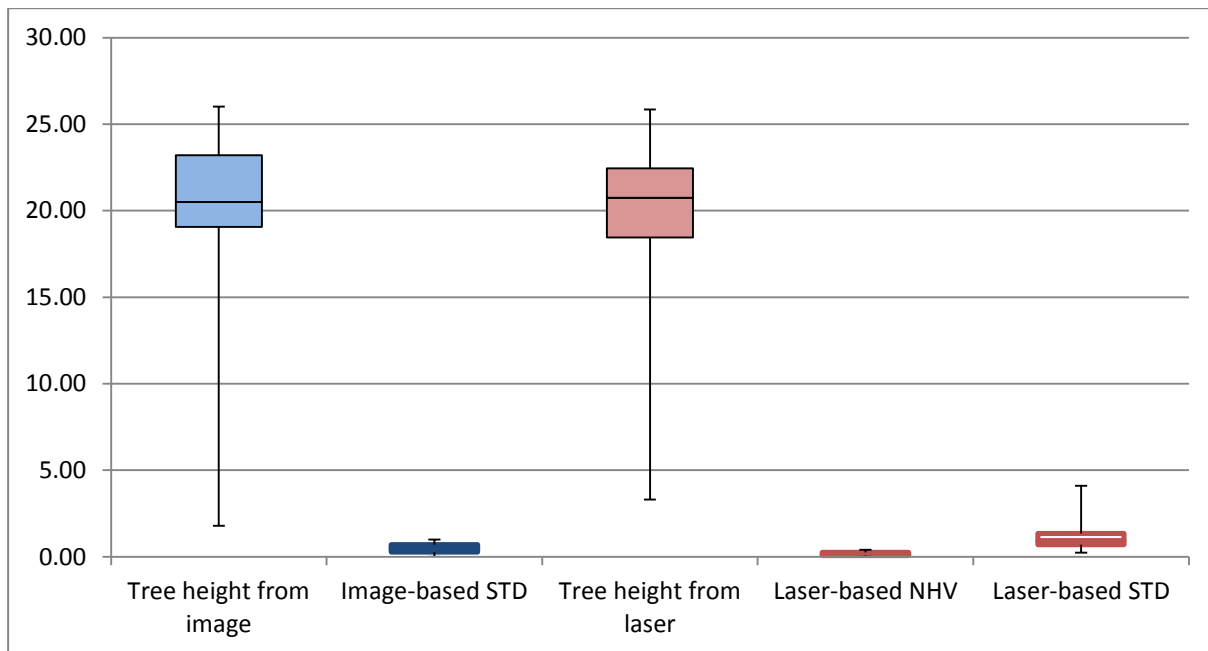


Figure 109: Segment specification of deciduous classification using roughness parameters on image-based and laser-based surface models (values in meter)

Although most of the segments are at the highest levels of elevation, the minimum value of less than 5m in the first quartile of both data types shows the participation of low vegetation in this classification. These segments can be easily filtered by their height values in the next steps.

For a better comparison, the roughness analyses for the coniferous and deciduous classes are expanded in Figure 110. Referring back to Table 12, the difference between mean values of coniferous and deciduous roughness in laser nDSM (1.65m for NHV and 1.91m for STD) is significantly higher than in the image-based surface model (0.63m for STD). This shows the advantage of laser data for better separation of the tree types, based on the surface characteristics.

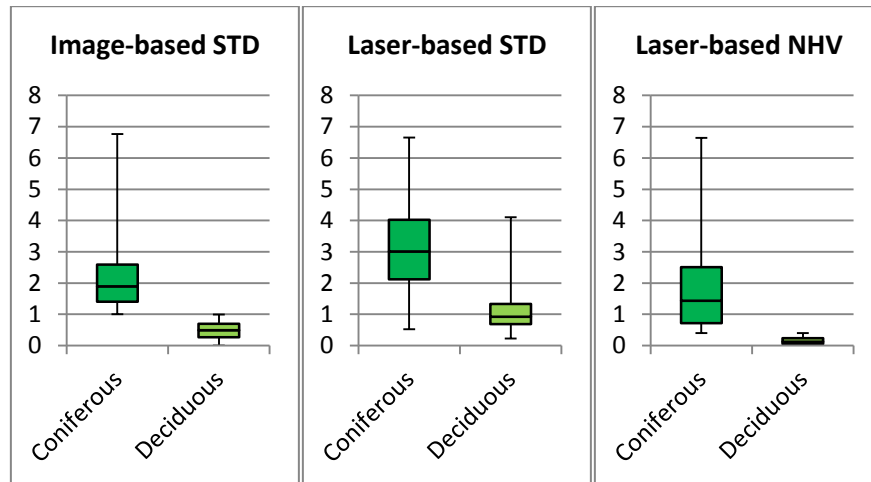


Figure 110: Comparison of the tree classes based on image-based and laser-based roughness parameter

The classification results of both image-based and laser-based features are visually demonstrated in Figure 111 and Figure 112. In this visual form, one can see that in the image-based segmentation some coniferous trees are classified as deciduous. This is due to the smoothed surface of the image-based models.

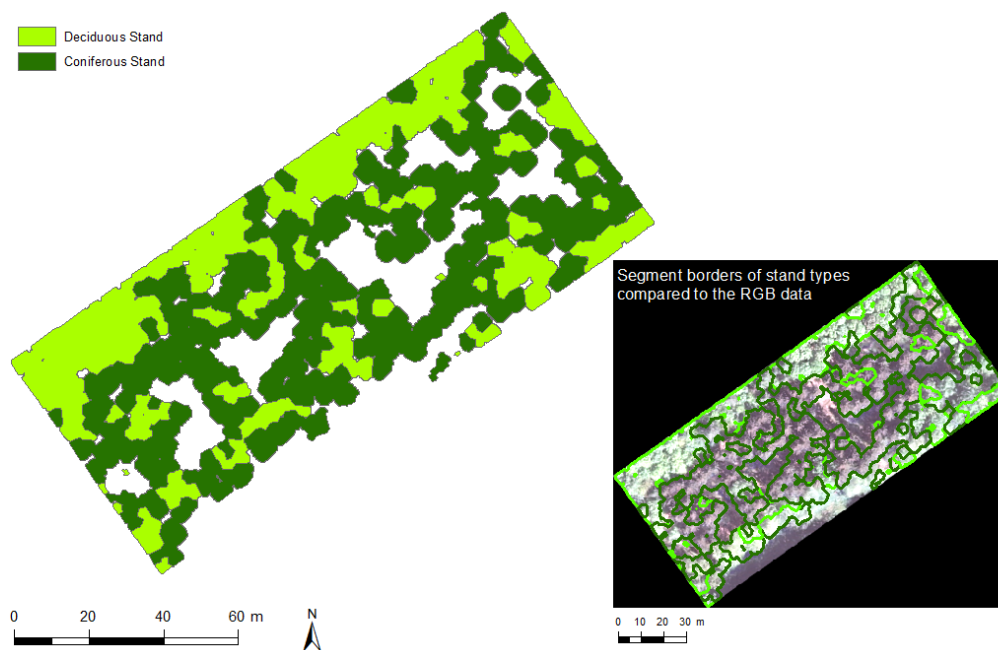


Figure 111: Classification results using image-based height variation feature STD (left), compared with RGB data (right).

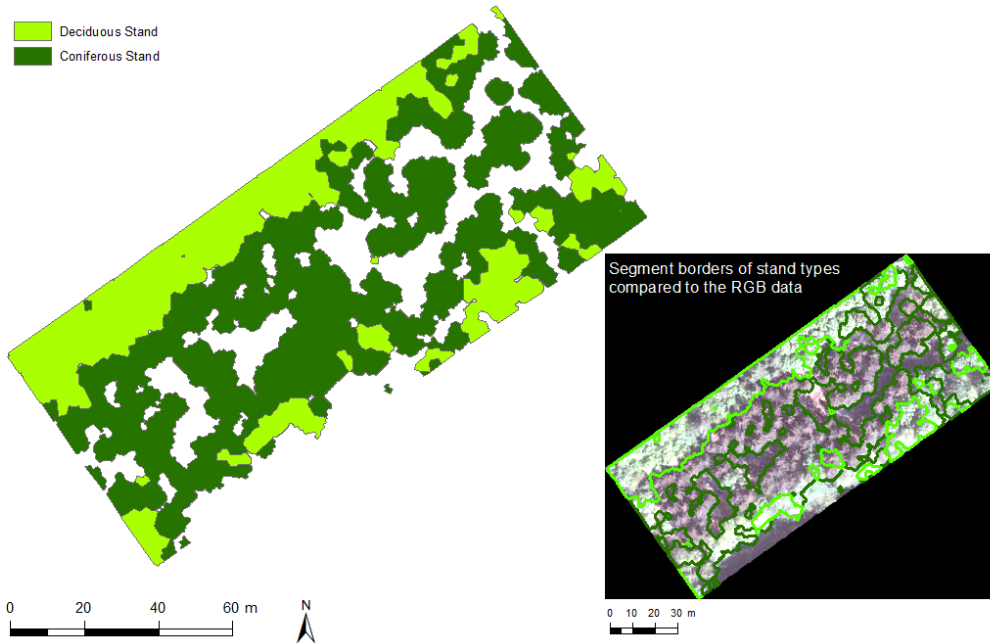


Figure 112: Classification results for laser-based height variation with feature NHV (left) compared with the RGB data (right).

6.4.2. Form analysis

In this section the form of the tree segments is evaluated based on the flatness analysis. For this, the geometry feature Mean Quasi Flatness (MQF) is implemented (see section 5.8). The hypothesis in this case is that the segments belonging to the deciduous trees are flatter than the coniferous ones. The classification results are demonstrated in Table 13.

Tree Type	Values for	Tree height from image	MQF image	Tree height from laser	MQF laser
Coniferous	Min	1.79	0.051	3.30	0.100
	1st Quartile	18.10	0.063	17.17	0.129
	Median	20.88	0.077	19.51	0.162
	3rd Quartile	22.88	0.099	21.28	0.230
	Max	26.76	0.424	25.88	0.600
	Mean	20.30	0.090	18.71	0.218
Deciduous	Min	11.17	0.000	8.93	0.024
	1st Quartile	19.38	0.022	19.03	0.057
	Median	20.73	0.032	20.77	0.073
	3rd Quartile	23.28	0.040	23.08	0.088
	Max	26.02	0.050	25.85	0.100
	Mean	21.04	0.031	20.74	0.070

Table 13: Analysis of form feature MQF on laser-based and image-based surface models

The distribution analyses of the coniferous and deciduous classes are represented in Figure 113 and Figure 114 respectively. Due to the small values of MQF, they are represented with factor 10 near the height values in the boxplots. Comparing the laser-based and image-based surface models, one can see that in both cases most of the segments are at the highest levels of elevations. However, due to the interpolation of the height values in the gap areas between the coniferous trees, the image-based elevation have even larger values compared to the laser data. The value of less than 4m for the minimum height of both datasets shows that some low vegetation segments are also categorized in this class. The reason is the small size of these segments which lead to higher values of MQF. These low vegetation areas can be simply excluded from the classification results by setting a threshold of height or segment size.

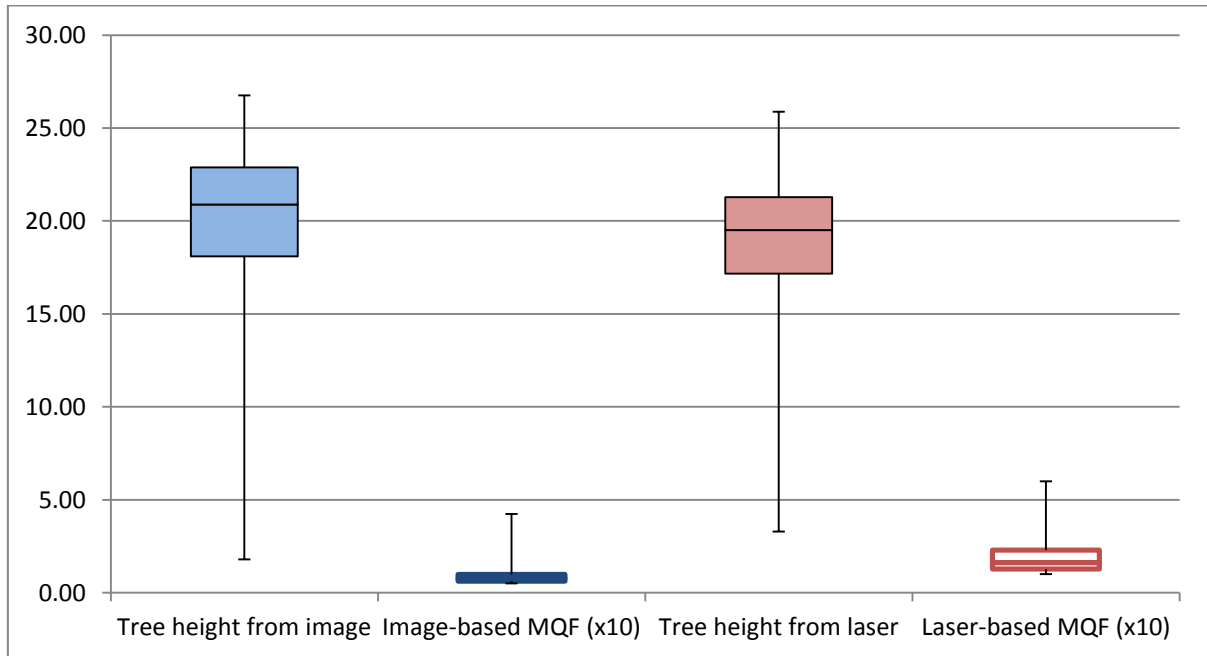


Figure 113: Segment specification of coniferous classification using the form parameters on image-based and laser-based surface models

Compared with the coniferous classes, the deciduous ones (Figure 114) lay also in the top elevations (more than 19m for laser and image data). In contrast with the coniferous classes, the deciduous segments, classified by MQF on the image-based nDSM, possess nearly the same range of laser-based values. This is due to the density of the deciduous canopy and consequently fewer shadows in the gap areas. The false elevations calculated from the height interpolation in these regions are less than the coniferous ones.

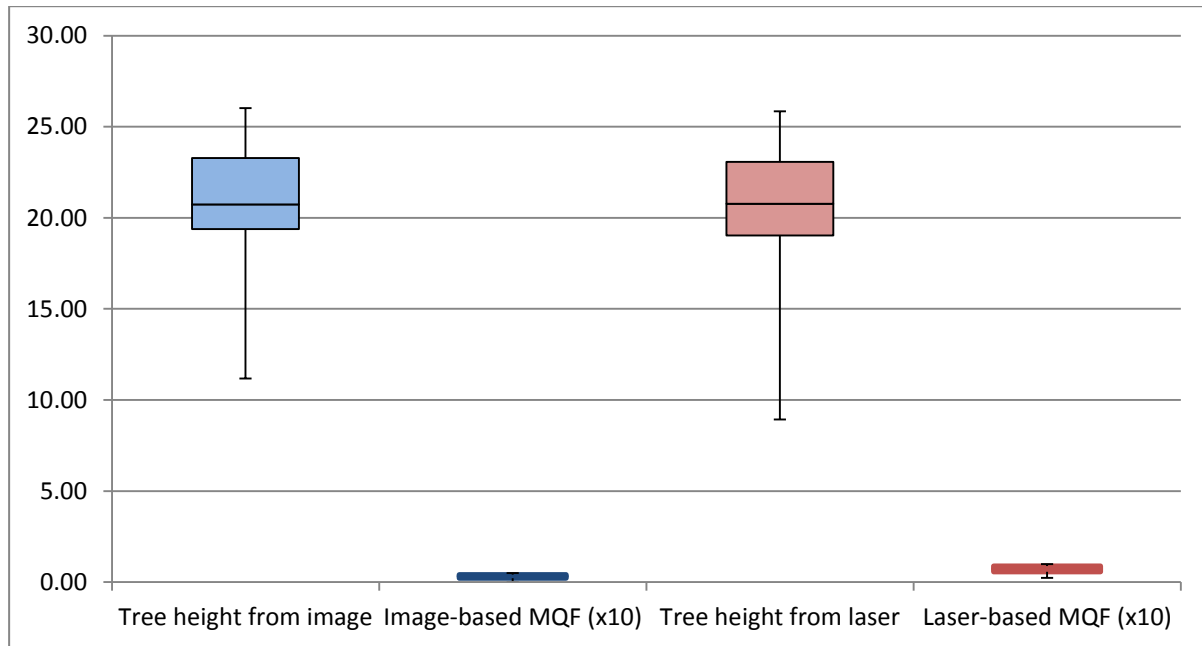


Figure 114: Segment specification of deciduous classification using form parameters on image-based and laser-based surface models

For a better illustration, the boxplot diagram of the coniferous and deciduous stands are compared and expanded in Figure 115. Referring back to Table 13, in both surface models, the MQF value of the coniferous segments are larger than the deciduous ones. This proves the hypothesis that deciduous trees are flatter than coniferous ones. The difference of mean values (0.059 difference for image-based and 0.148 for the laser-based nDSM) illustrates the greater efficiency of LIDAR compared to the photogrammetric method in keeping the geometric form of the trees. This is because of the smoothed form of the image surface models that the top point of the trees have less height than their true height in the nature.

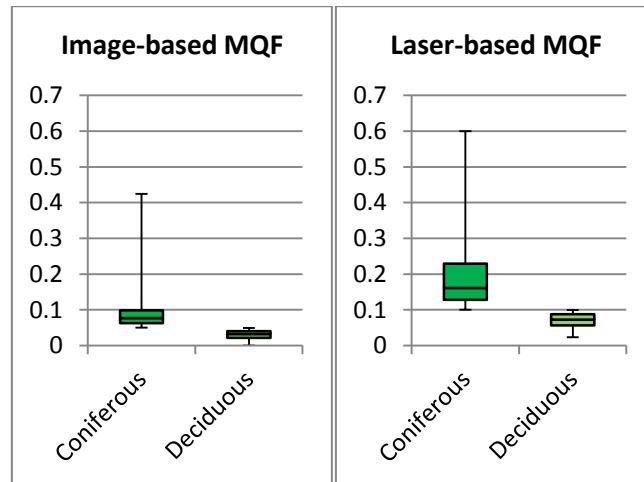


Figure 115: Comparison of the tree classes based on image-based and laser-based form parameter MFQ

The classification results are illustrated in Figure 116 and Figure 117. In both datasets, the MFQ feature can separate the coniferous and deciduous trees with more efficiency than the roughness feature. Even the isolated trees in both stand types (coniferous trees in deciduous stand and deciduous trees in coniferous stand) are significantly better distinguished using this geometry feature.

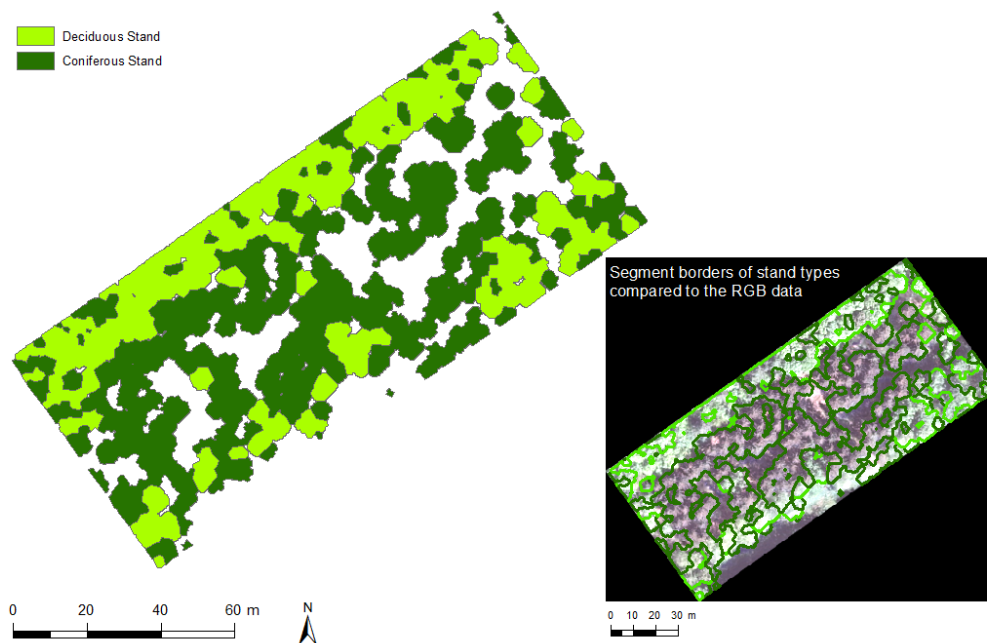


Figure 116: Classification results using laser-based form feature MQF (left), compared with RGB data (right).

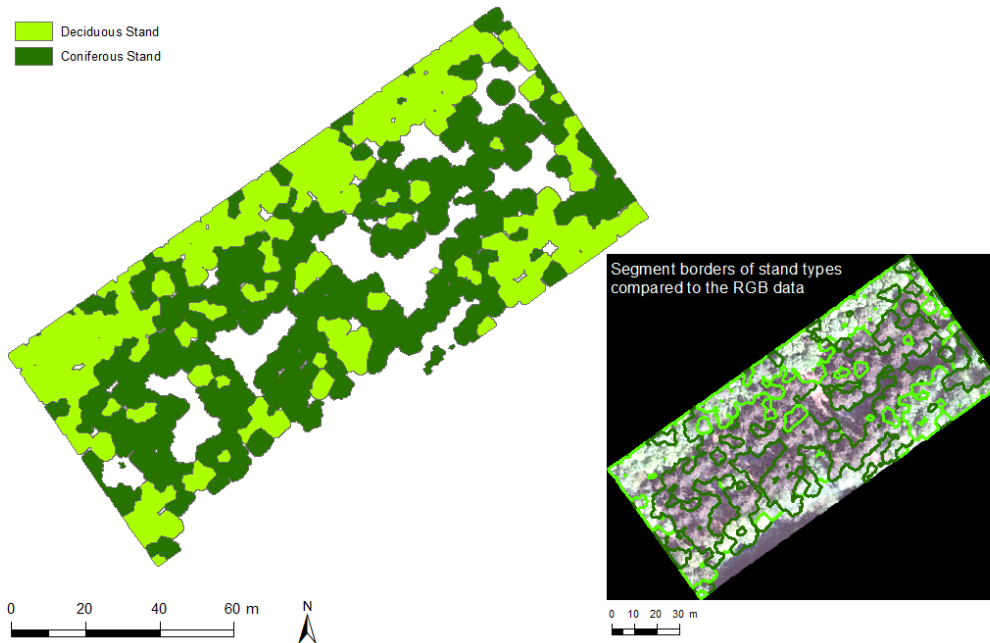


Figure 117: Classification results using image-based form feature MQF (left), compared with RGB data (right).

6.5. Quantitative evaluation of single tree delineation

For quantitative analysis of the single tree extraction algorithm, two aspects are taken into account; first the positioning accuracy of the single trees extraction and second the delineation of the crown regions. For this purpose, two datasets, called *reference* and *target*, are provided and compared. Each dataset contains vector data for tree positions in *point* format and for tree regions in the form of *polygons*. Evaluation of the tree regions, in this research, is undertaken on the basis of the spatial analysis of the reference and target polygons. The reference segments are simulated by the region growing of the segments on the surface models. The seed segments are the tree positions from reference segments. The growing procedure for each segment is weighted by the DBH, extracted from the terrestrial measurement (laser scanning and close-range photogrammetry) of the circles at breast height level. The tree regions are finally controlled with spectral data.

The tree positions in the reference dataset are extracted from the terrestrial methods (see section 6.2), whereas, in the target dataset, they are extracted from different features in the tree segment.

The tree positions, measured with the terrestrial laser scanning, are used to form a simulation of a reference dataset. To provide this simulated reference system the tree circles extracted from the combination of the close-range photogrammetry and the TLS data are used as seed objects. These will be converted into a thematic layer carrying the DBH characteristics in centimeter. This geometric value (segment area based on the DBH) will be used in a region growing algorithm as a weighting value, to simulate the tree crowns based on the available height data.

The positioning evaluation is based on the measurement of distance between reference and target points in Euclidean space. The allocation of an arbitrary reference point to its related neighboring target points is based on the overlapping target polygons. This means, the target polygons without any overlap with the reference segment will not get any allocation value. For the point-point evaluation, the tree positions (TP) are provided in four datasets (Table 14).

Reference points	Target points
<ul style="list-style-type: none"> • P: Position from TLS measurement of the tree circles at breast height • CR: Tree position from Centroid of Reference polygon 	<ul style="list-style-type: none"> • Mrb: Tree position from Marble Rolling segments • CT: Tree position from Centroid of Target polygon

Table 14: Point to point datasets

Among the allocated lines, the nearest point will be chosen as the related target point (Figure 118). In the next step, the completeness evaluation (producer accuracy) of the distances is calculated and categorized using 1m to 3m buffers. As can be seen in Table 15, for the laser-based data, the best quality of the evaluation is obtained from the comparison of the TLS measurements (P) and the positions of marble rolling (Mrb) segments. For single tree extraction with precision of less than 2m, the completeness of 87.2% and the correctness of 91% shows the efficiency of this method compared to the existing algorithms. In [Straub and Heipke 2007] these values were between 41% to 81% for completeness and 66% to 100% for correctness in single tree extraction of urban areas.

Point datasets	Buffer					
	Evaluation	D <3m	D <2.5m	D <2m	D <1.5m	D <1m
CR-CT	Completeness	96.2	94.9	85.3	72.4	48.7
	Correctness	92.3	85.1	72.9	62.4	42.0
	Quality	89.0	81.3	64.8	50.4	29.1
CR-Mrb	Completeness	94.2	91.7	80.1	71.8	46.2
	Correctness	92.8	86.7	76.8	65.7	39.8
	Quality	87.8	80.4	64.5	52.3	27.2
P-CT	Completeness	97.4	94.9	84.0	70.5	41.0
	Correctness	87.3	80.1	68.5	57.5	35.9
	Quality	85.3	76.8	60.9	46.3	23.7
P-Mrb	Completeness	95.5	95.5	87.2	78.2	56.4
	Correctness	98.7	96.8	91.0	81.4	56.4
	Quality	94.3	92.6	80.8	66.4	39.3

Table 15: Point-point evaluation (in %) of the laser-based data of the reference and target tree positions

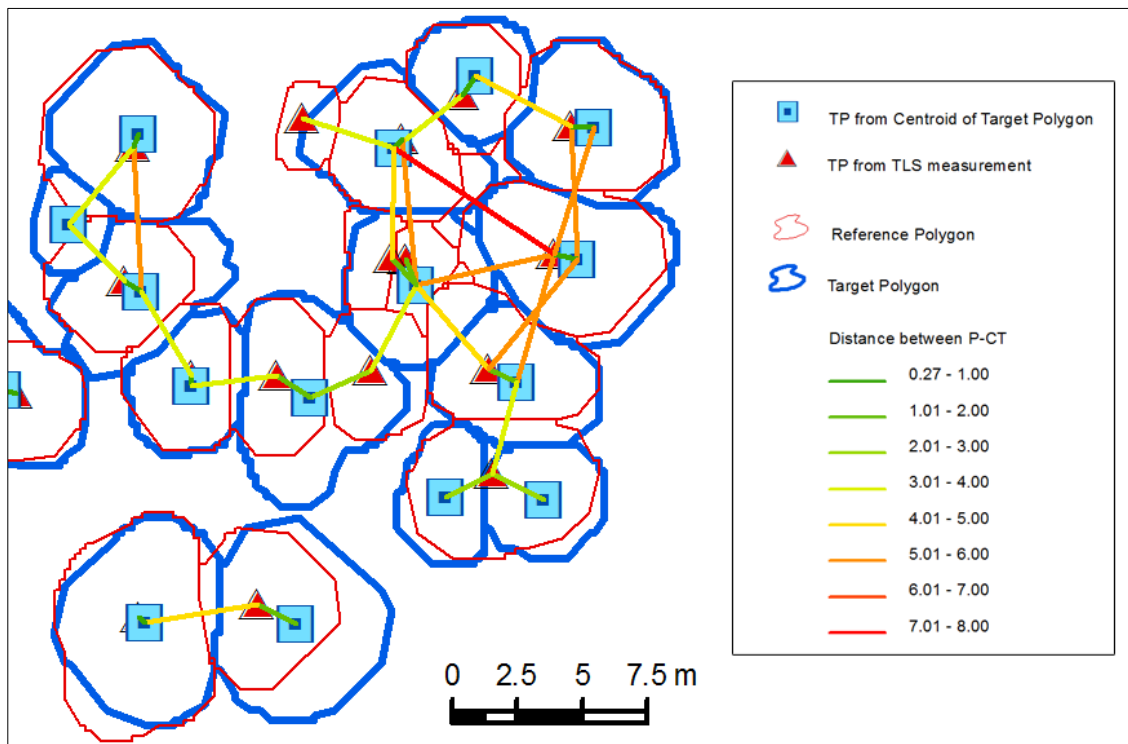


Figure 118: Allocation lines from the reference points to the target points in the case of P-CT datasets

In [Persson et al. 2002] 86% of the trees with a diameter of more than 15cm are automatically detected. These parameters increase in the lower positioning accuracies (less than 2.5m and 3m). The lower values for the accuracy of less than one meter are because of the different characteristics of the airborne and terrestrial datasets. The inclination of the trees is assumed as a reason for this difference.

In the image-based CHM (Table 16), for the distance buffer of less than 3m, the completeness of the extracted trees based on the centroid of the target segments (CT) shows better results (96.8% for CR-CT and 97.4% for P-CT). As the parameters CT and CR are dependent on the polygonal shape of the segment, these results are expected because of greater stability of the tree segments after region growing. The two independent parameters from region growing are the tree positions from the terrestrial measurements (P) and the marble rolling segments (Mrb). The completeness of 87.8% for positioning accuracy of less than 2m shows the high efficiency of this method in single tree extraction in coniferous stands. In Figure 119 the allocations of the extracted trees to the reference data are demonstrated for the buffer 2.5m.

Point datasets	Buffer	D <3m	D <2.5m	D <2m	D <1.5m	D <1m
	Evaluation					
CR-CT	Completeness	96.8	92.9	82.1	68.6	46.8
	Correctness	99.4	84.5	70.7	58.0	40.3
	Quality	96.3	79.4	61.2	45.8	27.7
CR-Mrb	Completeness	92.3	87.2	81.4	67.3	51.9
	Correctness	99.4	88.4	78.5	59.1	45.3
	Quality	91.8	78.2	66.5	45.9	31.9
P-CT	Completeness	96.8	92.9	84.6	73.7	46.8
	Correctness	92.3	80.7	70.2	60.8	39.2
	Quality	90.1	76.0	62.2	50.0	27.1
P-Mrb	Completeness	93.6	90.4	87.8	77.6	64.1
	Correctness	95.6	89.5	74.6	66.9	54.7
	Quality	89.7	81.7	67.6	56.0	41.9

Table 16: Point-point evaluation (in %) of the image-based data of the reference and target tree positions

In addition to positioning evaluation of the single tree extractor, to evaluate the quality of the segmentation the polygonal analyses are also incorporated in the next assessments.

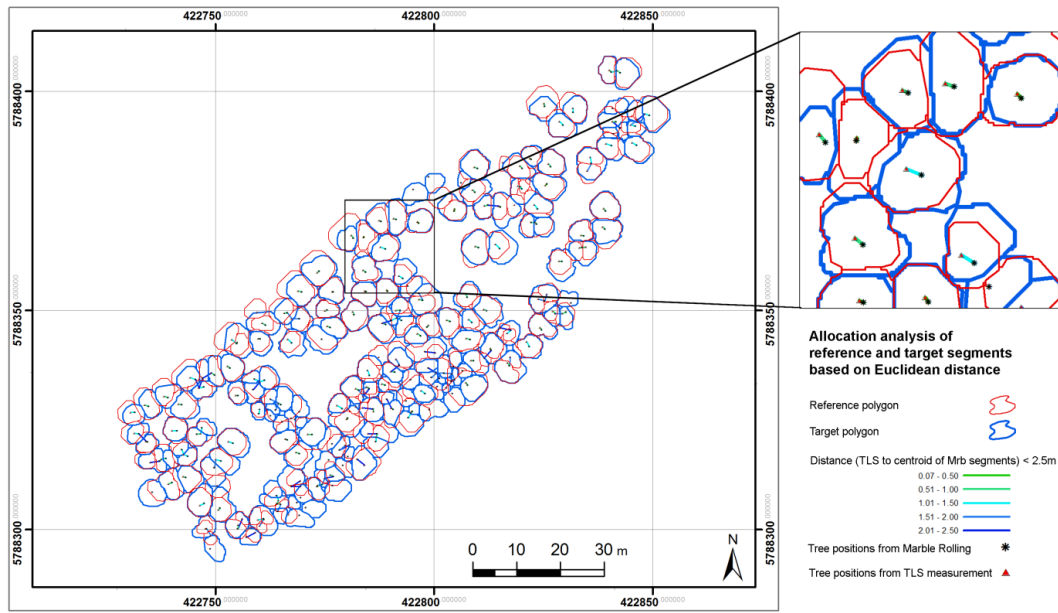


Figure 119: Allocated trees from target segments of the marble rolling segments laser-based data to the reference TLS segments for the 2.5m buffer

For the polygon-polygon analysis of the reference data and the extracted trees, the advanced overlapping factor (AOF) of reference and target segment is calculated (Figure 120).

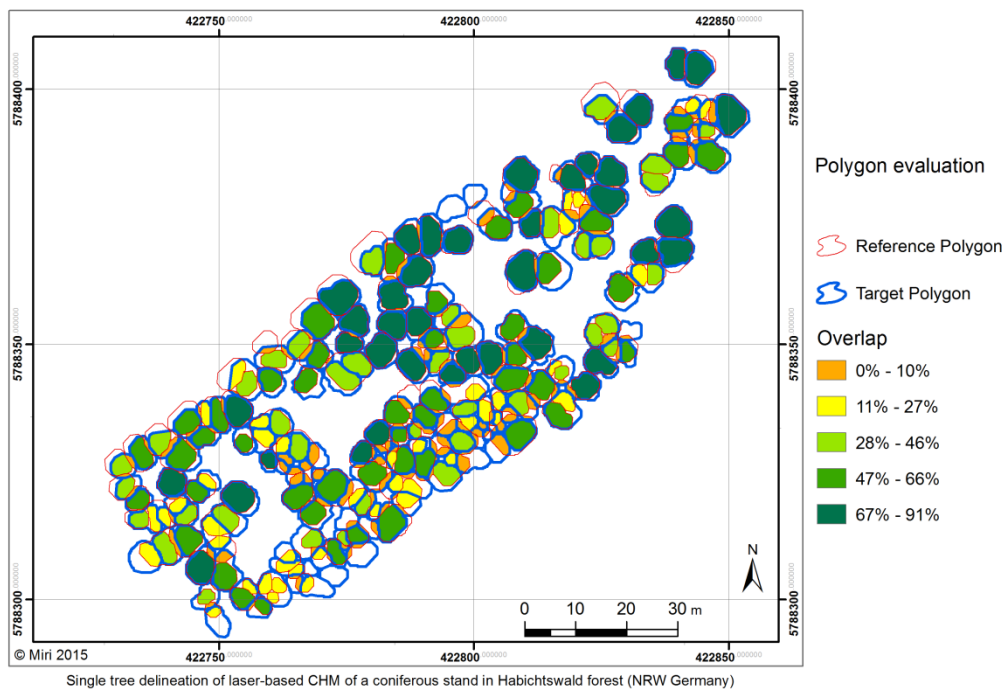


Figure 120: Quantitative evaluation based on overlapping factor of AOF

In addition to the overlapping ratio, the distance analysis is carried out based on the weighted distance (WD) factor.

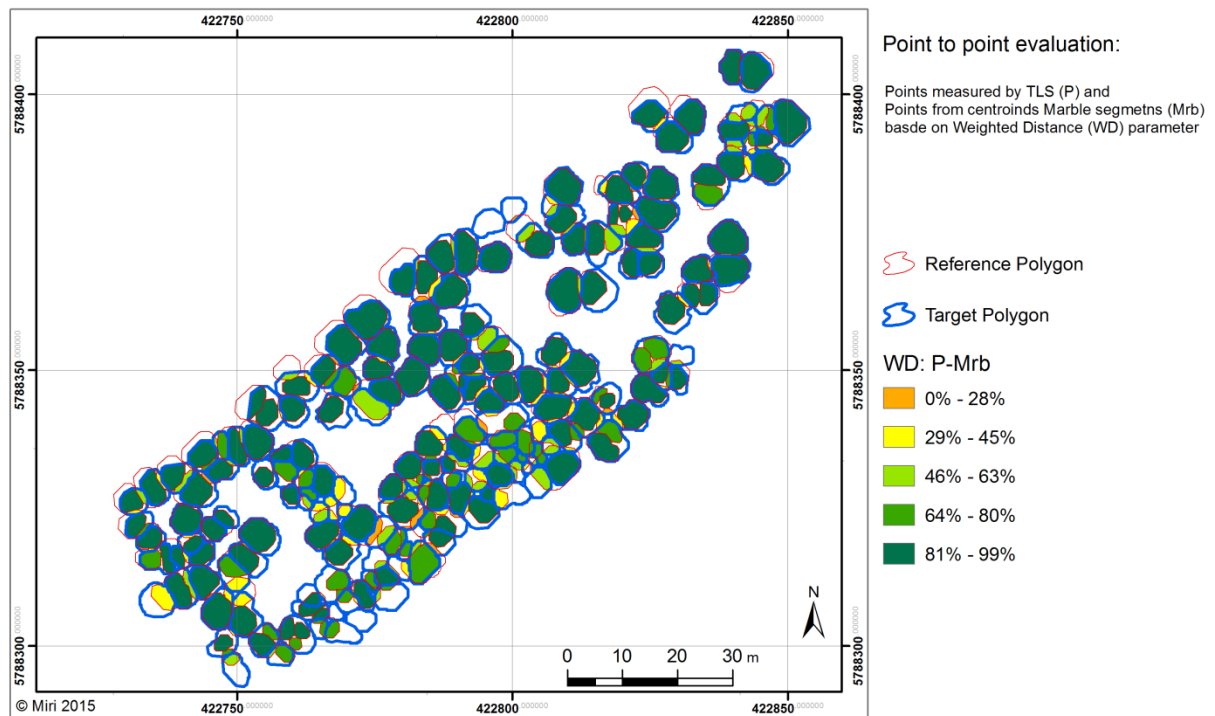


Figure 121: Point-point analyses of the reference and target datasets (P and Mrb) based on the weighted distance factor (WD)

To incorporate the overlapping ratio into the distance analyses and to provide a point-polygon quality evaluator, the WDO factor (see section 5.10) is calculated. In the ideal case, the target and reference segments are 100% the same if they cover each other completely and, furthermore, the positions should be the same (WD=100%).

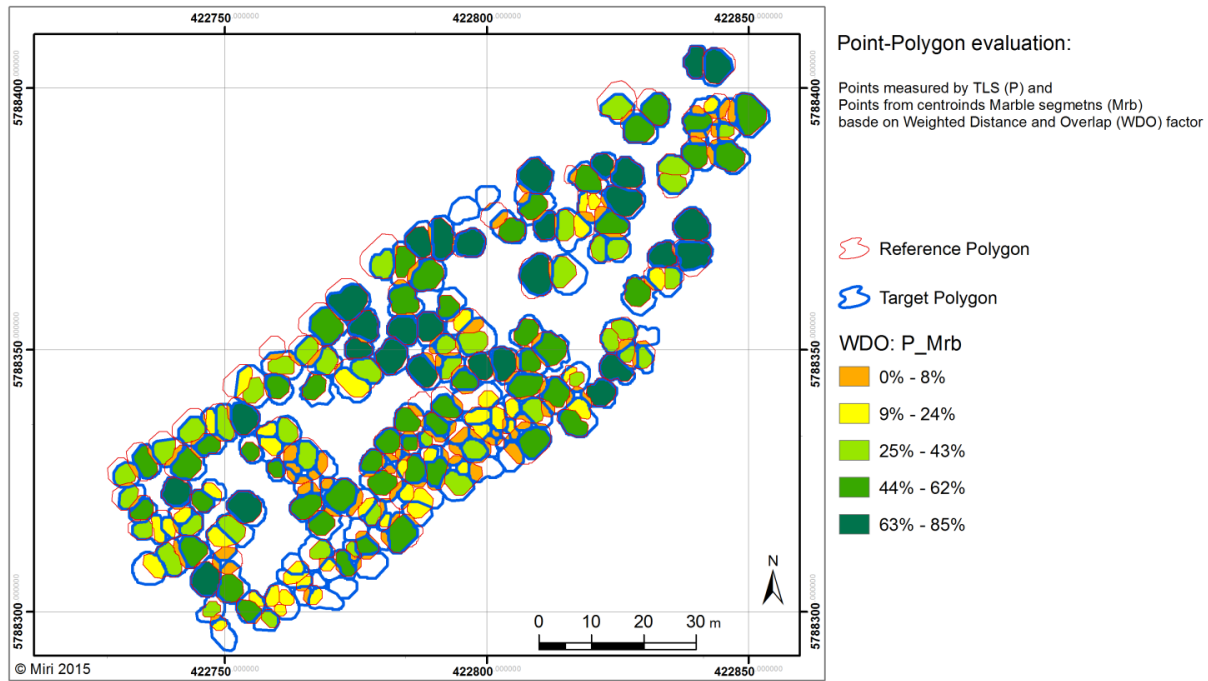


Figure 122: Point-polygon analyses of the reference and target datasets (P and Mrb) based on the weighted distance and overlapping factor (WDO) on LIDAR-based CHM

The target segments with $WDO < 10\%$ are defined as the low quality segments which are due to the large distance or very small overlap with the reference segments. These oversegmented regions are, for the most part, the broad-leaved trees and can be seen in orange in Figure 122 for the LIDAR-based dataset. The best results are obtained for the WD of the marble rolling (Mrb), which shows the higher quality of this dataset for evaluation of the tree positioning. For the image-based data, the oversegmentation of the extracted trees is greater than the LIDAR data, which reduces the quality of the segmentation (Figure 123).

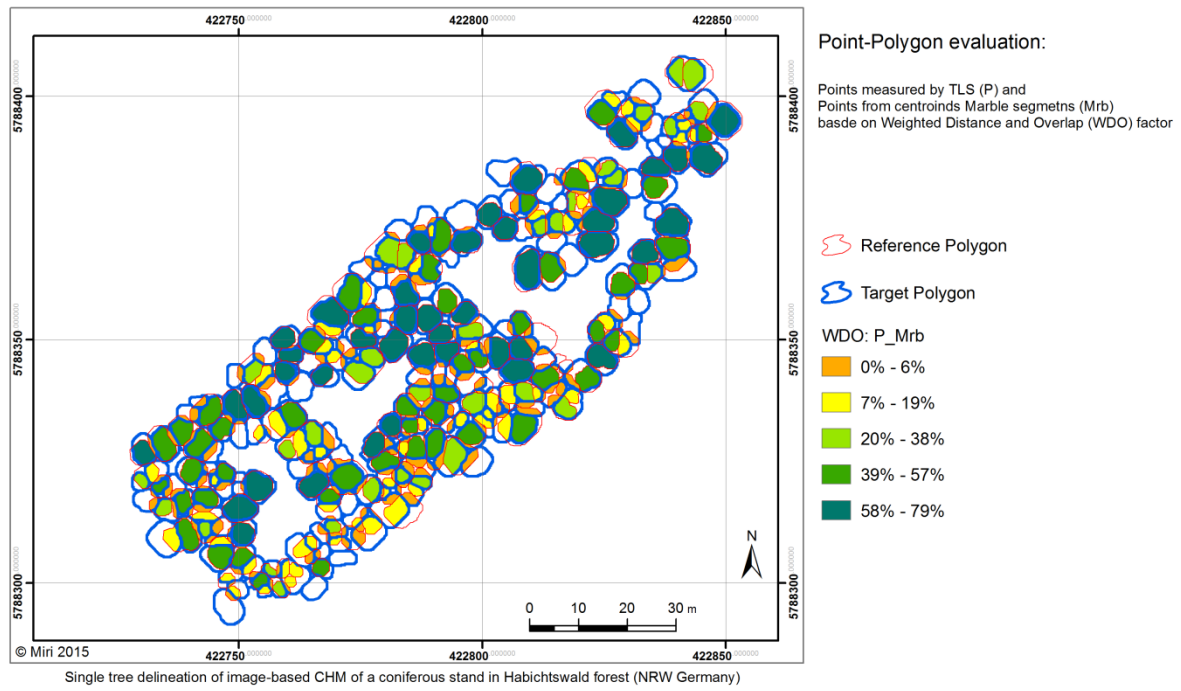


Figure 123: Point-polygon analyses of the reference and target datasets (P and Mrb) based on the weighted distance and overlapping factor (WDO) on image-based CHM



Conclusion and outlook

This chapter outlines the results of this research and the outlook for future work.

7.1. Height-based forest mensuration

The demand for more detailed mensuration of the individual trees is considered. Forest parameters at single tree level are for the most part related to tree height. In this research digital elevation models for European mixed forest are evaluated as an approach to single tree extraction. The focus is on comparison of laser-based and image-based digital elevation data. The spectral layers of aerial images are not implemented in this research for the following reasons:

- Firstly, the spectral data are compromised by the different textural characteristics of the trees in the image scene. Capturing different sides of the trees in stereo imagery, different illumination and the problem of the shadows are the main concerns in this regards.
- Secondly, the height of the trees is mostly used as a complementary layer in combination with the spectral data. As an important layer to describe the shape of the tree crowns, analyzing the CHM layers, independently from the spectral data, is necessary to consider the advantages and limitations of this layer for geospatial analysis in forestry.

While image-based DSM is suitable for detailed stand-wise analysis, the complementary data such as spectral channels and vitality indices are required for the purpose of single tree extraction. The problematic areas are the gaps between the trees and the shadows. These areas are normally interpolated in image-based DSMs. In open stands, the completeness of the single trees falls off in such datasets. The lower roughness is one of the disadvantages of this data for the young stands in mixed-forests, where the tree regions are not easy to distinguish. This suggests that, for practical purposes, implementation of image-based CHM is recommended in dense and old forests.

In the interests of completeness, due to the direct measurement of the tree crowns in LIDAR, these datasets are more reliable than the photogrammetric height data.

7.2. From stand-wise analysis to single tree extraction

The Roughness parameters are used to extract the characteristics of the stand, which is a method to define the stand type. Among the roughness parameters, the average based parameters provide general information about the stand geometry.

To define the appropriate parameters, e.g. scale space, a novel approach of marble rolling is proposed. Depending on the characteristics of the stands, the size of the marbles for single tree extraction can be identified. Having defined the stand type, the surface characteristics can be analyzed in further research to choose the appropriate parameters for marble rolling segmentation and region growing.

Filtering the height data is carried out with a non-smoothing algorithm. In addition to removing the noise data, the main task of this filter is to close the gap pixels within the tree crown without changing the crown shape. These small pixels are the main reason for oversegmentation in LIDAR datasets.

Surface analysis of the stand and crown height models can be used as an instrument for analyzing the characteristics of the forest areas and stand-wise partitioning of forests. Due to the influence of the peak and valley effect in evaluation of the surfaces, the roughness parameters related to the mean height of the stand, e.g. R_a , are reliable in the case of dense forests. To analyze the roughness of the tree surface models at finer scales the R_{fstd} feature is developed in this research. Using this surface evaluator the characteristics of the forests are evident at single tree level and can be employed as a feature in classification of the tree species. The results from different tree stands show that this parameter is independent from the stand density, the peak and valley effects or the stand type. Furthermore, the possibility of changing the sensitivity of the roughness evaluator is one of its great advantages. This parameter also serves to find the optimized strength and number of iterations in filtering the CHM data in the data preparation steps.

Extraction of the roughness attributes based on the standard deviation of image-based nDSM provides less information from the surface than the laser data. The roughness characteristics in the image-based surfaces are dependent on the conditions during the imagery and also the surface calculation in post processing steps. Gaps in DSM data (caused from matching problems) and the smoothing parameters in final processes remove the significant characteristics required for roughness evaluations.

The **Marble-rolling** method is proposed as a new and strong tool to extract seed objects. This method provides a solution to the problem of scale space. In the context of future work, the

author recommends development of this research in two aspects; firstly, to deepen the algorithms in different forest types and secondly, to exploit these techniques in other disciplines. For coniferous trees that might not have the expected cone form (like pine) the parameters should be set as for deciduous trees.

Stand boundaries are extracted based on the curvature analysis. As the height difference between the trees which are in the same aging group varies significantly, it is not recommended to use the curvature profiles for separation of single tree crown regions. An automatically supervised region growing algorithm is implemented in this research, based on the morphological structuring elements, to keep the tree form the seed objects while growing as a tree segment. This will partition the stand into tree regions.

However, for single trees in urban areas, the curvature parameters can succeed where sudden changes in elevation between the tree crown surface and the manmade objects (e.g. street, yard) occur. Separating the trees from the objects with close height values (like buildings in neighborhood) can be implemented considering the sudden changes in the textural characteristics and the homogeneity of the surface. Finding the appropriate settings for these features is a challenging approach in dense forests.

7.3. Outlook

To expand the techniques in forest classification, integration of this work with available forest information systems is advised. The roughness parameters can be used as main or complementary features, integrating with spectral layers for texture-based analyses. To define the geometric structure of the forests, e.g. the Stand Density Index (SDI), texture based surface analyses can be designed using developed roughness evaluators to extract the direction and wildness of the plantation. In this way, a detailed and extensive archive should be designed, in which each stand type is evaluated over different seasons and different ages.

In other disciplines, due to the complexity of single tree extraction in forest areas, it is expected that the algorithms and techniques designed in this research will be implemented for extraction of single trees in urban areas or even for small vegetation in open lands.

Due to the independence of the roughness parameter R_{fstd} from the height values, this evaluator can be employed also for change detection analyses in agricultural fields.

This algorithm can be studied in the case of different stand types. In coniferous stands, the growth direction of single trees can also be extracted in several marble projection layers.

Combination of laser data with full-wave-form and intensity data can enrich these elevation models for the purpose of more accurate classification of the tree types.



8

References

LITERATURE

- ACKERMANN, J., ADLER, P., ENGELS, F., ET AL. 2014. Forstliche Fernerkundung in den Bundesländern auf neuen Wegen. *AFZ-Der Wald* 9.
- ADAMS, R. 1993. Radial decomposition of disks and spheres. *CVGIP: Graphical models and image processing* 55, 5, 325–332.
- ADLER, P. 2001. Einsatz digitaler Photogrammetrie zur Beschreibung von Waldbeständen -. 198.
- ANDERSEN, H.-E., REUTEBUCH, S.E., AND SCHREUDER, G.F. 2001. Automated individual tree measurement through morphological analysis of a LIDAR-based canopy surface model. *Proc. International Precision Forestry Symposium, Seattle, WA, USA*, 11–21.
- ARBEITSGRUPPE FORSTLICHER LUFTBILDINTERPRETEN. 2012. *Das digitale Luftbild: ein Praxisleitfaden für Anwender im Forst-und Umweltbereich*. Universitätsverlag Göttingen.
- ASME_B46. 1. 1985. *Standard, ASME Surface Quality*. .
- BAATZ, M., HOFFMANN, C., AND WILLHAUCK, G. 2008. Progressing from object-based to object-oriented image analysis. *Object-Based Image Analysis*, 29–42.
- BAATZ, M. AND SCHÄPE, A. 2000. Multiresolution Segmentation : an optimization approach for high quality multi-scale image segmentation. *Angewandte Geographische Informationsverarbeitung XII*, 12–23.
- BALTSAVIAS, E. 1999a. Airborne laser scanning: basic relations and formulas. *ISPRS Journal of Photogrammetry and Remote Sensing* 54, 2-3, 199–214.
- BALTSAVIAS, E.P. 1999b. A comparison between photogrammetry and laser scanning. 83–94.
- BALTSAVIAS, E.P. 1999c. Airborne laser scanning: existing systems and firms and other resources. *ISPRS Journal of Photogrammetry and Remote Sensing* 54, 2-3, 164–198.
- BAYER, S., MIRI, M., AND BUCHER, T. 2013. Automatisierte Einzelbaumerfassung auf Basis von hochauflösten TrueOrtho-Mosaiken und photogrammetrisch abgeleiteten Oberflächenmodellen. *DGPF 2013, 33. Wissenschaftlich-Technischen Jahrestagung*, 26–35.
- BECHTEL, B. 2007. Objektextraktion von Bäumen aus Luftbildern: Vergleich und Steuerung von Segmentierungsverfahren zur Vorbereitung eines Expertensystems, Diplomarbeit. .
- BERALDIN, J.A., BLAIS, F., AND LOHR, U. 2010. Laser scanning technology. In: *Airborne and terrestrial laser scanning*. 1–42.

- BEUCHER, S. AND LANTUÉJOUL, C. 1979. Use of watersheds in contour detection. *international workshop on image processing: real-time edge and motion detection/estimation*.
- BLUNT, L. AND JIANG, X. 2003. *Advanced techniques for assessment surface topography: Development of a Basis for 3D Surface Texture Standards* "Surfstand." Elsevier.
- CASTILLA, G. AND HAY, G.J. 2008. Image objects and geographic objects. In: *Object-based image analysis*. Springer, 91–110.
- DEVENEZIA, K., WALKER, S., AND ZHANG, B. 2007. New approaches to generating and processing high resolution elevation data with imagery. *Photogrammetric Week*, 297–308.
- ECOGNITION. 2013. eCognition® Developer 8.9. In: *eCognition Reference Book*. Trimble Germany GmbH, München.
- EGENHOFER, M.J. AND FRANZOSA, R.D. 1991. Point-Set Topological Spatial Relations. *International Journal of Geographical Information Systems* 5, 2, 161–174.
- ERIKSON, M. AND OLOFSSON, K. 2005. Comparison of three individual tree crown detection methods. *Machine Vision and Applications* 16, 4, 258–265.
- FUCHS, H. 2003. Methodische Ansätze zur Erfassung von Waldbäumen mittels digitaler Luftbilddauswertung, PhD thesis. www.ediss.uni-goettingen.de.
- VON GADOW, K. 2005. *Forsteinrichtung: Analyse und Entwurf der Waldentwicklung*. Universitätsverlag Göttingen, Berlin.
- GERKE, M. 2006. Automatic Quality Assessment of Road Databases Using Remotely Sensed Imagery, PhD thesis. .
- GOUGEON, F.A. 1998. Automatic individual tree crown delineation using a valley-following algorithm and rule-based system. *Proc. International Forum on Automated Interpretation of High Spatial Resolution Digital Imagery for Forestry, Victoria, British Columbia, Canada*, 11–23.
- HAALA, N. AND WOLFF, K. 2009. Digitale photogrammetrische Luftbildkamarasysteme-Evaluation der automatischen Generierung von Höhenmodellen. *Proceedings of the Annual Meeting of the DGPF*, 1–10.
- HANBURY, A. 2008. Image Segmentation by Region Based and Watershed Algorithms. *Wiley Encyclopedia of Computer Science and Engineering*.
- HARALICK, R.M., SHANMUGAM, K., AND DINSTEN, I. 1973. Textural features for image classification. *IEEE Transactions on Systems, Man and Cybernetics SMC-3*, 6, 610–621.

- HASENAUER, H. AND MONSERUD, R.A. 1996. A crown ratio model for Austrian forests. *Forest Ecology and Management* 84, 1, 49–60.
- HEINZEL, J.N., WEINACKER, H., KOCH, B., AND FREIBURG, A. 2008. Full automatic detection of tree species based on delineated single tree crowns - a data fusion approach for airborne laser scanning data and aerial photographs. *SilviLaser 2008*, 76–85.
- HILDEBRANDT, G. 1969. *Bibliographie des Schrifttums auf dem Gebiet der forstlichen Luftbildauswertung 1887-1968*. Institut für Forsteinrichtung u. Forstliche Betriebswirtschaft d. Universität Freiburg im Breisgau.
- HIRSCHMULLER, H. 2005. Accurate and efficient stereo processing by semi-global matching and mutual information. *Computer Vision and Pattern Recognition, 2005. CVPR 2005. IEEE Computer Society Conference on, IEEE*, 807–814.
- HOLDAWAY, M.R. 1986. Modeling tree crown ratio. *The Forestry Chronicle* 62, 5, 451–455.
- HYYPÄ, J., HYYPPÄ, H., LITKEY, P., ET AL. 2004. Algorithms and methods of airborne laser-scanning for forest measurements. *International Archives of Photogrammetry, Remote Sensing and Spatial Information Sciences* 36, 8/W2, 82–89.
- ISO_4287. 1997. Geometrical product specifications (GPS)–Surface texture: Profile method–Terms, definitions and surface texture parameters. *Geometrical product specifications (GPS)–Surface texture: Profile method–Terms, definitions and surface texture parameters*.
- IWANOWSKI, M. AND SOILLE, P. 2005. Morphological refinement of an image segmentation. *Computer Analysis of Images and Patterns*, Springer, 538–545.
- JONES, R. AND SOILLE, P. 1996. Periodic lines: Definition, cascades, and application to granulometries. *Pattern Recognition Letters* 17, 10, 1057–1063.
- KENNEWEG, H. AND WEYER, G. 2014. Climate Change: How to Fight Destructive Effects in Urban Areas-Concepts, Planning Approaches and Measures in Germany. *Paranoá: cadernos de arquitetura e urbanismo* 7.
- KOCH, B., HEYDER, U., AND WEINACKER, H. 2006. Detection of Individual Tree Crowns in Airborne Lidar Data. *Photogrammetric Engineering & Remote Sensing Vol. 72, 4*, 357–363.
- LAAR, A. VAN AND AKÇA, A. 2007. *Forest Mensuration*. Springer Netherlands, Dordrecht.
- LANG, S. 2008. Object-based image analysis for remote sensing applications: modeling reality–dealing with complexity. In: *Object-based image analysis*. Springer, 3–27.
- LARSEN, M. 1997. Crown modelling to find tree top positions in aerial photographs. *International Airborne Remote Sensing Conference*.

- LECKIE, D., GOUGEON, F., HILL, D., QUINN, R., ARMSTRONG, L., AND SHREENAN, R. 2003. Combined high-density lidar and multispectral imagery for individual tree crown analysis. *Canadian Journal of Remote Sensing* 29, 5, 633–649.
- LEMAIRE, C. 2008. Aspects of the DSM production with high resolution images. *International Archives of the Photogrammetry, Remote ...*, 1143–1146.
- LINDBERG, T. 1993. *Scale-space theory in computer vision*. Kluwer Academic Publishers, Netherlands.
- LINDBERG, T. 1994. Scale-space theory: A basic tool for analyzing structures at different scales. *Journal of applied statistics* 21, 1-2, 225–270.
- MEISSNER, B., RICHTER, M., AND DOLP, S. 2004. FE-basiertes Wurzelschwamm-Monitoring in der Wiederaufforstung der Lausitzer Tagebau-Folgelandschaft. *Publ. d. DGPF, Bd 13*, 195–201.
- MEYER, F. 2001. An Overview of Morphological Segmentation. *International Journal of Pattern Recognition and Artificial Intelligence* 15, 07, 1089–1118.
- MIELONEN, T., MALTAMO, M., YU, X., HONKAVAARA, E., AND KAARTINEN, H. 2005. Using individual tree crown approach for forest volume extraction with aerial images and laser point clouds. 144–149.
- MIRI, M., BAYER, S., AND BUCHER, T. 2013. Evaluation of high resolution digital surface models for single tree extraction approaches in mixed forests. *DGPF 2013, 33. Wissenschaftlich-Technischen Jahrestagung*, 137–145.
- NAGEL, V.J. 2001. *Skript Waldmesslehre*. Georg-August-Universität, Göttingen, Fakultät für Forstwissenschaften und Waldökologie.
- NAJMAN, L. AND COUPRIE, M. 2003. Watershed algorithms and contrast preservation. *Discrete geometry for computer imagery*, Springer, 62–71.
- PERSSON, A., HOLMGREN, J., AND SÖDERMAN, U. 2002. Detecting and measuring individual trees using an airborne laser scanner. *Photogrammetric Engineering and Remote Sensing* 68, 9, 925–932.
- PFEIFER, N., BRIESE, C., AND SENSING, R. 2007. Geometrical Aspects of Airborne Laser Scanning and Terrestrial Laser Scanning. *IAPRS XXXVI*.
- POLLOCK, R.J. 1996. The automatic recognition of individual trees in aerial images of forest based on a systematic crown image model. 185.

- PYYSALO, U. AND HYYPPA, H. 2002. Reconstructing Tree Crowns from Laser Scanner Data for Feature Extraction. *Proceedings ISPRS Commission III, Symposium 2002 Photogrammetric Computer Vision*.
- ROERDINK, J.B.T.M. AND MEIJSTER, A. 2001. The watershed transform: Definitions, algorithms and parallelization strategies. *Fundamenta Informaticae* 41, 1, 187–228.
- RUTZINGER, M., ROTTENSTEINER, F., AND PFEIFER, N. 2009. A Comparison of Evaluation Techniques for Building Extraction From Airborne Laser Scanning. *Selected Topics in Applied Earth Observations and Remote Sensing IEEE Journal of 2.1 (2009)*, 11–20.
- SATO, T. 2010. Case applications for forest resource assessment. *International Archives of the Photogrammetry, Remote Sensing and Spatial Information Science XXXVIII*, part8, 715–718.
- SCHARDT, M., ZIEGLER, M., WIMMER, A., WACK, R., AND DATA, L.S. 2002. Assessment of forest parameters by means of laser scanning. *International archives of photogrammetry remote sensing and spatial information sciences*.
- SHAN, J. AND TOTH, C. 2009. *Topographic Laser Ranging and Scanning: Principles and Processing*. Taylor & Francis Group.
- SHENG, Y., GONG, P., BLGLNG, G.S., AND BIGING, G.S. 2001. Model-Based Conifer-Crown Surface Reconstruction from High-Resolution Aerial Images. *Photogrammetric engineering and remote sensing* 67, 8, 957–965.
- SMITH, S.W.S. AND SCIENTIST, T. 1999. *The Scientist and Engineer's Guide to Digital Signal Processing, 1999*. California Technical Publishing, San Diego.
- SOILLE, P. 2003. *Morphological image analysis*. Springer, Berlin [u.a.].
- SOLBERG, S., NAESSET, E., AND BOLLANDSAS, O. 2006. Single tree segmentation using airborne laser scanner data in a structurally heterogeneous spruce forest. *Photogrammetric Engineering & Remote Sensing* 72, 12, 1369–1378.
- STRAUB, B. AND HEIPKE, C. 2004. Concepts for internal and external evaluation of automatically delineated tree tops. *International Archives of Photogrammetry, Remote Sensing and Spatial Information Sciences* 36, 8, 62–65.
- STRAUB, B.-M. 2003. Automatische Extraktion von Bäumen aus Fernerkundungsdaten. 100.
- STRAUB, B.-M. AND HEIPKE, C. 2007. Automatic extraction and delineation of single trees from remote sensing data. *Machine Vision and Applications* 18, 5, 317–330.
- STRAUB, C. AND SEITZ, R. 2011. No Title. *Proceedings of the DGPF conference*.

- STRAUB, C., STEPPER, C., SEITZ, R., AND WASER, L.T. 2013. Potential of UltraCamX stereo images for estimating timber volume and basal area at the plot level in mixed European forests. *Canadian Journal of Forest Research* 43, 8, 731–741.
- VINCENT, L. 1992. Recent developments in morphological algorithms. *ACTA STEREOLOGICA* 11, 521–532.
- VINCENT, L. AND SOILLE, P. 1991. Watersheds in digital spaces: an efficient algorithm based on immersion simulations. *IEEE transactions on pattern analysis and machine intelligence* 13, 6, 583–598.
- WAH, B. 2008. Wiley Encyclopedia of Computer Science and Engineering. *Wiley Encyclopedia of Computer Science and Engineering* 1. <http://dl.acm.org/>.
- WANG, Z., BOESCH, R., GINZLER, C., AND VII, W.G. 2008. Integration of high resolution aerial images and airborne LIDAR data for forest delineation. *The International Archives of the Photogrammetry, Remote Sensing and Spatial Information Sciences* Vol. XXXVI, 1203–1208.
- WEHR, A. AND LOHR, U. 1999. Airborne laser scanning—an introduction and overview. *ISPRS Journal of Photogrammetry and Remote Sensing* 54, 2-3, 68–82.
- WINTER, S. 2000. Uncertain topological relations between imprecise regions. *International Journal of Geographical Information Science* 14, 5, 411–430.
- YOUNG, I.T., GERBRANDS, J.J., AND VAN VLIET, L.J. 2007. *Fundamentals of image processing*. Delft University of Technology Delft, The Netherlands.

REFERENCE TABLE OF FIGURES

Figure 1: Tree height based on definition of [Laar and Akça 2007].....	8
Figure 2: Measurement of height with a vertical scale	9
Figure 3: Forest parameters based on characteristics of the tree crown	11
Figure 4: Artificial reflectance of the crown surface, setting the light source at a height of 45 degree and azimuth of (from left to right) 0, 90, 180 and 270 degree	13
Figure 5: Illumination elements in spectral imagery of tree crown [Larsen 1997].....	13
Figure 6: Different texture caused from the shadows on tree surface (left) and from the tree height on the ground (middle) and effect of the shadows on colored data (right).....	14
Figure 7: Multiresolution segmentation of shaded surface of a single tree with roughness shadows (left) and height shadows (middle) compared with spectral data (right).	15
Figure 8: The length of shadows (S) in aerial images.....	16
Figure 9: Occluded areas (black) and projected surface of the tree crowns (green) in aerial images	17
Figure 10: Different viewing angles and templates for STE from high resolution images [Larsen 1997]	17
Figure 11: Stereoscopic measurement of tree height in flat (left) and topographic (right) areas (Laar and Akça, 2007)	19
Figure 12: Transmitted (A_T) and received amplitude (A_R) in time-of-flight ranging [Wehr and Lohr 1999].....	19
Figure 13: Left, ALS units from data acquisition to processing phases, right: Vector setup for geocoded LIDAR data [Shan and Toth 2009]	20
Figure 14: Measuring principle of pulse (left) and continuous waves (right) [Shan and Toth 2009]	21

- Figure 15: Typical reflectivity of deciduous and coniferous trees (in percent) in comparison with various diffuse materials for 900nm wavelength (values from Wehr and Lohr, 1999). 22
- Figure 16: Footprint (a, b, c) and swath width (d) in scanning geometry [Baltsavias 1999a] 23
- Figure 17: nDSM of a single tree from LIDAR data (left) and the shaded model of the point cloud (right). The lack of data at the occluded area shows where the laser beam could not reach the ground. 23
- Figure 18: True-orthophoto of the test area Hoppengarten [Miri et al. 2013]. 26
- Figure 19: Test area Hoppengarten; DSM Laser 40cm, photogrammetric DSM 8cm and 20cm, RGB 8cm [Miri et al. 2013]. 27
- Figure 20: Top: difference images with colorized height differences in decimeter; DSM_image_8cm – DSM_LIDAR_40cm (left), DSM_image_20cm – DSM_LIDAR_40cm (right). Bottom: True orthophotos 8cm (left) and 20cm (right)[Miri et al. 2013]. 28
- Figure 21: Existence of single trees in clearing areas: left and right; the existence of the trees through their shadows in the true-orthophoto and laser-based DSM, middle; the lack of the trees in image-based DSM. 29
- Figure 22: The generic procedure of object-oriented image analysis (left) and the fractal approach of segmentation and classification in a workflow [Baatz et al. 2008]. 33
- Figure 23: Schematic 3D demonstration of the scale-space representation of a 1D signal [Lindeberg 1993] 35
- Figure 24: Different phases of watershed segmentation by flooding on the landscape. The segment boundaries are demonstrated with thick lines [Wah 2008] 37
- Figure 25: Construction of a partition hierarchy by synchronous flooding using depth function. On top of each diagram, the separated segment values caused from connection weights of depth are demonstrated in different gray values [Wah 2008] 39
- Figure 26: Chess-board segmentation of an image-based nDSM with grid size of 10 pixel (2m) 40

Figure 27: Quad-tree segmentation of image-based (top) and laser-based (bottom) nDSM of a single tree with scale parameter of 10, 50, 100 and 200 (left to right)	41
Figure 28: Contrast split segmentation with step 10, chessboard object size 10 pixels or 2m (left and top-right) and 100 pixels (right-down).....	42
Figure 29: The small difference in Contrast Split with step 10 (left) and step 20 (right) with chessboard object size of 100 (the red subset from previous figure).....	42
Figure 30: Spectral difference segmentation of image-based (top) and laser-based (bottom) nDOM with maximum difference of 1, 5 and 10 (left to right) after a chessboard segmentation at pixel size	43
Figure 31: CHM image segmented with multiresolution algorithm in eCognition with scale parameters 100 (left) and 200 (right) with shape parameters 0.1 and compactness of 0.5.....	44
Figure 32: Multiresolution segmentation of laser-based (up) and image-based (bottom) nDSM of a single tree with scale parameter of 10, 50, 100 and 200 (left to right)	45
Figure 33: Chessboard 10 pixel or 2m (the cell represented in red) under a multiresolution with scale 200 (left) and spectral difference segmentation (sp.diff. =100) on LIDAR nDOM after a multiresolution segmentation with scale 100 (right).....	46
Figure 34: Spectral difference segmentation on nDOM with 10 maximum difference after a chessboard segmentation at pixel size	46
Figure 35: Top-down or model-driven (up) and bottom-up or data-driven approach in tree extraction [Straub 2003].....	50
Figure 36: Different projection of trees in true orthophotos with resolutions of 8cm (left) and 20cm (right).....	51
Figure 37: Generalized ellipsoid of revolution with $a = b = n = 2$	52
Figure 38: Top hat segments on an image-based nDSM with 20cm resolution (top left) using spectral difference segmentation (top right), multiresolution segmentation (down left) and Quadtree segmentation (down right).....	54

Figure 39: Different top hat levels (green segments) and local maxima (red pixels) in different nDSM; image-based (left) and laser-based (right)	55
Figure 40: Processing workflow of the feature-based evaluation of the DSM data at the level of THS (red) [Miri et al. 2013]	55
Figure 41: 2D and 3D fitness of structural elements in five scale spaces and different height sections for the hat with the formula of $za^2 + x^2 + y^2b^2 = 1$, with $a = 2$, $b = 2$	56
Figure 42: Results of micrometric measurement of a concrete surface using coherence scanning interferometry demonstrated in 2D, 3D and profile on the blue line (www.nanovea.com).....	57
Figure 43: Top: True-color and false-color surface model of a mixed forest near to other flat surfaces. Down: 2D profile of the laser-based nDSM the rough surface (black) and the filtered surface (red).....	58
Figure 44: Object oriented workflow for single tree extraction	65
Figure 45: The problematic points in the laser-based height data.....	67
Figure 46: Non-smoothing filtering of the laser-based nDSM data	69
Figure 47: The problematic pixels in laser surface models of deciduous and coniferous trees	70
Figure 48: Laser-based nDSM data before (left) and after (right) filter.....	71
Figure 49: The outer boundary (red) and some inner boundaries (blue) of the mixed <i>Stand 1</i> on laser-based (left) and image based (right) canopy height model.....	71
Figure 50: Image-based nDSM (left) and its curvature along the slope (right) of a mixed forest area.....	72
Figure 51: Laser-based nDSM (left) and its curvature profile (right) of a mixed forest area	73
Figure 52: Morphological operations on an object in a binary image space [Smith and Scientist 1999].....	75
Figure 53: Profile of a tree height model (left) after dilation (middle) and erosion (right) with a spherical structural element	76

Figure 54: Profile of a tree height model with a ground threshold (left) and the inverted one (right)	77
Figure 55: Marble rolling with different marble sizes (top and middle) and combined format	78
Figure 56: The voxel spheres in 2D (left) and 3D (right) with diameters of 8 pixels (top) 20 pixels (middle) and 50 pixels (bottom).....	79
Figure 57: Binary images of the 3D marbles with 2m and 3m radius in a coniferous stand	80
Figure 58: Multi-layer demonstration of the structural elements for three marble sizes	81
Figure 59: Multiresolution segmentation of marble layers of a coniferous stand in eCognition with parameters: shape 0.1, compactness 0.5 and scales 10 (left) and 50 (right). Marble layers are weighted from 0.0 to 1.0 with 0.1 intervals	81
Figure 60: Multiresolution segmentation of marble layers of a deciduous stand in eCognition with parameters: shape 0.1, compactness 0.5 and scales 10 (left) and 50 (right). Marble layers have the same weighing value of one.....	82
Figure 61: Multiresolution segmentation of marble layers of a laser-based nDSM of a coniferous stand before (left) and after (right) merging the marble segments	83
Figure 62: Multiresolution segmentation of marble layers of an image-based nDSM of a coniferous stand before (left) and after (right) merging the marble segments.....	83
Figure 63: Multiresolution segmentation of marble layers on a laser-based nDSM of coniferous stand in eCognition. Inversed nDSM is involved (left) and is not involved (right) as weighting values	84
Figure 64: Definition of amount and direction of tree inclination using marble rolling layers	85
Figure 65: Definition of growing limits with setting height threshold (left) and recognition of changes in curvature values (right)	86
Figure 66: Curvature profiles of image-based and laser-based nDSM in a coniferous stand.....	87
Figure 67: Definition of the inner border and the outer border of a segment	88

Figure 68: Candidate border pixels (with orange boundaries) based on curvature values before (left) and after (right) merging.....	88
Figure 69: Start of the region growing of the non-tree area (with yellow boundaries) at the first (left) and second (right) growth iteration	89
Figure 70: Region growing of the non-tree area (yellow-green) from the first to the last growth iteration.....	89
Figure 71: Segmentation refinement of the not-tree area in a laser-based nDSM	91
Figure 72: Final result of the segmentation refinement of the not-tree areas (yellow) in a laser-based nDSM of a coniferous stand.....	92
Figure 73: The problem of region growing based on height value of the current growing pixel as absolute reference comparing with the mean height of the inner border pixels (left) or the mean height of the segment (right)	94
Figure 74: Uncontrolled segmentation of the single trees based on extreme values of compactness (left) and shape (right) parameters leads to wrong region growing of the seed objects.....	95
Figure 75: Schema of a supervised region growing model	97
Figure 76: Definitions of the length and width of a segment based on the ellipse parameters in the bounding box (left) or the main line of the skeleton polygon (right).....	98
Figure 77: Circular opening elements among the MEs within an allocation rule-set	99
Figure 78: Result of a supervised region growing model on LIDAR-Data (for better demonstration of the regions, the scale at height values is set to 0.1).....	99
Figure 79: Final segmentation results with the gaps between trees (left) and the extended tree regions without the final implementation of MEs (right).....	100
Figure 80: Comparison of IQF on laser-based nDSM (left) and image-based nDSM (right) at low segmentation level for ■ coniferous and ■ deciduous tree types from [Miri et al. 2013]	101
Figure 81: 2D and 3D demonstration of the results of region growing-comparison of the segments in a dense coniferous area (S1 to S3) with a deciduous tree (S4 to S7)	102




Figure 82: Geometry of the final segments in 2D and 3D space	103
Figure 83: Comparison of AHV on laser-based nDSM (left) and image-based nDSM (right) at low segmentation level for ■ coniferous and ■ deciduous tree types [Miri et al. 2013]	104
Figure 84: Roughness and height variations considering different reference values for calculating the standard deviation of a segment	105
Figure 85: Allocation areas for the automatically found tree positions (blue points) with search buffers of 1m, 2m and 3m (green, yellow and orange lines) around the reference trees (red points)	107
Figure 86: Topological relations between the reference dataset (red circles) and the target tree segments (blue squares) based on [Gerke 2006] and [Straub and Heipke 2004]	108
Figure 87: The explanation of completeness and correctness according to [Straub 2003].....	109
Figure 88: The study area Habichtswald in the state of NRW, Germany	115
Figure 89: Difference image of DSM data (LIDAR - Image)	116
Figure 90: Contribution of the assessment patches around the study area	117
Figure 91: Roughness parameters (in decimeter) on image-based ■ and laser-based ■ surface models based on the arithmetic average of different deciduous stands	119
Figure 92: Roughness parameters (in decimeter) on image-based ■ and laser-based ■ surface models based on the standard deviation of different deciduous stands	120
Figure 93: Roughness parameters (in decimeter) on image-based ■ and laser-based ■ surface models based on the arithmetic average of different coniferous stands	121
Figure 94: Roughness parameters (in decimeter) on image-based ■ and laser-based ■ surface models based on the standard deviation of different coniferous stands.....	122
Figure 95: Roughness analysis (in decimeter) over the CHM of an old beech stand using the R_{fstd} evaluator with window size of 3 pixels in different filter iterations	124

Figure 96: Roughness analysis (in decimeter) over laser (red) or image (blue) CHM of a young spruce (Con) stand (432a1) and an old beech (Dec) stand (437a1) using the R_{fstd} evaluator in eleven filter iterations	125
Figure 97: Roughness analysis (in decimeter) over laser (La) or image (Im) CHM of a very young mixed deciduous stand (430c6) and a young beech stand (430c4) using the R_{fstd} evaluator in eleven filter iterations	125
Figure 98: Experimenting the preparation of the reference data using traditional methods in forestry.....	127
Figure 99: Complexity of tree positioning and counting.....	127
Figure 100: Point cloud of a TLS station in a coniferous stand with true colors (left) and height false colors (right).....	128
Figure 101: Panorama view of the point cloud of a scan position with RGB information	128
Figure 102: Panorama view of the point cloud of a scan position with intensity values	129
Figure 103: Leica HDS 7000, Riegl LMS Z620	129
Figure 104: Surveying the reference points at field, required for geo-referencing the terrestrial dataset	130
Figure 105: Terrestrial laser scanning of the targets in the clearing area for the global registration (right) and the single trees within the stand (left).....	131
Figure 106: Terrestrial data acquisition of the single trees with TLS and close range photogrammetry in PHIDIAS.....	132
Figure 107: Multiple-views for provision of the reference data. Top-left: the DBH circles (blue) and the 1.3m breast height (red lines); Top-right: the test area (marked with orange dashed lines). Below: colored point clouds	133
Figure 108: Segment specification of coniferous classification using roughness parameters on image-based and laser-based surface models (values in meter).....	135

Figure 109: Segment specification of deciduous classification using roughness parameters on image-based and laser-based surface models (values in meter)	136
Figure 110: Comparison of the tree classes based on image-based and laser-based roughness parameter.....	137
Figure 111: Classification results using image-based height variation feature STD (left), compared with RGB data (right).....	137
Figure 112: Classification results for laser-based height variation with feature NHV (left) compared with the RGB data (right).....	138
Figure 113: Segment specification of coniferous classification using the form parameters on image-based and laser-based surface models.....	139
Figure 114: Segment specification of deciduous classification using form parameters on image-based and laser-based surface models.....	140
Figure 115: Comparison of the tree classes based on image-based and laser-based form parameter MFQ.....	141
Figure 116: Classification results using laser-based form feature MQF (left), compared with RGB data (right).....	141
Figure 117: Classification results using image-based form feature MQF (left), compared with RGB data (right).....	142
Figure 118: Allocation lines from the reference points to the target points in the case of P-CT datasets	144
Figure 119: Allocated trees from target segments of the marble rolling segments laser-based data to the reference TLS segments for the 2.5m buffer	146
Figure 120: Quantitative evaluation based on overlapping factor of AOF.....	146
Figure 121: Point- point analyses of the reference and target datasets (P and Mrb) based on the weighted distance factor (WD)	147

Figure 122: Point-polygon analyses of the reference and target datasets (P and Mrb) based on the weighted distance and overlapping factor (WDO) on LIDAR-based CHM	148
Figure 123: Point-polygon analyses of the reference and target datasets (P and Mrb) based on the weighted distance and overlapping factor (WDO) on image-based CHM.....	149

REFERENCE OF TABLES

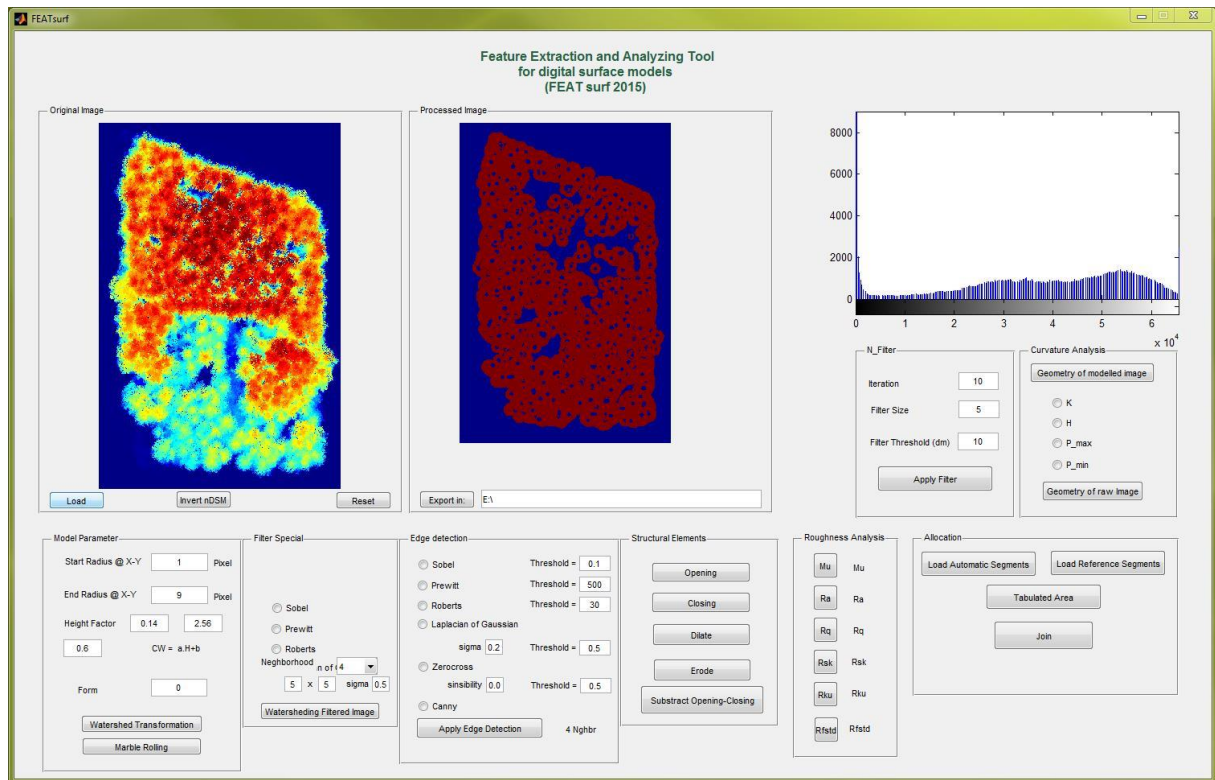
Table 1: Comparison of ranging methods in ALS systems	21
Table 2: Comparison of laser-based and image-based data potential for forestry applications (potential level:  high;  medium;  low) [Miri et al. 2013].....	25
Table 3: The S-Parameter Set	59
Table 4: The R-Parameter Set.....	59
Table 5: Some geospatial filters in software ArcGIS 10.1	68
Table 6: The geometry-based features of a segment.....	103
Table 7: The sixteen specifications of binary topological relations and the terminology for the nine relations (grey rows) between two spatial regions	108
Table 8: Technical data for airborne sensors used for the test area Habichtswald (HBW)	115
Table 9: Statistical assessment of difference surfaces of laser-based and image-based DSM	117
Table 10: The sets of roughness parameters in 2D form	118
Table 11: Characteristics of the sample areas in the forest region of Habichtswald	118
Table 12: Analysis of roughness parameters on laser-based and image-based surface models ..	134
Table 13: Analysis of form feature MQF on laser-based and image-based surface models	138
Table 14: Point to point datasets	143
Table 15: Point-point evaluation (in %) of the laser-based data of the reference and target tree positions	144
Table 16: Point-point evaluation (in %) of the image-based data of the reference and target tree positions	145



9

Appendices

Appendix 2: Environment of the *Feature Extraction and Analyzing Tool (FEATsurf)* developed using the GUI in MATLAB including the Marble-rolling tool, Roughness evaluators, and non-smoothing filter, Edge detection and Curvature analyses.



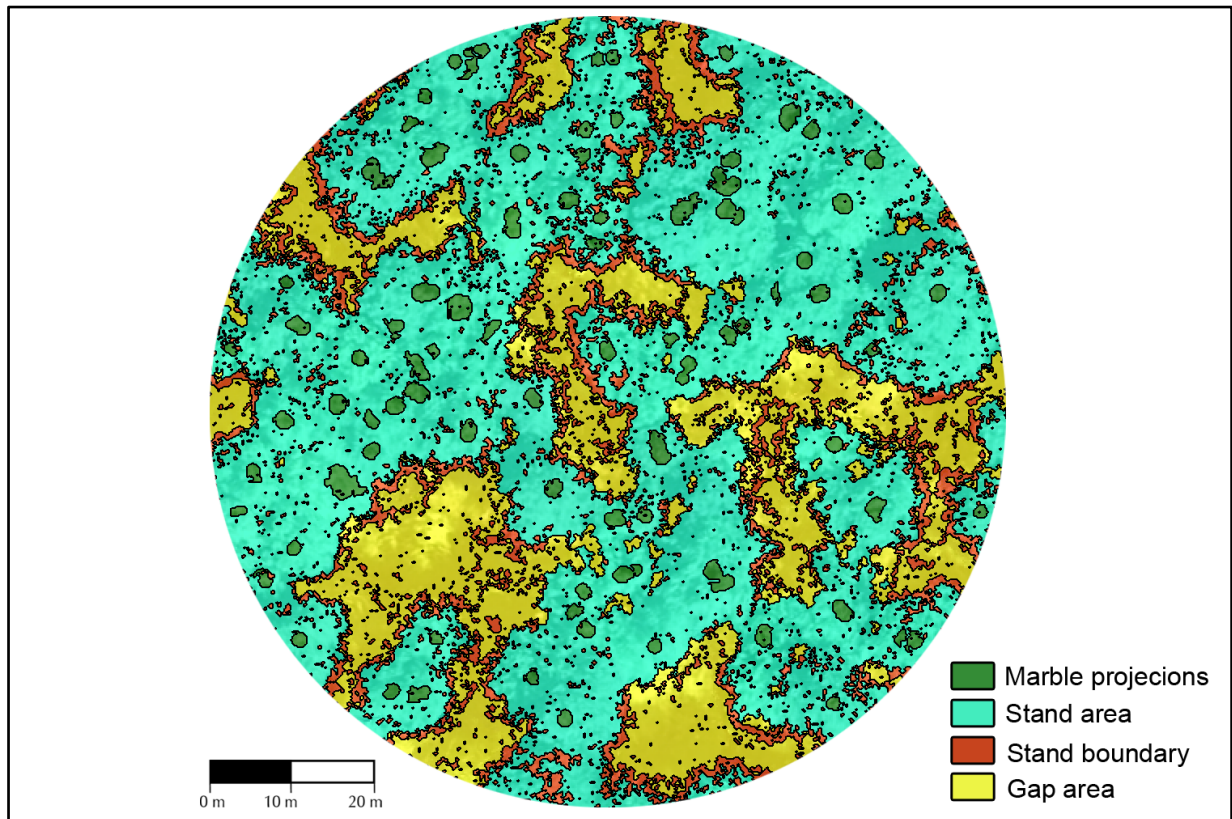
Appendix 3: Partial representation of the *FEATsurf* developed in MATLAB (Function Marble Rolling)

```

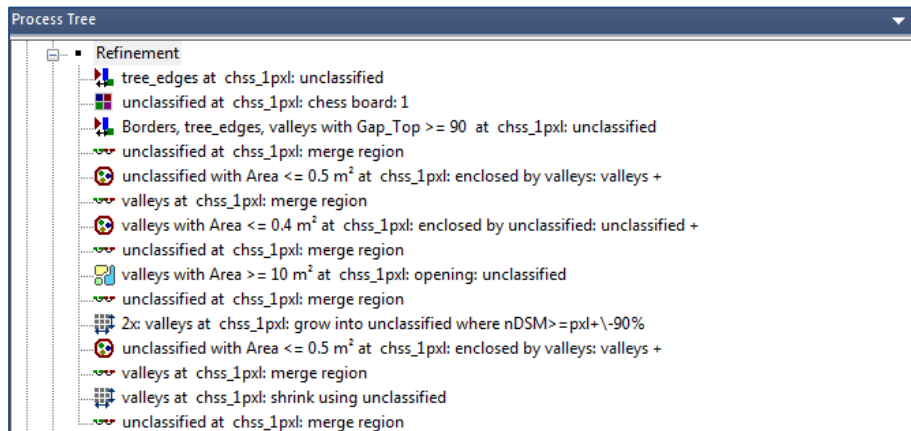
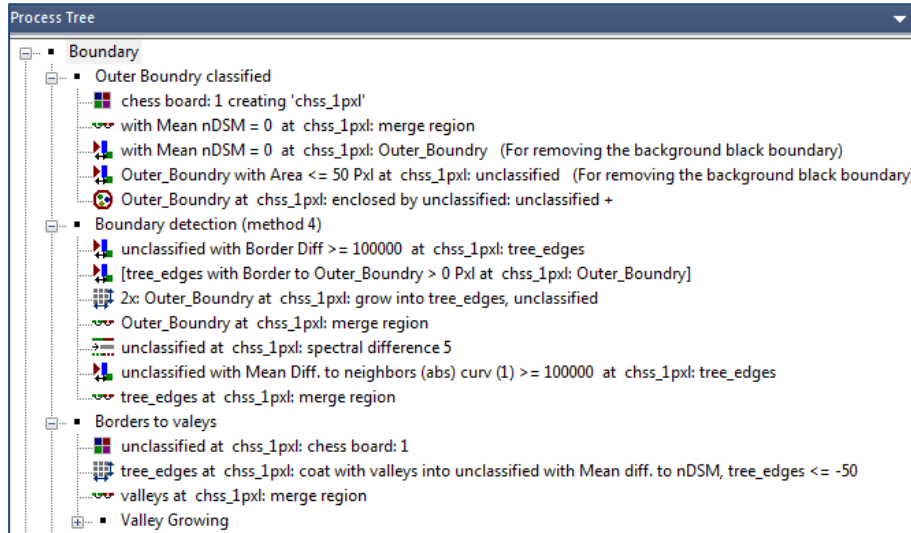
2547 % --- Executes on button press in marble_rolling.
2548 function marble_rolling_Callback(hObject, eventdata, handles)
2549 % hObject    handle to marble_rolling (see GCBO)
2550 % eventdata  reserved - to be defined in a future version of MATLAB
2551 % handles    structure with handles and user data (see GUIDATA)
2552
2553 global im2 SP xmin xmax ymin ymax zmin zmax cmin cmax N maxval m n load_path
2554
2555 img_f = im2;
2556
2557 %% Scaling Parameters:
2558 Start_Rad = str2double(get(handles.morpho_radi,'String'));
2559 End_Rad   = str2double(get(handles.morpho_radi_end,'String'));
2560 HF        = str2double(get(handles.f_radi,'String'));
2561 Form      = str2double(get(handles.form_factor,'String'));
2562
2563 %% ----- Variables
2564 SP        = (End_Rad-Start_Rad)/2; %Scaling Parameter
2565 xmin     = 0;
2566 xmax     = n;
2567 ymin     = 0;
2568 ymax     = m;
2569 zmin     = 0;
2570 zmax     = maxval;
2571 cmin     = 0;
2572 cmax     = 255;
2573
2574 %% ----- PREPARATION
2575
2576 % Morphologic
2577 remain = zeros(m,n,End_Rad-Start_Rad+1); % (prepares matrix with depth of
''End-Start'')
2578 % Geometric
2579 gradmag = zeros(m,n,End_Rad-Start_Rad+1); % (prepares matrix with depth of
''End-Start'' for gradmag)
2580 hy = fspecial('sobel');
2581 hx = hy';
2582
2583 %% ----- PROCESS
2584
2585 exp_folder_path = 'E:\Marble_Rolling_im\';
2586
2587     F_Num = 0; % Functioned Number or the remain layer
2588
2589     for Rad = Start_Rad:End_Rad
2590
2591         clear im_remain Ix Iy
2592         F_Num = F_Num +1;
2593
2594         %% MORPHOLOGICAL Function
2595
2596         remain (:,:,F_Num) = imopen(img_f, strel('ball', Rad, HF*Rad, Form));
2597
2598         %% GEOMETRY
2599
2600         Iy = imfilter(double(remain (:,:,F_Num)), hy, 'replicate');
2601         Ix = imfilter(double(remain (:,:,F_Num)), hx, 'replicate');
2602         gradmag (:,:,F_Num) = sqrt(Ix.^2 + Iy.^2);
2603
2604         % Exportin results in severela files %
2605         Rad_txt = ['rad_' num2str(Rad) '_' ];
2606         HF_txt = ['hf_' num2str(HF) '_' ];
2607         Form_txt = ['form_' num2str(Form) ];
2608         file_detail = [Rad_txt HF_txt Form_txt];
2609         file_path = [ exp_folder_path '06_MatExp_' file_detail '.tif'];
2610         imwrite(gradmag (:,:,F_Num),file_path,'tif', 'Compression','none');
2611
2612     end

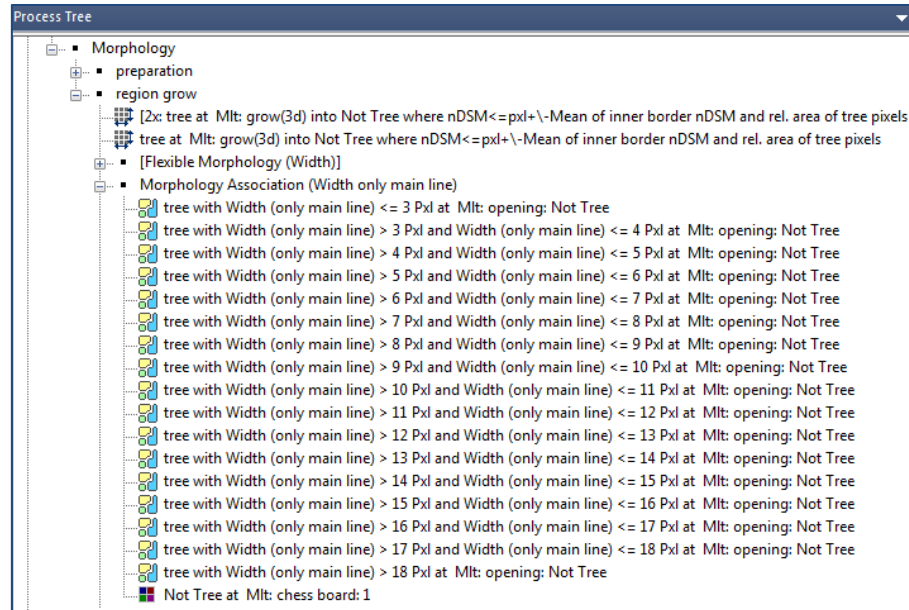
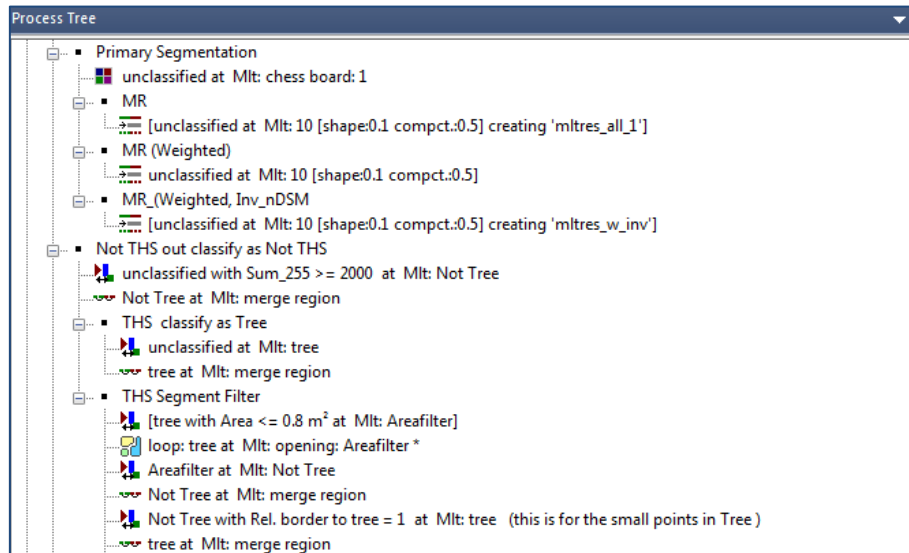
```

Appendix 4: Combined classes before segmentation refinement of a laser CHM of a deciduous stand.

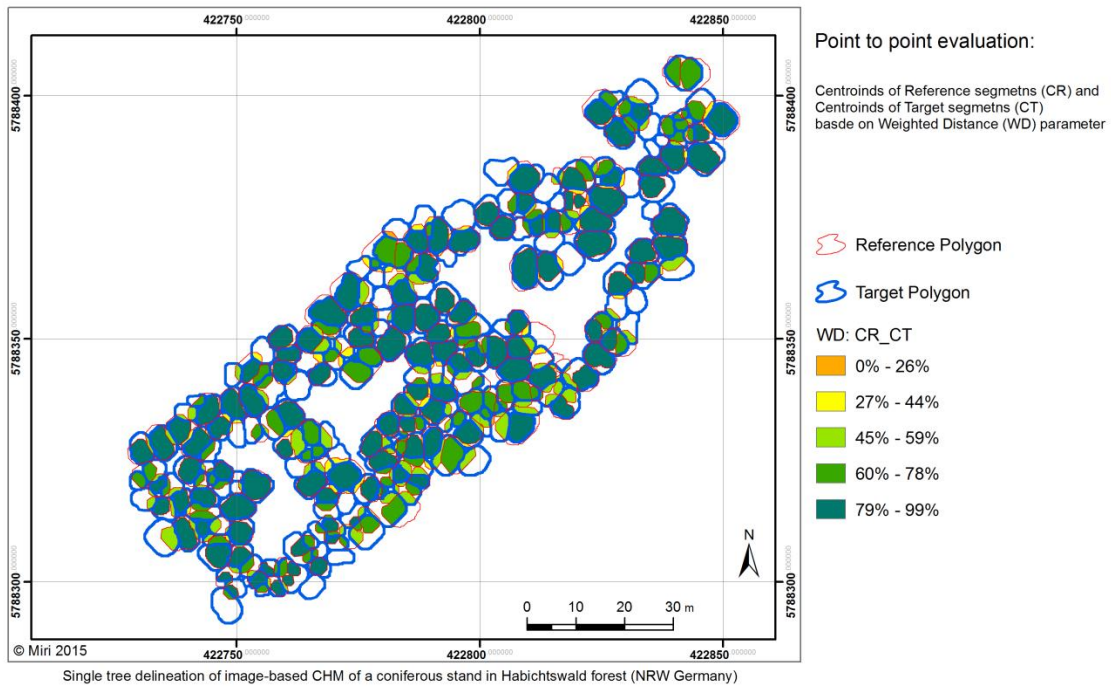
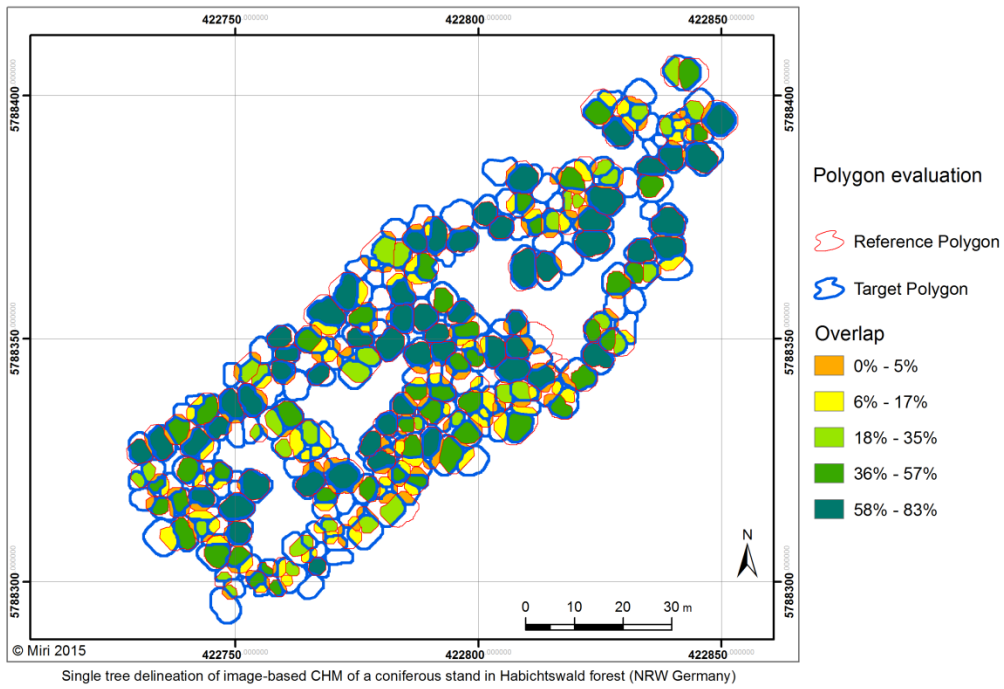


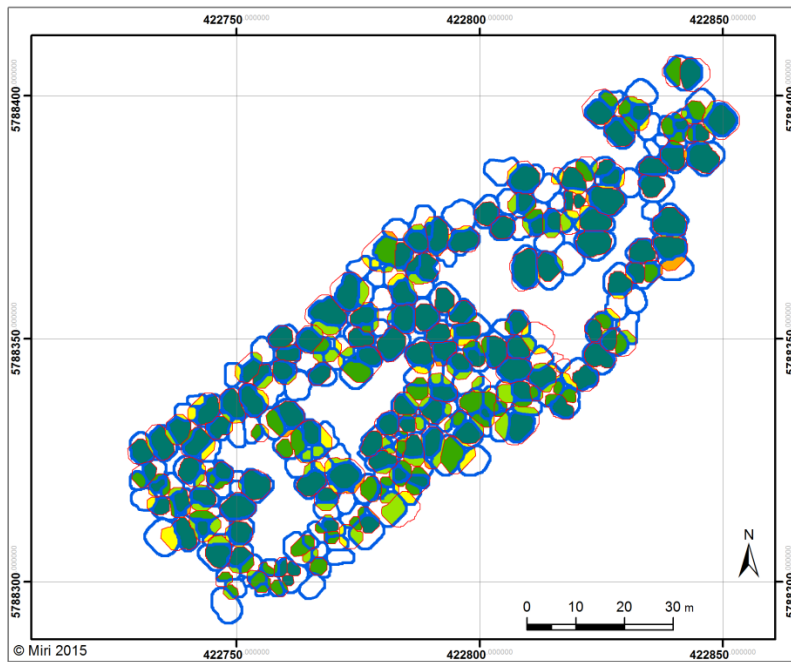
Appendix 5: Partial representation of the implemented rule-sets designed and developed in the object-oriented environment of the software eCognition.





Appendix 6: Polygonal and point analyses of the image-based canopy height models







Single tree delineation of image-based CHM of a coniferous stand in Habichtswald forest (NRW Germany)


Point to point evaluation:


Points measured by TLS (P) and
Points from centroids Marble segments (Mrb)
basde on Weighted Distance (WD) parameter


 Reference Polygon

 Target Polygon


WD: P_Mrb

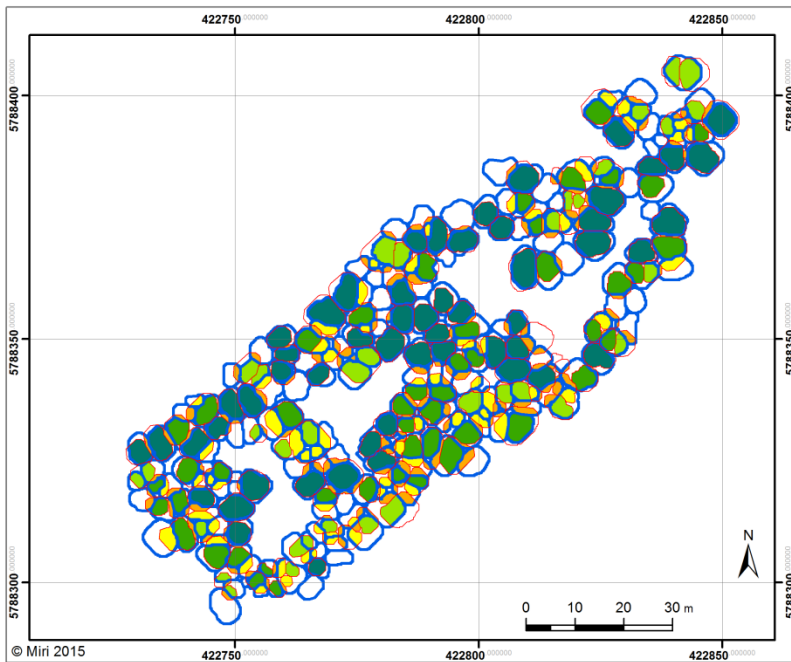
 0% - 36%

 37% - 52%

 53% - 67%

 68% - 84%


 85% - 99%



Single tree delineation of image-based CHM of a coniferous stand in Habichtswald forest (NRW Germany)


Point-Polygon evaluation:

Centroids of Reference segments (CR) and
Centroids of Target segments (CT)
basde on Weighted Distance and Overlap (WDO) factor


 Reference Polygon


 Target Polygon


WDO: CR_CT

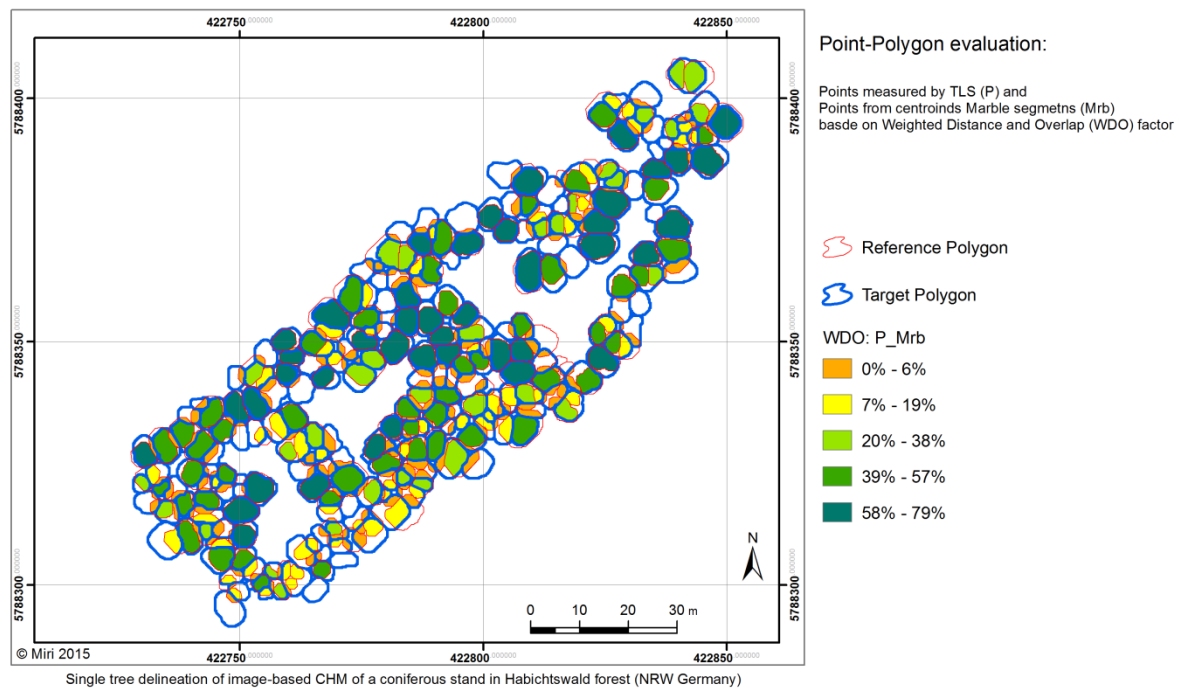
 0% - 4%

 5% - 13%

 14% - 29%

 30% - 52%

 53% - 81%






10

Abbreviations

AHV	Averaged Height Variations
ALS	Airborne Laser Scanning
CHM	Canopy Height Model
CW	Crown Width
DBH	Diameter at Breast Height
DEM	Digital Elevation Model
DMC	Digital Mapping Camera
DSM	Digital Surface Model
DTM	Digital Terrain Model
fSTD	Filtered Standard Deviation
FWF	Full Wave Form
GSD	Ground Sampling Distance
HBW	Habichtswald
HRDI	High Resolution Digital Images
HRSC	High Resolution Stereo Cameras
IMU	Inertial Measurement Unit
IQF	Inversed Quasi Flatness
LIDAR	Light Detection And Ranging
LOD	Level Of Detail
ME	Morphological Element
MQF	Mean Quasi Flatness
Mrb/MR	Marble Rolling
nDSM	Normalized Digital Surface Model
NHV	Normalized Height Variations
OBIA	Object Based Image Analyses
RGB	Red, Green, Blue
RMS	Root Mean Square
SDI	Stand Density Index
SE	Structural Element
SGM	Semi Global Matching
STD	Standard Deviation
TLS	Terrestrial Laser Scanning
VHSR	Very High Spatial Resolution
WD	Weighting Distance
WDO	Weighted Distance and Overlapping



11

Curriculum Vitae

For reasons of data protection, the Curriculum Vitae is not published in the online version.

For reasons of data protection, the Curriculum Vitae is not published in the online version.